A DENSITY APPROACH TO CHEMICAL BINDING

A DENSITY APPROACH
TO
CHEMICAL BINDING

By

HARRY JOHN THOMAS PRESTON, B.Sc.

A Thesis

Submitted to the Faculty of Graduate Studies

in Partial Fulfilment of the Requirements

for the Degree

Doctor of Philosophy

McMaster University

May, 1969

DOCTOR OF PHILOSOPHY
(Chemistry)

McMASTER UNIVERSITY
Hamilton, Ontario.

TITLE: A Density Approach to Chemical Binding

AUTHOR: Harry John Thomas Preston, B.Sc. (McMaster University)

SUPERVISOR: Professor R. F. W. Bader

NUMBER OF PAGES: ix, 239

SCOPE AND CONTENTS:

The material presented in this thesis is an attempt to obtain an increased understanding of the electronic structure and chemical binding in molecular systems. The one-electron charge distribution in methane, which is derived by considering only one-electron dependent properties of the system, is used to analyze the chemical binding in this molecule. A theoretical method, which allows one to determine the effect of the Pauli exclusion principle on the one-electron density distribution, is used to test the concepts underlying the electron pair repulsion theory as applied to H_2O and NH_3. Kinetic energy distributions are defined in order to examine the relationship between the topographical features of the molecular one-electron charge distribution and the kinetic energy of the system.

PREFACE

The electronic structure and chemical binding in molecular systems are of major concern to many experimentalists and theoreticians. A basic understanding of these properties is essential to a fundamental interpretation of the stability and chemical behaviour exhibited by molecules. The work presented in this thesis, which is couched in terms of a density approach, is an attempt to obtain a more complete knowledge of molecular binding.

A one-electron charge distribution is obtained for the methane molecule using only one-electron properties of the system. This charge distribution is used to analyze the chemical binding in methane. The effect of the Pauli exclusion principle on the one-electron charge distribution in three dimensional space is discussed. The topography of the one-electron charge distribution in molecules is related to the kinetic energy of the system by considering a number of kinetic energy distributions.

During the course of my research I have been very dependent on the computer facilities that were supplied. I wish to thank the computer staff at McMaster University for their valuable assistance in the use of the IBM 7040 computer. I am also indebted to the people associated with the Quantum Chemistry Program Exchange who supplied many of the programs used for the calculations considered in this thesis.

I thank my research supervisor, R. F. W. Bader, who suggested the problems considered in this thesis. His valuable assistance and enthusiastic encouragement have been a great asset to the successful

completion of this work. To him I owe my interpretation of molecular binding.

I wish to acknowledge the assistance of my fellow graduate students, Mr. A. Bandrauk, Mr. I. Keaveny and Mr. W. Henneker. Their many valuable discussions have made the tasks of preparing this thesis much easier. I thank the National Research Council of Canada for their financial assistance. I wish to express my sincere thanks to Mrs. S. Hawley for the competent typing of this thesis.

I wish to express the deepest appreciation to my parents for their moral support and for making this thesis possible. Finally, to my wife Rosemary, I dedicate this thesis with love and gratitude.

TABLE OF CONTENTS

TABLE OF CONTENTS-Continued

LIST OF TABLES

LIST OF FIGURES

LIST OF FIGURES-Continued

GENERAL INTRODUCTION

All but the smallest atoms and molecules are dynamic systems of great complexity. At present, exact calculation of the properties of such many-particle systems are not possible since Schrödinger's wave equation has not been solved exactly for the many-body problem. Thus, certain assumptions and approximations must first be made in order to carry out any theoretical calculations. It is important, however, to be guided by physical considerations, for the purpose of analysis is not just to account for the properties of a particular molecule as closely as possible but also to discern features that are shared by other molecular systems.

It was with the intention of better understanding the electronic structure and chemical binding in polyatomic systems that the work presented in this thesis was undertaken. Since many molecular properties[1] are directly determined by the three-dimensional charge distribution in the molecule, much can be gained by analyzing the characteristics of this distribution. In this thesis a "Density Approach" is used as a means of aquiring this knowledge.

In Chapter I a ground state one-electron density distribution for the methane molecule is determined by requiring this distribution to give zero forces on the nuclei and the correct expectation value for the diamagnetic proton magnetic shielding. This electrostatic approach, which utilizes only one-electron properties, was used rather than the generally accepted method of energy minimization which necessarily involves difficult

two-electron integral calculations. This derived density distribution is used to calculate a set of experimentally observable physical properties in order to assess the merits of this approach. The chemical binding in methane is analyzed in terms of the derived charge distribution. An answer is given to the question, "Does the method of energy minimization necessarily give the best one-electron charge density for polyatomic molecules using a limited basis set?"

Chapter II deals with a theoretical method which is used to test the concepts underlying the electron pair repulsion theory of molecular geometry.[2] This theoretical method allows one to determine the effect of the Pauli exclusion principle on the one-electron density distribution. It is shown that pictures of overlapping orbitals, which are so commonly used in discussions of molecular geometry, do not in general correspond to the actual effect which the Pauli principle has on the three-dimensional charge density. An alternative electrostatic approach, involving the concept of a binding region for a polyatomic molecule, is proposed to account for the observed molecular geometries.

The material in Chapter III is concerned with a new dynamic approach to the binding in molecules. This approach is a complement to the electrostatic approach[3,4,5,6] which interprets chemical binding in terms of the spatial characteristics of the molecular charge distribution and the forces which it exerts on the nuclei. This new approach examines the relationship between the topographical features of a molecular charge distribution and the kinetic energy of the system. Specifically, the spatial contributions to the kinetic energy are related to the Laplacian of the total charge density and to the gradients of the natural orbital densities. It is shown that the

charge density accumulated in the internuclear region of a stable molecule is distributed in such a way as to keep the accompanying increase in the kinetic energy to a minimum. A comparison of the contribution to the kinetic energy from the atomic and molecular charge distributions indicates that in the formation of a stable molecule the contribution to the kinetic energy from the molecular charge density in the binding region is decreased to that of the atoms.

Concluding remarks concerning the binding in molecules from a "Density Approach" are given.

Some of the results presented in this thesis have been accepted for publication[7]; others have been published in the Canadian Journal of Chemistry[8].

I. A DENSITY APPROACH TO CHEMICAL BINDING IN METHANE

I.1 Introduction

a) Historical Survey

The high symmetry possessed by the methane molecule has resulted in many theoretical investigations of its electronic structure. The literature on the determination of the electronic wavefunction of methane is rather extensive[9-30] and includes various approaches and different degrees of accuracy. In the past, accurate wavefunctions for polyatomic molecules such as CH_4 were not attempted because it was impossible to evaluate the many-centered two-electron integrals which were required by the self-consistent-field (SCF) procedure. Only recently have some polyatomic wavefunctions become available which for their accuracy[21,24,26-29] can be compared to those derived for diatomic molecules by the SCF LCAO MO method[31,32].

The tetrahedral symmetry of the methane molecule, which can almost be considered spherical to a good approximation, makes it an ideal molecule for testing one-center expansion[9-14,17-20,22,30] (OCE) techniques. This one-center method, which requires the evaluation of only one-center integrals, was used by early workers to circumvent the calculation of the difficult multicenter integrals. The failure of this method to produce a good charge distribution around the hydrogen atoms and in the outer regions of the molecule has often led to criticism[24] of this approach.

The attempts to use Gaussian-type orbitals[16,21,28] (GTO's) in multi-center expansions have met with some success even though such orbitals do not fulfill the cusp conditions as well as the exponentials. The use of

Gaussian instead of Slater-type functions for the radial part decreases the computational difficulties, but it is clear[16] that the Gaussians form an inferior basis set, and probably about 40% more such functions are needed[33] to achieve comparable results. Using an extremely large Gaussian basis set Ritchie and King[28] have determined a wavefunction for methane that gives one of the better energies, -40.198 a.u., for this molecule. Similar results for other molecules indicate the great success of the Gaussian approach.

Only recently have extensive polycenter analytic SCF calculations[24, 26,27,29] been attempted using Slater-type orbitals (STO's) in minimal or rather limited basis sets. These results for polyatomic systems are very promising even though the calculated energies do not approach the Hartree-Fock limit as closely as do the results for diatomic molecules. Because of the computational difficulties with multi-center integrals, fully optimized polycenter wavefunctions using large extended basis sets of Slater-type orbitals have not been attempted for molecules such as CH_4. The best wavefunction to date for methane, from a minimum energy criterion, has been obtained by Arrighini et al[29] using a multi-center basis set of thirty-nine Slater-type orbitals. They obtain an energy of -40.20542 a.u., which is approaching the Hartree-Fock limit, and determine good expectation values for a number of physical properties. Even though theoretical calculations such as these are in good agreement with experiment, accurate Hartree-Fock wavefunctions for polyatomic molecules await advances in numerical computations.

Since obtaining molecular wavefunctions using the minimization of energy criterion[34] requires so much computation time, particularly for

polyatomic systems, other methods of determining wavefunctions have been suggested. Bader and Jones[35], and Keaveny[36] have shown that certain one-electron properties, which are much simpler than energies to calculate, can be used to determine a set of unknown parameters in a very generalized set of basis orbitals. This method, which depends solely on the one-electron density, was adopted in the present work to determine a one-electron density distribution for methane, which could then be used to analyze the chemical binding in this molecule.

Many models have been proposed to account for the known facts of the chemical behaviour of molecules. The idea that a chemical bond consists of a pair of electrons, in close association with each other, shared between two atoms was first conceived by Lewis[37]. This idea of the electron pair bond was further considered in the theoretical treatment of molecules by Heitler[38] and London[39]. Sidgwick and Powell[40] were the first to point out that molecules with four pairs of electrons in the valency shell were either tetrahedral in shape (CH_4) or were related to the basic tetrahedral geometry, e.g., the nearly tetrahedral bond angles found in NH_3 and H_2O. Lennard-Jones[41] demonstrated that the antisymmetrization requirements of the Pauli principle forces the electrons of an inert gas, such as neon, to dispose themselves so that those of the same spin subtend tetrahedral angles at the nucleus. He also showed that there was no correlation between the two tetrahedra resulting from the electrons with α and β spin. Pople[42] postulated that as one considered the withdrawal of successive protons from the Ne nucleus to form HF, H_2O, NH_3 and CH_4 respectively, the motion of the two tetrahedra would become correlated so as to concentrate a pair of electrons with opposite spin along each bond to a hydrogen atom. In

this way the electron density in these molecules were directly related to the tetrahedral hybridization (sp^3) of Ne. The sp^3 hybridization is in fact altered by polarization-type hybridization[43] due to the protons.

The methane molecule, which has four pairs of valence electrons, can thus be expected to have its electron density concentrated along the molecular bond axes in almost sp^3 hybridization. The actual positioning of the density along these bonds determines how polar the bonds are. In order to analyze these characteristics of the charge distribution, contour maps of the derived molecular density $\rho(\vec{x}_1)$ and the difference density $\Delta\rho(\vec{x}_1)$, which is obtained by subtracting the superimposed densities of the component undistorted atoms placed at the equilibrium bond lengths from the molecular density also evaluated at the equilibrium bond distance, are considered.

The one-electron density distribution of the ground state accounts for many of the physical properties of a molecule. In order to determine how closely the derived density distribution for methane resembles the real physical density a number of these physical properties are calculated, using the derived density, and compared with their experimental counterparts. The agreement of these results will be used as a measure of the quality of the derived one-electron density distribution.

b) Theoretical Background

Within the confines of Quantum Mechanics a complete knowledge of the time-independent properties of a system consisting of nuclei and electrons can be obtained by finding solutions to Schrödinger's wave equation

$$H\psi = E\psi \,, \qquad (1.1)$$

where H is the quantum mechanical Hamiltonian operator for the system, ψ is the energy eigenfunction and E is the corresponding energy eigen value. In Equation (1.1) the Hamiltonian is a function of the coordinates and momenta of both the electrons and the nuclei, and ψ is a function of the space and spin coordinates of all the particles. To find solutions to Equation (1.1) is not an easy task since this equation can not be solved exactly for many particle systems and approximate methods must be used.

Within the Born-Oppenheimer[44] approximation, which allows one to separate the electronic and nuclear motions, the basic problem of finding solutions to Equation (1.1) is reduced to finding solutions to the electronic wave equation

$$H_e \psi_e = E_e \psi_e \tag{1.2}$$

for various fixed nuclear configurations. In Equation (1.2) the electronic Hamiltonian, H_e, is given by

$$H_e = -\frac{1}{2}\sum_{i=1}^{n} \nabla_i^2 - \sum_{i=1}^{n}\sum_{\alpha=1}^{N} \frac{Z_\alpha}{r_{i\alpha}} + \sum_{i>j=1}^{n} \frac{1}{r_{ij}} \quad , \tag{1.3}$$

where n and N are the number of electrons and nuclei respectively, ∇_i^2 is the Laplacian operator for the i^{th} electron, r_{ij} is the distance between the i^{th} and j^{th} electrons, Z_α is the charge on the α^{th} nucleus and $r_{i\alpha}$ is the distance between the i^{th} electron and the α^{th} nucleus. Atomic units (a.u.) are employed throughout. The electronic wavefunction, ψ_e, will thus depend on the spin and space coordinates of the electrons and on the fixed nuclear geometry through the terms $(Z_\alpha/r_{i\alpha})$ in H_e. Exact solutions to Equation (1.2) are also not possible except for very simple cases and

thus further approximations are required.

The next step, the Hartree-Fock approximation, is to assume the total electronic wavefunction ψ_e to be given by an antisymmetrized product of orthonormal one electron spin functions, designated as spin orbitals. Thus, for a system of n electrons the wavefunction is represented by

$$\psi_e = 1/\sqrt{n!}\,||\lambda_1(1)\lambda_2(2).....\lambda_n(n)|| \quad , \tag{1.4}$$

where the λ_i's are the spin orbitals, each being a product of a space function ϕ_i, called an atomic or molecular orbital, and an α or β spin function. The double bars in Equation (1.4) denote a determinant. In 1930, Fock[45], using the determinantal wavefunction represented by Equation (1.4) which satisfies the Pauli principle, devised a self-consistent-field (SCF) procedure, proposed earlier by Hartree[46], for finding approximate solutions to Equation (1.2). This SCF method[47], which has the variational principle built into it, involves an iterative procedure of first guessing a set of spin orbitals λ_i, determining the "Fock" matrix, solving for a new set of λ_i and comparing them with those guessed; the steps are repeated until self-consistency is reached.

The SCF procedure is ideal for atoms, but when dealing with molecules the SCF method is replaced by the LCAO SCF method first proposed by Roothaan[34]. He assumed that the molecular orbitals, ϕ_i, are represented to a good approximation by a linear combination of basis functions, χ_j, centered on each of the constituent atoms. Thus

$$\phi_i = \sum_j C_{ij}\chi_j \quad , \tag{1.5}$$

where the C_{ij}'s are the variable atomic coefficients. The criterion of

energy minimization is used to optimize the variable parameters, including the atomic coefficients, C_{ij}, in the molecular wavefunction. If enough atomic functions χ_j are included in the expansion for the molecular orbitals then no error will be introduced by this LCAO approximation.

The single-determinantal wavefunction represented by Equation (1.4) does not represent an exact solution of the electronic Schrödinger wave equation, Equation (1.2). Such a wavefunction, although it satisfies the Pauli principle by keeping electrons with parallel spin apart, does not prevent electrons with opposite spin from being in the same space orbital and this is energetically unfavourable because of the coulombic repulsions of the electrons. The error introduced by the single-determinantal Hartree-Fock wavefunction is called the correlation error and it arises because of the electrostatic interactions of electrons with opposite spin. Löwdin[48] has shown that a linear combination of several single-determinantal wavefunctions, each formed from different spin orbitals, can give a significant improvement in the total wavefunction and if the expansion is carried far enough such a wavefunction can lead to a true solution of Equation (1.2). This is the method of configuration interaction which is often applied to open-shell configurations.

In the present work, which is concerned with deriving a ground state one-electron density distribution for the methane molecule, all the molecular orbitals are doubly occupied and thus the molecular wavefunction is assumed to be given to a good approximation by a single-determinantal wavefunction.

Because of computational difficulties with integrals in the SCF procedure the basis sets used to represent the molecular orbitals in polyatomic systems are not complete. The more accurate calculations generally result

in numerical solutions which have no simple physical interpretation. Using limited basis sets, which are less accurate than numerical solutions, one can often correlate properties of the molecular wavefunction with certain physical properties of the molecule and thus achieve some chemical insight into binding. In the present work a large but limited basis set, rather than just a minimal set, is used to determine a groundstate density distribution for methane. The limited basis set consists of large SCF atomic orbital set centered on carbon and a single 1s orbital on each hydrogen. The derived density distribution is used to consider the binding in the methane molecule.

Many molecular properties are related directly to the one-electron density distribution. These properties, which are one-electron properties, can be calculated simply from a knowledge of the first order density matrix[48] given by

$$\gamma(1|1')_{\vec{x}_1'=\vec{x}_1} = n\int\psi^*(1,2.....n)\psi(1,2.....n)d\tau_2 ds_2.....d\tau_n ds_n \ , \quad (1.6)$$

where n is the number of electrons, $d\tau_i$ and ds_i are the space and spin elements respectively of electron i. This expression is n times the probability of finding electron one at the position $\vec{x}_1$ with spin s_1 irrespective of the spin and space coordinates of the other (n-1) electrons. The one-electron density is then given by

$$\rho(\vec{x}_1) = \int\gamma(1|1')_{\vec{x}_1'=\vec{x}_1} ds_1 = n\int\psi^*\psi ds_1 d\tau_2 ds_2.....d\tau_n ds_n \ , \quad (1.7)$$

where now $\rho(\vec{x}_1)$ is independent of spin and is a function only of position in three-dimensional space. It is this one-electron density which is responsible for the scattering of X-rays and electrons and which determines

the electrical properties of the molecule.

One-electron properties, which depend only on the coordinates of one electron at a time, are evaluated in quantum mechanics by averaging the molecular wavefunction over the appropriate one-electron operators. A one-electron operator can be represented by

$$Q = \sum_{i=1}^{n} Op(i) \ , \tag{1.8}$$

where i refers to the i^{th} electron. The average value of this operator is given by

$$\langle Q \rangle = \int \psi^*(1,2,....n) \sum_{i=1}^{n} Op(i) \psi(1,2,....n) d\tau_1 ds_1 .... d\tau_n ds_n$$

$$= \int Op(1) \gamma(1|1')_{\vec{x}'=\vec{x}} d\tau_1 s_1 \ . \tag{1.9}$$

If the operator is spin independent then

$$\langle Q \rangle = \int Op(1) \rho(\vec{x}_1) d\tau_1 \ . \tag{1.10}$$

Within the molecular orbital approximation to the wavefunction, Equations (1.7) and (1.10) have particularly simple forms. These are respectively

$$\rho(\vec{x}_1) = \sum_i n_i \phi_i^*(1) \phi_i(1) \tag{1.11}$$

$$\langle Q \rangle = \sum_i n_i \langle \phi_i^*(1) | Op(1) | \phi_i(1) \rangle \ , \tag{1.12}$$

where the ϕ_i's are the orthogonal set of molecular orbitals and the n_i's are the orbital occupation numbers equal to one or two.

As already indicated, the general procedure for determining the approximate molecular wavefunction satisfying Equation (1.2) is the Hartree-Fock-Roothaan method. This approach utilizes the minimization of energy

constraint to optimize the variable parameters in the wavefunction. But does the resulting approximate wavefunction, which yields the best energy, predict the best one-electron charge distribution or other one-electron properties? This does not necessarily need to be the case since the energy operator, which depends simultaneously on the coordinates of two electrons, weighs more heavily different regions of space than do most one-electron operators.

Mukherji and Karplus[49] have shown that, within a limited basis set, a better one-electron distribution for hydrogen fluoride is obtained when additional constraints, besides the minimization of energy criterion, are used. They indicate that by requiring the wavefunction to predict the correct experimental dipole moment and quadrupole coupling constant the other molecular properties are given more accurately with only a slight increase in the energy. Thus one would conclude that certain one-electron properties are useful in determining the form of the wavefunction.

This was the approach used in the present work to determine a charge distribution for methane. The one-electron properties used as constraints on the wavefunction are the electric field (i.e., the forces) and the diamagnetic part of the magnetic shielding, both occurring at a proton. Since these are one-electron properties they can both be determined from the first-order density matrix or more precisely from the one-electron density distribution.

The forces acting on the nuclei can be calculated most readily by applying the electrostatic Hellmann-Feynman theorem[50]. This theorem was stated by Feynman as follows:

"The force on any nucleus (considered fixed) in a

system of nuclei and electrons is just the classical electrostatic attraction exerted on the nucleus in question by the other nuclei and by the electron density distribution for all the electrons."

A simple proof of this theorem is given here.

If ψ is the molecular wavefunction satisfying Equation (1.1) then the energy of the system is

$$E = \langle\psi|H|\psi\rangle \ , \tag{1.13}$$

where ψ is normalized to unity.

The force, $\vec{F}_{\alpha q}$, acting on nucleus α in the direction $\vec{q}\alpha$ is given by $-\partial E/\partial\vec{q}\alpha$, where $\partial\vec{q}\alpha$ is the displacement coordinate of nucleus α with all other nuclei held fixed. Thus the force is

$$\vec{F}_{\alpha q} = -\frac{\partial E}{\partial \vec{q}\alpha} = -\langle\psi|\frac{\partial H}{\partial \vec{q}\alpha}|\psi\rangle - \langle\frac{\partial\psi}{\partial \vec{q}\alpha}|H|\psi\rangle - \langle\psi|H|\frac{\partial\psi}{\partial \vec{q}\alpha}\rangle \tag{1.14}$$

$$= -\langle\psi|\frac{\partial H}{\partial \vec{q}\alpha}|\psi\rangle - E\,\frac{\partial}{\partial \vec{q}\alpha}(\langle\psi|\psi\rangle) \tag{1.15}$$

$$= -\langle\psi|\frac{\partial H}{\partial \vec{q}\alpha}|\psi\rangle \ , \tag{1.16}$$

which follows since H is Hermitian and

$$\frac{\partial}{\partial \vec{q}\alpha}(\langle\psi|\psi\rangle) = \frac{\partial}{\partial \vec{q}\alpha}(1) = 0 \ . \tag{1.17}$$

Within the Born-Oppenheimer[44] approximation the Hamiltonian operator, H, for a system of N nuclei and n electrons and including the nuclear repulsion terms, is given by

$$H = -\frac{1}{2}\sum_{i=1}^{n}\nabla_i^2 - \sum_{i=1}^{n}\sum_{\alpha=1}^{N}\frac{Z_\alpha}{r_{i\alpha}} + \sum_{i>j=1}^{n}\frac{1}{r_{ij}} + \sum_{\alpha>\beta=1}^{N}\frac{Z_\alpha Z_\beta}{r_{\alpha\beta}} \quad , \tag{1.18}$$

where the symbols have been defined previously except for $r_{\alpha\beta}$ which is the separation between the nuclei α and β, and the terms in the expression are respectively the kinetic energy of the electrons, the electron-nuclear attractions, the electron-electron repulsions and the nuclear-nuclear repulsions. Since the kinetic energy of the electrons and the electron-electron repulsion terms are independent of the nuclear coordinates, it follows that

$$\frac{\partial H}{\partial \vec{q}_\alpha} = -\frac{\partial}{\partial \vec{q}_\alpha}\sum_{i=1}^{n}\sum_{\alpha=1}^{N}\frac{Z_\alpha}{r_{i\alpha}} + \frac{\partial}{\partial \vec{q}_\alpha}\sum_{\alpha>\beta=1}^{N}\frac{Z_\alpha Z_\beta}{r_{\alpha\beta}} \tag{1.19}$$

$$= \sum_{i=1}^{n}\frac{\partial}{\partial \vec{q}_\alpha}V_i + \frac{\partial}{\partial \vec{q}_\alpha}V_N \quad , \tag{1.20}$$

where $V_i = -\sum_{\alpha=1}^{N} Z_\alpha / r_{i\alpha}$ is the potential experienced by electron i in the field of all N nuclei and V_N is the potential energy of nuclear repulsions. The operator given by Equation (1.20) is a one-electron operator as defined by Equation (1.8) and thus, with the use of Equation (1.10), the force on nucleus α can be written as

$$\vec{F}_{\alpha q} = -\frac{\partial V_N}{\partial \vec{q}_\alpha} - \int \frac{\partial V_1}{\partial \vec{q}_\alpha}\rho(\vec{x}_1)\,d\tau_1 \quad . \tag{1.21}$$

Within a molecular orbital approximation to the wavefunction it is easily shown, with the use of Equation (1.12), that the magnitude of the force on nucleus α in the direction of $\vec{q}_\alpha$ is

$$F_{\alpha q} = \sum_{\substack{\beta=1 \\ \beta\neq\alpha}}^{N} Z_\alpha Z_\beta \frac{\cos\theta_{\alpha\beta}}{r_{\alpha\beta}^2}$$

$$- Z_\alpha \sum_j n_j \left\langle \phi_j(1) \left| \frac{\cos\theta_{\alpha 1}}{r_{1\alpha}^2} \right| \phi_j(1) \right\rangle \qquad (1.22)$$

$$= F^N \text{ (nuclear)} + F^e \text{ (electronic)} ,$$

where $\theta_{\alpha\beta}$ is the angle between $\vec{r}_{\alpha\beta}$ and $\vec{q}\alpha$, $\theta_{\alpha 1}$ is the angle between $\vec{r}_{1\alpha}$ and $\vec{q}\alpha$, and the sign convention is that $F_{\alpha q}$ is positive for a repulsive force and negative for an attractive force. This force, via the Hellmann-Feynmann theorem, is a one-electron property that can be calculated if the wavefunction is known. Or, alternatively, the equilibrium density distribution can be partially determined from a number of constraints imposed by the zero force requirements that a proposed equilibrium density distribution must satisfy. These force constraints together with the constraint that the equilibrium density distribution must predict the experimental diamagnetic part of the proton magnetic shielding, referred to later in this thesis, were used to determine a density distribution for the methane molecule.

Since the equilibrium framework of methane is tetrahedral, it is often convenient to work with orbitals that transform in the same manner as the irreducible representation of the tetrahedral group. These type of orbitals, referred to as molecular orbitals, are used in the Hartree-Fock SCF treatment as already discussed and are useful in determining certain molecular properties such as ionization potentials. But from a chemical point of view where the properties of a particular bond are of interest molecular orbitals are not the most convenient orbitals to use.

In order to understand the binding in molecules one often wishes to think in terms of localized bonds and directed charge distributions. It is therefore convenient to transform the molecular orbitals into another

set of orbitals that are not necessarily a basis for the irreducible representations of the molecular point group. This is particularly of interest when a molecule possesses two or more chemical bonds that can be termed "equivalent".

Lennard-Jones and co-workers[51] have shown that the fully delocalized molecular orbitals can be converted into a new set of orbitals called "Equivalent Molecular Orbitals" (EMO's) by a unitary transformation which leaves the wavefunction and the total molecular properties calculated from this wavefunction unchanged. This new set of orbitals have the property of being localized in certain regions of space, particularly along the bond directions which have been termed "equivalent". Within the equivalent orbital representation one retains the concepts of bonds and bonding electrons and for this reason this approach was used in the present work.

It should be noted that the Hellmann-Feynman theorem gives the correct forces on the nuclei only if the electron charge distribution has been determined from the exact electronic wavefunction or from a wavefunction in which all the parameters have been fully optimized with respect to the nuclear coordinates[52]. In order to insure that the wavefunction used in the present work fulfills these requirements as closely as possible the additional constraints imposed by the proton magnetic shielding is applied and an accurate set of Hartree-Fock self-consistent-field atomic functions is used to describe the 1s, 2s and 2p orbitals on the carbon nucleus. These SCF functions have been determined by Clementi[53] et al for the ^3P configuration of the carbon atom using a linear combination of six Slater functions to describe the 1s and 2s atomic

orbitals and a linear conbination of four Slater functions to describe the 2p atomic orbitals. The use of this large but limited basis set, rather than a minimal basis set, will greatly increase the mathematical computations but a better density distribution will be obtained.

The general procedure followed in the present work in determining a one-electron density distribution for methane is very similar to the approach used by Bader and Jones[35] and Keaveny[36] in determining a one-electron density distribution for the water molecule. The differences are that the methane molecule contains more atoms, possesses greater symmetry and does not contain lone-pairs. The essential features of the chemical binding in methane are expected to be similar to those for the water molecule and can be conveniently discussed in terms of the ground-state one-electron density distribution.

Having derived a one-electron density distribution for methane the next step is to determine how accurate a density distribution has been obtained using this electrostatic approach. By far the simplest way to assess this accuracy is to calculate the expectation value of a number of one-electron operators and compare these properties with their experimental counterparts. The properties used as testing devices in the present work are the diamagnetic susceptibility, the bond dipole, the octupole moment, and the electric field gradients arising from a force constant analysis. How well these properties are predicted will indicate how accurately the density distribution is given near the protons, near the carbon nucleus and in the outer regions of the molecule.

Since the wavefunction has been determined solely on the basis of one-electron properties a crucial test of the derived density distribution

would be to calculate the total energy for the molecule. This energy is given by Equation (1.13) and within the molecular orbital approximation can be represented by[47]

$$E = 2 \sum_i \langle \phi_i(1) | -\tfrac{1}{2}\nabla_1^2 | \phi_i(1) \rangle + 2 \sum_\alpha \sum_i \langle \phi_i(1) | -\frac{Z_\alpha}{r_{1\alpha}} | \phi_i(1) \rangle$$

$$+ \sum_i \sum_j \left(2\langle \phi_i(1)\phi_j(2) | \frac{1}{r_{12}} | \phi_i(1)\phi_j(2) \rangle \right.$$

$$\left. - \langle \phi_i(1)\phi_j(2) | \frac{1}{r_{12}} | \phi_j(1)\phi_i(2) \rangle \right)$$

$$+ \sum_{\alpha<\beta} \sum \frac{Z_\alpha Z_\beta}{r_{\alpha\beta}} , \qquad (1.23)$$

where the indicies i and j run over the doubly-occupied orthonormal equivalent space orbitals ϕ_i and the indicies α and β run over the number of atoms in the molecule. For polyatomic systems like methane such an energy calculation involves the evaluation of many integrals, particularly two-electron integrals, which is very time-consuming. This was the major reason why the electrostatic approach, rather than the method of energy minimization, was used to determine a groundstate one-electron density distribution for the methane molecule.

From the derived density distribution the total energy for the methane molecule was determined. The calculated result is compared with the experimental and other theoretical values in order to assess the merits of the electrostatic approach.

In summary, the derived groundstate one-electron density distribution, obtained solely from one-electron considerations, is tested by calculating a number of physical properties, including the total energy. This distribution is used to explain the nature of the bonding in the

methane molecule and the final conclusions that have been reached.

I.2 Determination of the Density Distribution

a) The Equivalent Orbital Representation for CH_4

The equilibrium tetrahedral configuration of methane is represented by the coordinate system shown in Figure I.1. The molecule is inscribed in a cube of side 2a, where $a = R/\sqrt{3}$ and R is the C-H equilibrium bond distance in atomic units (a.u.). The atomic coordinates of the five atoms C, H_1, H_2, H_3 and H_4 are (o,o,o), (a,a,a), $(a,\bar{a},\bar{a})$, $(\bar{a},a,\bar{a})$ and $(\bar{a},\bar{a},a)$ respectively.

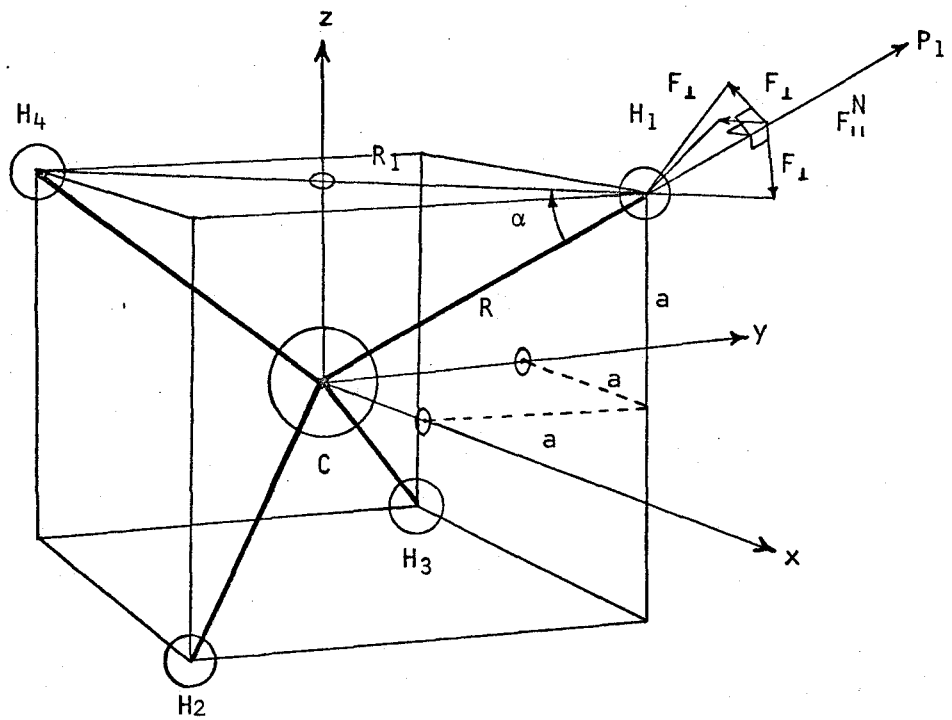

FIGURE I.1. Coordinate system for methane

The total groundstate electronic wavefunction was assumed to be represented, to a good approximation, by a single Slater determinant as indicated by Equation (I.4). The ten electrons in the methane molecule were placed in five doubly-occupied space orbitals which were constructed from a limited basis set consisting of 1s, 2s, $2p_x$, $2p_y$ and $2p_z$ type

functions centered on carbon and a single 1s function centered on each of the hydrogens. The 1s, 2s and 2p functions used on carbon were the SCF atomic orbitals for the ^3P configuration of the carbon atom as determined by Clementi[53] et al (see Appendix 1). The SCF 1s and 2s atomic orbitals were each constructed of a linear combination of six Slater functions and each 2p orbital was constructed of four Slater functions. The 1s function used on each of the hydrogen centers was just a simple Slater 1s orbital in which the orbital exponent was allowed to vary.

Similar to the method of Bader and Jones[35], the orbital wavefunctions were written in their most general form in terms of "equivalent molecular orbitals"[51] (see page 17 of this thesis). The first orbital, ϕ_o, is just the 1s core orbital on carbon (i.e., $\phi_o = 1s_c$). The remaining four orbitals are equivalent to each other and are labeled bonding orbitals. These bonding orbitals are defined as

$$\phi_{b1} = \lambda(\cos(\varepsilon b)\cdot 2s_c + \sin(\varepsilon b)\cdot P_1) + \mu(h_1 - \delta(h_2+h_3+h_4) - C_o\cdot 1s_c)$$

$$\phi_{b2} = \lambda(\cos(\varepsilon b)\cdot 2s_c + \sin(\varepsilon b)\cdot P_2) + \mu(h_2 - \delta(h_1+h_3+h_4) - C_o\cdot 1s_c)$$

$$\phi_{b3} = \lambda(\cos(\varepsilon b)\cdot 2s_c + \sin(\varepsilon b)\cdot P_3) + \mu(h_3 - \delta(h_1+h_2+h_4) - C_o\cdot 1s_c)$$

$$\phi_{b4} = \lambda(\cos(\varepsilon b)\cdot 2s_c + \sin(\varepsilon b)\cdot P_4) + \mu(h_4 - \delta(h_1+h_2+h_3) - C_o\cdot 1s_c)$$

where the following definitions are used.

1) $1s_c$ is the 1s function on carbon;

2) $2s_c$ is the 2s function on carbon;

3) P_1, P_2, P_3 and P_4 are localized p-type functions on carbon which point at H_1, H_2, H_3 and H_4 respectively. In terms of $2p_x$, $2p_y$ and $2p_z$, the localized P orbitals are defined as:

$$P_1 = 1/\sqrt{3}(2p_x + 2p_y + 2p_z)$$

$$P_2 = 1/\sqrt{3}(2p_x - 2p_y - 2p_z)$$

$$P_3 = 1/\sqrt{3}(-2p_x + 2p_y - 2p_z)$$

$$P_4 = 1/\sqrt{3}(-2p_x - 2p_y + 2p_z)$$

4) h_1, h_2, h_3 and h_4 are 1s Slater atomic orbitals on the hydrogen centers H_1, H_2, H_3 and H_4 respectively.

5) $C_o \equiv \langle h_1 | 1s_c \rangle (1 - 3\delta) + \lambda/\mu \cos\varepsilon b \langle 1s_c | 2s_c \rangle^*$. This coefficient is required to make ϕ_o (the core orbital) orthogonal to ϕ_{bi} (the bonding orbitals).

6) λ, μ, εb and δ are variable parameters that are obtained by putting constraints on the wavefunction. These parameters have the following definitions:

εb is the hybridization parameter;

λ/μ is the polarity factor;

δ is a parameter which determines the extent of delocalization in the equivalent orbitals.

Within the single determinantal representation given by Equation (1.4) the total molecular wavefunction for methane can be written in terms of the equivalent molecular orbitals as follows.

$$\psi_e = 1/\sqrt{10!}\,||\phi_o\bar{\phi}_o\phi_{b1}\bar{\phi}_{b1}\phi_{b2}\bar{\phi}_{b2}\phi_{b3}\bar{\phi}_{b3}\phi_{b4}\bar{\phi}_{b4}|| \quad . \tag{1.24}$$

Further, requiring the equivalent molecular orbitals to be normalized and mutually orthogonal (i.e., $\langle \phi_{bi} | \phi_{bi} \rangle = 1.0$ and $\langle \phi_{bi} | \phi_{bj} \rangle = 0$, $i \neq j$; ϕ_o is already normalized and orthogonal to the bonding orbitals) permits the total one-electron density to be written in the simple form (see Equation (1.11))

$$\rho(\vec{x}_1) = 2(\phi_o^2 + \phi_{b1}^2 + \phi_{b2}^2 + \phi_{b3}^2 + \phi_{b4}^2) \quad . \tag{1.25}$$

---

* The symbol $\langle \chi_1 | \chi_2 \rangle$ represents the overlap integral between the orbitals χ_1 and χ_2.

The normalization and orthogonality conditions provide two equations which can be used to determine two of the four unknown parameters λ, μ, εb and δ which appear in the generalized set of equivalent orbitals. The two remaining parameters are obtained by requiring the total density distribution to give a zero resultant force on the proton along the C-H bond axis and also to give the correct (experimental) value for the diamagnetic part of the proton magnetic shielding. The reason for choosing these two properties will be made clear later in this thesis. The conditions imposed on the density distribution will now be considered in more detail.

b) Orthogonality and Normalization Conditions

The normalization of the bonding orbital ϕ_{b1} gives

$$\begin{aligned} 1.0 = {} & \lambda^2(1.0 - \cos^2(\varepsilon b)\cdot\langle 1s_c|2s_c\rangle^2) \\ & + 2\lambda\mu(\cos(\varepsilon b)\cdot(1-3\delta)\cdot(\langle h_1|2s_c\rangle - \langle h_1|1s_c\rangle\cdot\langle 1s_c|2s_c\rangle) \\ & \qquad + \sin(\varepsilon b)\cdot(1+\delta)\cdot\langle h_1|P_1\rangle) \\ & + \mu^2(1.0 - \langle h_1|1s_c\rangle^2 - 6\delta(\langle h_1|h_2\rangle - \langle h_1|1s_c\rangle^2) \\ & \qquad + \delta^2(3.0 + 6\langle h_1|h_2\rangle - 9\langle h_1|1s_c\rangle^2)) \quad . \quad (1.26) \end{aligned}$$

Similarly the orthogonality condition between ϕ_{b1} and ϕ_{b4} gives

$$\begin{aligned} 0.0 = {} & \lambda^2(1.0 - \cos^2(\varepsilon b)\cdot\langle 1s_c|2s_c\rangle^2 - 4\sin^2(\varepsilon b)/3) \\ & + 2\lambda\mu\ (\cos(\varepsilon b)\cdot(1-3\delta)\cdot(\langle h_1|2s_c\rangle - \langle h_1|1s_c\rangle\cdot\langle 1s_c|2s_c\rangle) \\ & \qquad - \sin(\varepsilon b)\cdot(1+\delta)\cdot\langle h_1|P_1\rangle/3) \\ & + \mu^2(\langle h_1|h_2\rangle - \langle h_1|1s_c\rangle^2 - 2\delta(1.0 + 2\langle h_1|h_2\rangle - 3\langle h_1|1s_c\rangle^2) \\ & \qquad + \delta^2(2.0 + 7\langle h_1|h_2\rangle - 9\langle h_1|1s_c\rangle^2)) \quad . \quad (1.27) \end{aligned}$$

Equations (1.26) and (1.27) which contain the four unknown parameters λ, μ, εb, and δ can be used to solve for εb and λ. The solving of these two equations is best carried out by constructing two new equations. Subtracting Equation (1.27) from Equation (1.26) gives

$$1.0 = 4\lambda^2\sin^2(\varepsilon b)/3 + 8\lambda\mu\sin(\varepsilon b)\cdot(1+\delta)\cdot\langle h_1|P_1\rangle/3 + \mu^2\cdot(1+\delta)^2\cdot(1.0 - \langle h_1|h_2\rangle) \quad . \qquad (1.28)$$

Adding Equation (1.26) and three times Equation (1.27) gives

$$1.0 = 4\lambda^2\cos^2(\varepsilon b)\cdot(1.0 - \langle 1s_c|2s_c\rangle^2) + 8\lambda\mu\cos(\varepsilon b)\cdot(1-3\delta)\cdot(\langle h_1|2s_c\rangle - \langle h_1|1s_c\rangle\cdot\langle 1s_c|2s_c\rangle) + \mu^2\cdot(1-3\delta)^2\cdot(1.0 + 3\langle h_1|h_2\rangle - 4\langle h_1|1s_c\rangle^2) \quad . \qquad (1.29)$$

Equations (1.28) and (1.29) can be solved as quadratic equations for $\sin(\varepsilon b)$ and $\cos(\varepsilon b)$ to give

$$\sin(\varepsilon b) = \frac{\mu}{\lambda}(1+\delta)(-b\pm\sqrt{b^2 - a}) \qquad (1.30)$$

and

$$\cos(\varepsilon b) = \frac{\mu}{\lambda}(1-3\delta)(-b_1\pm\sqrt{b_1^2 - a_1}) \quad , \qquad (1.31)$$

where

$$b = \langle h_1|P_1\rangle$$

$$a = 3(1.0 - \langle h_1|h_2) - 1/\mu^2(1+\delta)^2)/4$$

$$b_1 = \frac{(\langle h_1|2s_c\rangle - \langle h_1|1s_c\rangle\langle 1s_c|2s_c\rangle)}{(1.0 - \langle 1s_c|2s_c\rangle^2)}$$

$$a_1 = \frac{(1.0 + 3\langle h_1|h_2\rangle - 4\langle h_1|1s_c\rangle^2 - 1/\mu^2(1-3\delta)^2)}{4(1.0 - \langle 1s_c|2s_c\rangle^2)} \quad .$$

Using the trignometric relation $\sin^2(\varepsilon b) + \cos^2(\varepsilon b) = 1.0$, Equations (1.30) and (1.31) can be used to solve for λ in terms of μ, δ and the appropriate overlap integrals. Thus

$$\lambda^2 = \mu^2((1+\delta)^2\cdot(2b^2 - a\mp 2b\sqrt{b^2 - a}) + (1-3\delta)^2\cdot(2b_1^2 - a\mp 2b_1\sqrt{b_1^2 - a_1})) \quad , \qquad (1.32)$$

where both a and a_1 are functions of μ and δ.

Using the calculated values for the overlap integrals in Equations

(1.30) and (1.31) one finds that $\sin(\varepsilon b)$ and $\cos(\varepsilon b)$ have imaginary values unless μ and δ satisfy the following condition

$$0.0 < |\mu(1-3\delta)| \tilde{} |\mu(1+\delta)| \leq \sqrt{2.0} \ .$$

Also since the present work is concerned with deriving a ground state wavefucntion for methane the only orbital wavefunctions of interest are those which give the lowest energy. This criterion is satisfied if the sign of λ and μ are the same, assumed positive without any loss in generality, and $\sin(\varepsilon b)$ and $\cos(\varepsilon b)$ are both positive (i.e., $0° \leq \varepsilon b \leq 90°$). These conditions assure that the orbitals obtained are "bonding orbitals" and not "antibonding orbitals" of higher energy. These are some of the restrictions that can be placed on the unknown parameters if a real physical solution exists.

The values of $\sin(\varepsilon b)$, $\cos(\varepsilon b)$ and λ are given by Equations (1.30), (1.31) and (1.32) respectively if the values of μ and δ are known. The correct sign to use for the square root in these equations can be determined from the restrictions indicated above. The final values of μ and δ are fixed by the force and proton magnetic shielding constraints.

c) Force Constraint

In the methane molecule the only force that is not zero by symmetry is the force on the hydrogen nucleus parallel to the C-H bond axis. Since the force on each hydrogen is identical, all calculations are carried out considering the force on H_1 only. This force is labeled F_{11} as indicated in Figure 1.1.

There must be no net forces acting on the nuclei in the equilibrium configuration. Thus, the nuclear forces of repulsion at H_1 must be balanced by the electrostatic forces of attraction. The nuclear force of repulsion

along the C-H bond axis, F_{11}^N, can be easily calculated using Equation (1.22) (see Figure 1.1).

$$F_{11}^N = (6.0 + 3/(4\cos(\alpha)))/R^2 = 1.62763214 \text{ a.u.}^* \qquad (1.33)$$

The electrostatic force of attraction, F_{11}^e, which must equal F_{11}^N, can most readily be obtained using the Hellmann-Feynman theorem[50] (see page 13 of this thesis). Since the equivalent orbitals are orthonormal the force exerted on H_1 by the electron density distribution is simply the sum of the forces exerted by density obtained from each of the orbitals as indicated by the second term of Equation (1.22). Thus, at electrostatic equilibrium

$$F_{11}^e = F_{11}(\phi_o^2) + F_{11}(\phi_{b1}^2) + F_{11}(\phi_{b2}^2) + F_{11}(\phi_{b3}^2) + F_{11}(\phi_{b4}^2)$$

$$= F_{11}^N = (6.0 + 3/(4\cos\alpha))/R^2 \ , \qquad (1.34)$$

where $F_{11}(\phi_i^2) \equiv 2\langle\phi_i(1)|F_{op}|\phi_i(1)\rangle$ is the force exerted on H_1 by the electron density contained in the ith equivalent orbital and $F_{op} \equiv \cos\theta_{H_1}/r_{H_1}^2$. Expressions for these orbital forces are given in Appendix 2.

d) Proton Magnetic Shielding Constraint

Ramsey[55] has shown that the proton magnetic shielding consists of a diamagnetic term, depending on the groundstate wavefunction, and a paramagnetic term, involving excited state functions. This can be represented by

$$\sigma = \sigma^{(d)} + \sigma^{(p)} \ . \qquad (1.35)$$

---

* The C-H bond length, R, for the calculations in this thesis is 2.06172 a.u. This is obtained using the experimental bond length of 1.0910 Å.[54]

The paramagnetic term can be calculated from the proton spin-rotation constant C (obtained from molecular beam studies[56]) and the general expression[57,58]

$$\sigma^{(p)} = -(e^2/3mc^2) \sum_{B(\neq A)} (Z_B/R_{AB}) + (2\pi e Mp S_A/6mc\mu_N\mu_A) \sum_{\alpha=1}^{3} I_\alpha C_{\alpha\alpha} , \quad (1.36)$$

where the first summation is over all nuclei of charge Z_B at a distance R_{AB} from nucleus A, S_A is the nuclear spin on A, Mp is the proton mass, and μ_A is the magnetic moment in units of the nuclear magneton μ_N. Using the experimental value[56] C = 10.40±0.10 kc/sec the paramagnetic part of the proton magnetic shielding can be determined to be $\sigma_H^{(p)} = -56.45 \times 10^{-6}$ e.m.u.[57] at the equilibrium bond length. The total proton magnetic shielding has also been determined experimentally. It can be obtained by adding the value for the proton shielding[59] in H_2 ($26.43\pm0.60 \times 10^{-6}$) to the observed[60] proton shift (4.20×10^{-6}) between methane and H_2. This gives the result

$$\sigma = 30.63\pm0.60 \times 10^{-6} \text{ e.m.u.}$$

From these two experimental values the diamagnetic term can be calculated

$$\sigma^{(d)} = \sigma - \sigma^{(p)} \quad (1.37)$$
$$= 30.63 \times 10^{-6} + 56.45 \times 10^{-6} = 87.09 \times 10^{-6} \text{ e.m.u.}$$
$$= 4.90588209 \text{ a.u.}$$

The diamagnetic term, $\sigma^{(d)}$, is a measure of the first-order shielding of the proton by the electron density when placed in a magnetic field. This effect is a measure of the potential energy of the proton in the electric field of the charge density. It can be evaluated from the groundstate

wavefunction using the one-electron operator $1/r_{H_1}$[55] and Equation (1.12). Thus at equilibrium

$$\sigma^{(d)} = \frac{e^2}{3mc^2} (\sigma(\phi_o^2) + \sigma(\phi_{b1}^2) + \sigma(\phi_{b2}^2) + \sigma(\phi_{b3}^2) + \sigma(\phi_{b4}^2))$$

$$= 87.09 \times 10^{-6} \text{ e.m.u.} , \qquad (1.38)$$

where $\sigma(\phi_i^2) \equiv 2\langle\phi_i(1)|1/r_{H_1}|\phi_i(1)\rangle$ is the magnetic shielding for the density in the i^{th} molecular orbital. The operator $1/r_{H_1}$ weighs very heavily the density near the proton. Expressions for the orbital shielding terms are given in Appendix 2.

Equations (1.34) and (1.38) can not be readily solved for the parameters μ and δ because of their complicated mathematical form, see Appendix 2. For this reason a general method of proceeding towards a solution was adopted. The parameters were obtained essentially by trial and error. The following steps were followed.

First δ is assigned an arbitrary value. Then μ is set equal to an initial value and λ, $\sin\varepsilon b$ and $\cos\varepsilon b$ are calculated from Equations (1.32), (1.30) and (1.31) respectively. These results are then used to calculate the force F_{μ}^{e}. μ is varied at random until Equation (1.34) is satisfied. When the force is finally balanced the proton magnetic shielding, $\sigma^{(d)}$, is calculated. If the result does not satisfy Equation (1.38) a new value of δ is assigned and the steps above are repeated. Following this simple procedure both δ and μ were varied until Equations (1.34) and (1.38) were both satisfied.

Using the above technique a number of trial wavefunctions for methane were tested. Two cases will be considered here.

e) Case I: A Hydrogen Orbital Exponent of 1.245

In all the calculations in this thesis the atomic orbitals on carbon were represented by the SCF atomic orbitals obtained by Clementi[53] et al (see Appendix 1). The next step was to determine a screening coefficient for the 1s Slater orbitals on the hydrogens.

From variational and SCF calculations it is a well-known fact that there is a substantial increase in the hydrogen 1s orbital exponent over the free atom value when hydrogen is involved in bond formation. Taking this into consideration, the first attempt to find a wavefunction for methane used a screening coefficient of 1.245 for the 1s orbital on the hydrogens. This figure was obtained by using an empirical rule discussed by Bader[61] which relates the screening coefficient in the separated atom (1.0) to that in the united atom. By this rule $\alpha_H = Z_S - \Delta Z e^{-R}$, where $\Delta Z = Z_s - Z_u$ and R is the bond length. The Z_s and Z_u refer to the effective nuclear charges calculated by Slater's rules (including the factor 1/n where n is the principle quantum number) for the electron in the separated and united atom respectively.

In Table I.1 are listed the variable parameters at different values of δ where the electronic force has been balanced to the experimental value of 1.62763214 a.u. The screening coefficient on the hydrogens is 1.245.

For values of δ much below -0.7 and above 1.4 the values of $\sin(\varepsilon b)$ and $\cos(\varepsilon b)$ from Equations (I.30) and (I.31) become imaginary for any reasonable choice of μ. As can be seen from Table I.1 the electronic force can be balanced for any given choice of δ in the range indicated. Increasing δ requires the polarity factor, λ/μ, to increase and the hybridization εb, to decrease in order to obtain the experimental electronic force. With this

TABLE I.1

Variable Parameters that Balance the Force with a Hydrogen Orbital Exponent of 1.245

δ	μ	λ	εb	Force (electronic)[a]	$\sigma^{(d)}$ a.u.
-0.7	0.24267	0.82857	86.657°	1.62763213	4.7070950
-0.4	0.28578	0.47202	80.116°	1.62763213	4.7201877
0.0	0.33192	0.73427	64.541°	1.62763213	4.7485827
0.1	0.33545	0.74674	59.869°	1.62763213	4.7566407
0.3	0.32809	0.77526	51.437°	1.62763213	4.7709287
0.8	0.26074	0.88268	33.995°	1.62763214	4.7807176
1.4	0.18703	0.96219	33.288°	1.62763214	4.7876415

[a] Force given in atomic units (a.u.).

required change in variables the magnetic shielding varies very slowly as δ is increased with the result that it was impossible to get the magnetic shielding as high as the experimental value of 4.9058821 a.u. using a hydrogen screening coefficient of 1.245. In order to obtain the experimental shielding and retain real solutions further considerations were necessary.

f) Case 2: A Hydrogen Orbital Exponent of 1.5

Since the proton magnetic shielding is largely determined by the density around the proton it would appear that the screening coefficient in the 1s orbital on the hydrogens should be increased. To justify such a move consider Woznick's[24] wavefunction for methane. In his rather elaborate set of orbitals two 1s orbitals on each of the hydrogens were used, one with an orbital exponent of 1.0 and another with an orbital exponent of 1.5. An analysis of his wavefunction shows that the coefficients for the 1s orbital with exponent 1.5 are relatively larger than those for the orbital with exponent 1.0. This would suggest that the orbital with exponent 1.5 is the dominant one on the hydrogens.

With these ideas in mind the 1s screening coefficient used in the orbital on the hydrogens was increased in steps from 1.245 to 1.5 and beyond. The best result was found to occur when the hydrogen 1s exponent was set equal to 1.5. In Table 1.2 is a list of values, similar to Table 1.1, for $\alpha_H = 1.5$. This table indicates that a balance can be obtained for both the electronic force and the proton magnetic shielding. This balance occurs when the parameters have the values $\delta = 0.12139750$, $\mu = 0.36865974$, $\lambda = 0.72735440$ and $\varepsilon b = 57.564934°$.*

* More significant figures are given then are really warranted by the experimental data used; but these figures are recorded to permit future checking of the results.

TABLE I.2

Variable Parameters that Balance the Force with $\alpha_H = 1.5$

δ	μ	λ	εb	Force (electronic)[a]	$\sigma^{(d)}$ a.u.
0.000	0.36867	0.72082	63.572°	1.62763213	4.8963473
0.06	0.36990	0.72241	60.554°	1.62763213	4.9013944
0.12	0.36872	0.72721	57.631°	1.62763213	4.90578842
†0.12139750	0.36865974	0.72735440	57.564934°	1.62763213	4.90588209
0.13	0.36829	0.72830	57.160°	1.62763213	4.90644957
0.20	0.36349	0.73806	54.035°	1.62763213	4.9104684
0.33	0.34747	0.76339	49.234°	1.62763213	4.9150885

† Final balance point.

[a] Force given in atomic units (a.u.).

The atomic integral $\langle h_1 | 1/r_{H_1} | h_1 \rangle$ makes a major contribution to the magnetic shielding. By increasing the orbital exponent on the hydrogens from 1.245 to 1.5 this integral is increased from 1.245 a.u. to 1.5 a.u. It is the increase in this integral which gives a balance for the magnetic shielding as well as the electronic force when $\alpha_H = 1.5$ even though no balance was obtained for $\alpha_H = 1.245$. All remaining calculations for methane in this thesis use the wavefunction determined at this balance point. The final orbital representations are:

$$\phi_o = 1s_c$$

$$\phi_{b1} = 0.39011176(2s_c) + 0.35442782(P_1) - 0.012828560(1s_c) + 0.36865974(h_1) - 0.044754370(h_2 + h_3 + h_4)$$

$$\phi_{b2} = 0.39011176(2s_c) + 0.35442782(P_2) - 0.012828560(1s_c) + 0.36865974(h_2) - 0.044754370(h_1 + h_3 + h_4)$$

$$\phi_{b3} = 0.39011176(2s_c) + 0.35442782(P_3) - 0.012828560(1s_c) + 0.36865974(h_3) - 0.044754370(h_1 + h_2 + h_4)$$

$$\phi_{b4} = 0.39011176(2s_c) + 0.35442782(P_4) - 0.012828560(1s_c) + 0.36865974(h_4) - 0.044754370(h_1 + h_2 + h_3) \ .$$

Table 1.3 gives the orbital contributions to the electronic force and proton magnetic shielding using the orbital representations above. The results are recorded to only six decimal places, which is the limit of the experimental results used in the calculations.

The wavefunction that has been derived gives both the correct experimental electronic force and diamagnetic part of the proton shielding. The results indicate that the hybridization, εb, is close to sp^3. The actual value of εb is 57.565°. sp^3 hybridization occurs when $\varepsilon b = 60°$. This result is to be expected since the tetrahedral symmetry of methane

TABLE 1.3

Orbital Contributions to the Force and Magnetic Shielding at the Proton

Orbital†	Electronic Force on H_1 (a.u.)	$\sigma^{(d)}$ at H_1 (a.u.)
ϕ_o	0.470511	0.970064
ϕ_{b1}	0.520551	1.817005
ϕ_{b2}	0.212190	0.706271
ϕ_{b3}	0.212190	0.706271
ϕ_{b4}	0.212190	0.706271
TOTAL	1.627632	4.905882
EXPERIMENTAL	1.627632	4.905882

† NOTE: Each orbital contribution is for two electrons in that orbital.

suggest approximate sp^3 hybridization in order give an energy minimum[42]. The polarity factor, λ/μ, which has the value 1.9730, is somewhat higher than the result obtained for this ratio by Keaveny[36] for the water molecule. The delocalization δ, which has the value 0.1214, is small as was expected since the methane equivalent orbitals are strongly localized as anticipated for this tetrahedral symmetry. All further discussion concerning the derived wavefunction and the comparison of this wavefunction with those derived for other hydride molecules will be left for the final summary.

1.3 One-Electron Property Determinations

In the derivation of the molecular charge distribution for methane the only one-electron properties used to determine the unknown parameters in the wavefunction were (1) the force and (2) the proton magnetic shielding both occurring at the hydrogen atom H_1. If this derived density distribution is to have any physical significance it must be able to predict good expectation values for other physical properties that depend on the one-electron density. There are a number of these properties that can be calculated such as the diamagnetic susceptibility, the bond dipole, the octupole moment and the electric field gradient at a hydrogen nucleus. These one-electron properties were evaluated for the methane molecule using the derived density distribution. The agreement of these calculated values with the appropriate experimental quantities is used as the basis of determining how closely the derived density distribution approximates the true physical density.

a) Diamagnetic Susceptibility

As is the case for the proton magnetic shielding, Van Vleck[62] has

shown that the total magnetic susceptibility of a molecule with no resultant spin can be broken down into two parts: (1) the diamagnetic or Larmor term depending only on the ground state wavefunction, and (2) the paramagnetic or "high frequency" term, often referred to as the "Van Vleck paramagnetism", which is a temperature independent term depending on excited states. The total diamagnetic susceptibility, χ, can thus be expressed as

$$\chi = \chi^{(d)} + \chi^{(p)} \quad . \tag{1.39}$$

The paramagnetic term, $\chi^{(p)}$, can be obtained from the components of the rotational-magnetic-moment tensor g_{gg} measured in molecular beam or Zeeman effect microwave experiments. The mathematical expression[63] used to calculate $\chi^{(p)}$ is

$$\chi^{(p)} = \frac{-N_o e^2}{12\, m\, c^2\, Mp} \sum_{g=1}^{3} g''_{gg}\, I_g \,, \tag{1.40}$$

where g''_{gg}, the electronic part of g_{gg}, is obtained by subtracting the nuclear contribution

$$g'_{gg} = (Mp/e I_g) \sum_k Z_k (r_k^2 - g_k^2), \tag{1.41}$$

where Z_k is the charge on the k^{th} nucleus at a distance $(r_k^2 - g_k^2)^{1/2}$ from the principal rotational axis g, I_g is the moment of inertia about this axis, and Mp is the proton mass. Using the value 0.3133±0.002 n.m. for g_{gg}, obtained from molecular beam experiments[56], the molar paramagnetic susceptibility of methane, $\chi^{(p)}$, calculated at the center of mass[57] has the value 9.29×10^{-6} e.m.u. The total magnetic susceptibility for methane has been measured by Barter et al[64]. They find that $\chi = -17.4 \pm 0.8 \times 10^{-6}$ e.m.u. From this most recent result, the diamagnetic term, $\chi^{(d)}$, can be calculated to be

$$\chi^{(d)} = \chi - \chi^{(p)}$$
$$= -17.4 \times 10^{-6} - 9.29 \times 10^{-6}$$
$$= -26.69 \times 10^{-6} \text{ e.m.u.} \qquad (1.42)$$

This diamagnetic term can also be obtained by averaging the ground state wavefunction over the operator r_c^2, where r_c is the distance measured from the center of mass. Within the orbital approximation this diamagnetic term is given by

$$\chi(d) = \frac{-N_o e^2}{6mc^2}[\chi(\phi_o^2) + \chi(\phi_{b1}^2) + \chi(\phi_{b2}^2) + \chi(\phi_{b3}^2) + \chi(\phi_{b4}^2)] , \qquad (1.43)$$

where $\chi(\phi_i^2) \equiv 2\langle\phi_i|r_c^2|\phi_i\rangle$ is the magnetic susceptibility for the i^{th} molecular orbital. These orbital contributions have been evaluated (see Appendix 5), and the total diamagnetic susceptibility calculated for the methane molecule using the previously determined wavefunction.

The value obtained for $\chi^{(d)}$ in the present work and its orbital contributions are listed in Table 1.4 along with the results recorded by Hegstrom and Lipscomb[57] for the magnetic susceptibility calculated from other methane wavefunctions.

In general, the calculated $\chi^{(d)}$ values are somewhat larger than the experimental value of -26.69×10^{-6} e.m.u. This is also true for most of the values for $\chi^{(d)}$ determined by Banyard[66] from earlier methane wavefunctions. This is probably because of the fact that the operator r_c^2 weighs heavily the density in the outer regions of the molecule and these earlier wavefunctions over estimate the density in these regions. The result obtained using Coulson's wavefunction is in good agreement with the experimental value but Hegstrom and Lipscomb[57] suggest that this may be fortuitous because of the unusually large choice of 2.98 for the orbital

TABLE I.4

Results for Diamagnetic Susceptibility for Methane

Wavefunction	$\chi^{(d)} \times 10^6$ e.m.u.	Orbital*	$\chi^{(d)}$ (a.u.)
Coulson[a]	-26.4	ϕ_{bo}	0.19440
Palke-Lipscomb[b]	-28.1	ϕ_{b1}	8.52480
Pitzer[c]	-27.9	ϕ_{b2}	8.52480
Woznick[d]	-28.7	ϕ_{b3}	8.52480
Present Work	-27.17	ϕ_{b4}	8.52480
Experimental	-26.69	TOTAL	34.29360

* NOTE: Each orbital contribution is for two electrons in that orbital.

[a] Reference 65

[b] Reference 26

[c] Reference 27

[d] Reference 24

exponent of the carbon 2s atomic orbital (the Slater exponent is 1.625).

The value obtained for $\chi^{(d)}$ in the present work is in excellent agreement with the experimental result, the calculated value being only about 2% larger. This agreement is due to the fact that the density around carbon is better represented by the SCF atomic orbitals that are used on carbon instead of single Slater orbitals. Also, the use of the large orbital exponent (1.5) on the hydrogens contracts the density around the hydrogen nuclei making the density less diffuse in the outer regions of the molecule and thus lowering the value of the susceptibility. The rather high polarity factor (λ/μ = 1.9730) found for the bonding orbitals contracts the density around the carbon nucleus and contributes to a lowering in the susceptibility, thus giving rise to a better result than obtained from earlier wavefunctions.

The excellent agreement between the calculated diamagnetic susceptibility and the actual experimental value indicates that the density distribution obtained by the present method has many of the features of the true density. As a matter of fact, it would have been possible to use the diamagnetic susceptibility as a constraint in place of the proton magnetic shielding to obtain the variable parameters in the wavefunction without changing the final results significantly. Thus, the derived charge distribution can adequately predict either of these two properties.

b) Bond Dipole Moment

For a system of nuclei and electrons possessing tetrahedral symmetry the total charge distribution can be expanded in terms of tetrahedral harmonics. In such an expansion the individual terms can be related to the multipole moments of the total charge distribution. It is easy to show

the first non-zero multipole moment for a tetrahedral system is the octupole moment, which will be considered in the next section. Even though the total dipole moment is zero for methane, it is still useful to consider the moments for particular parts of the total charge distribution. In this section we are interested in determining the dipole moment of the C-H bond.

Using an orthonormal set of molecular orbitals, ϕ_i, the total dipole moment of a molecule is given by

$$\vec{\mu} = e \sum_i n_i \langle \phi_i | \vec{r} | \phi_i \rangle - e \sum_j Z_j \vec{r}_j \ , \qquad (1.44)$$

where e is the electronic charge, $\vec{r}$ is the vector r cosθ from an arbitrary origion, Z_j is the nuclear charge on atom j, and the n_i's are the orbital occupation numbers. The first sum is over all occupied orbitals and the second sum is over all the nuclei in the molecule. The total moment given by Equation (1.44) is zero for methane. However, quantum mechanical calculations[23,27] of the charge distribution for this molecule indicate that the electronic charge is strongly localized along the C-H bond directions; this will also be found to be true when we consider $\rho(\vec{x}_1)$ contour maps. For this reason it is convenient[67] to consider this localized charge as characteristic of a single bond and to specify a bond moment for this rather specialized part of the molecule. The vector sum of the bond moments gives the total dipole moment.

Experimentally, a C-H bond moment can be determined from infrared intensity data[68] and the usually accepted value is about 0.5 D. From this data the direction of the moment can not be directly obtained and Hornig and McKean[69] have given a good review on the difficulties attending such a procedure both in derivation and interpretation of the moments obtained from

experimental data. It is not at all clear that the bond moments deduced from vibrational data should be the same as the static moments deduced from dipole moment studies.

There is no unique procedure for obtaining theoretical bond moments for molecules. The usual procedure is to transform the SCF molecular orbitals into "equivalent orbitals" as specified by Lennard-Jones[51]. This decomposition into equivalent orbitals has the advantage that these new orbitals are strongly localized and can be considered as the result of a particular bond. In the equivalent orbital representation one then just considers the dipole moment of each orbital and associates this moment with a particular bond in the molecule.

For the methane molecule the bond dipole moment resulting from the bonding orbital ϕ_{b1}, which is already in the equivalent orbital representation, was determined at the carbon nucleus (i.e., the operator $\vec{r}$ is equal to $r_c \cos\theta_c$). This bond moment is given by

$$\mu_{b1} = e(D(\phi_{b1}^2) - R) \quad , \tag{1.45}$$

where $D(\phi_{b1}^2) \equiv \langle\phi_{b1}|r_c \cos\theta_c|\phi_{b1}\rangle$ is the electronic contribution to the bond moment from the orbital ϕ_{b1} and the remaining term is the nuclear contribution from the hydrogen nucleus H_1, R being the C-H_1 bond length. A negative value for μ_{b1} means that the direction of the dipole is $C_{(+)} - H_{(-)}$.

The calculated electronic contribution (see Appendix 6) is -2.533 a.u. This gives a total bond dipole moment of -0.4713 a.u. or -1.198 D using the derived density distribution for methane. This is in better agreement with the experimental value of ±0.5 D than the other theoretical results which are listed in Table 1.5

TABLE I.5

Bond Dipole Moment for Different Wavefunctions

Wavefunction	μ^{*}_{CH}
Nesbet[a]	-1.58 D
Moccia[b]	-1.52 D
Klessinger[c]	-1.88 D
Sinai[d]	-1.93 D
Arrighini[e]	-1.792 D
Present Work	-1.198 D

* The negative sign indicates that the bond moment is $C_{(+)} - H_{(-)}$.

[a] Reference 16

[b] Reference 22

[c] Reference 25

[d] Reference 23

[e] Reference 29

c) Octupole Moment

As already indicated the first non-vanishing multipole moment in the multipole expansion of the total charge distribution for methane is the octupole moment. The only non-vanishing component of the electric octupole moment is given by averaging the wavefunction over the operator $\sqrt{15}\, X_c Y_c Z_c$ (see Appendix 7). Thus the total octupole moment is given by[70]

$$I_3 = -\sqrt{15}\, 2 \sum_{i=1}^{5} \langle \phi_i(1) | X_c Y_c Z_c | \phi_i(1) \rangle + \sqrt{15} \sum_{j=1}^{5} Z_j X_j Y_j Z_j \qquad (1.46)$$

$$= I_3^e \text{ (electronic)} + I_3^N \text{ (nuclear)} ,$$

where the first summation is over the occupied orbitals and the second summation is over the number of atoms with charge Z_j and coordinates X_j, Y_j, Z_j. In Table 1.6 are listed the electronic and nuclear contributions to the total octupole moment for methane obtained from the wavefunction derived in the present work and from some other recent wavefunctions[29,71].

In Table 1.6 there is no sign given for the experimental values of the total octupole moment since it is not known. The plus sign on the other values have been determined theoretically. The actual value, +9.628 a.u., for the total octupole moment determined in the present work is in excellent agreement with the recommended value[71] of +9.796 a.u. This recommended value has been obtained as an average result of a one-center calculation, a value from second virial coefficient data and a value from static dielectric constant data. The agreement of the present result with other theoretical values is satisfactory with the exception of the theoretical results given by Sinai[70], which are lower than the value determined in the present work.

d) Electric Field Gradient

TABLE I.6

Contributions to the Octupole Moment for Methane

Wavefunction	Electronic Contribution (a.u.)	Nuclear Contribution (a.u.)	Total (a.u.)
Albasiny[a]			+ 9.71
Turner[b]	-11.00	23.85	+12.85
Sinai[c]	-17.87	23.85	+ 5.98
Woznick[c]	-23.099	26.311	+ 3.212
Krauss[c]	-22.464	26.311	+ 3.847
King[d]			+12.299
Arrighini[e]	-21.805	26.346	+ 4.541
Present Work	-16.500	26.128	+ 9.628
Experimental results by:			
Second virial data[f]			10.884
Second virial data for mixture with Argon[f]			17.414
Static dielectric constant[g]			8.707
Phase transition data for solid CD_4[h]			3.396
Recommended value[i]			+9.796

[a] Reference 72
[b] Reference 73
[c] Reference 70
[d] Reference 74
[e] Reference 29
[f] Reference 75
[g] Reference 76
[h] Reference 77
[i] Reference 71

Another important experimentally-observable one-electron property is the electric field gradient at the proton H_1. This quantity is obtained theoretically by averaging the total charge density over the operator $Ga \equiv (3\cos^2\theta_{H_1} - 1)/r^3_{H_1}$, where r_{H_1} is the distance from the hydrogen center H_1 and θ_{H_1} is the angle between the C-H_1 bond axis and the vector $\vec{r}_{H_1}$. The electric field gradient is related to the experimental quadrupole coupling constant via the equation

$$\text{quadrupole coupling constant} = eqQ/h \ , \tag{1.47}$$

where Q is the deuteron quadrupole moment and q is the calculated total electric field gradient at the proton H_1.

The electric field gradient has a nuclear and electronic contribution. Thus

$$q = q_N + q_e \ , \tag{1.48}$$

where q_N is the nuclear field gradient at H_1 produced by the carbon nucleus and the other protons, and q_e is the electronic field gradient at H_1 produced by the electronic charge density $\rho(\vec{x}_1)$. The nuclear contribution is given by

$$q_N = \frac{12}{R^3} + \frac{9\sqrt{3}}{16\sqrt{2}R} = 1.44789 \text{ a.u.} \tag{1.49}$$

Within the equivalent orbital representation the electronic contribution is given by

$$q_e = -e(G(\phi_0^2) + G(\phi_{b1}^2) + G(\phi_{b2}^2) + G(\phi_{b3}^2) + G(\phi_{b4}^2)), \tag{1.50}$$

where $G(\phi_i^2) \equiv 2\langle\phi_i|(3\cos^2\theta_{H_1} - 1)/r^3_{H_1}|\phi_i\rangle$ is the contribution to the electronic field gradient at H_1 resulting from the electron density contained in the i^{th} equivalent orbital. Expressions for these orbital

contributions are given in Appendix 8. Using the derived density distribution for methane all the required integrals were evaluated and the numerical value for q_e is -1.14934 a.u., where the orbital contributions have the values $G(\phi_0^2)$ =0.45643, $G(\phi_{b1}^2)$ = 0.37453, and $G(\phi_{b2}^2) = G(\phi_{b3}^2) = G(\phi_{b4}^2)$ = 0.10613; all values being in atomic units. Thus the total electric field gradient is

$$q = q_N + q_e = 0.29847 \text{ a.u.} \qquad (1.51)$$

From the computed electric field gradient q and the value $+2.796 \times 10^{-27}$ cm^2 for the deuteron quadrupole moment Q[78], the deuteron quadrupole coupling constant in CH_3D is calculated to be

$$eqQ/h = 196.1 \text{ kc/sec.} \qquad (1.52)$$

This value is in excellent agreement with the results of Caves and Karplus[79], who estimate this quantity to be 210±30 kc/sec, and Pitzer[27], who derived a value of 224 kc/sec. Arrighini et al[29] calculate a value for the deuteron quadrupole coupling constant of 207.7 kc/sec and indicate that their result should be a very reliable estimate of such a quantity. At present, only a very uncertain experimental value of 100±50 kc/sec for the quadrupole coupling of the deuteron in methane[80] is available.

1.4 Energy Determination for Methane

The present wavefunction for methane was determined by varying the parameters to satisfy one-electron dependant properties, rather than by minimizing the energy, a property determined by the two-electron probability distribution. Therefore, it is of interest to evaluate the expectation value of the energy operator for the wavefunction presently derived, to determine whether or not the emphasis which has been placed

on the one-electron nature of the wavefunction has had an adverse effect on the value of the energy calculated for the system.

The total energy can be obtained by evaluating all the terms in Equation (I.23) for the methane molecule. All the required one-, two-, three-, and four-center integrals were evaluated using programs obtained from Quantum Chemistry Program Exchange[81] (see Appendix 3). In order to be certain that the programs were operating correctly the energy for the Palke and Lipscomb[25] wavefunction was duplicated to six figure accuracy. Using the same programs, the energy was evaluated for the one-electron density distribution that has been derived in the present work. The numerical results obtained for the orbital contributions to the energy and the final energy results are given in Table I.7.

From this table we see that the virial theorem is not satisfied since V/T is -1.9886 and the correct value should be -2.000. This agreement is acceptable since the virial was not used as a constraint on the charge distribution. Also, since we have derived the "best" one-electron density distribution from one-electron property considerations and not from the energy minimization criterion it is expected that the kinetic energy, which is a one-electron property, will be given more accurately than the total energy which is a two-electron property. This fact alone would suggest that the virial theorem will not be completely satisfied.

Summarized in Table I.8 are the results obtained for the energy of the methane molecule from a number of molecular wavefunctions. This table is a revised table of the one given by Moccia[22].

The calculated value of the total energy is in very satisfactory agreement with the experimental and other theoretical results. The derived

TABLE I.7

Orbital Contributions to the Energy for Methane[a]

Orbital	Orbital Energy (a.u.)	
ϕ_0	-11.0531	
ϕ_{b1}	- 0.5993	
ϕ_{b2}	- 0.5993	
ϕ_{b3}	- 0.5993	
ϕ_{b4}	- 0.5993	
Electronic energy	-53.5792	Kinetic energy 40.6212
Nuclear repulsion	13.4229	
Total energy	-40.1563	
Viriam theorem V/T =	-1.9886	

[a] All energies are in atomic units (a.u.).

TABLE 1.8

Summary of Energy Calculations for CH_4[a]

Reference	Method of calculation	Number and type of basis functions[b]	C-H distance (a.u.)	Molecular energy (a.u.)
Buckingham[9]	one-center, SCF, single detor ℓ up to 1	Slater-like functions with variable exponents	2.000	-39.47
Bernal[11]	one-center, single detor with angular terms		1.975	-39.33
Kaide[14]	one-center, single detor with ℓ up to 3		2.000	-39.80
Mills[17]	one-center, SCF single detor with f terms		2.000	-39.62
Saturno[30,c]	V.B. one-center single detor ℓ up to 1		2.052	-39.503
Saturno[30,c]	V.B. one-center 6 detor ℓ up to 5		2.000	-39.844
Albasiny[18]	one-center, numerical SCF, ℓ up to 1		2.000	-39.53
Albasiny[18]	one-center, numerical SCF, ℓ up to 3		2.000	-39.90
Sinai[23]	single detor SCF LCAO MO	9 STO (S)	2.000	-39.86
Krauss[21]	single detor SCF LCAO MO	33 GTO (PO)	2.0665	-40.167

TABLE I.8--Cont'd.

Reference	Method of calculation	Number and type of basis functions[b]	C-H distance (a.u.)	Molecular energy (a.u.)
Moccia[22]	single detor SCF OCE MO, ℓ up to 3	26 GTO (PO)	2.080	-39.866
Woznick[24]	single detor SCF LCAO MO	27 STO (S)	2.0665	-40.181
Lipscomb[26]	single detor SCF LCAO MO	9 STO (S)	2.0665	-40.114
Pitzer[27]	single detor SCF LCAO MO	9 STO (PO)	2.050	-40.128
Ritchie[28]	single detor SCF LCAO MO	52 GTO (PO)	2.12	-40.198
Arrighini[29]	single detor SCF LCAO MO	39 STO (PO)	2.065	-40.205
Present Work	single detor LCAO MO Hellmann-Feynman approach	22 STO (S)	2.06172	-40.156
Experimental[d]			2.067	-40.525

[a] (PO) = Partial optimization of the exponents.

[b] Linear combinations of n functions are counted as n basis functions, and p_x, p_y, and p_z are counted separately.

[c] The values are those revised by Bishop.

[d] Reference 28.

value of -40.156 a.u. is only slightly higher by 0.049 a.u. than the best energy obtained for this molecule by Arrighini et al[29] using a very large basis set of thirty-nine STO's. In our calculation there are an equivalent of 22 STO's used with no optimization of exponents beyond the SCF atomic orbital functions obtained by Clementi[53] et al. Our calculated result is in excellent agreement with the values determined with multi-centered limited basis sets by Krauss[21] and Woznick[24], and considerably better than the results obtained with one-center expansions[22,30] or minimal basis representations[23,26,27]. The only energies that are significantly better than the result obtained in the present work were obtained using extremely large basis sets; in one case fifty-two GTO's[28] and in the other thirty-nine STO's[29] are used. Thus, we see that the one-electron charge distribution determined by the present electrostatic approach gives a very reasonable energy, one that is approaching the estimated Hartree-Fock limit of -40.22 a.u.[82].

The experimental value of the total energy[28] is -40.525 a.u. which differs from the calculated value by 0.369 a.u. or 0.91%. Using the atomic energy of -37.689 a.u.[53] for carbon and a zero-point vibrational energy of -0.044 a.u.[83] the calculated binding energy for methane, using the derived density distribution, is 0.443 a.u. This differs from the experimental binding energy of 0.625 a.u.[83] by 29%. This is much better than might be expected from the present approach since it does not use the minimization of energy criterion.

Although the virial theorem does not hold exactly for the derived charge distribution it does hold for the real charge distribution and thus the kinetic energy, which is minus the total energy, has an experimental

value of -40.525 a.u. The calculated value is -40.621 a.u., which is larger than the experimental result by only 0.2%. This accuracy might be expected since the kinetic energy operator is a one-electron operator and it has already been suggested that the derived one-electron density distribution should yield excellent one-electron properties.

Not only has the derived one-electron charge density for methane given excellent one-electron properties, but it has just been shown that this distribution also yields a respectable energy, a two-electron property, for this molecule. Since the calculated total energy is in very good agreement with the other results, the present electrostatic approach has been justified as a satisfactory method of determining a one-electron charge distribution for methane. Such an approach might well be considered an acceptable method for determining one-electron density distributions for other polyatomic molecules.

1.5 Discussion of the Electrostatic Method

Because of the computational difficulties with the SCF method for polyatomic molecules other methods, such as the electrostatic method used in the present work, have been used to determine molecular charge distributions. The electrostatic method has been used frequently[35,36,84,85] to determine one-electron charge distributions for a number of hydride molecules and has been further applied here to the methane molecule.

It has been shown (see Section 1.3) that the one-electron properties calculated from the derived charge distribution for methane are in excellent agreement with the corresponding experimental quantities. In almost every case it is found that these properties as determined from the one-electron

density distribution obtained in the present electrostatic approach are in better agreement with experiment than the results calculated from density distributions obtained by the energy minimization method. Thus, one may conclude that within a limited basis set the energy minimization criterion does not necessarily give the "best" one-electron density; that is to say, a one-electron density that yields the "best" one-electron properties. It is only in the limit of large extended basis sets that exact one-electron density distributions are expected to be given by either method.

The calculation of the energy for the methane molecule (see Section 1.4) shows that the derived one-electron density distribution also yields a very satisfactory total molecular energy. The total energy calculated from the wavefunction determined by the present electrostatic approach is only slightly higher than the best results obtained to date[29] by the SCF procedure. The electrostatic approach utilizes only one-electron properties and thus is easier to apply than the energy minimization procedure which necessarily involves difficult two-electron integral calculations. Because of the simplicity in the calculations and the excellent agreement of the calculated physical properties with experiment the electrostatic method has proven to be a very useful way of determining a good one-electron distribution for methane. From this work one can conclude that when using a limited basis set, not necessarily a minimal basis set, the better method of determining the "best" one-electron charge density and thus the "best" one-electron properties for a polyatomic molecule is the present electrostatic approach.

As a further note of interest it is known that the SCF method, which utilizes the energy minimization procedure, does not yield as good

a wavefunction for molecules obtained from the second and third-row atoms as it does for molecules obtained from the first-row atoms. This fact can be observed in the work of Matcha[86] for NaCℓ for example or by comparing the density distributions and force analyses of the first[4] and second[6] row hydrides. The decrease in accuracy of the SCF results for molecules obtained from the second and third-row atoms is partially owing to the fact that when one determines a molecular wavefunction by the energy minimization criterion the core orbitals of the larger molecules, because of their very large contributions to the total energy, are more stringently weighted by the minimization procedure than are the valence orbitals. The result is that as the molecular size increases the core density is more accurately determined than the valence density by the SCF method.

In the present electrostatic approach the primary role of the core density is to simply shield an equivalent amount of nuclear charge. The forces, however, are very sensitive to the exact form of the valence density. Thus in an electrostatic determination of the charge density $\rho(\vec{x}_1)$, the valence density, the density responsible for binding the nuclei, dominates the calculation and is more accurately determined than in an energy calculation which is dominated by that part of the wavefunction near the nuclei. Since the very important valence density is heavily weighted by the electrostatic approach this method would be ideal for determining charge distributions for molecules obtained from the second and third-row atoms. This will be particularly true for molecules that have almost spherical symmetry such as SiH_4 and GeH_4, for then the first possible core polarization (which is omitted in this method) is an

octupolar one.

1.6 Analysis and Interpretation of the One-Electron Density

The derived one-electron density distribution for the methane molecule has been shown to yield expectation values for both one- and two-electron properties that are in excellent agreement with experiment. Some of the one-electron properties that have been considered are the octupole moment, the diamagnetic susceptibility, the proton magnetic shielding, the force, and the electric field gradient. These properties depend on the average values of r_C^3, r_C^2, $1/r_{H_1}$, $1/r_{H_1}^2$ and $1/r_{H_1}^3$ respectively. Since each of these properties separately measure the accuracy of the charge density in different regions of space, the agreement of their calculated expectation values with experiment clearly indicates that the derived charge distribution has the correct physical behavior in all regions of space. It is of interest to use this charge distribution, since it must closely resemble the actual physical density, to analyze the chemical binding in the methane molecule. By comparing this charge distribution with those for other molecules the stability of the methane molecule will be better understood.

Considering first the molecular wavefunction we note that in the present work equivalent orbitals have been used. For the purpose of comparison of these results with others, the molecular orbitals of Palke and Lipscomb's[26] wavefunction for methane have been transformed, by the unitary transformation given by Lennard-Jones[51], into equivalent orbitals. The parameters λ, μ, εb and δ, which appear in our wavefunction, were determined from the transformed equivalent orbitals. These results

together with the present results are listed in Table 1.9.

From this table we see that the parameters εb and δ are almost identical. The ratio λ/μ is somewhat higher for our wavefunction. This is mainly due to the SCF atomic orbital basis set which is used on carbon in the present calculation, where Palke and Lipscomb use a minimal basis set of Slater orbitals. Also, Palke and Lipscomb use an orbital exponent of 1.2 on the hydrogens instead of value of 1.5 which is used in the present work. Because of these orbital changes one might well expect the λ/μ ratio to be higher for the present calculation. For these same reasons the wavefunction derived in the present work yields better one-electron properties (see Section 1.3) and even a better energy (see Section 1.4) than Palke and Lipscomb's wavefunction.

Using the electrostatic method, one-electron distributions have been obtained for the water molecule[35,36] and the ammonia molecule[84]. The differences between the equivalent orbitals derived in the present work for methane and the equivalent orbitals obtained for water and ammonia are quite marked. As already indicated for methane the hybridization in the bonding orbitals is almost sp^3. In particular, the hybridization εb is 57.565° which is very close to the sp^3 hybridization angle of 60°. Using bent bonds (i.e., the bonding orbitals do not point along the bond axies) in both the water[35,36] and the ammonia[84] molecules allows electrostatic equilibrium to be obtained but this increases the p character and decreases the s character of the bonding orbitals beyond that of sp^3 hybridization. In the case of the methane molecule the tetrahedral symmetry can not be maintained unless the bonding orbitals are at the tetrahedral angle with the result that they must point along the C-H

TABLE I.9

Comparison of Parameters in Wavefunctions for CH_4

Parameter	From Palke and Lipscomb's[a] transformed wavefunction	From present wavefunction
λ	0.6127	0.7274
μ	0.5070	0.3687
εb	57.167°	57.565°
δ	0.1243	0.1214

[a] Reference 26.

bond axies. Thus, in order to form the most stable distribution the hybridization should be close to the sp^3 hybridization of the Ne atom as was suggested by Pople[42]. The stability is achieved since the sp^3 hybridization places the maximum amount of charge density along the bond axies. The fact that the hybridization is not exactly sp^3 is because of the polarization-type hybridization[43] contributed by the hydrogen orbitals.

Keaveny[36] found that, when using an SCF atomic orbital basis set to describe the density on the oxygen center in the water molecule, the polarity factor λ/μ was larger than that found by Bader and Jones[35] using just simple Slater orbitals on the oxygen. Similarly, the use of an SCF atomic basis set on carbon in the present work has resulted in a large λ/μ ratio of 1.973 for methane, which is even higher than the value of 1.735 obtained for the water molecule by Keaveny. This would suggest that the bonding orbitals in methane are more polar than in water, but this ratio is strongly dependent on the basis sets used in the bonding orbitals. For example, different orbital exponents on the hydrogens place different amounts of density on these centers and the λ/μ ratio will fluctuate in order to partially compensate for this change in the exponents. In the case of methane, the use of a high orbital exponent of 1.5 in the 1s orbitals on the hydrogens places a lot of density at the hydrogens, but this increase is offset by the high ratio of λ/μ which weighs more heavily the density on the carbon center than on the hydrogen centers. This is the main reason for the low value of -1.198 D for the bond dipole moment of methane determined from the present wave-function. This value is in better agreement with the commonly quoted

value of ±0.5 D than other calculated results which are generally higher than our result.

One should also note the differences in the orbital exponents used on the hydrogens in these hydride molecules. Keaveny[36] used an orbital exponent of 1.32 on the hydrogens in water and Bader and Jones[84] used an orbital exponent of 1.29 on the hydrogens in ammonia. This would suggest that one should use an orbital exponent less than 1.29 (for example, 1.245) on the hydrogens in methane. But it was found in the present work that the best results were obtained with an orbital exponent of 1.5 on the hydrogens in methane. It is felt that when using an SCF atomic orbital set on the heavy atom one should use a large orbital exponent on the hydrogens. This exponent should be larger than the value used when just simple Slater orbitals are placed on the heavy atom. If Keaveny[36] had used a larger exponent than 1.32 on the hydrogens in the water molecule perhaps better balance points could have been obtained for the forces and dipole moment.

The delocalization parameter δ for methane is small (i.e., $\delta = 0.1214$) compared to the value 0.388 for water[36] and 0.280 for ammonia[84]. This result is expected since the high symmetry and the large tetrahedral bond angles in methane tend to localize the bonding orbitals along the bond directions to a greater extent than found in the water and ammonia molecules. Any further connections between the orbital description of these hydride molecules will be seen in Chapter II where the water and ammonia molecules are considered in more detail.

Relating the chemical binding in molecules to the properties of the molecular orbitals is by no means an unique method of understanding

the processes of bond formation. An infinite number of sets of orbitals, all related by unitary transformations, can be constructed that give identical results for the expectation values of the total molecular properties, but different results for the orbital contributions. Thus, any analysis of chemical binding based upon the orbital description is dependant upon the type of orbital set used. It is desirous to consider chemical binding in terms of a more stationary framework.

Instead of considering the molecular orbital functions let us consider the one-electron density function $\rho(\vec{x}_1)$ (see Equation (I.11)). This function, which is independent of the orbital description, is a function in three-dimensional space and can be easily pictured in coordinate space. Contour plots can be made of the total one-electron density by evaluating $\rho(\vec{x}_1)$ at a large number of points in space and then joining up points of equal density thus forming the density contour lines. Considerable use will be made of contour plotting in this and the remaining sections of this thesis. Many of the contour plots given in this thesis are obtained by programming an IBM 7040 computer to produce a magnetic output tape which contained the necessary information for a Benson-Lehner plotter to produce the required contour diagrams.

Before considering contour diagrams of $\rho(\vec{x}_1)$ for methane let us first consider another density function, the difference density $\Delta\rho(\vec{x}_1)$. Following the work of Berlin[87] for diatomic molecules, a polyatomic molecule can be divided into binding and antibinding regions[88]. Electron density placed in the binding region of a molecule creates attractive forces that tend to pull all the nuclei together. Placing density in the antibinding regions creates larger forces on some nuclei than others in

such a way that it tends to pull the molecule apart into its separated atoms or a mixture of simpler molecular species. Thus, the binding region is that region in which electron density must be concentrated in order to achieve electrostatic equilibrium. Once the boundary curves between the binding and antibinding regions have been determined for a polyatomic molecule how much charge must be placed in the binding region in order to attain a state of electrostatic equilibrium? This question is best answered by choosing a standard density distribution which is known to be electrostatically unstable because it places an insufficient amount of charge in the binding region. By comparing the molecular density with the standard density the electrostatic stability of the molecular density can be better understood. For example, if the molecular density concentrates more charge in the binding region than the standard density then the molecular density is electrostatically more stable than the standard density. The purpose of constructing the difference density distribution $\Delta\rho(\vec{x}_1)$ is to determine the rearrangement that the charge density represented by the standard charge distribution must undergo in order to attain a state of electrostatic equilibrium in the molecule.

The difference density distribution $\Delta\rho(\vec{x}_1)$ is obtained by subtracting the superimposed densities of the component undistorted atoms placed at the equilibrium bond length from the molecular density, also evaluated at the equilibrium distance. Thus

$$\Delta\rho(\vec{x}_1) = \rho(\vec{x}_1) \text{ (molecular)} - \rho_A(\vec{x}_1) \text{ (atomic)} , \tag{1.53}$$

where $\rho_A(\vec{x}_1)$ is the standard atomic density distribution which can be

shown to be electrostatically unstable.* If contour plots of the density difference distribution $\Delta\rho(\vec{x}_1)$ are constructed one can determine the regions in which the molecular distribution $\rho(\vec{x}_1)$ has more charge concentrated than the standard atomic distribution $\rho_A(\vec{x}_1)$. In regions where $\Delta\rho(\vec{x}_1)$ is positive the molecular charge density exceeds the atomic density, while in regions where $\Delta\rho(\vec{x}_1)$ is negative the atomic density exceeds the molecular one. If $\Delta\rho(\vec{x}_1)$ is positive in the binding region, the molecular charge distribution is electrostatically more stable than the atomic charge distribution. Thus for a stable molecular species, $\Delta\rho(\vec{x}_1)$ must be negative in the antibinding region since the integral of $\Delta\rho(\vec{x}_1)$ over the coordinates of $\vec{x}_1$ yields zero. By analyzing the difference density contour diagrams one can consider the molecular stability with respect to the separated atoms.

Contour diagrams of the one-electron density $\rho(\vec{x}_1)$ and the difference density $\Delta\rho(\vec{x}_1)$ have been used extensively[3,4,5,6] as interpretive devices in understanding the chemical binding and the forces operative in diatomic molecules. These diagrams dramatically show the areas of density concentration, and the regions of density increase and decrease accompanying molecular bond formation. In Figure I.2 are given plots of $\rho(\vec{x}_1)$ and $\Delta\rho(\vec{x}_1)$ in the plane of the carbon and two hydrogen nuclei for the methane molecule as determined from the derived wavefunction.

From the plot of $\rho(\vec{x}_1)$ we see that the one-electron charge density

---

* In the standard atomic charge distribution the nucleus of each atom will penetrate the spherical atomic charge density of the other atoms. By applying Gauss' theorem it can be shown that there will always be a net force of repulsion between all the nuclei resulting in a state of non-equilibrium.

Figure 1.2. The total density $\rho(\vec{x}_1)$ and difference density $\Delta\rho(\vec{x}_1)$ contour maps obtained from the derived one-electron charge distribution for methane. The plots are in a plane containing the carbon and two hydrogen nuclei. The dotted lines on the $\Delta\rho(\vec{x}_1)$ map are the boundary curves between the binding region (above and between the two dotted lines) and the antibinding regions. The C-H bond length in this and subsequent diagrams for methane is 2.06172 atomic units (a.u.). All contour values used in this thesis are given in atomic units.

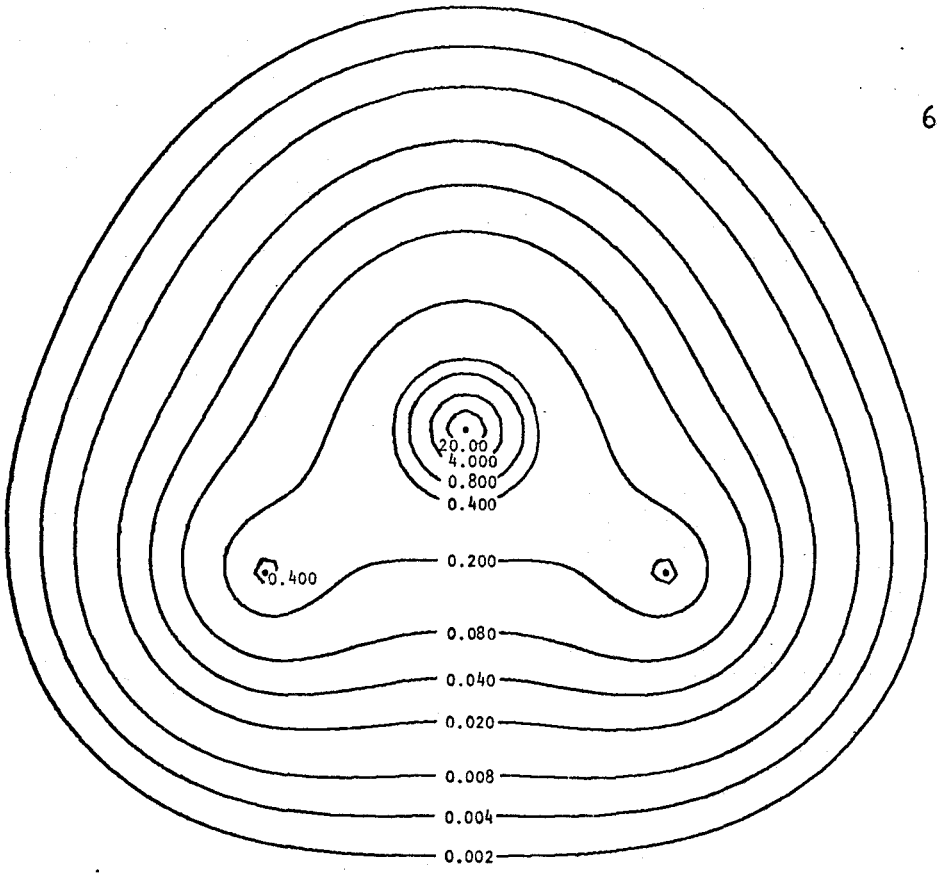

$\rho(\bar{x})$

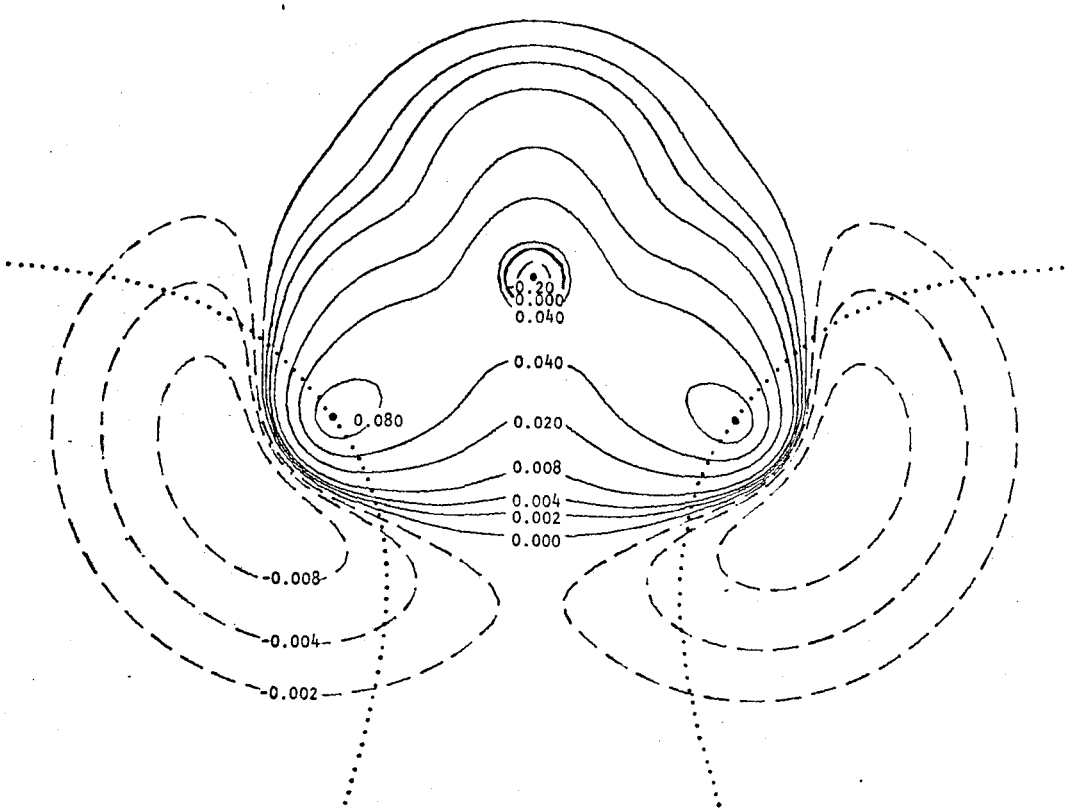

$\Delta\rho(\bar{x})$

for methane has the required tetrahedral symmetry and that the density is well localized along the C-H molecular bond axies as was suggested when the bond dipole moment was determined. This large concentration of charge density along the bond directions justifies the use of the equivalent orbital description and the break-down of density into its bond components. Note that the charge distribution is almost spherical except for the regions right along the bond axies. It is because of this almost spherical symmetry that one-center expansions have been moderately successful in the past when used to determine a wavefunction for methane. The fact that the density at the protons is very highly peaked, a condition that can not be well taken care of in one-center expansions, is the main reason that the one-center method has been replaced by the more accurate multi-center technique.

From the $\Delta\rho(\vec{x}_1)$ contour plot* in Figure 1.2 one notes that the charge density right at the carbon nucleus has decreased on the formation of the methane molecule from the sphericalized constituent atoms. Thus, the density is not as highly peaked at the carbon nucleus in the molecule as in the carbon atom itself. Also, the density at the hydrogen nuclei has increased over the atomic value, the contours around the hydrogens in the $\Delta\rho(\vec{x}_1)$ plot being positive. This peaking of the density on the hydrogens is a well-known fact[4,6] that always occurs when the hydrogen atom undergoes bond formation. In the case of methane this density increase is accomplished by the use of the large 1s orbital exponent of 1.5 on the hydrogens.

---

* In the $\Delta\rho(\vec{x}_1)$ contour plots the atomic density used for the carbon atom is obtained from the ^3P atomic orbital set determined by Clementi[53] et al and the atomic density for hydrogen is obtained using a simple Slater 1s orbital with an exponent of 1.0.

The electrostatic stability of the methane molecule is easily understood from the $\Delta\rho(\vec{x}_1)$ contour map. On the $\Delta\rho(\vec{x}_1)$ contour map is shown the boundary curve, the dotted line, between the binding and anti-binding regions. This boundary curve is derived on the basis that the charge distribution for methane must reflect the tetrahedral symmetry of the nuclear framework. Thus one must consider the forces exerted on the nuclei by a symmetrically equivalent set of point charges in deriving the binding region. Symmetrically equivalent charge points placed above and between the two boundary curves will exert forces on the nuclei such as to decrease all the nuclear separations. Charge density placed outside of this boundary curve will tend to separate the molecule. The positions of these boundary curves clearly indicate where charge density must be concentrated in order to achieve a state of electrostatic equilibrium upon molecular formation.

From the $\Delta\rho(\vec{x}_1)$ map we see that as the atoms combine to form the methane molecule there is a large transfer of charge density from the outer regions of the atomic system, particularly behind the protons, into the region between the carbon and hydrogen atoms, which is the all-important binding region. This build-up of charge, which is dominant along the C-H bond axes , strongly binds the carbon and hydrogen nuclei together. Although there is a slight increase in charge density along the H-H bond axes , this increase is not as large as the increase in charge density between the hydrogens found in the water[36] and ammonia[84] (see page 108 of this thesis) molecules. The increase in charge density in the water and ammonia molecules occurs predominantly in the regions above and below the heavy nucleus and between hydrogen nuclei, where as

in methane the largest density increases occur along the C-H bond axies. Methane, for this reason and also because of the fact that its total density is almost spherical and as such is not easily polarized, is much less reactive than the water and ammonia molecules, which both have large local and over-all dipolar moments in their charge distributions.

In order to obtain a more detailed picture of how the density distribution in the methane molecule has rearranged from that of the original atomic densities, contour plots of $\rho(\vec{x}_1)$ and $\Delta\rho(\vec{x}_1)$ are given in Figure I.3 for a number of planes perpendicular to one of the three-fold symmetry axes . The plots in Part (a) are through a single proton. Note the spherical shape of the total charge density $\rho(\vec{x}_1)$ and the large increase in density at the proton with the corresponding decrease in density further from the proton accompanying bond formation as indicated in the $\Delta\rho(\vec{x}_1)$ map. The plots in Part (b) are half way along the C-H bond axis and they clearly indicate the large increase in density that occurs along the C-H bond axis as the methane molecule is formed from its constituent atoms. The plots in Part (c) are in the plane through the carbon nucleus and perpendicular to a three-fold symmetry axis. These diagrams again show the decrease of the density at the carbon nucleus, the strong build-up of charge along the C-H bond axies and the decrease in charge behind the proton brought about by the formation of an electrostatically stable molecular species. The final plots in Part (d) are through the plane of three protons. Clearly there is a build-up of charge density at each of the protons and a decrease in charge density behind each of the protons as the atomic densities rearrange

Figure 1.3. Contour plots of the total density $\rho(\vec{x}_1)$ (to the left of the diagram) and the difference density $\Delta\rho(\vec{x}_1)$ (to the right of the diagram) for a number of planes perpendicular to one of the three-fold symmetry axies in methane. (a) a plot through the single hydrogen nucleus. (b) a plot half-way along the single C-H bond axis. (c) a plot through the carbon nucleus. (d) a plot through the plane containing three protons. The crosses indicate the vertical projections of the positions of the other nuclei not in the plane.

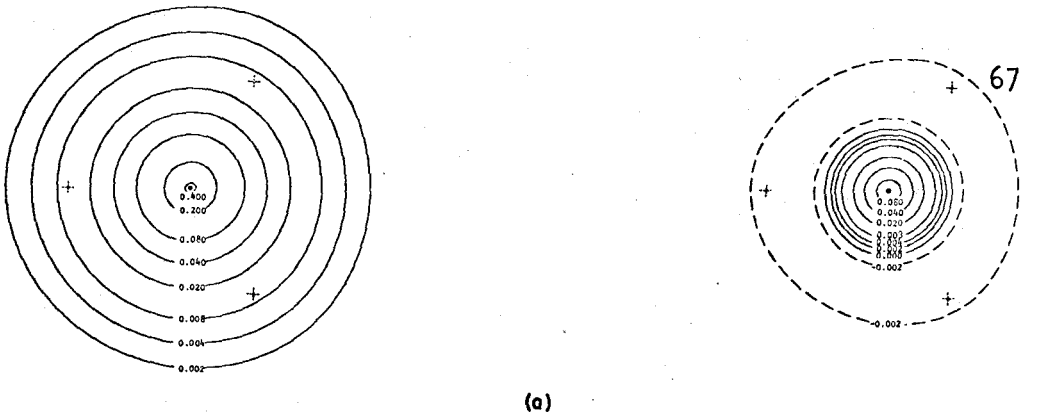
0.400
0.200
0.080
0.040
0.020
0.008
0.004
0.002
0.080
0.040
0.020
-0.002
-0.002

(a)

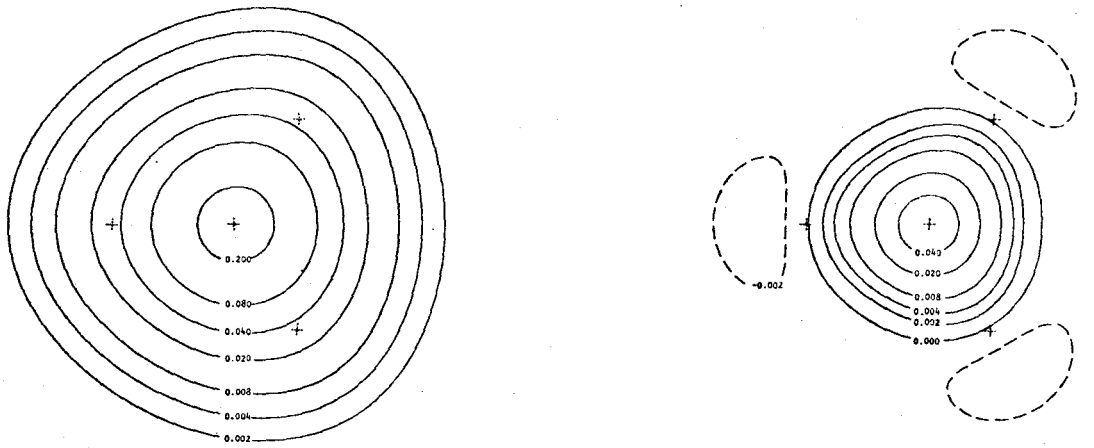
0.200
0.080
0.040
0.020
0.008
0.004
0.002
-0.002
0.040
0.020
0.008
0.004
0.002
0.000

(b)

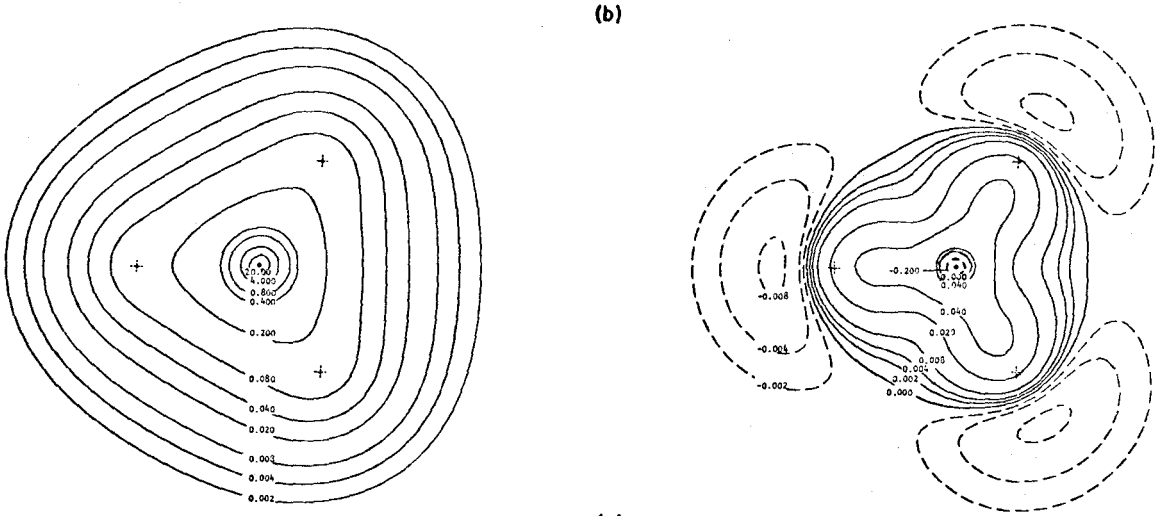
0.200
0.080
0.040
0.020
0.008
0.004
0.002
-0.200
-0.008
-0.004
-0.002
0.040
0.020
0.008
0.004
0.002
0.000

(c)

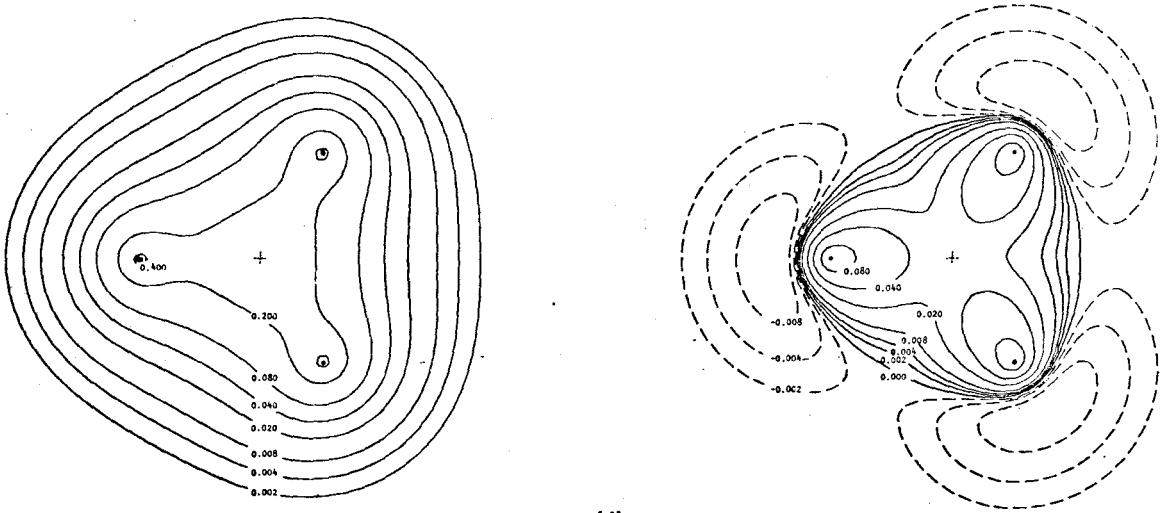
0.400
0.200
0.080
0.040
0.020
0.008
0.004
0.002
0.080
0.040
0.020
0.008
0.004
0.002
0.000
-0.008
-0.004
-0.002

(d)

to form the molecule. The increase in charge density in the middle of the plane of the three protons is not as pronounced as in the case of the ammonia molecule[84]. Thus, the portion of the charge density that is mainly responsible for the binding in the methane molecule is that density which is concentrated along the C-H bond axies. This is different from the case of the water[36] or the ammonia[84] molecule. In these two molecules the binding charge density is concentrated in a region where it attracts all nuclei simultaneously (i.e., immediately below and on the hydrogen side of the oxygen or nitrogen nucleus and symmetrically placed with respect to the hydrogen nuclei) and not directly along the heavy nucleus-hydrogen bond axies. Also, note the almost spherical shape of the total charge density $\rho(\vec{x}_1)$ that occurs in all four planes. It is this spherical shape of the methane charge distribution, since it has no large local moments, that makes it so unreactive towards other molecules.

The interpretation of chemical binding in terms of the equilibrium charge distribution is a static one and perhaps more could be understood about the binding in the methane molecule if one considered distortions in the equilibrium configuration. An interesting property of the molecular charge distribution is to determine how it changes as the nuclei are displaced from their equilibrium positions during a normal mode of vibration. Considering only the A_1 or symmetric stretch mode, the change in the charge distribution is dealt with in the following manner.

One-electron charge distributions are determined for a contraction (bond distance = 2.03672 a.u.) and extension (bond distance = 2.08672 a.u.) of the C-H bond from its equilibrium value of 2.06172 a.u. The charge distributions for these changed bond lengths are obtained by balancing the

sum of the nuclear and electronic forces not to zero, as was done for the equilibrium case, but to the net force acting on the proton H_1 in the new positions as determined from the experimental force constant. Thus, the electronic force of attraction is balanced to the new force

$$F_{11}^{New} \text{ (at new bond length)} = (6.0 + 3\sqrt{3}/4\sqrt{2})/R_N^2 - \Delta R \cdot k_1 \ , \qquad (1.54)$$

where R_N is the new bond length, $\Delta R = R_N - R$, and k_1 is the force constant for the A_1 mode (see Equation (1.83)). The first term in Equation (1.54) is the nuclear force of repulsion on the proton for the new geometry and the second term is the net force, with the proper sign, acting on the proton because of the distorted configuration. In the equilibrium configuration F_{11}^{New} is equal to the nuclear force alone.

Using the same basis orbitals as for the equilibrium distribution, the parameters λ, μ and εb were determined for the different one-electron charge distributions of the distorted methane molecule by satisfying the orthogonality and normalization conditions, and the appropriate force constraint. The delocalization δ is assumed to be equal to the equilibrium value of 0.12140, a condition which should be nearly satisfied, and thus, an additional constraint such as the proton magnetic shielding is not required to obtain this parameter. The results obtained for the variable parameters and the expectation values of a few properties for the one-electron charge distributions determined at each different bond distance are listed in Table 1.10.

From Table 1.10 we see that the electronic force of attraction is balanced to the force F_{11}^{New} and that the variable parameters vary smoothly as the C-H bond is increased; the polarity factor λ/μ decreasing from

TABLE I.10

List of Parameters and Expectation Values for the Determined Density Distributions at Three C-H Bond Lengths for Methane

Parameter or Physical Property	C-H Bond Length (a.u.)		
	2.03672	2.06172[a]	2.08672
λ	0.73137	0.72735	0.72426
μ	0.36204	0.36866	0.37424
εb	57.702°	57.565°	57.439°
δ	0.12140	0.12140	0.12140
F_{11}^{New} (a.u.)	1.65841	1.62763	1.59829
F_{11}^{e} (a.u.)	1.65841	1.62763	1.59829
$\sigma^{(d)}$ (a.u.)	4.94364	4.90588	4.86791
$\chi^{(d)}$ (a.u.)	33.94108	34.29360	34.63963

[a] Results obtained for the equilibrium configuration.

2.0201 to 1.9352, the hybridization angle εb decreasing from 57.702° to 57.439° and the delocalization δ being held constant as the C-H bond length is changed from 2.03672 a.u. to 2.08672 a.u. The two physical properties $\sigma^{(d)}$ and $\chi^{(d)}$ decrease and increase respectively as the bond length is increased in agreement with what might have been expected from purely physical consideration.

The purpose of deriving the one-electron charge distributions for the distorted configurations of the methane molecule was to determine how the molecular charge density rearranges as the molecule moves from its equilibrium configuration. In order to best facilitate this analysis, density contour diagrams are again considered. The desired diagrams are obtained by plotting the function $\Delta\rho_D(\vec{x}_1)$, where

$$\Delta\rho_D(\vec{x}_1) = \rho_D(\vec{x}_1) - \rho(\vec{x}_1) \ . \tag{1.55}$$

In this expression $\rho_D(\vec{x}_1)$ is the one-electron charge density evaluated for the distorted configuration (i.e., either an extension or contraction of the molecular bonds) and $\rho(\vec{x}_1)$ is the one-electron charge density determined for the equilibrium configuration of the molecule. Contour plots of $\Delta\rho_D(\vec{x}_1)$ for the methane molecule are given in Figure 1.4 for an extension (Part (a)) and a contraction (Part (b)) of the C-H bonds leaving the carbon atom fixed.

Inasmuch as bond stretching is the undoing of molecular-bond formation, the change in the charge density for bond extension should be characterized by a reversal of the charge transfer that occurred as the molecule is formed from its constituent separated atoms. Thus, it is expected that a density plot of $\Delta\rho_D(\vec{x}_1)$ (extended minus equilibrium density)

Figure 1.4. Contour plots of the density shift $\Delta\rho_D(\vec{x}_1)$ for an extension (a) and a contraction (b) of the C-H bond in methane.

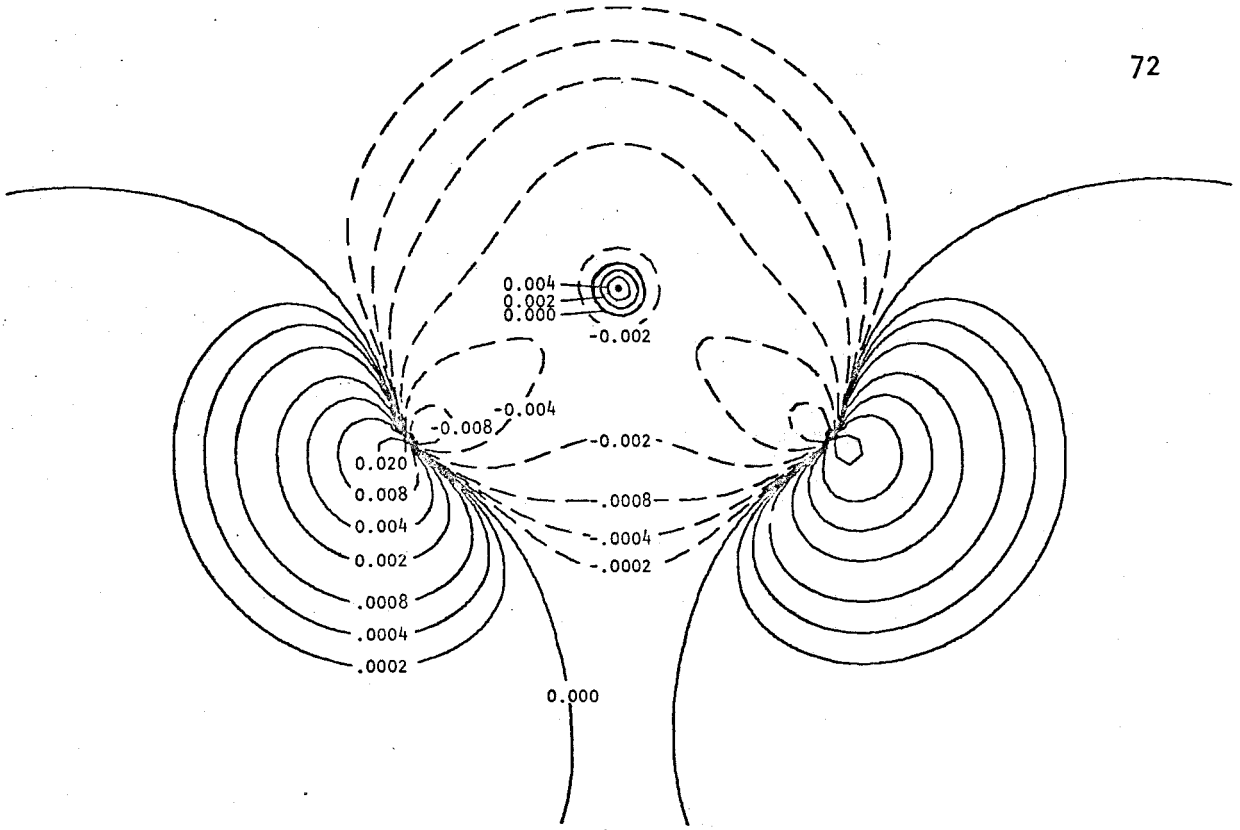
0.004
0.002
0.000
-0.002
-0.004
-0.008
-0.002
0.020
0.008
0.004
0.002
.0008
.0004
.0002
.0008
.0004
.0002
0.000

(a)

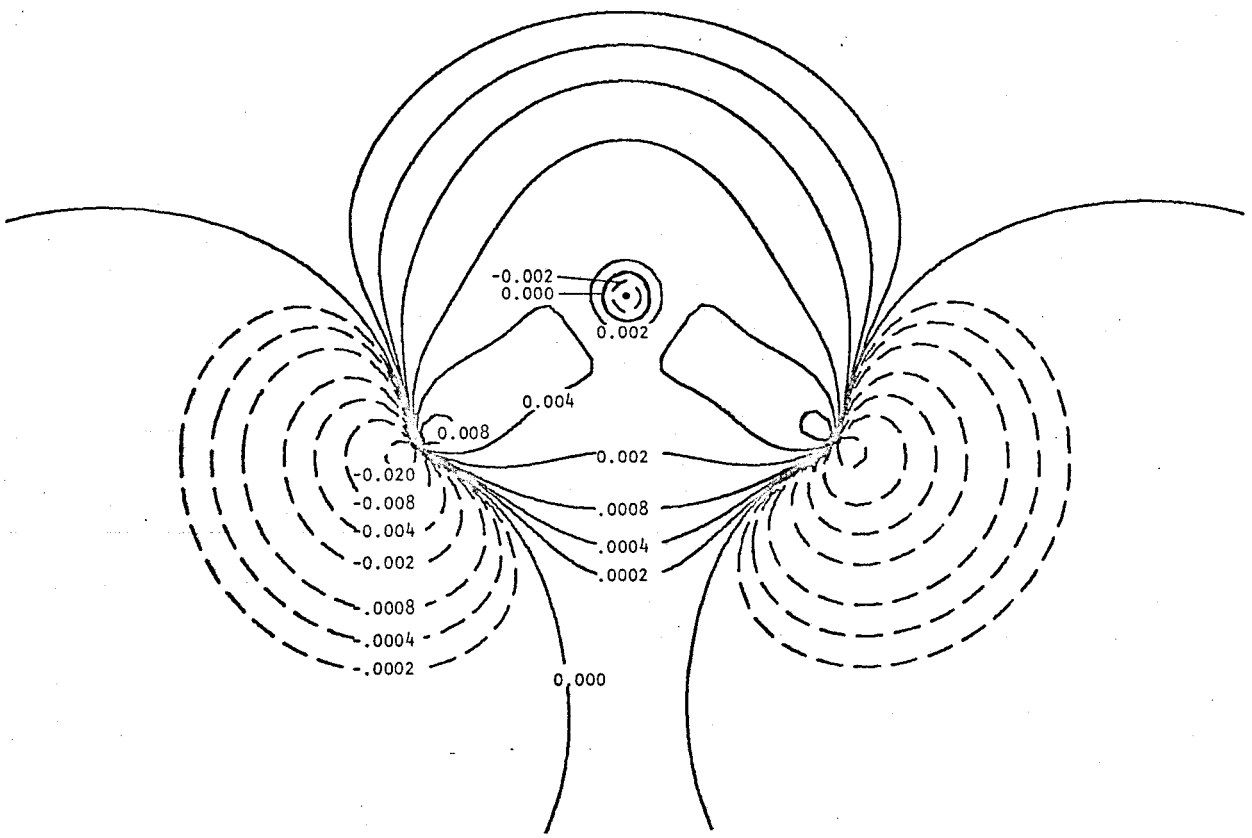
-0.002
0.000
0.002
0.004
0.008
0.002
-0.020
-0.008
-0.004
-0.002
.0008
.0004
.0002
.0008
.0004
-.0002
0.000

(b)

for an extension of the C-H bond will indicate a relaxation of the charge density which is just the reverse of the $\Delta\rho(\vec{x}_1)$ plot. Comparing the $\Delta\rho_D(\vec{x}_1)$ map for a bond extension (Figure I.4, Part (a)) with the $\Delta\rho(\vec{x}_1)$ map (Figure I.2) we see that our prediction is correct. Instead of a decrease in density at the carbon nucleus there is a charge build-up in the $\Delta\rho_D(\vec{x}_1)$ map. The charge decrease behind the protons in the $\Delta\rho(\vec{x}_1)$ is replaced by a charge increase behind the protons in the $\Delta\rho_D(\vec{x}_1)$ map for a bond extention. In a similar manner it is expected that the $\Delta\rho_D(\vec{x}_1)$ map for a bond contraction should show almost identical regions of charge increase and decrease as indicated in the $\Delta\rho(\vec{x}_1)$ map. This prediction is also found to be true as can be seen in the $\Delta\rho_D(\vec{x}_1)$ map for a bond contraction (Figure I.4, Part (b)).

Since all the major density changes in the $\Delta\rho_D(\vec{x}_1)$ contour maps occur along the C-H bond axies we may conclude that it is this density between the hydrogen and carbon nuclei that is mainly responsible for the chemical binding in the methane molecule. This fact was shown in the $\Delta\rho(\vec{x}_1)$ map where there is a large density increase along the C-H bonds as the methane molecule is formed from its constituent atoms. The density accumulated along the C-H bond, since this is the major part of the all-important binding region, produces a state of electrostatic equilibrium in the methane molecule which is more stable than the separated atoms.

Further knowledge can be obtained from the $\Delta\rho_D(\vec{x}_1)$ maps. If the density followed rigidly the motion of the protons then we would expect symmetrical positive and negative contours near the protons. This is not found to be the case in the $\Delta\rho_D(\vec{x}_1)$ map for bond extension since there is a larger increase in density behind the protons than there is in front of

them. This suggests that more density has been transferred to the region behind the protons upon bond extension than would normally have occurred if the density moved rigidly with the protons. Thus, the transfer of charge density following bond extension aids in the motion of the protons by placing density ahead of the moving nuclei. This same effect is apparent in the $\Delta\rho_D(\vec{x}_1)$ map for a bond contraction (Figure 1.4, Part (b)).

Bader and Bandrauk[89] have shown that the relaxation of the charge density in such a way as to aid the motion of the nuclei is directly reflected in an overall decrease in the force constant for the normal mode of vibration under consideration. In an effort to obtain a better understanding of how the relaxation of the charge density, accompanying the displacement of the nuclei from their equilibrium positions, affects the molecular force constant we will consider a theoretical analysis of the force constants for the normal vibrations, particularly the symmetric stretch vibration, for the methane molecule. It is possible to give a theoretical expression for the force constant which relates its magnitude to certain static properties of the equilibrium density and to the manner in which this charge density relaxes during a normal vibration. The contributions from the static density and from the change in the density to the force constant will be discussed and interpreted.

Methane, having tetrahedral symmetry, has nine normal modes; one with A_1 symmetry, a doubly degenerate set of E symmetry and two triply degenerate sets of T_2 symmetry. In a normal coordinate analysis, the potential energy of a system of nuclei relative to the equilibrium con-

figuration can be expanded as

$$V = \frac{1}{2} \sum_i k_i Q_i^2 \quad , \tag{1.56}$$

where the k_i are the appropriate harmonic force constants for the different normal modes which are represented by the normal coordinates Q_i. These harmonic force constants can be evaluated theoretically from a knowledge of the one-electron density distribution. A theoretical analysis of these normal mode force constants for the methane molecule is considered following closely the work of Salem[90], and Gerratt and Mills[91] for diatomic molecules using the Hellmann-Feynman theorem.

If we consider a system of electrons and nuclei, within the Born-Oppenheimer approximation, having a Hamiltonian operator H given by Equation (1.18) and an energy eigenfunction of this operator given by ψ, then the energy of the system is given by the expectation value

$$E = \langle \psi | H | \psi \rangle \quad , \tag{1.57}$$

where ψ is normalized to unity. Theoretically, the separate force constants, k_i, can be evaluated by taking the second partial derivative of the energy E with respect to the appropriate normal coordinate. This gives

$$k_i = (\partial^2 E / \partial Q_i^2) \quad , \tag{1.58}$$

where the partial derivative is taken at equilibrium.

The first derivative of E can be easily obtained with the aid of Hellmann-Feynman theorem[50]. From Equations (1.16) and (1.21) we have

$$\frac{\partial E}{\partial Q_i} = \langle \psi | \frac{\partial H}{\partial Q_i} | \psi \rangle = \frac{\partial V_N}{\partial Q_i} + \int \frac{\partial V_1}{\partial Q_i} \rho(\vec{x}_1) d\tau_1 \quad , \tag{1.59}$$

where V_N and V_1 are one-electron potential operators defined by Equation

(1.20). The equalities in these equations hold only if ψ is an exact eigenfunction of the Hamiltonian operator or the variable parameters in ψ have been fully optimized with respect to the normal coordinate. The force constant k_i is then given by

$$k_i = \left(\frac{\partial^2 E}{\partial Q_i^2}\right)_0 = \frac{\partial^2 V_N}{\partial Q_i^2}\bigg|_0 + \int \frac{\partial^2 V_1}{\partial Q_i^2}\,\rho(\vec{x}_1)\,d\tau_1\bigg|_0 + \int \frac{\partial V_1}{\partial Q_i}\,\frac{\partial \rho(\vec{x}_1)}{\partial Q_i}\,d\tau_1\bigg|_0 , \quad (1.60)$$

where $\rho(\vec{x}_1)$ is the one-electron density distribution defined by Equation (1.7). A similar expression to Equation (1.60) was obtained by Salem[90] for a diatomic molecule.

In order to evaluate the first term in Equation (1.60) for the methane molecule it is advantageous to work with symmetry coordinates instead of normal coordinates. The normal coordinates are related to these symmetry coordinates by a linear unitary transformation. The symmetry coordinates[92] are defined below, where the internal coordinates r_i = C-H_i distance and α_{ij} = <H_iCH_j are used and the numbering of the atoms in relation to the cartesian axies is shown in Figure 1.1.

$$S_1 = \frac{1}{2}(r_1 + r_2 + r_3 + r_4) . \quad (1.61)$$

$$S_{2a} = \frac{R}{2\sqrt{3}}(2\alpha_{12} + 2\alpha_{34} - \alpha_{13} - \alpha_{24} - \alpha_{32} - \alpha_{41}) .$$
$$S_{2b} = \frac{R}{2}(\alpha_{13} - \alpha_{32} + \alpha_{24} - \alpha_{41}) . \quad (1.62)$$

$$S_{3a} = \frac{1}{2}(r_1 + r_4 - r_2 - r_3) . \quad (1.63)$$

$$S_{4a} = \frac{R}{\sqrt{2}}(\alpha_{23} - \alpha_{14}) . \quad (1.64)$$

The other components of the three-fold degenerate coordinates S_3 and S_4 are obtianed by permuting the subscripts 2,3 and 4 on the internal coordinates in Equations (1.63) and (1.64) respectively. From these symmetry coordinates

the theoretical contributions to the force constants for the different normal modes can be obtained.

The actual theoretical contributions to the force constant for the symmetric stretch mode of A_1 symmetry, which involves the normal coordinate Q_1, can be easily worked out.* From Equation (1.60) we have

$$k_1 = \left(\frac{\partial^2 E}{\partial Q_i^2}\right)_0 = \frac{\partial^2 V_N}{\partial Q_1^2}\bigg|_0 + \int \frac{\partial^2 V_1}{\partial Q_1^2}\rho(\vec{x}_1)\,d\tau_1\bigg|_0 + \int \frac{\partial V_1}{\partial Q_1}\frac{\partial \rho(\vec{x}_1)}{dQ_1}\,d\tau_1\bigg|_0 \quad . \tag{1.65}$$

The normal coordinate Q_1 is equivalent to the symmetry coordinate S_1. Thus

$$Q_1 = \frac{1}{2}(r_1 + r_2 + r_3 + r_4) \quad . \tag{1.66}$$

Since Q_1 is a function of the internal coordinate r_i it is easily shown that

$$\frac{\partial^2 V_N}{\partial Q_1^2} = \sum_{i=1}^{4}\sum_{j=1}^{4}\frac{\partial r_i}{\partial Q_1}\frac{\partial r_j}{\partial Q_1}\frac{\partial^2 V_N}{\partial r_i \partial r_j} \tag{1.67}$$

and a similar expression is obtained for $(\partial^2 V_1/\partial Q_1^2)$. If all displacements r_i are assumed to be equivalent then it is easily shown that

$$\frac{\partial r_1}{\partial Q_1} = \frac{\partial r_2}{\partial Q_1} = \frac{\partial r_3}{\partial Q_1} = \frac{\partial r_4}{\partial Q} = \frac{1}{2} \quad , \tag{1.68}$$

and that

$$\begin{aligned} \frac{\partial^2 V_N}{\partial Q_1^2} &= \frac{\partial^2 V_N}{\partial r_1^2} + 3\frac{\partial^2 V_N}{\partial r_1 \partial r_2} \quad . \\ \frac{\partial^2 V_1}{\partial Q_1^2} &= \frac{\partial^2 V_1}{\partial r_1^2} + 3\frac{\partial^2 V_1}{\partial r_1 r_2} \quad . \end{aligned} \tag{1.69}$$

---

* Only the symmetric stretch mode is considered in detail in this thesis. The mathematical expressions required to analyze the force constant for an infra-red active T_2 mode have been worked out and are given in Appendix 8.

For the methane molecule the potentials V_N and V_1 are given by (see Equation (I.20))

$$V_N = \sum_{\alpha=1}^{4} \frac{6}{r_{c\alpha}} + \sum_{\alpha>\beta=1}^{4} \frac{1}{r_{\alpha\beta}} \tag{I.70}$$

and

$$V_1 = - \sum_{\alpha=1}^{4} \frac{1}{r_{1\alpha}} - \frac{6}{r_{1c}} , \tag{I.71}$$

where the summation over α and β are over the number of hydrogen atoms, $r_{1\alpha}$ is the distance between hydrogen atom α and electron one, r_{1c} is the distance between the carbon atom and electron one, $r_{c\alpha}$ is the C-H_α bond distance and $r_{\alpha\beta}$ is the H_α-H_β bond distance. Thus, the terms in Equation (I.69) are given by

$$\begin{aligned}
\frac{\partial^2 V_N}{\partial r_1^2} &= \sum_{\alpha=2}^{4} \frac{\partial^2}{\partial r^2} \left(\frac{1}{r_{\alpha 1}}\right) + \frac{\partial^2}{\partial r^2} \left(\frac{6}{r_{c1}}\right) . \\
\frac{\partial^2 V_N}{\partial r_1 \partial r_2} &= \frac{\partial^2}{\partial r_1 \partial r_2} \left(\frac{1}{r_{12}}\right) . \\
\frac{\partial^2 V_1}{\partial r_1^2} &= - \frac{\partial^2}{\partial r_1^2} \left(\frac{1}{r_{11}}\right) . \\
\frac{\partial^2 V_1}{\partial r_1 \partial r_2} &= 0 .
\end{aligned} \tag{I.72}$$

Substituting these expressions into the first two terms in Equation (I.65) one obtains

$$\begin{aligned}
\frac{\partial^2 V_N}{\partial Q_1^2}\bigg|_0 &= \frac{\partial^2 V_N}{\partial r_1^2}\bigg|_0 + 3 \frac{\partial^2 V_N}{\partial r_1 \partial r_2}\bigg|_0 \\
&= \sum_{\alpha=2}^{4} \frac{\partial^2}{\partial r_1^2} \left(\frac{1}{r_{\alpha 1}}\right)\bigg|_0 + \frac{\partial^2}{\partial r_1^2} \left(\frac{6}{r_{c1}}\right)\bigg|_0 + 3 \frac{\partial^2}{\partial r_1 \partial r_2} \left(\frac{1}{r_{12}}\right)\bigg|_0 ,
\end{aligned} \tag{I.73}$$

and

$$\int \frac{\partial^2 V_1}{\partial Q_1} \rho(\vec{x}_1) d\tau_1 \Big|_0 = \int \frac{\partial^2 V_1}{\partial r_1^2} \rho(\vec{x}_1) d\tau_1 \Big|_0 + 3 \int \frac{\partial^2 V_1}{\partial r_1 \partial r_2} \rho(\vec{x}_1) d\tau_1 \Big|_0$$

$$= - \int \frac{\partial^2}{\partial r_1^2} \left(\frac{1}{r_{11}}\right) \rho(\vec{x}_1) d\tau_1 \Big|_0 . \qquad (1.74)$$

All the terms required in Equations (1.73) and (1.74) have been evaluated for the equilibrium configuration for the methane molecule using the derived density distribution. These terms are given by the following expressions.

$$\sum_{\alpha=2}^{4} \frac{\partial^2}{\partial r_1^2} \left(\frac{1}{r_{\alpha 1}}\right) \Big|_0 = 9\sqrt{3}/16\sqrt{2}\ R^3 . \qquad (1.75)$$

$$\frac{\partial^2}{\partial r_1} \left(\frac{6}{r_{c1}}\right) \Big|_0 = 12/R^3 . \qquad (1.76)$$

$$3 \frac{\partial^2}{\partial r_1 \partial r_2} \left(\frac{1}{r_{12}}\right) \Big|_0 = 15\sqrt{3}/16\sqrt{2}\ R^3 . \qquad (1.77)$$

In these expressions R is the equilibrium C-H bond distance.

$$\int \frac{\partial^2}{\partial r_1^2} \left(\frac{1}{r_{11}}\right) \rho(\vec{x}_1) d\tau_1 \Big|_0 = \int \frac{(3\cos^2\theta_{H_1} - 1)}{r_{H_1}^3} \rho(\vec{x}_1) d\tau_1 - \frac{4\pi}{3} \rho_o(H_1) , \qquad (1.78)$$

where $\rho_o(H_1)$ is the density evaluated right at the hydrogen nucleus H_1.

Thus, the force constant k_1 for the symmetric stretch normal mode of vibration is given by

$$k_1 = (24\sqrt{2} + 3\sqrt{3})/2\sqrt{2}\ R^3 - \int \frac{(3\cos^2\theta_{H_1} - 1)}{r_{H_1}^3} \rho(\vec{x}_1) d\tau_1 + \frac{4\pi}{3} \rho_o(H_1)$$

$$+ \int \frac{\partial V_1}{\partial Q_1} \frac{\partial \rho(\vec{x}_1)}{\partial Q_1} d\tau_1 . \qquad (1.79)$$

The first term in this equation is a nuclear field gradient term G^N, which

depends only on the nuclear configuration. This term is easy to evaluate and has the value

$$G^N = (24\sqrt{2} + 3\sqrt{3})/2\sqrt{2}\ R^3 = 1.57891 \text{ a.u.} \tag{1.80}$$

The second term is an electronic field gradient term which arises from the static charge distribution $\rho(\vec{x}_1)$ as the nuclei are allowed to move. This term has already been evaluated in determining the electric field gradient at the proton (see Section 1.4, Part (d)) and it has the value given by

$$G^e = -q_e = \int \frac{(3\cos^2\theta_{H_1} - 1)}{r_{H_1}^3} \rho(\vec{x}_1) d\tau_1 = 1.14934 \tag{1.81}$$

The third term is an electronic field gradient term arising from the density situated right at the hydrogen nucleus H_1 [89]. The numerical value of this term is

$$4\pi\rho_o(H_1)/3 = 2.10387 \text{ a.u.} \tag{1.82}$$

These three terms are determined by the equilibrium properties of the charge distribution. The final term in Equation (1.79) is often referred to as a "relaxation" term[89,91]. It represents the field gradient generated by the electronic charge following the motions of the nuclei as they are allowed to move, thereby leading to a lowering of the otherwise large energy increase obtained for the displacement of the nuclei in a rigid charge distribution[93]. This term is not easy to evaluate directly by any theoretical means for a polyatomic molecule since it requires one to know how the density changes upon molecular vibration. The value of this term has been evaluated in the present work by using the experimental force constant for the symmetric stretch normal vibration.

The experimental force constants for methane have been obtained

by Jones and McDowell[94]. Using their notation and the values they give for the methane force constants, the force constant for the A_1 mode is

$$k_1 = F_r + 3F_{rr} = 5.867 \text{ milli dynes/A}$$
$$= 0.37688 \text{ a.u.} \qquad (1.83)$$

Using this experimental result the "relaxation term" can be evaluated as

$$\int \frac{\partial V_1}{\partial Q_1} \frac{\partial \rho(\vec{x}_1)}{\partial Q_1} d\tau_1 = k_1 + G^e - G^N - \frac{4\pi}{3} \rho_o(H_1) = -2.15656 \text{ a.u.} \qquad (1.84)$$

Thus, the "relaxation term" contributes a negative quantity to the overall force constant, as can be shown to always be the case for diagonal force constants. This follows from the fact that there is a one to one correspondence between the "relaxation term" obtained in the present Hellmann-Feynman approach and the term

$$2 \sum_k \frac{\langle \psi_k | \sum_{i=1}^{n} \partial^2 V_i / \partial Q_1^2 | \psi \rangle^2}{E - E_k}$$

obtained by Byers Brown[95] using perturbation theory, where the ψ_k represent the complete set of excited electronic states for the equilibrium nuclear configuration and V_i is given by Equation (I.20). This term, which is for a diagonal force constant, is always negative.

The "relaxation term" almost cancels completely the $4\pi\rho_o(H_1)/3$ term, a result which has been noted by Salem[90] and Schwendeman[96] for force constants expressed in the form of Equation (I.79). Since we are dealing here only with the force constant at a proton the cancellation is not as obvious as in the case of determining the force constant at a heavy nucleus such as that of nitrogen where the third and fourth terms for the force constant are much larger. As a matter of fact, Bader and Bandrauk[89] have

shown that for a simple diatomic molecule AB there is a complete cancellation of terms of the form

$$-\int \frac{\partial V_1}{\partial X_A} \frac{\partial \rho(\vec{x}_1)}{\partial X_A} d\tau_1 = \frac{4}{3}\pi\rho_o(A) - \int \frac{(3\cos^2\theta_A - 1)}{r_A^3} \rho(\vec{x}_1) d\tau_1 \qquad (1.85)$$

when the density $\rho(\vec{x}_1)$ follows rigidly the displacement of nucleus A with nucleus B held fixed. In Equation (1.85) X_A is the displacement coordinate of nucleus A. In our polyatomic system if the density around the protons in methane rigidly followed the nuclear displacements of the hydrogens accompanying the normal A_1 vibration then one would expect a complete cancellation of the terms $-G^e$ and $4\pi\rho_o(H_1)/3$ with the "relaxation term". The actual result is

$$G_T^e = -G^e + \frac{4\pi}{3}\rho_o(H_1)/3 + \int \frac{\partial V_1}{\partial Q_1} \frac{\partial \rho(\vec{x}_1)}{\partial Q_1} d\tau_1 = -1.20203 \text{ a.u.} \qquad (1.86)$$

The quantity expressed by G_T^e is the total electronic contribution to the force constant, the nuclear contribution being G^N. Since G_T^e is negative and not zero the charge density does not rigidly follow the motion of protons but relaxes in such a manner that the electronic contribution decreases the overall force constant k_1.

It has been shown in the $\Delta\rho_D(\vec{x}_1)$ contour plots (Figure 1.4) that the charge density does not rigidly follow the motion of the protons during a normal vibration but relaxes in such a manner that it aids in the motion of the nuclei. Electronic charge is built up ahead of the moving nuclei thus leading to a decrease in the overall force constant for the vibration. It is this relaxation of the charge density that is mainly responsible for the large negative value of the "relaxation term" and thus for its corresponding reduction in the force constant k_1. This force constant analysis

clearly indicates the crucial role played by the change in the one-electron charge distribution in lowering the otherwise large increase in energy of the system when the nuclei are displaced from their equilibrium positions.

In conclusion, the "best" one-electron density distribution for the equilibrium configuration of methane has been determined by requiring this distribution to give zero forces on the nuclei and the correct expectation value for the diamagnetic proton magnetic shielding. This charge distribution was shown to give excellent one-electron properties and a very acceptable energy (a two-electron property). The distribution was used to show that the chemical binding in methane is mainly the result of a large accumulation of charge along the C-H bond axies which makes the molecule electrostatically more stable than the separated atoms. It is the almost spherical shape of the total charge density $\rho(\vec{x}_1)$ which accounts for the methane molecule being very unreactive. The theoretical analysis of the force constant for the A_1 mode indicates that the relaxation of the charge density accompanying a normal vibration aids in the motion of the nuclei and thus leads to a decrease in the overall force constant.

II. PAULI REPULSIONS AND MOLECULAR GEOMETRY

2.1. Introduction

In Chapter I a one-electron density distribution for methane was obtained using only one-electron properties of the system. Using this method it is not necessary to calculate the energy in order to derive the required wavefunction. It is the long arduous task of calculating the energy integrals (namely, the two-electron integrals) that makes the SCF procedure for polyatomic molecules very cumbersome. This difficulty is bypassed by using the present electrostatic method since only one-electron integrals need be calculated. This electrostatic approach not only produced a one-electron density distribution for methane that predicted good one-electron properties but also gave a charge distribution with a very acceptable total molecular energy (a two-electron property).

It is hoped that other similar electrostatic methods can be developed for polyatomic systems which can be used to determine the relative stability of model molecular charge distributions. In this section a theoretical method, which allows one to determine the effect of the Pauli exclusion principle on the one-electron density distribution, is considered and an electrostatic approach, involving the concept of a binding region, is proposed to account for the observed molecular geometries in polyatomic molecules.

Gillespie and Nyholm[2] have advanced a theory of molecular geometry "on the idea that the arrangement of all electron pairs (bonding pairs and lone pairs) in the valency shell of the central atom is determined by the

operation of the Pauli exclusion principle". The molecular geometry, which is directly dependent on the three-dimensional charge distribution, is thus related to "Pauli repulsions" between pairs of electrons in either bond or lone pair orbitals. Since lone pairs of electrons are assumed to be associated only with one nucleus they are considered to occupy a more diffuse orbital than bonding electron pairs, which encompass at least two nuclei. For this reason lone pair-lone pair repulsions are assumed larger than lone pair-bond repulsions which in turn are more important than bond-bond repulsions. "Pauli repulsions", when applied in this manner, will be given a theoretical basis in this chapter.

The Pauli principle in its most general form demands that a wave-function be antisymmetric with respect to permuting the space and spin coordinates of all the electrons present in the system. Or alternatively, within the orbital approximation, the Pauli principle is satisfied if no more than two electrons with opposite spin are placed in any one space orbital taken from an orthogonal basis set. The important feature for the present discussion is that the Pauli principle demands that the set of orbitals, atomic or molecular, used to describe the system be orthogonal,

$$\langle \phi_i | \phi_j \rangle = \delta_{ij} \ . \qquad (2.1)$$

Thus for a system of n electrons requiring a minimal set of n/2 space orbitals (or (n+1)/2 if n is odd), the Pauli principle is in reality an orthogonality restraint imposed in an (n/2)- or ((n+1)/2)-dimensional mathematical space. This is the source of confusion regarding "Pauli repulsions" which are treated as occurring in the three-dimensional physical space of the molecular system. To state that the Pauli principle

gives rise to repulsions between filled orbitals in three-dimensional space is not the same as requiring these orbitals to be orthogonal in the many-dimensional space required to define the orbitals. The only function of the electronic coordinates which can be pictured in three-dimensional space is the one-electron density distribution, not the orbitals. Thus to determine what effect the Pauli principle has on the molecular shape or the electronic arrangement in physical space, one must ask the question, "what effect does the requirement of orthogonality of the orbitals in the many-dimensional orbital space have on the one-electron density distribution in three-dimensional space?" The answer to this problem is not obvious and does not in general follow from pictures of "colliding" orbitals in physical space. It is possible to formulate a technique which does show the effect of the orthogonality requirements of the Pauli principle on the three-dimensional one-electron density distribution. This method will be illustrated with a number of examples.

2.2 Pauli Repulsions Present in the Approach of Two Helium Atoms

The one-electron density distribution, which is the probability of finding electronic charge at some point in real three-dimensional space, is given by Equation (1.7). For a molecule in a stationary state, this one-electron density distribution can be interpreted as a static distribution of negative charge, rather than as a probability function. Within an orbital approximation to a wavefunction, the one-electron density has the very simple form (see Equation (1.11))

$$\rho(\vec{x}_1) = \sum_i n_i \phi_i \phi_i \ , \tag{2.2}$$

where the ϕ_i's are an orthogonal set of orbitals and the n_i's are the

orbital occupation numbers.

For a system described by an orthogonal set of orbitals there are no Pauli repulsion effects since the Pauli principle is satisfied. The effect of the Pauli principle on a wavefunction or density can be determined by first considering a system described by a set of orbitals which are orthogonal because of some restraint. This restraint may be artificial or be the result of a large separation between the orbitals. Then the effects of the nonorthogonality (i.e., "Pauli repulsions") are determined when the restraint is removed. Consider, for example, the effects of the Pauli exclusion principle on the electron density distribution obtained when two helium atoms approach one another. Let ϕ_a and ϕ_b be doubly occupied atomic orbitals on the two atoms a and b respectively. At a large separation of the atoms the overlap between the orbitals is zero and the one-electron density is then simply

$$\rho_o(\vec{x}_1) = 2(\phi_a^2 + \phi_b^2) \quad . \tag{2.3}$$

At small values of the internuclear separation this same expression would hold for the density if the orbitals did not overlap. But in reality this is not the case since the orbitals do overlap and thus, the Pauli exclusion principle demands the corrected form of the density

$$\rho(\vec{x}_1) = \rho_o(\vec{x}_1) + \Delta\rho_p(\vec{x}_1) \quad . \tag{2.4}$$

The quantity $\Delta\rho_p(\vec{x}_1)$ is the change in the one-electron density which arises from the orthogonality requirements of the Pauli exclusion principle. Longuet-Higgins and Salem*,[97] have shown that when $\rho(\vec{x}_1)$ is expressed in

---

* The general theorem for $\Delta\rho_p(\vec{x}_1)$ was contributed by H.C. Longuet-Higgins.

the form of Equation (2.4), $\Delta\rho_p(\vec{x}_1)$ has the form

$$\Delta\rho_p(\vec{x}_1) = -4S\phi_a\phi_b + 2S^2(\phi_a^2 + \phi_b^2) \ , \tag{2.5}$$

where S is the overlap between ϕ_a and ϕ_b. Expression (2.5) for $\Delta\rho_p(\vec{x}_1)$ is correct to the order S^2 and goes to zero as S goes to zero. From this expression it is seen that there exist regions where $\Delta\rho_p(\vec{x}_1)$ is negative, giving a total density $\rho(\vec{x}_1)$ that is less than that of the original atomic densities, and regions where $\Delta\rho_p(\vec{x}_1)$ is positive, giving a total density which is greater than the original atomic densities. Since, by definition, the integration of $\rho(\vec{x}_1)$ over all space must yield the total number of electrons, four in this case, and this is given by the integration of $\rho_o(\vec{x}_1)$ itself it follows that the integration over $\Delta\rho_p(\vec{x}_1)$ must yield zero,

$$\int \Delta\rho_p(\vec{x}_1)\, d\tau_1 = 0 \ . \tag{2.6}$$

The positive and negative regions of $\Delta\rho_p(\vec{x}_1)$ exactly balance so that the decrease in density in certain regions from the value given by $\rho_o(\vec{x}_1)$ must be equal to the increase over the $\rho_o(\vec{x}_1)$ values in other regions. The quantity $\Delta\rho_p(\vec{x}_1)$ thus gives a three-dimensional picture of the charge density which is transferred relative to the original set of orbitals because of the operation of the Pauli exclusion principle. In this simple example where ϕ_a, ϕ_b and S are all positive, the expression for $\Delta\rho_p(\vec{x}_1)$ shows that charge of the total amount $4S\phi_a\phi_b$ must be removed from regions where the orbitals overlap and transferred to regions where ϕ_a^2 and ϕ_b^2 are large. A contour plot of $\Delta\rho_p(\vec{x}_1)$ in the molecular plane for two He atoms at an internuclear separation of 2.5 a.u. is given in Figure 2.1. This plot shows dramatically the operation of the Pauli exclusion principle on two over-

Figure 2.1. A contour plot of $\Delta\rho_p(\vec{x}_1)$ for two He atoms at an internuclear separation of 2.5 atomic units (a.u.). The solid and dashed contours represent positive and negative $\Delta\rho_p(\vec{x}_1)$ values respectively. The dotted lines through the nuclei are the boundary curves which separate the binding and antibinding regions.

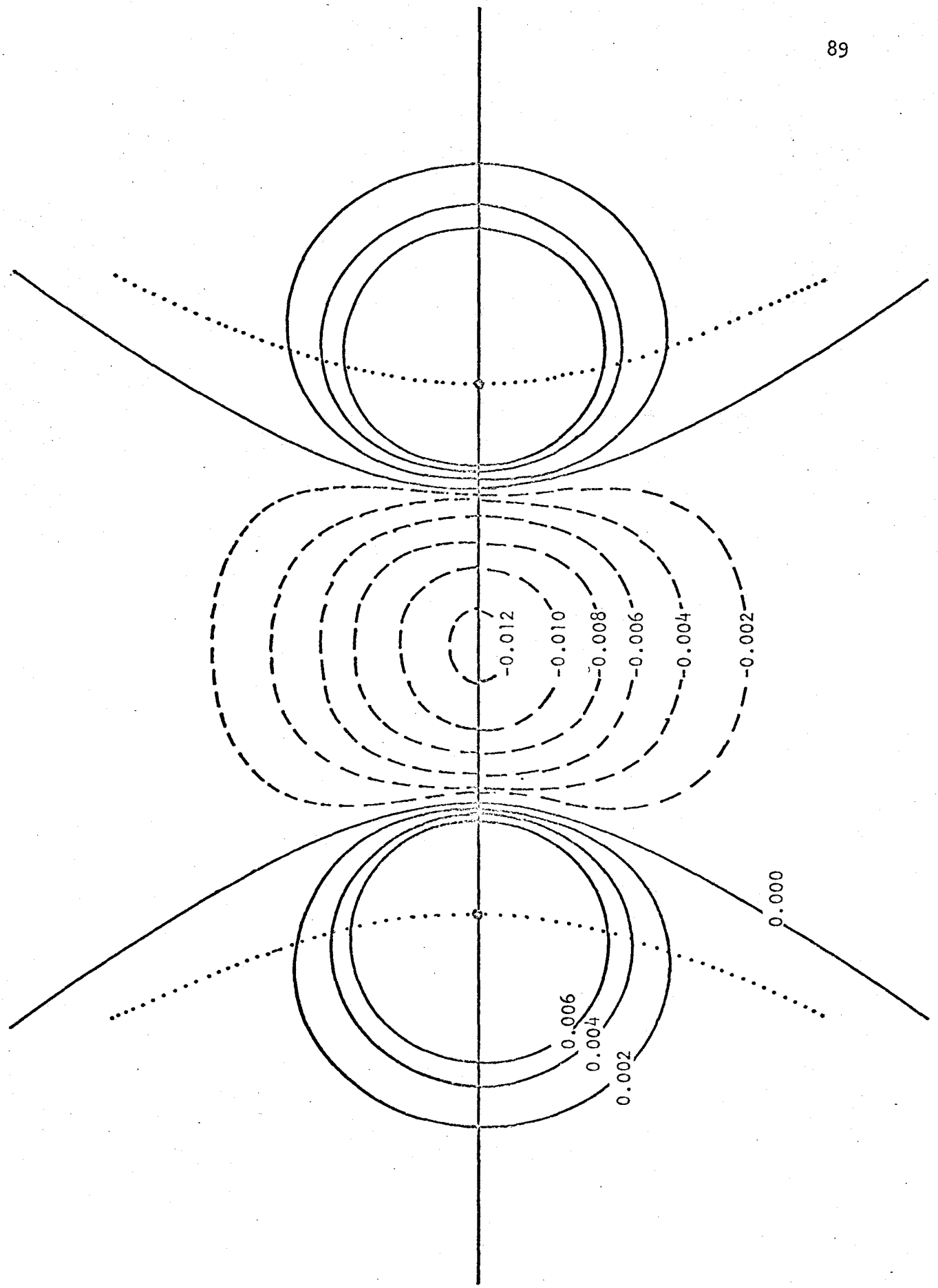
-0.012
-0.010
-0.008
-0.006
-0.004
-0.002
0.000
0.006
0.004
0.002

lapping, doubly filled orbitals, or if one wishes, the effect of Pauli repulsions. In the internuclear region, where the overlap of the original atomic orbitals is large, $\Delta\rho_p(\vec{x}_1)$ is negative showing that electron density has been forced to migrate away from this region. The density is transferred to regions behind each nucleus, where $\Delta\rho_p(\vec{x}_1)$ is positive. The region between the nuclei is one of low potential energy, and is the region where charge density must be concentrated to achieve a stable chemical bond and electrostatic equilibrium. This is the origin of the Pauli repulsions. The operation of the Pauli exclusion principle requires that density be removed from the region of low potential energy and be placed in less favoured regions. The electronic energy is thus raised above that of the separated atoms and a repulsive force results. Thus while there are no Pauli repulsive forces as such, the Pauli exclusion principle does place restraints on the distribution of the electronic charge and this in turn determines the electronic energy of the system.

The energy, since it is determined by the second-order or two-electron probability distribution[98], is not simply related to the one-electron density distribution. However, the forces acting on the nuclei are explicable in terms of classical electrostatics and are determined from the one-electron density distribution by the application of the Hellmann-Feynman theorem[50] (see page 13 of this thesis). Therefore, the change in stability brought about by the charge which is transferred as a result of the Pauli principle is best discussed in terms of the forces acting on the nuclei. Consider, for example, the case of the two He atoms. By applying Gauss' theorem it is easily shown that for any finite value of internuclear

separation the density distribution obtained from the overlap of the original spherical atomic densities, $\rho_o(\vec{x}_1)$, results in a net force of repulsion on both nuclei (see footnote on page 62 of this thesis). According to Berlin[87] one can define a region, called the binding region, in which charge must be concentrated to overcome the nuclear forces of repulsion and achieve electrostatic equilibrium in a diatomic molecule. The boundary curves separating the binding region from the antibinding regions are indicated by the dotted lines on Figure 2.1 for the homonuclear diatomic molecule. Any charge density placed between the two boundary curves exerts an attractive force on both nuclei pulling them together. Any charge placed outside these two curves exerts a greater force on one nucleus than on the other and leads to a separation of the molecule into atoms. Charge density on the boundary curve exerts equal forces on both nuclei along the bond axis. From Figure 1.2 it is evident that $\Delta\rho_p(\vec{x}_1)$ is primarily negative in the binding region between the nuclei and positive in the antibinding regions behind the nuclei. Since the sum of the original atomic densities, $\rho_o(\vec{x}_1)$, does not bind the nuclei, the density transferred because of the operation of the Pauli exclusion principle, $\Delta\rho_p(\vec{x}_1)$, will clearly result in an even larger force of repulsion on both nuclei. This follows from the fact that the change in density $\Delta\rho_p(\vec{x}_1)$ leads to a decrease in electronic charge in the binding region over that present in the original atomic distribution $\rho_o(\vec{x}_1)$. The atomic distribution itself has insufficient charge in the binding region to balance the forces of nuclear repulsion and as such is unstable. The result is the final density $\rho(\vec{x}_1)$ is less stable than the original atomic density, $\rho_o(\vec{x}_1)$.

In this simple example of two He atoms, the form of $\Delta\rho_p(\vec{x}_1)$ fits in well with the concept of "Pauli repulsions" as they are usually applied[2]. In a sense the orbitals do appear to "collide". However, it should be remembered that the resulting instability is an electrostatic one, resulting from the forced migration of charge from the binding region and the consequent increase in the nuclear forces of repulsion. The analogy of $\Delta\rho_p(\vec{x}_1)$ with that of colliding orbitals in real three-dimensional space breaks down when one considers more complicated examples with more orbitals.

The theoretical expression for $\Delta\rho_p(\vec{x}_1)$[97] and the concept of a binding region[88] can be extended to a polyatomic system. For any molecular system we can first determine $\Delta\rho_p(\vec{x}_1)$, the charge which is transferred because of the Pauli principle, and secondly, determine what effect this transfer has on the stability of the system by noting whether or not it corresponds to an accumulation in the binding region. The general expression for $\Delta\rho_p(\vec{x}_1)$ for doubly occupied orbitals is[97]

$$\Delta\rho_p(\vec{x}_1) = \sum_{i<j} (-4S_{ij}\phi_i\phi_j + 2S_{ij}^2(\phi_i^2 + \phi_j^2)) \qquad (2.7)$$

and the total density is given by

$$\rho(\vec{x}_1) = 2 \sum_i \phi_i\phi_i + \Delta\rho_p(\vec{x}_1) \ . \qquad (2.8)$$

There is a contribution to $\Delta\rho_p(\vec{x}_1)$ from every pair of overlapping orbitals which is identical in form to that obtained for the two He atoms. The form of $\Delta\rho_p(\vec{x}_1)$ is determined by the initial choice for the set of orbitals ϕ_i. If they are chosen as an orthogonal set, then $\Delta\rho_p(\vec{x}_1)$ is zero at every point in space. However, in discussions of chemical bonding, comparisons between different systems are often employed, either between the separated atoms

and the molecule or between different members of an isoelectronic series. For example, we may consider the classic ten-electron Ne atom and what effect the Pauli principle has on the relationship between its one-electron density distribution and that of the isoelectronic hydride molecules H_2O, NH_3 and CH_4.

2.3 An Analysis of the Assumed Pauli Repulsions in H_2O and NH_3

In Chapter I (see page 6 of this thesis) it has been indicated that the electron density in molecules such as H_2O and NH_3, which have four pairs of electrons in their valency shell, was previously[42] thought to be directly related to the tetrahedral hybridization (sp^3) of Ne and thus one could account for the nearly tetrahedral bond angles in H_2O and NH_3. Gillespie and Nyholm[2], in their original paper, also considered the orbital descriptions of H_2O and NH_3 to be sp^3 and related to that of Ne. By postulating that the repulsions between the lone pair and bond orbitals is greater than those between the bond orbitals themselves they accounted for the fact that the bond angle in NH_3 is slightly less than the tetrahedral angle. Similarly in the case of H_2O, the larger lone pair-lone pair "repulsion" causes an even greater decrease in the basic tetrahedral angle between the bonding pairs. In both these examples the important assumptions are the essentially tetrahedral arrangement of the electron pairs and the effect of the Pauli repulsions on these pairs as the original equality of the orbitals in the basic Ne structure is perturbed by the change in the number of bonded protons. The physical basis of the "repulsion theory" can be investigated by first determining $\Delta\rho_p(\vec{x}_1)$ and comparing this with the assumed repulsions between the orbitals, and secondly, by

determining the stability of the tetrahedral density arrangement by means of the concept of a binding region. It will be shown that the polarizations made necessary by the presence of the protons are indeed of crucial importance.

The one-electron density (ignoring the inner 1s electrons) in Ne is given by

$$\rho(\vec{x}_1) = 2 \sum_{i=1}^{4} \phi_i \phi_i \ , \tag{2.9}$$

where each ϕ_i may be considered as an sp^3 hybrid orbital. These form an orthogonal set and $\Delta\rho_p(\vec{x}_1)$ is zero. The density $\rho(\vec{x}_1)$ is of course spherical. The effects of perturbing this density distribution by extracting three protons from the Ne nucleus, one into each of three of the sp^3 hybrids, to form a tetrahedral NH_3 molecule will be considered. The presence of protons destroys the orthogonality between the original Ne orbitals and the resulting change in density $\Delta\rho_p(\vec{x}_1)$ will be directly determined by the effects of the Pauli exclusion principle arising from this nonorthogonality. The final molecular density distribution for tetrahedral NH_3 expressed in terms of equivalent orbitals is

$$\rho(\vec{x}_1) = 2(\phi_\ell^2 + \phi_{b1}^2 + \phi_{b2}^2 + \phi_{b3}^2) + \Delta\rho_{p\ell b}(\vec{x}_1) + \Delta\rho_{pbb}(\vec{x}_1) \ , \tag{2.10}$$

where ϕ_ℓ is an original unperturbed Ne orbital (the lone pair) and the ϕ_{bi} are bonding orbitals of the form*

$$\phi_{bi} = \lambda[(1/2)2s + (\sqrt{3}/2)P_i] + \mu h_i \ , \tag{2.11}$$

---

* The atomic orbitals employed in the calculations of the density distributions are Slater functions. It has been shown[88] that the use of Slater functions rather than the Hartree-Fock expressions does not alter the appearance or the general characteristics of the calculated one-electron density plots.

λ/μ being a polarity factor and P_i a nitrogen 2p orbital directed at the hydrogen orbital h_i. The term in square brackets defines an sp^3 orbital. The λ/μ ratio must be close to unity to obtain the correct order of magnitude for the molecular dipole moment[84] and was taken as one in the present calculations for NH_3. In any event, the variation of this ratio over a wide range of reasonable values does not alter the conclusions discussed below. Since the total change in density $\Delta\rho_p(\vec{x}_1)$ required by the Pauli exclusion principle is constructed of terms from pairs of overlapping orbitals, it can be divided into separate contributions, one resulting from the lone pair orbital overlapping with the bonding orbitals and one resulting from the bond orbitals overlapping with each other. By this procedure the lone pair-bond "repulsions" and the bond-bond "repulsions" can be determined individually. Thus, the two change in density terms in Equation (2.10) arising from these separate "repulsions" have the forms

$$\Delta\rho_{p\ell b}(\vec{x}_1) = -4S_{\ell b}(\Sigma_i \phi_\ell \phi_{bi}) + 2S^2_{\ell b}(\Sigma_i(\phi^2_\ell + \phi^2_{bi})) \tag{2.12}$$

$$\Delta\rho_{pbb}(\vec{x}_1) = -4S_{bb}(\Sigma_{i<j} \phi_{bi}\phi_{bj}) + 2S^2_{bb}(2\Sigma_i \phi^2_{bi}) , \tag{2.13}$$

where $S_{\ell b}$ and S_{bb} are the overlap integrals between the lone pair orbital and bond orbital and between two bond orbitals respectively.

In Figure 2.2 is shown a contour plot of $\Delta\rho_{p\ell b}(\vec{x}_1)$ for the tetrahedral NH_3 molecules. Clearly the charge migration which results from the finite overlap of the lone pair and bonding orbitals corresponds to a depletion in the density above the N nucleus and to its accumulation below, between the three hydrogen nuclei. The direction of charge migration is easy to understand in terms of the nonorthogonalities. Since the nitrogen

Figure 2.2. A contour plot of the density shift, $\Delta\rho_{p\ell b}(\vec{x}_1)$, resulting from the interaction of the lone pair orbital with the bonding orbitals in tetrahedral NH_3. This and the subsequent diagrams for ammonia are plotted in the plane parallel to the three-fold symmetry axis and along an N-H bond. The vertical line is the three-fold symmetry axis and the line joining the two points (the positions of the nuclei) is the N-H bond.

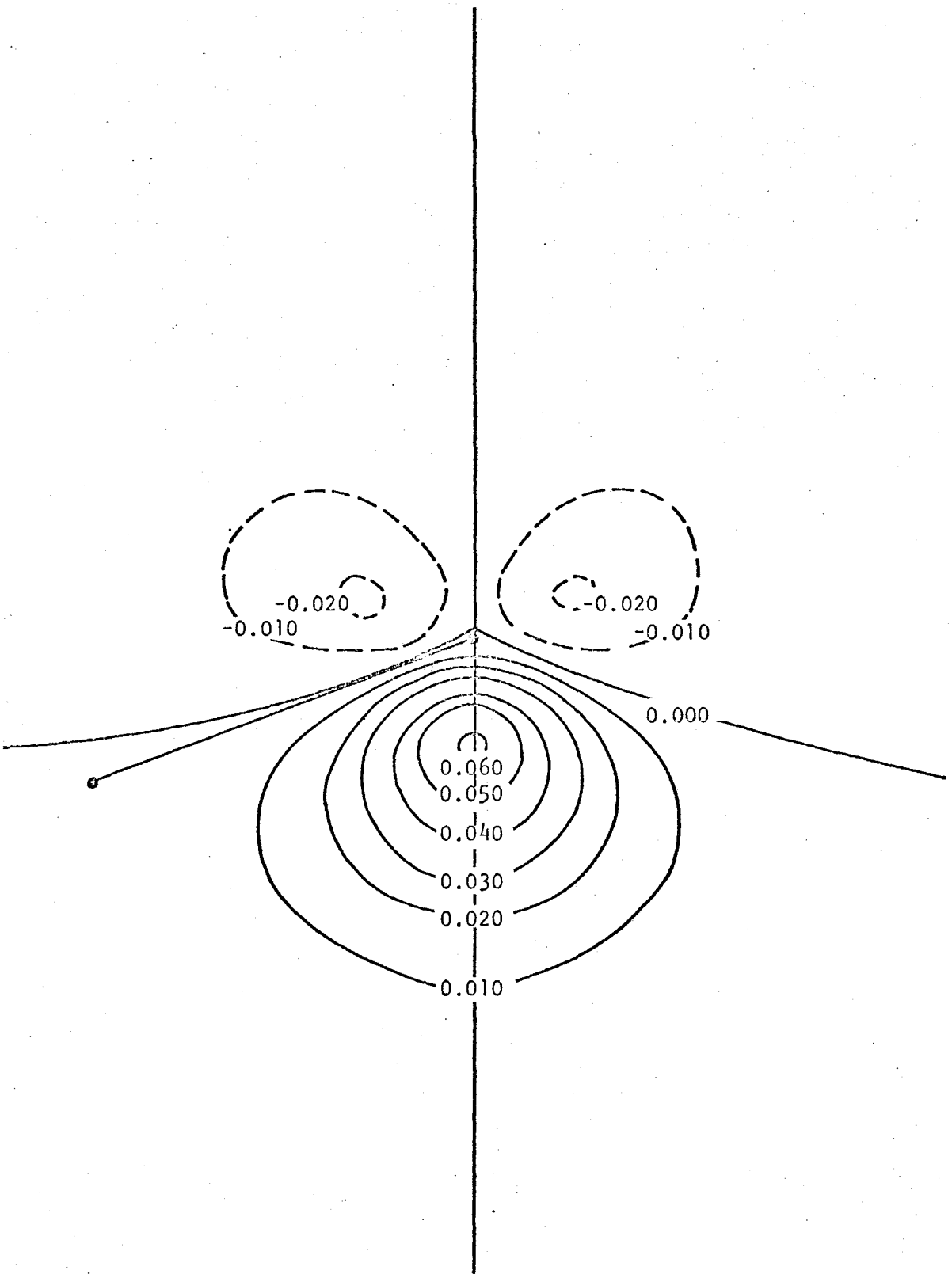
-0.020
-0.010
-0.020
-0.010
0.000
0.060
0.050
0.040
0.030
0.020
0.010

sp^3 orbital contributions to the ϕ_{bi} are still orthogonal to the sp^3 orbital which comprises ϕ_ℓ, the whole of $S_{\ell b}$ arises from the overlap of ϕ_ℓ with only the hydrogen orbitals in the ϕ_{bi}. Thus

$$S_{\ell b} = \mu[(1/2)S_2 - (1/2\sqrt{3})S_3] \ , \tag{2.14}$$

where S_2 and S_3 are respectively the overlap integrals of a 2s and a 2p orbital on nitrogen with a hydrogen orbital. $S_{\ell b}$ for the tetrahedral NH_3 molecule equals +0.06381. Since $S_{\ell b}$ is positive, the first set of terms in Equation (2.12) will decrease the density where the product $\phi_\ell\phi_{bi}$ is positive and increase it where this product is negative. The orbital ϕ_ℓ, since it has a 2p orbital contribution, is positive above the nitrogen and negative below it. The second term in $\Delta\rho_{p\ell b}$ is positive in all regions.

A contour plot of $\Delta\rho_{pbb}(\vec{x}_1)$, the density which is transferred because of the nonorthogonality between the bonding orbitals, is given in Figure 2.3. The migration of charge in this plot is close to the reverse of that found in the $\Delta\rho_{p\ell b}(\vec{x}_1)$ plot, as it shows a decrease in density in the region below the N nucleus and its concentration above. The bond-bond interaction is greater than the bond-lone pair interaction, however, since the value of S_{bb} (0.1284) is greater than that of $S_{\ell b}$. The nonorthogonality between the bonding orbitals is again entirely because of the hydrogens,

$$S_{bb} = \mu^2 S_1 + \lambda\mu[(1/2)S_2 - (1/2\sqrt{3})S_3] \ . \tag{2.15}$$

The first term in this expression arises from the overlap of two hydrogen orbitals and the second from the overlap of the hydrogen in one bonding orbital with the sp^3 hybrid from another. The bonding orbitals will over-

Figure 2.3. A contour plot of the density shift, $\Delta\rho_{pbb}(\vec{x}_1)$, resulting from the bond-bond interactions in tetrahedral NH_3.

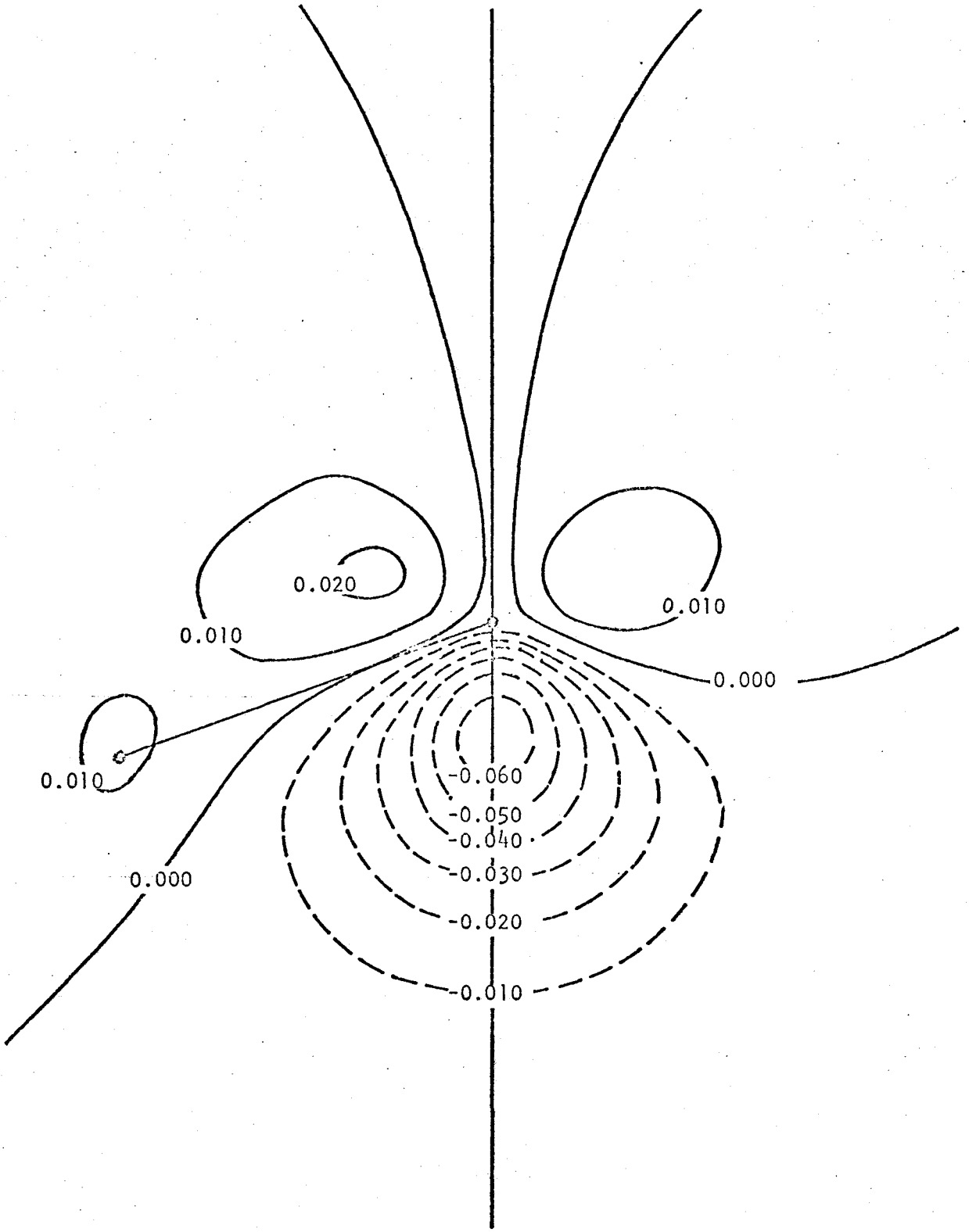
0.020
0.010
0.010
0.000
0.010
0.000
-0.060
-0.050
-0.040
-0.030
-0.020
-0.010

lap one another most strongly in the region between all four nuclei and thus $\Delta\rho_{pbb}(\vec{x}_1)$ is negative in this region. The net result of the lone pair-bond and bond-bond overlaps is shown in Figure 2.4 which is a contour plot of the total charge migration $\Delta\rho_p(\vec{x}_1)$ as determined by the orthogonality requirements of the Pauli principle. Charge density is removed from above and below the N nucleus along the three-fold symmetry axis and is concentrated in the region of each hydrogen nucleus. Figure 2.4 thus shows the effect of the Pauli exclusion principle on the three-dimensional one-electron density distribution for the NH_3 molecule when this distribution is related to an idealized tetrahedral one. The question now to be asked is whether the form of $\Delta\rho_p(\vec{x}_1)$ is such that it will lead to a decrease in the tetrahedral bond angle. In order that the bond angle decrease, electron density must be concentrated in the region below the nitrogen nucleus, between the three hydrogen nuclei. Such a charge migration would exert attractive forces on the three protons, drawing them together. The form of $\Delta\rho_p(\vec{x}_1)$ does not meet this requirement. There is a greater amount of charge placed above the proton along the N-H bond axis than below it and the charge is depleted in the region between all four nuclei. Thus, one finds that the basic assumptions of the electron pair repulsion theory are not met. The interactions between the bonding orbitals are larger than those involving the lone pair orbitals, and the overall migration of the charge density resulting from the "Pauli repulsions" is such as to lead to an increase rather than the predicted decrease in the tetrahedral bond angle.

The application of this type of theoretical analysis to the water molecule leads to similar conclusions. Consider, for example, the one-

Figure 2.4. A contour plot of the total charge migration, $\Delta\rho_p(\vec{x}_1)$, required by the Pauli exclusion principle for tetrahedral NH_3 with sp^3 hybridization.

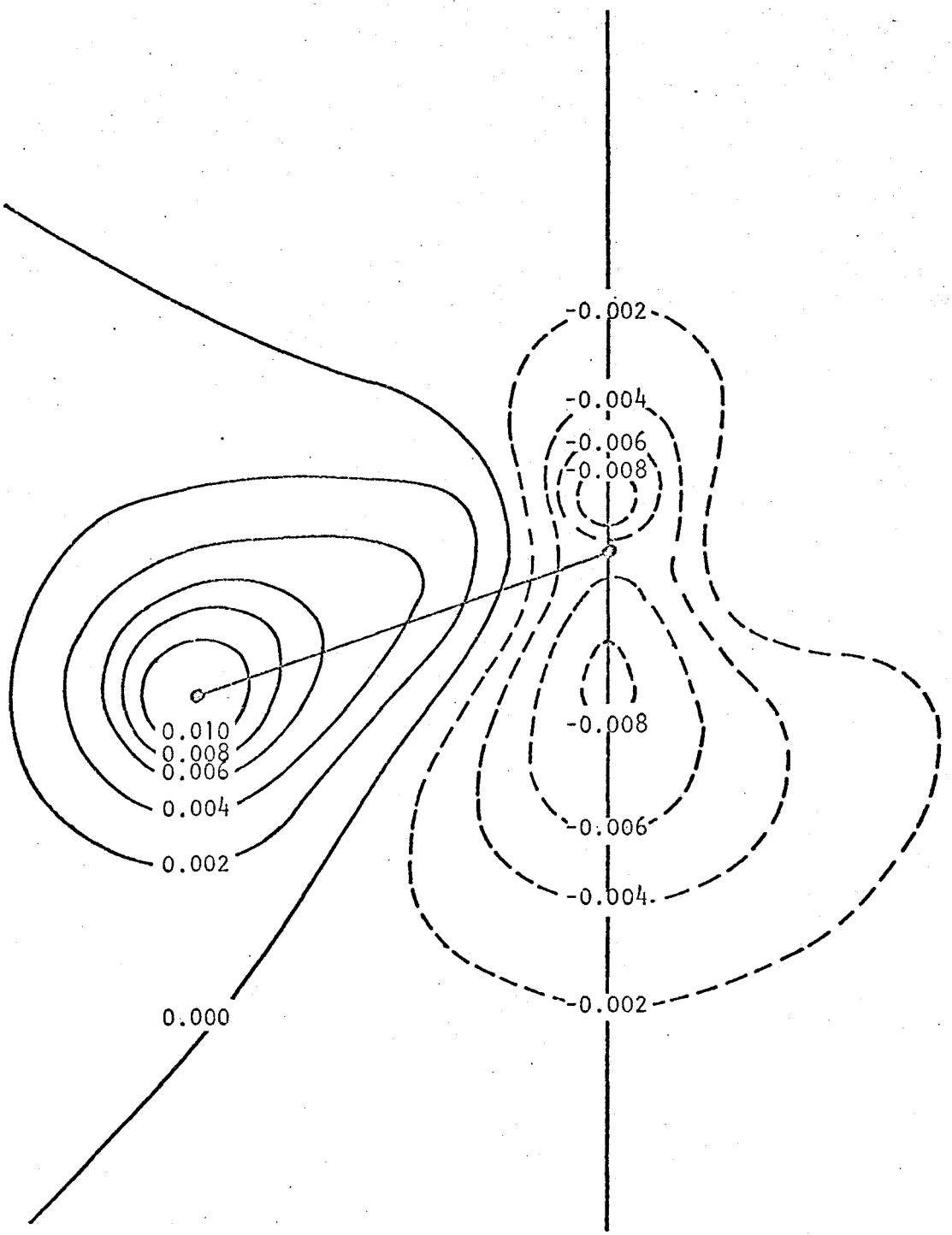

electron density distribution of water to be tetrahedral in character and derived from that of neon by the removal of two protons from the neon nucleus. Since the two lone pair orbitals in the resulting water molecule would remain orthogonal, $\Delta\rho_{p\ell\ell}(\vec{x}_1)$, the density transferred because of the overlap of the two lone pair orbitals, would be zero. Thus, there are no Pauli repulsions at all between the lone pairs in the water molecule when its electron density is related to that of neon. The same result would be obtained by relating the density distribution to that of the tetrahedral methane molecule. The fact that the two lone pair orbitals in the water molecule overlap one another when pictured in three-dimensional space does not preclude the possibility that their total overlap is still zero, i.e.,

$$\int \phi_{\ell 1}\phi_{\ell 2} d\tau = 0 \ . \tag{2.16}$$

Thus, a pair of electrons can coexist in both lone pair orbitals with no shift in electron density as the Pauli exclusion principle is satisfied. The electron density distribution in certain regions of real space will contain contributions from both of the lone pair orbitals. This is permissible as long as the orbitals are orthogonal in orbital space.* The forms of $\Delta\rho_{p\ell b}(\vec{x}_1)$ and $\Delta\rho_{pbb}(\vec{x}_1)$ are similar to those calculated for ammonia, resulting in a total charge migration which would tend to increase rather than decrease the tetrahedral bond angle. In addition, there is no charge migration due to the interaction of the lone pairs, i.e., $\Delta\rho_{p\ell\ell}(\vec{x}_1)$ is zero. Thus, the concept that the bond angle in the water molecule is less than the tetrahedral value because of Pauli repulsions between the lone pair orbitals is incorrect.

---

* Lone pair-lone pair Pauli repulsions will never exist between equivalent lone pair orbitals centered on the same nucleus. They will be orthogonal by definition.

The identification of "Pauli repulsions" between filled orbitals with shifts in the three-dimensional one-electron charge density has demonstrated that their interpretation in terms of overlapping orbitals in real space can be misleading. In the simple case of two He atoms, where the overlapping orbitals are s orbitals centered on different atoms, the form of $\Delta\rho_p(\vec{x}_1)$ fits in with the simple interpretation of "colliding" orbitals. However, when a number of orbitals, including p orbitals, are centered on one nucleus, such as in H_2O or NH_3, this is no longer true. The order of magnitude of the shifts, $\Delta\rho_{pbb}(\vec{x}_1) > \Delta\rho_{p\ell b}(\vec{x}_1) > \Delta\rho_{p\ell\ell}(\vec{x}_1)$, is in contradiction with the proposals of the electron pair repulsion theory and, more important, $\Delta\rho_{p\ell\ell}(\vec{x}_1)$ is actually zero. The latter point is especially important in emphasizing that the overlap of orbitals when pictured in real space does not preclude the possibility that they are orthogonal and hence satisfy the Pauli principle. Furthermore, the density shift arising from the requirements of the Pauli principle as calculated for the tetrahedral distribution does not predict a decrease in the tetrahedral bond angle. Thus, the second basic assumption of the repulsion theory, that the one-electron density distribution in these molecules can be related to a tetrahedrally oriented set of orbitals, is incorrect. This conclusion is necessary not only because $\Delta\rho_p(\vec{x}_1)$ does not lead to a decrease in the bond angle but for an even more fundamental electrostatic reason which will be considered in the next section.

2.4 Analysis of the Charge Distributions for H_2O and NH_3 in Terms of Their Binding Regions

The concept of a binding region in polyatomic molecules[88] was

discussed in Chapter I (see page 60 of this thesis). By placing electron density in this region one can overcome the nuclear forces of repulsion and thus attain a state of electrostatic equilibrium. Using this approach it can be shown that the tetrahedral one-electron density distributions for water and ammonia do not concentrate sufficient density in the binding region to bind the nuclei, and for this reason are unacceptable as stable distributions.

The boundary curve between the binding and antibinding regions is indicated by the dotted line in Figure 2.5. The binding region is derived by considering the forces exerted on the nuclei by a symmetrically equivalent set of charge points following the same procedure used for methane (see page 65 of this thesis). This set of symmetrically equivalent points reduces to a single one for charge along the three-fold axis, to a set of three for charge in the symmetry planes, and to a set of six for charge placed in any other regions. Any such set of symmetrically equivalent charge points placed below the boundary curve will exert forces on the nuclei such as to decrease all the internuclear separations. Charge density outside of this boundary curve will tend to separate the molecule into either a diatomic molecule and two atoms or into four atoms.* Charge density must be concentrated in this binding region if the molecule is to achieve equilibrium. The existence and shape of the binding region and the necessity of concentrating charge in this region illustrate the

---

* One can also construct a binding region by considering the forces exerted on the nuclei by only a single point charge at a time. The binding region thus obtained is equivalent to the superposition of all the possible diatomic boundary curves. Such a region has been given previously for the water molecule[88] and corresponds to the region between all three nuclei defined by an angular boundary curve subtended at the oxygen nucleus with an angle less than the bond angle. A similar less extended binding region for the ammonia molecule would be pyramidal in shape, enclosed within the region of all four nuclei with its apex at the nitrogen nucleus.

importance of the requirements imposed on the density distribution by the the presence of the protons. The shape of the binding region will in fact determine the polarization-type hybridization induced by the protons which was referred to by Sinanoglu[43].

The question as to how much charge must be placed in the binding region was discussed in Chapter I (see page 61 of this thesis). By plotting the difference density function (see Equation (I.53))

$$\Delta\rho(\vec{x}_1) = \rho(\vec{x}_1)\ \text{(molecule)} - \rho_A(\vec{x}_1)\ \text{(atomic)}\ , \qquad (2.17)$$

where $\rho_A(\vec{x}_1)$ is a standard atomic density distribution* which does not place sufficient charge in the binding region to bind the nuclei, one can determine the acceptability of a proposed molecular density distribution $\rho(\vec{x}_1)$. A distribution which gives a positive $\Delta\rho(\vec{x}_1)$ in the binding region is acceptable, while one which gives a negative $\Delta\rho(\vec{x}_1)$ in the binding region is unacceptable since it places less charge density in the crucial binding region than does the standard atomic distribution which is known to be insufficient in this regard.

A contour plot of $\Delta\rho(\vec{x}_1)$ for the tetrahedrally based NH_3 density distribution is shown in Figure 2.5. There is less charge density between every pair of nuclei than in that obtained from the simple overlap of the atomic densities. Thus, there will be larger forces of repulsion acting on all the nuclei. In particular, the large accumulation of charge density above the nitrogen and its depletion below will result in large forces tending to increase the bond angle. Thus not only does the form of $\Delta\rho_p(\vec{x}_1)$,

* The standard atomic density distribution is the one obtained by placing the constituent atoms at the same internuclear separations present in the molecule, each with its original atomic density.

Figure 2.5. A contour plot of the difference density $\Delta\rho(\vec{x}_1)$ (molecular density - atomic density) for tetrahedral NH_3 with sp^3 hybridization. The dotted line divides the binding region (below the line) from the antibinding region.

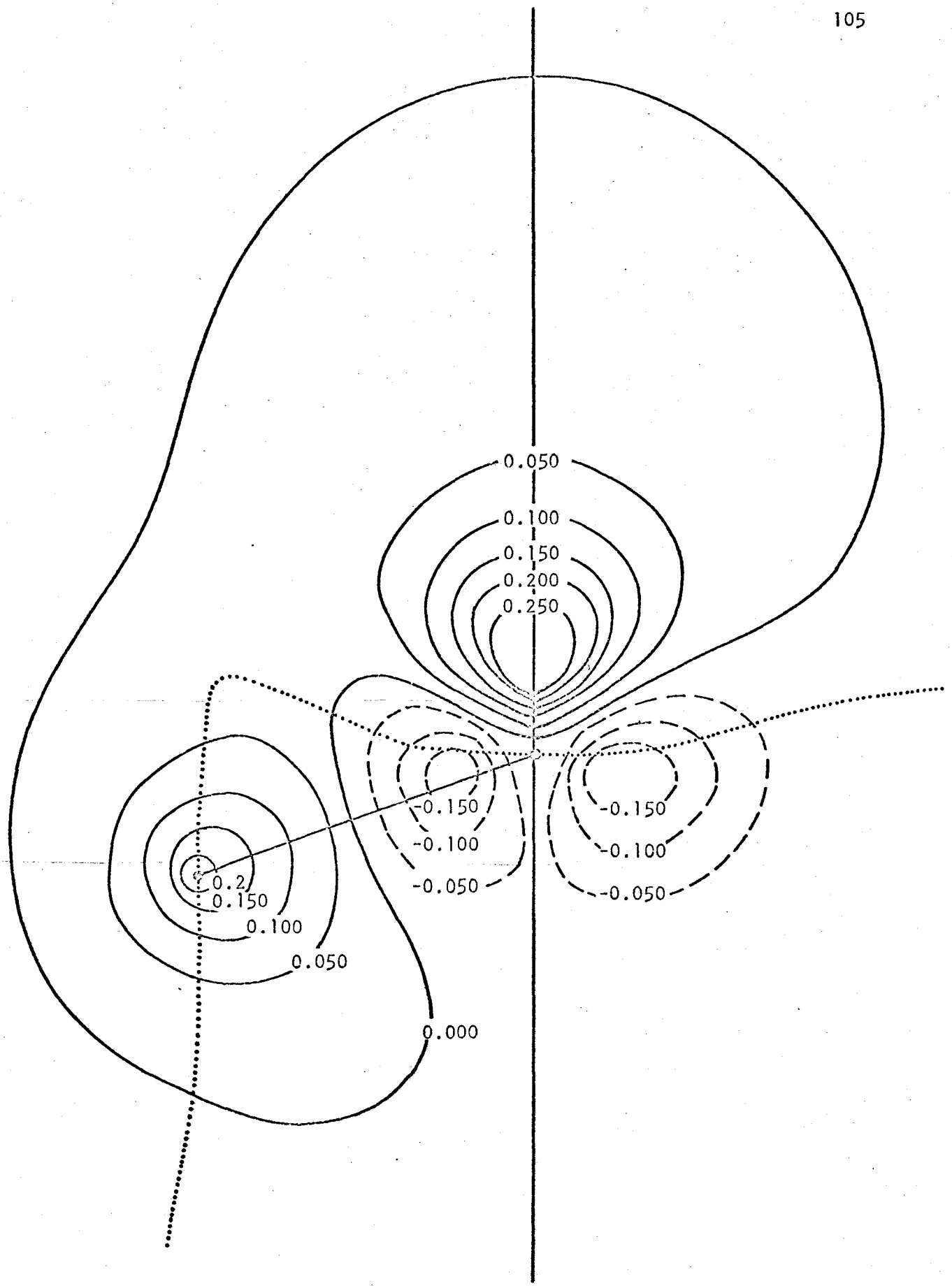
0.050
0.100
0.150
0.200
0.250
-0.150
-0.100
-0.050
-0.150
-0.100
-0.050
0.2
0.150
0.100
0.050
0.000

the density shift required by Pauli repulsions, predict an increase in bond angle for a tetrahedral distribution, but the form of the distribution itself predicts even larger forces of repulsion on the nuclei than the atomic density $\rho_A(\vec{x}_1)$.

A contour plot of $\Delta\rho(\vec{x}_1)$ for a tetrahedral density distribution for the water molecule has been given previously[88] and illustrates the same general features as those noted for the ammonia molecule. The value of $\Delta\rho(\vec{x}_1)$ is negative in the binding region and in regions between all three nuclei, and is large and positive in the antibinding region above the oxygen nucleus. The large decrease in the electron density in the binding region found for the tetrahedral distributions is because of the sp^3 hybridization assumed for the lone pair electrons. When an sp^3 hybrid orbital is squared, there is a contribution to the electron density of $(\sqrt{3}/2)$ sp per electron. This term is positive above the nodal plane of the p orbital (where it leads to an increase in the electron density) and negative below it (where it leads to a decrease in the electron density). In Ne the four cross terms for each orbital are all equally weighted and a spherical density distribution is obtained. In ammonia, the lone pair orbital contributes a term $\sqrt{3}\ sP_\ell$, which increases the density in the antibinding region above the nitrogen nucleus at the expense of the density in the binding region. However, the density in a bonding orbital is shared between the nitrogen (a fraction equal to $\lambda^2 \simeq 0.5$) and a hydrogen (a fraction equal to μ^2). Thus, the bonding orbitals in ammonia contribute $3\lambda^2\sqrt{3}\ sP_i$ rather than the $3\sqrt{3}\ sP_i$ necessary to just balance the charge migration due to the lone pair. It is clear that the hybridization of the lone pair must be reduced and must approach pure s character in order to

concentrate charge density in the binding region of the water and ammonia molecules. At the same time, the demands of the Pauli principle require the bonding orbitals to acquire more p character from the nitrogen or the oxygen as the lone pair becomes more s-like. Figure 2.6 is a contour plot of $\Delta\rho(\vec{x}_1)$ for the ammonia molecule in which the molecular one-electron density possesses a lone pair in a pure 2s orbital and the bonding orbitals are close to pure 2p in character from the nitrogen. The bonding orbitals contain a small amount of 2s character but it is of negative sign. This distribution does accumulate charge density in the binding region and does balance all the forces exerted on the nuclei[84]. In addition, the values calculated for the other physical properties which depend upon the one-electron density are in excellent agreement with experiment. Density distributions for the water molecule[35,36] which do concentrate density in the binding region and which do balance the forces on all the nuclei are similar in character to that found for the ammonia molecule. The oxygen contributions to the bond orbitals are almost pure 2p character and the lone pair orbitals are sp hybrids. (The lone pair may also be viewed as one orbital of pure 2s character and another of pure 2p, perpendicular to the molecular plane.) Contour plots of $\Delta\rho(\vec{x}_1)$ for these type of distributions for the water molecule appear in the literature[36,88].

One can envisage a whole spectrum of possible hybridization for the nitrogen and oxygen in the ammonia and water molecule, extending from the one extreme of sp^3 hybrids to the other in which the lone pair is pure 2s (and in water, a second of pure 2p, perpendicular to the molecular plane) and the bonds pure 2p. The analysis of the resulting charge distributions in terms of the amount of charge shifted to the binding region has shown

Figure 2.6. A contour plot of the difference density $\Delta\rho(\vec{x}_1)$ for NH_3 with the experimental bond angle of 107.3° and for a density distribution which balances all the forces on the nuclei and has the correct dipole moment[84].

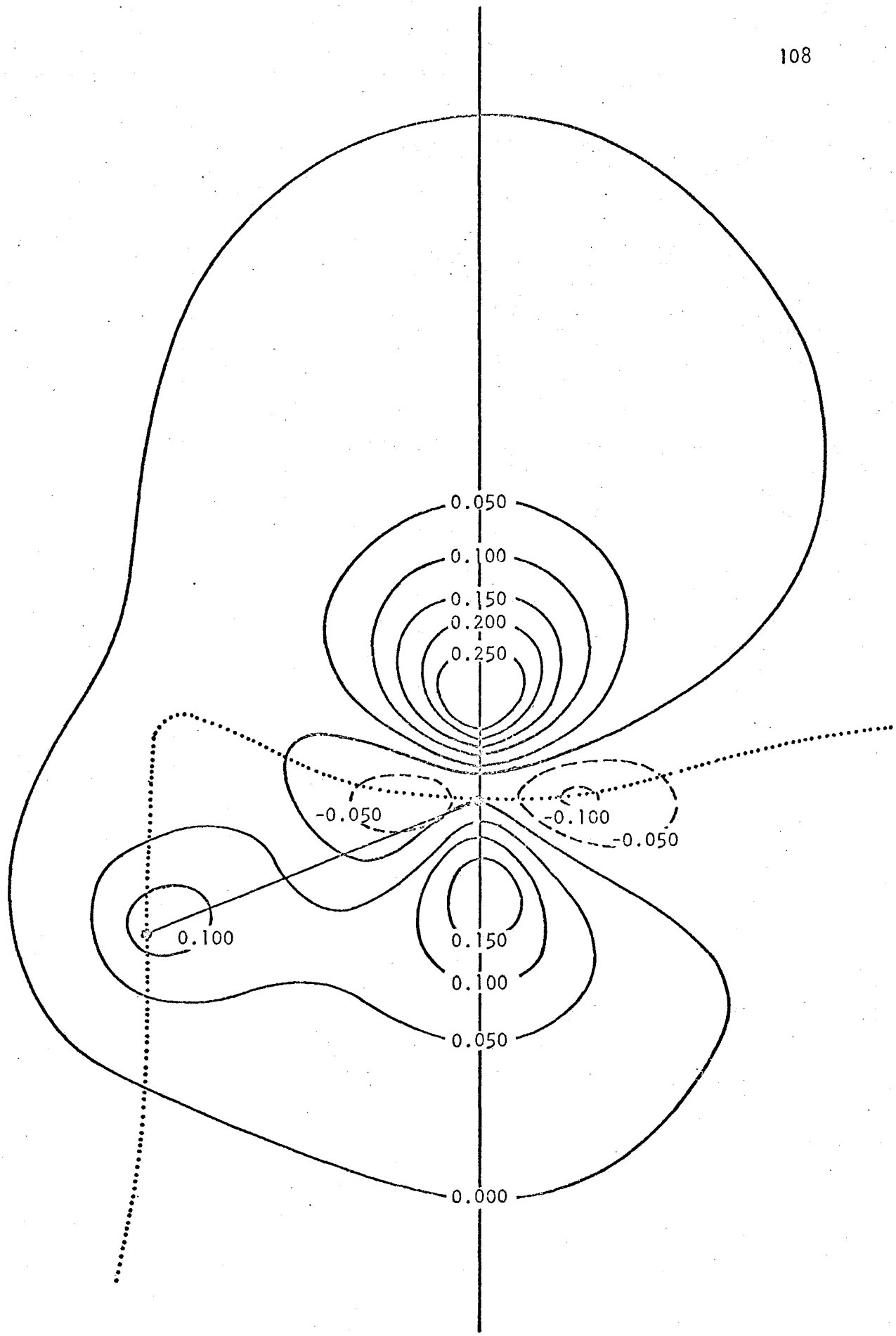
0.050
0.100
0.150
0.200
0.250
-0.050
-0.100
-0.050
0.100
0.150
0.100
0.050
0.000

that only the latter of the extremes of hybridization is satisfactory in this respect. Thus, a theory which assumes that the charge distribution in these molecules arises from a perturbed neon-like distribution will be unsatisfactory as the unperturbed density is chosen from the wrong end of the hybridization spectrum. Rather, the charge distribution should be considered as arising from a perturbation of the original ground state electronic densities for the nitrogen and oxygen atoms. This is, of course, more realistic on energetic grounds as well. In both the water and ammonia molecules an orbital angle less than the bond angle is necessary to concentrate density in the binding region and along the bonds in three-dimensional space. In a sense one must have "bent orbitals" in these molecules in order to obtain chemical bonds in terms of the density distribution in real space.

In the preceeding discussion of the water and ammonia molecules it has been shown that charge density must be concentrated in the binding region between all nuclei in order to attain a state of electrostatic equilibrium. The appropriate one-electron charge distribution for either of these two molecules can not be obtained by considering a tetrahedral geometry and sp^3 hybridization of the central atom. In contrast, the methane molecule, which by necessity has tetrahedral symmetry and close to sp^3 hybridization fo the bonding orbitals, has its one-electron density primarily concentrated along the C-H bond axies (see Figure I.2). It is this charge build-up, which does in fact occur in the all-important binding region, that is responsible for the attainment of a state of electrostatic equilibrium and for the binding between the hydrogens and the central carbon nuclei in methane. The $\Delta\rho(\vec{x}_1)$ contour map for methane (Figure I.2)

clearly indicates the necessity of charge accumulation in the binding region to balance the nuclear forces of repulsion and thus, produce a stable molecular one-electron charge distribution.

2.5 Concluding Remarks

The acceptable one-electron density distributions for the H_2O and NH_3 molecules (with the 2s lone pairs) are interesting in that they concentrate density above and below the heavy nucleus to almost identical extents as do the distributions with sp^3 lone pairs. However, in the distributions with the 2s lone pair this increase is not because of the lone pair. The lone pair density, in fact, cancels out in the determination of $\Delta\rho(\vec{x}_1)$ as the 2s orbital is unchanged from the atomic distribution. Instead, the increase in $\Delta\rho(\vec{x}_1)$ above the nitrogen or oxygen nucleus arises from the density contained in the bonding orbitals. A 2p orbital concentrates density on both sides of the nucleus it is centered on. Thus bonds formed from 2p orbitals will necessarily place density above and below the nitrogen nucleus. In addition, the negative 2s character found in the bonding orbitals also contributes to this build-up of charge above the heavy nucleus. However, the fact that there is an increase in the electron density above the nitrogen and oxygen nuclei over that found in the atomic cases indicates that the ammonia and water molecules do possess directed lone pairs. Perhaps an excellent definition of a lone or unshared pair would be the concentration of electron density in an antibinding region. The fact that the positive $\Delta\rho(\vec{x}_1)$ values in the antibinding regions arises from the density in the bonding orbitals is irrelevant. An infinite number of choices as to the forms of the orbitals is possible and to express the density (which is invariant to an unitary transformation of the molecular

orbitals) in terms of equivalent orbitals as done here is but one of many possibilities. Only the total density distribution is of significance and the concentration of charge density in the antibinding region, where by definition it plays no role in binding the nuclei together, must correspond to the existance of a lone pair or at least unshared electrons. The results of self-consistent field (SCF) calculations, when expressed in terms of equivalent orbitals[84,85], exhibit the same characteristics as determined by the present considerations of concentrating density in the binding region. Thus one finds for these variationally determined functions that the bonding orbitals are primarily of 2p character with negative 2s contributions, that the orbital angle is less than the bond angle, and that the lone pairs approach the limiting 2s form. This has been pointed out by Peters[99] for the diatomic hydride functions of Ransil[100]. Ruedenberg and Edmiston[101] have shown that when the molecular orbitals describing these wavefunctions are transformed into a new set, one which minimizes the overall interorbital coulombic and exchange interactions, bonding orbitals are obtained which now contain 2p and 2s character of the same sign and the lone pair orbitals are directed behind the heavy nucleus. However, the definition of a lone pair orbital is now changed, for the orbitals labelled as lone pairs by Ruedenberg no longer consist of atomic orbitals centered only on the heavy atom. Rather, they contain contributions from the hydrogen orbitals as well, with negative coefficients. In fact, Ruedenberg ascribes the origin of nonbonded interactions to the antibonding nature of these lone pair orbitals. A definition of a lone pair based on the final density distribution avoids the ambiguities associated with an orbital definition. There is but one density distribution but many possible

orbital descriptions of it.

One can give an electrostatic interpretation as to why the ammonia and water molecules are pyramidal and bent, respectively. In a planar ammonia molecule the unshared pair of electrons would necessarily be placed in a 2p orbital perpendicular to the plane of the molecule. A p_π orbital is very inefficient at screening a nucleus, since density is placed above and below the bond axis or the molecular plane. By bending the bonds out of the plane the lone pair takes on an increasing amount of s character. The electrons in a 2s orbital are much more efficient at screening a nucleus since the density is distributed spherically about it. In addition, the 2s orbital is easily polarized (by the admixture of 2p) to place density in the binding region below the nitrogen nucleus in a pyramidal molecule. Thus, the total density between the nuclei obtained from s-p hybrid bonds and a p_π lone pair in the planar molecule is less than that obtained from bonds composed of p orbitals and a 2s lone pair for the pyramidal geometry. In the case of the water molecule one lone pair remains in a p_π orbital (perpendicular to the molecular plane) whether the molecule is linear or bent. The second lone pair, however, changes from a p_π orbital in the linear case through a range of s-p hybridizations to the limiting form of an s orbital when the bonding orbitals are pure p and the molecule is bent. Again one finds that to achieve maximum screening of the heavy nucleus and to achieve the maximum electron density along the bonds, the bonding orbitals must be approximately pure p orbitals and one lone pair must be placed in an s orbital. This corresponds to the bent geometry. The $\Delta\rho(\vec{x}_1)$ plots for the tetrahedral density distributions again illustrate the importance of considering the total density distribution. The sp^3 bonding orbitals in a

tetrahedral density distribution for NH_3 or H_2O do concentrate a maximum amount of density along the bonds. However, the orthogonality restraints of the Pauli exclusion principle demand that the lone pair must be strongly s-p hybridized when the bonds are s-p hybrids. The result of the forced hybridization of the lone pair is the removal of more density from the binding region and from between the nuclei than was concentrated by the sp^3 bonding orbitals. The net effect is a distribution which places less charge density between the nuclei than that obtained from the simple overlap of the atomic densities. Thus, the presence or absence of lone pairs does affect the geometry of a molecule, but not in the sense of exerting Pauli repulsions. Rather, the geometry can be interpreted as being determined by the molecule attaining a density distribution which provides a maximum screening of the nuclei, and places a maximum amount of electron density along the bonds and in the binding region.

It has been shown that the effects of the Pauli exclusion principle on the one-electron density distribution of simple molecules is not what is commonly pictured. However, one is still faced with the fact that the electron pair repulsion theory is remarkably successful. In recent papers Gillespie (see for example, Reference 102) has purposely avoided any reference to the degree of hybridization. Instead, the distortions from the most probable arrangement of a given number of initially equivalent pairs of electrons is determined by the arguments based on the relative size of the orbitals. Thus orbitals which are lone pairs in the molecule become more diffuse and less directional and occupy a larger volume of space. In terms of the arguments put forward in the present work this would correspond to an increase in the s character of the lone pair orbitals.

Similarly the bonding orbitals are stated to be contracted and polarized by the presence of the ligands. This description coincides with the predicted increase in the p character of the bonding orbitals found in the present work. However, the present appraoch arrives at these conclusions by a determination of which one-electron density distribution places the maximum charge in the binding region, and not by arguments based on orbital "repulsions". It will be interesting to determine whether or not the parallelism between the two approaches noted above will continue to hold the non-hydride polyatomic molecules as well.

The fact that charge must be accumulated in the binding region of a stable molecular species is made clear by previous work[3,4,5,6] for diatomic molecules using SCF wavefunctions. Consider, for example, the case of the homonuclear diatomic molecules Li_2, B_2, C_2, N_2, O_2 and F_2.[3] The $\Delta\rho(\vec{x}_1)$ contour maps for these stable molecules* clearly indicate a charge accumulation in the binding region between the nuclei at the expense of a decrease in charge in the antibinding regions. For most of these molecules there is also a large build-up of charge in the antibinding region behind each of the nuclei which reveals the existence of lone pairs or unshared electrons as defined in the present work. As a note of caution, one might further consider the $\Delta\rho(\vec{x}_1)$ contour map for the unstable molecule Be_2[3] (see Figure 3.11). For this molecule, the $\Delta\rho(\vec{x}_1)$ map also shows an increase in charge density in the internuclear or binding region. However, this increase is very small when compared to the large accumulation of charge in the antibinding regions behind the nuclei which creates large

---

* The $\Delta\rho(\vec{x}_1)$ contour diagram for N_2 is given in Figure 3.10 of this thesis.

electrostatic forces that tend to separate the molecule. Thus, when one is determining the stability or instability of a molecular charge distribution by considering the $\Delta\rho(\vec{x}_1)$ contour diagrams and the accumulation of charge in the binding region it may be necessary to calculate the forces exerted on the nuclei. Whether one is considering a force analysis or the $\Delta\rho(\vec{x}_1)$ contour maps the main feature that is always necessary for the production of a stable molecular species is the build-up of charge in the crucial binding region.

III. THE KINETIC ENERGY OF MOLECULAR CHARGE DISTRIBUTIONS AND MOLECULAR STABILITY

3.1 Introduction

The electrostatic approach as exemplified in the preceeding two chapters permits a classification and interpretation of chemical binding[3,4,5,6] based on the spacial characteristics of the molecular one-electron charge distribution and the forces which it exerts on the nuclei. This approach provides an essentially static view of chemical binding. The net reorganization of the one-electron charge density of the separated atoms accompanying the formation of a molecule is obtained by subtracting the superimposed densities of the component (undistorted) atoms separated at R_e from the molecular one-electron density, also evaluated at $R = R_e$. The discussion of the stability of the molecular system relative to the separated atoms which results from the charge reorganization depicted in the density difference, $\Delta\rho(\vec{x}_1)$, contour maps is couched in the language of classical electrostatics via the Hellmann-Feynman theorem[50]. Thus in certain diatomic molecules[3,4,5,6] the charge distribution is found to be characterized by the transfer of charge from the region of one nucleus to the neighbourhood of the other and the bond is described as "ionic". In ionic binding[3] the charge density which exerts the net binding force on both nuclei is found to be localized in the region of a single nucleus. In "covalent" binding[3], the formation of the molecule results in a charge increase localized in the region between the nuclei and it is the force exerted by this shared density increase which binds the nuclei.

Many systems, of course, fall between the ionic and covalent extremes

which represent two limiting manners in which the one-electron charge density may be distributed to achieve electrostatic equilibrium. Given the one-electron charge distribution, the binding in a molecule may be classified and the binding mechanism understood in terms of classical electrostatics. Of equal or perhaps greater interest, however, is the question as to how the one-electron charge density must be distributed in order to obtain the necessary balance between the kinetic energy increase and the potential energy decrease required for the formation of a stable molecular species. In this chapter we wish to complement the electrostatic approach with a dynamic one, one which relates the kinetic energy and potential energies of the system to the topographical features of the one-electron charge distribution. The charge density in a molecular system is not, for example, a functional of the potential as it is predicted to be in Thomas-Fermi statistical theory. Thus, equi-density surfaces of a molecular charge distribution are not equipotential surfaces. In fact, Balàzs[103] has shown that a stable molecule can not exist (stable with respect to separated atoms or ions) if the charge density is a simple functional of the potential alone. The departure of the charge density from being a functional of the potential is a result of the form and requirements of the kinetic energy operator in quantum mechanics[104]. Perhaps the most striking difference between the classical and quantum predictions regarding the behaviour of a bound charged distribution is that the former predicts a distribution of zero extent while the later predicts one of infinite extent. There are two causes for the non-collapse of a fermion system, the antisymmetry condition imposed by the Pauli exclusion principle and the Heisenberg uncertainty principle. The

effect of this latter principle is made manifest through the kinetic energy of the charge distribution. Through a study of the kinetic energy of the charge distribution, "the kinetic energy density", an explanation can be obtained for the manner in which the one-electron charge density is distributed in a molecule. In this chapter we will restrict the discussion to homonuclear diatomic molecules.

3.2 Kinetic Energy Density

The first requirement is to obtain an expression for the kinetic energy as a function of the one-electron charge distribution. This can be done by first expanding the one-electron charge distribution $\rho(\vec{x}_1)$ in terms of its natural orbitals[105], which are taken to be real,

$$\rho(\vec{x}_1) = \sum_i \lambda_i \phi_i(\vec{x}_1)\phi_i(\vec{x}_1) = \sum_i \rho_i(\vec{x}_1) \quad . \tag{3.1}$$

The gradient and the Laplacian of $\rho(\vec{x}_1)$ are respectively

$$\vec{\nabla}\rho(\vec{x}_1) = \sum_i \lambda_i 2\phi_i(\vec{x}_1)\vec{\nabla}\phi_i(\vec{x}_1) \tag{3.2}$$

$$\nabla^2\rho(\vec{x}_1) = \sum_i \lambda_i [2\phi_i(\vec{x}_1)\nabla^2\phi_i(\vec{x}_1) + 2\vec{\nabla}\phi_i(\vec{x}_1)\cdot\vec{\nabla}\phi_i(\vec{x}_1)] \quad . \tag{3.3}$$

Writing the kinetic energy operator in the form usual for the Schrödinger representation and allowing it to operate on the first-order density matrix[106]

$$T_{op}\rho(\vec{x}_1|\vec{x}_1') = -\frac{1}{2}\sum_i \lambda_i \phi_i(\vec{x}_1)\nabla^2\phi_i(\vec{x}') \tag{3.4}$$

one obtains from Equation (3.3)

$$T_{op}\rho(\vec{x}_1|\vec{x}_1')_{\vec{x}_1'=\vec{x}_1} = -\frac{1}{4}\nabla^2\rho(\vec{x}_1) + \frac{1}{8}\sum_i \frac{\vec{\nabla}\rho_i(\vec{x}_1)\cdot\nabla\rho_i(\vec{x}_1)}{\rho_i(\vec{x}_1)} \quad . \tag{3.5}$$

Let

$$T_{op}\rho(\vec{x}_1|\vec{x}_1')_{\vec{x}_1'=\vec{x}_1} \equiv K(\vec{x}_1) \quad . \tag{3.6}$$

Also let $L(\vec{x}_1)$ denote the contribution to $K(\vec{x}_1)$ from the Laplacian of $\rho(\vec{x}_1)$

$$L(\vec{x}_1) \equiv -\frac{1}{4}\nabla^2\rho(\vec{x}_1) \tag{3.7a}$$

and let $G(\vec{x}_1)$ denote the gradient contribution

$$G(\vec{x}_1) \equiv \frac{1}{8}\sum_i \frac{\vec{\nabla}\rho_i(\vec{x}_1)\cdot\vec{\nabla}\rho_i(\vec{x}_1)}{\rho_i(\vec{x}_1)} = \frac{1}{2}\sum_i \lambda_i \vec{\nabla}\phi_i(\vec{x}_1)\cdot\vec{\nabla}\phi_i(\vec{x}_1) \quad . \tag{3.7b}$$

Then

$$K(\vec{x}_1) = L(\vec{x}_1) + G(\vec{x}_1) \quad . \tag{3.8}$$

Equation (3.8), or Equation (3.5), then represents one possible relationship between the variation in the kinetic energy of the system and the properties of the one-electron charge density. Specially $K(\vec{x}_1)$ at each point in space is determined by the Laplacian of the total density distribution and by the values and gradients of its component natural orbital densities. The value of $K(\vec{x}_1)d\tau_1$ is the contribution to the total kinetic energy from the charge density in the volume $d\tau_1$, and the integration of $K(\vec{x}_1)d\tau_1$ over all space yields the total average kinetic energy of the system.

$$\int K(\vec{x}_1)d\tau_1 = \bar{T} \quad . \tag{3.9}$$

The probability density in coordinate space describes the one-electron charge distribution in real space, and the associated distribution in momentum space, as investigated by Coulson[107] and more recently by Henneker and Cade[108], yields the momentum density of the system. The function $K(\vec{x}_1)$, however, contains information pertaining to both the distri-

bution of charge and the magnitude of momentum throughout coordinate space.

Equation (3.8) shows an immediate consequence of Heisenberg's uncertainty relationship. The Laplacian of a function is negative in those regions where the function is a maximum. Thus, a local concentration of charge density, such as occurs in regions of low potential, will result in a negative curvature for $\rho(\vec{x}_1)$, in a positive value for $L(\vec{x}_1)$ and from Equation (3.8), in a positive contribution to the kinetic energy. A compression of the charge density leads to a large local contribution to the kinetic energy. Thus, any lowering in energy obtained by concentrating charge density in a region of low potential is gained only at the expense of a corresponding increase in the kinetic energy of the system for the same region of space. This observation regarding the contribution to the kinetic energy from a given region of space is independent of the virial theorem which states that for a coulomb potential, the average kinetic energy must be equal to minus one-half the average potential energy when no external forces are acting on the system.

When Equation (3.5) is written for a single electron $[\rho(\vec{x}_1) \equiv \rho_i(\vec{x}_1)]$ and divided by $\rho(\vec{x}_1)$, the resulting R.H.S. of the equation is identical with Bohm's[109] "quantum potential". The quantum potential plays a central role in Bohm's attempt to replace the probabilistic interpretation of quantum mechanics by a precise and objective description of a physical process. Bohm ascribes the stability of a stationary state in a quantum system to the balancing of the classical force exerted on the particle, $-\nabla V_{op}$, by the quantum mechanical force which is given by the gradient of the "quantum potential". In the hydrogen atom $\nabla[G(\vec{x}_1)/\rho(\vec{x}_1)] = 0$.

Thus, the force balancing the electrostatic force of attraction and preventing the collapse of the atom is given by the gradient of the Laplacian contribution $\nabla[L(\vec{x}_1)/\rho(\vec{x}_1)]$, the same term through which the Heisenberg's uncertainty principle is made manifest. Jørgensen[110] has considered an equation similar to Equation (3.5) (but not expressed in terms of the charge density) for the one-electron case and has attempted to relate the terms corresponding to $G(\vec{x}_1)$ and $L(\vec{x}_1)$ to separate contributions to the energy in Dirac's bubble-surface model of an electron.

Making use of the fact that the functions $\rho_i(\vec{x}_1)$ and $\phi_i(\vec{x}_1)$ are analytic and must vanish at infinity, Green's theorem shows that

$$\frac{1}{8}\sum_i \int \frac{\vec{\nabla}\rho_i(\vec{x}_1)\cdot\vec{\nabla}\rho_i(\vec{x}_1)}{\rho_i(\vec{x}_1)}\, d\tau_1 = -\frac{1}{2}\sum_i \lambda_i \int \phi_i(\vec{x}_1)\nabla^2\phi_i(\vec{x}_1)\, d\tau_1 = \bar{T} \,. \qquad (3.10)$$

Thus it follows from Equation (3.5) or (3.8) that

$$\int \nabla^2\rho(\vec{x}_1)\, d\tau_1 = \int L(\vec{x}_1)\, d\tau_1 = 0 \,. \qquad (3.11)$$

The total kinetic energy of the system is given by the contributions from $G(\vec{x}_1)$ alone. The positive contributions of $L(\vec{x}_1)$ in regions where $\rho(\vec{x}_1)$ is a maximum, exactly balancing the negative contributions of $L(\vec{x}_1)$ obtained from regions where $\rho(\vec{x}_1)$ is a minimum. While the integrated contribution of $L(\vec{x}_1)$ to the total kinetic energy is zero, it is the presence of this term in the expression for $K(\vec{x}_1)$ which imposes quantum mechanical restrictions on the form of the density distribution. The term $G(\vec{x}_1)$ exhibits a behaviour more characteristic of a classical

kinetic energy density. Its value is everywhere positive and finite and the sum of its local contributions yields the total kinetic energy of the system.* It is the term $L(\vec{x}_1)$ which imparts to $K(\vec{x}_1)$ its classically impossible negative values.

Consider the following Expression (3.13) obtained from

$$\psi^*(\vec{x})(T_{op} + V_{op})\psi(\vec{x}) = E\psi^*(\vec{x})\psi(\vec{x}) \tag{3.12}$$

for a one electron system.

$$L(\vec{x}_1) = E\rho(\vec{x}_1) - G(\vec{x}_1) - V_{op}\rho(\vec{x}_1) \ . \tag{3.13}$$

In a classical system, the R.H.S. of Equation (3.13) should equal zero not only when integrated over all space, but for every point in space as well, since it is simply the difference between the total energy density $E\rho(\vec{x}_1)$ and the sum of the potential and kinetic energy densities at every point in space. In a quantum mechanical system, however, this difference is in general not zero and is instead equal to $L(\vec{x}_1)$ which is proportional to the curvature of the one-electron density distribution. The fact that $L(\vec{x}_1)$ is in general different from zero imposes restrictions on the form of $\rho(\vec{x}_1)$. For example, the singularities at the positions of the nuclei which occur in V_{op} when it represents a coulomb potential, require that the curvature of the

---

* The function $G(\vec{x}_1)$, because of the cusp conditions, may exhibit a finite discontinuity at the positions of the nuclei in the case of a molecular charge distribution.

density at the positions of these singularities be infinitely negative. This requirement on $\rho(\vec{x}_1)$ together with the further requirement that it be finite demands that $\rho(\vec{x}_1)$ behave as $e^{-\alpha r}$ at the singular points, i.e., that $\psi(\vec{x}_1)$ and $\rho(\vec{x}_1)$ have cusps at the positions of the nuclei. It is always true that $E\rho(\vec{x}_1) < 0$ and $G(\vec{x}_1) > 0$. Thus it follows from Equation (3.13) that the curvature of $\rho(\vec{x}_1)$ will be negative and $L(\vec{x}_1)$ positive in those regions where the potential energy density exceeds in absolute value the difference between the energy density $E\rho(\vec{x}_1)$ and the kinetic contribution $G(\vec{x}_1)$. $L(\vec{x}_1)$ will be negative in regions where the absolute value of the potential energy density is less than this difference. Thus, $L(\vec{x}_1)$ is a measure of the departure of the behaviour of the system from that of a classical model. The value of $L(\vec{x}_1)$ where the curvature is negative is a measure of the extent to which the charge density may be concentrated in regions of low potential beyond that anticipated on classical grounds. An equation similar in form to Equation (3.13) holds for the individual orbitals in the Hartree-Fock approximation to the one-electron density; the curvature of a Hartree-Fock one-electron density distribution being related to the orbital energy densities by

$$L(\vec{x}_1) = \frac{1}{4}\nabla^2\rho(\vec{x}_1) = \sum_i \varepsilon_i \rho_i(\vec{x}_1) - \sum_\alpha (-Z_\alpha/r_\alpha)\rho(\vec{x}_1) - G(\vec{x}_1) - \int \frac{\Gamma(\vec{x}_1\vec{x}_2|\vec{x}_1\vec{x}_2)}{r_{12}}\, d\tau_2. \qquad (3.14)$$

The integral involving the second-order density matrix in Equation (3.14)

represents the total electronic repulsion experienced by the one-electron charge density at the position $\vec{x}_1$ from all possible pairs of electrons, the interaction being averaged over the whole space of the second electron. Equation (3.14) again integrates to zero

$$0 = E - \overline{T} - \overline{V} \tag{3.15}$$

as the double counting of the electronic repulsions in the sum of the orbital energies is accounted for by the doubling of the same terms in the final integral over the second-order density matrix.

According to Equations (3.13) and (3.14), the regions of space in which $L(\vec{x}_1) > 0$, denote regions in which the potential energy density attains its maximum stability. While the integration of $L(\vec{x}_1)$ over all space must yield zero, thus signifying the existence of regions in which $L(\vec{x}_1) < 0$ and in which the potential energy density is relatively less stable, it will be demonstrated that the relative positioning, in the nuclear potential field, of the regions in which $L(\vec{x}_1) \gtrless 0$ is critical in determining the stability of the system. Thus in certain cases, whether the overall curvature at the saddle point of a charge distribution (the mid point of the bond in a homonuclear diatomic species) is greater than or less than zero determines whether the resulting molecule is unstable or stable respectively with respect to the separated atoms.

The presence of a kinetic energy, since it is always positive in value, is to destabilize a system. The virial theorem as applied to a system at equilibrium with coulomb interactions demands that a potential decrease may be obtained only at the expense of an increase in the kinetic energy. Thus, chemical binding has been ascribed to a

lowering of the potential energy of the system in spite of an increase in the kinetic energy. Ruedenberg[111] has presented arguments to prove his contention that in spite of the validity of the virial theorem, the formation of a chemical bond should be interpreted as the result of a lowering of the kinetic energy. Ruedenberg considers it essential that the kinetic and potential energies of the molecule be compared not with the same quantities for the separated atoms, but with the kinetic and potential energies of atoms in special "promotion states". The promotion state corresponds to one in which the valence electrons contract towards the nucleus. Such a "contractive promotion" has two obvious effects on the energy of the system; the potential energy is decreased and the kinetic energy increased above their final equilibrium values. The formation of the molecule from atoms in promoted states thus results in an increase in potential energy and a <u>decrease</u> in the kinetic energy. The "promotion state" is, however, not a real one and difficult to define precisely. It seems an arbitrary decision to insist that chemical bonding must be discussed with reference to such an unreal and imprecisely defined state of the system. If one wishes to retain as a reference state the states of the separated atoms from which the particular molecular state is formed or into which it dissociates, then indeed the virial theorem applies, and the kinetic energy must increase if a stable molecule is formed. However, the real question to be answered is how the system can realize a distribution of charge density which possesses a kinetic energy which does not exceed $(1/2)\overline{V}$ in absolute value. The virial theorem in its most

general form applies whether the system is at equilibrium or not[112],

$$2\overline{T} = -\overline{V} - (RdE/dR) \quad . \tag{3.16}$$

Any value of $2\overline{T}$ which is less than or equal to $|\overline{V}|$ implies either the existence of an attractive force ($dE/dR > 0$) drawing the nuclei together or a situation of electrostatic equilibrium ($dE/dR = 0$). Either situation implies the existence of a stable molecular state. Only when the average value of the kinetic energy exceeds $(1/2)|\overline{V}|$ in value over the complete range of internuclear distances (disregarding the Van der Waal's minimum) is the existence of a repulsive force and hence an unstable molecular state indicated. Thus, one must determine how the charge density which is accumulated in the internuclear region of a stable molecule is distributed so as to attain a decrease in the potential energy with the least possible increase in its kinetic energy, one which does not exceed $(1/2)|\overline{V}|$ over some range of R values. In addition one must inquire as to why the removal of charge density from the internuclear region, such as occurs in He_2, results in a molecular one-electron charge distribution which possesses a kinetic energy in excess of $(1/2)|\overline{V}|$.

Since the integration of the gradient contribution $G(\vec{x}_1)$ yields $\overline{T}$, a knowledge of this distribution enables one to relate the final value of the kinetic energy to the spacial properties of the one-electron charge distribution. The Laplacian distribution in turn, whether it is greater or less than zero indicates the regions of space in which the charge density attains its maximum stability. The

functions $G(\vec{x}_1)$ and $L(\vec{x}_1)$ taken together thus provides a detailed explanation of the stability or instability of the system in terms of the spatial distribution of the one-electron charge density. In this chapter we investigate the stability or instability (with respect to the separated atoms) of a molecular one-electron charge distribution as evidenced by the properties of $K(\vec{x}_1)$ and its components $G(\vec{x}_1)$ and $L(\vec{x}_1)$.

Previous studies[5] have shown that the deformations which the atomic densities undergo on bond formation are characterized by either dipolar or quadrupolar polarizations. The density difference distribution, $\Delta\rho(\vec{x}_1)$, for a molecule formed from atoms which employ principally s orbitals is found to differ significantly from that for a molecule formed from atoms which employ orbitals with non-zero angular momentum (primarily p orbitals). The principal polarization of the charge density of a hydrogen, helium, lithium or sodium atom density on bond formation, whether the bond is ionic, polar or covalent, is dipolar in character. For example, the $\Delta\rho(\vec{x}_1)$ maps for H_2 and Li_2 indicate that the charge increase is confined almost entirely to the nuclei and the binding region between the nuclei, while the charge decrease occurs in the antibinding regions behind the nuclei. The redistribution of charge found in the $\Delta\rho(\vec{x}_1)$ distributions for the Be → F or Mg → Cℓ atoms is characterized by an increase of the charge density along the bond axis in both the binding and antibinding regions of the nucleus and its removal from a region perpendicular to the bond axis at the position of the nucleus. Such a quadrupolar polarization results in a gross accumulation of charge density in the antibinding as well as in the binding region.

We will first consider the consequences which the simpler, dipolar type charge reorganization has on the kinetic energy of a system, as exemplified by H_2 and He_2. Then the effect which the more complex, quadrupolar type charge reorganization has on the kinetic energy of a system, such as presented by N_2 and Be_2, will be considered.

3.3 The Kinetic Energy Distributions of the H_2 and He_2 Molecules

Contour maps of the total one-electron charge density $\rho(\vec{x}_1)$, the distribution $K(\vec{x}_1)$ and its contributions $G(\vec{x}_1)$ and $L(\vec{x}_1)$ for the hydrogen molecule at the equilibrium internuclear separation of 1.4 a.u. are shown in Figure 3.1.* The maps were determined using the Das and Wahl[113] extended wavefunction for H_2, a function which yields over 90% of the correlation energy.

A comparison of the $\rho(\vec{x}_1)$ and $K(\vec{x}_1)$ distributions indicates that $K(\vec{x}_1)$ is greatest in those regions where the charge density is most concentrated; at the nuclei and in the internuclear region. This is the expected consequence of Equation (3.8) which dictates that $K(\vec{x}_1)$ be large in regions where the concentration of charge leads to large gradients in the $\rho_i(\vec{x}_1)$ and to negative curvatures for $\rho(\vec{x}_1)$. The distributions $G(\vec{x}_1)$ and $L(\vec{x}_1)$ will indicate the origin of the kinetic energy contributions depicted in the $K(\vec{x}_1)$ distributions; whether they arise from a direct increase in the classical-like contributions to the kinetic energy $G(\vec{x}_1)$

---

* The distributions $K(\vec{x}_1) = -\frac{1}{2}\sum_i \lambda_i \phi_i(\vec{x}_1)\nabla^2\phi_i(\vec{x}_1)$ and $G(\vec{x}_1) = \frac{1}{2}\sum_i \lambda_i \vec{\nabla}\phi_i(\vec{x}_1)\cdot\vec{\nabla}\phi_i(\vec{x}_1)$ were evaluated using the expressions given for $\nabla^2\phi_i(\vec{x}_1)$ and $\vec{\nabla}\phi_i(\vec{x}_1)$ in Appendix 9. $L(\vec{x}_1)$ was determined by subtracting $G(\vec{x}_1)$ from $K(\vec{x}_1)$.

Figure 3.1. Contour maps and profiles of the total one-electron charge distribution $\rho(\vec{x}_1)$, the kinetic energy distribution $K(\vec{x}_1)$ and its components $G(\vec{x}_1)$ and $L(\vec{x}_1)$ for H_2 at its equilibrium separation of 1.4 a.u. These and the subsequent distributions are all given in atomic units (a.u.). The scale on the internuclear axis of the profile diagrams is in divisions of 0.5 a.u. Note that the ordinate scales differ between the profile diagrams.

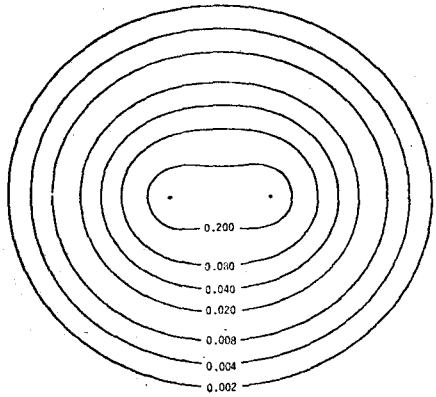

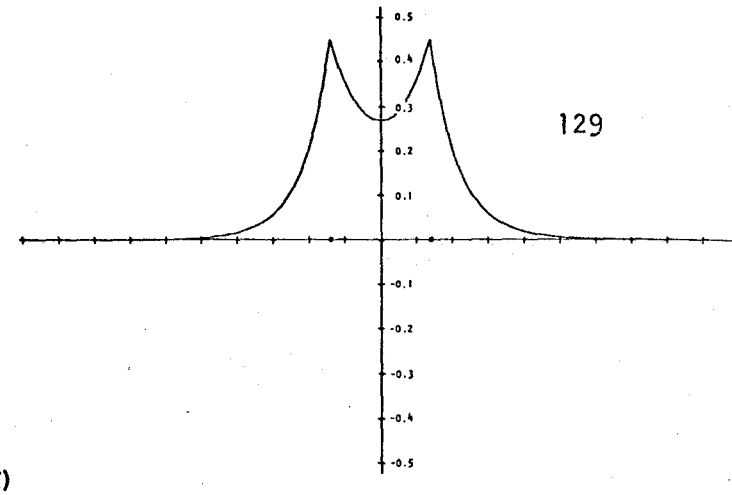

$\rho(\bar{x})$

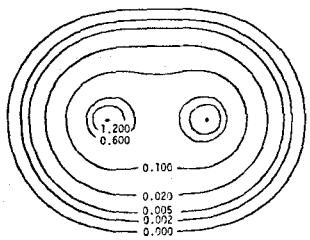

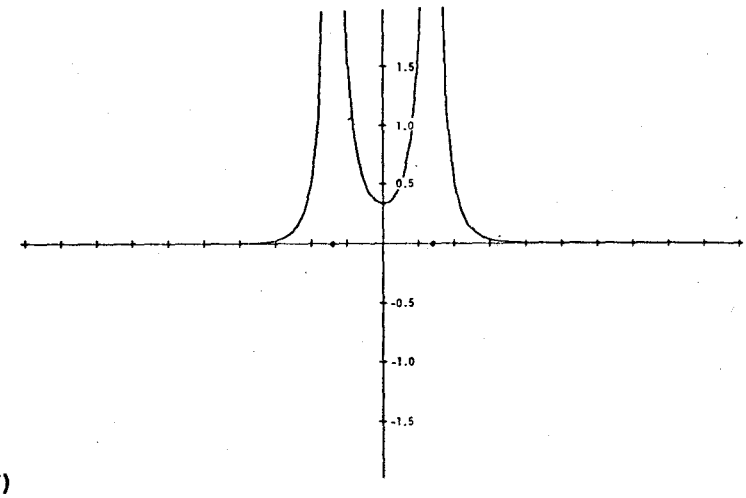

$K(\bar{x})$

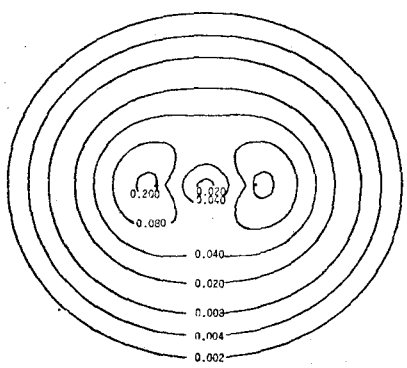

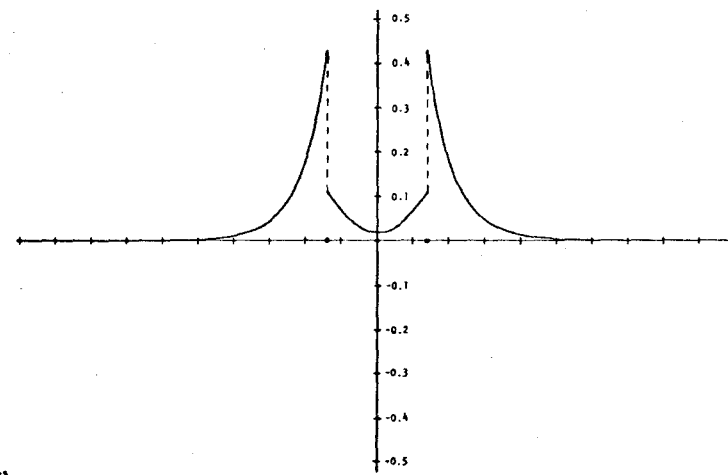

$G(\bar{x})$

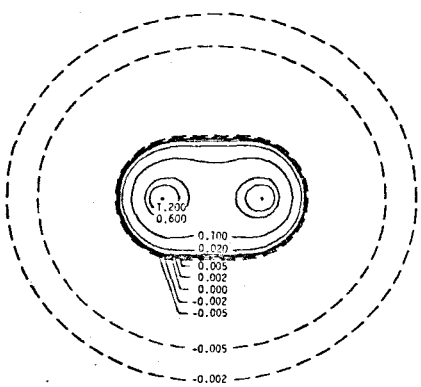

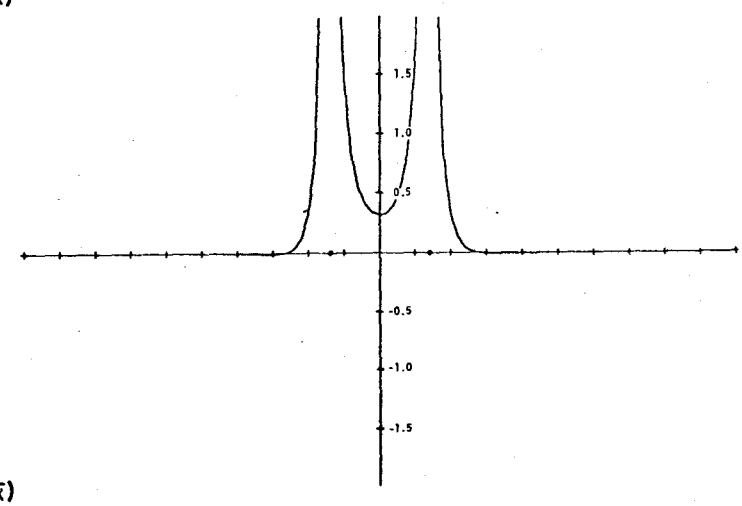

$L(\bar{x})$

or whether they are the result of an extreme non-classical reduction in the potential energy of the system as denoted by regions in which $L(\vec{x}_1) > 0$.

A molecular one-electron charge distribution possesses a saddle point in the internuclear region. The sign of the Laplacian contribution $L(\vec{x}_1)$ in the region of this saddle point is determined by the relative magnitudes of the two competing curvatures. The curvature of $\rho(\vec{x}_1)$ in a direction parallel to the bond axis is positive and hence makes negative contributions to $L(\vec{x}_1)$ and $K(\vec{x}_1)$ whereas the curvature perpendicular to the bond axis is negative and gives positive contributions to $L(\vec{x}_1)$ and $K(\vec{x}_1)$. In a stable molecule such as hydrogen, the accumulation of charge density in the region between the nuclei decreases the positive curvature of $\rho(\vec{x}_1)$ along the bond axis. This minimizes the negative contributions to $L(\vec{x}_1)$ and hence to $K(\vec{x}_1)$. A concomitant peaking of the accumulated charge density along the bond axis leads to a large negative curvature in $\rho(\vec{x}_1)$ perpendicular to the axis. This negative curvature is dominant in H_2 and overall $L(\vec{x}_1) > 0$ in the internuclear or binding region. It is the contraction of the charge density in directions perpendicular to the bond axis which is responsible for the positive sign of $L(\vec{x}_1)$ and $K(\vec{x}_1)$ in the binding region and therefore, for the excess stability of the potential energy density in this critical region of space. The values of $K(\vec{x}_1)$ and $L(\vec{x}_1)$ right at the bond mid-point are 0.323 a.u. and 0.306 a.u. respectively. Thus, the increase in $K(\vec{x}_1)$ at the center of the binding region is primarily the result of an extreme stability in the potential energy rather than from a large contribution to the kinetic energy from $G(\vec{x}_1)$.

The gradient contribution $G(\vec{x}_1)$ is a less rapidly varying function than $K(\vec{x}_1)$. In fact, aside from the internuclear region, the contours of

$G(\vec{x}_1)$ are similar to those for $\rho(\vec{x}_1)$ itself. $G(\vec{x}_1)$, like $\rho(\vec{x}_1)$, increases regularly from the outer regions to maximum values at the nuclei and to ridge-like increases on either side of the internuclear axis in the binding region. Unlike $\rho(\vec{x}_1)$ however, $G(\vec{x}_1)$ exhibits a steep minimum in the region of the bond mid-point. The $1\sigma_g^2$ configuration accounts for 98% of the charge density in the H_2 molecule, and thus the properties of $G(\vec{x}_1)$ are determined almost entirely by the gradient of the density resulting from this configuration. Since the gradients of the $1\sigma_g$ orbital distribution (or any σ_g distribution) both parallel and perpendicular to the internuclear axies at the bond mid-point are zero, the central minimum in the $G(\vec{x}_1)$ contour map is understandable. The value of $G(\vec{x}_1)$ at the bond mid-point (0.0165 a.u.) is the result of the small contribution from the $1\sigma_u$ orbital. It is clear from the second expression for $G(\vec{x}_1)$ given in Equation (3.7b) that an orbital of "u" symmetry will contribute to $G(\vec{x}_1)$ at the bond mid-point as a result of the presence of a node which introduces a non-zero slope for ϕ_i in the direction of the bond axis at the nodal plane. Thus, the bonding ("g" symmetry) or the antibonding ("u" symmetry) character of an orbital (or, in general, the presence or absence of a node in $\rho_i(\vec{x}_1)$ between the nuclei) has a very pronounced effect on the value of $G(\vec{x})$ in the binding region and hence in the contributions to the total kinetic energy from the density in the binding region. The density distribution of a bonding orbital results in a smaller value for $G(\vec{x}_1)$ in the binding region and hence in smaller contributions to $\overline{T}$ than does the density of an antibinding orbital. From the shape of the contours of $\rho(\vec{x}_1)$ it is clear that because of the accumulation of charge between the nuclei, the gradient of $\rho(\vec{x}_1)$ at a point in the internuclear region and in a direction

parallel to the bond axis is less than that perpendicular to the bond axis. This is a reflection of the dominance of the perpendicular curvature over the parallel one in determining the sign of $L(\vec{x}_1)$ in the same region of space. The decrease in the parallel gradient of $\rho(\vec{x}_1)$ in the binding region is further reflected in the nature of the discontinuity illustrated in the profile of the $G(\vec{x}_1)$ distribution. The discontinuous decrease in $G(\vec{x}_1)$ on the binding side of each nucleus dramatizes the great reduction in the magnitude of the parallel gradients in the internuclear region. These characteristics of the charge build-up parallel and perpendicular to the internuclear axis have opposing effects in determining the resultant value of $G(\vec{x}_1)$ at each point in this region. The low value of the gradient in directions parallel to the bond axis leads to small contributions to $G(\vec{x}_1)$ and hence to $\overline{T}$ while the contraction of $\rho(\vec{x}_1)$ perpendicular to the bond axis gives large contributions. The one-electron charge density in the binding region of a stable molecule is therefore, distributed in such a way as to keep the accompanying increase in the kinetic energy to a minimun. The otherwise large increase in $G(\vec{x}_1)$ resulting from the contraction of $\rho(\vec{x}_1)$ perpendicular to the bond, the effect responsible for the reduction in the potential energy, is partially offset by the smaller contributions to $G(\vec{x}_1)$ and hence to $\overline{T}$ as a result of the softening of $\rho(\vec{x}_1)$ along the bond direction.

The differing behaviour of the gradients of $\rho(\vec{x}_1)$ parallel and perpendicular to the bond axis in the internuclear region are so very pronounced in H_2 that it is reflected in the <u>average</u> values of the parallel and perpendicular contribution to the total kinetic energy of the system. The form of the kinetic energy operator

$$T_{op} = -\frac{1}{2}\left(\frac{\partial^2}{\partial_x{}^2} + \frac{\partial^2}{\partial_y{}^2} + \frac{\partial^2}{\partial_z{}^2}\right) \tag{3.17}$$

allows one to evaluate separately the parallel

$$\overline{T}_{\parallel} = -\frac{1}{2}\langle\psi|\frac{\partial^2}{\partial_z{}^2}|\psi\rangle \tag{3.18}$$

and perpendicular

$$\overline{T}_{\perp} = -\frac{1}{2}\langle\psi|\frac{\partial^2}{\partial_x{}^2} + \frac{\partial^2}{\partial_y{}^2}|\psi\rangle \tag{3.19}$$

contributions to the total, average kinetic energy. The integrals required to evaluate $\overline{T}_{\parallel}$ and $\overline{T}_{\perp}$, where the z coordinate is along the bond axis, are given in Appendix 9. In the separated hydrogen atoms the spherical nature of the charge distribution demands that $\overline{T}_{\parallel} = (1/2)\overline{T}_{\perp}$ or that $(\overline{T}_{\perp}-\overline{T}_{\parallel})/\overline{T} = 1/3$. The change in the value of $(\overline{T}_{\perp}-\overline{T}_{\parallel})/\overline{T}$ from its atomic value of 1/3 provides a measure of the extent to which the formation of the molecule effects a differentiation in the distribution of $\rho(\vec{x}_1)$ parallel and perpendicular to the bond axis. In the stable hydrogen molecule one finds (see Table 3.1) that $\overline{T}_{\parallel}$ has decreased in value from that for two hydrogen atoms, while $\overline{T}_{\perp}$ has increased. The value of $(\overline{T}_{\perp}-\overline{T}_{\parallel})/\overline{T}$ is increased in value from 1/3 to 0.4740. Thus, the formation of the molecule results in a considerable differentiation between the distribution of the charge density parallel and perpendicular to the bond axis. The reduction in the gradient of $\rho(\vec{x}_1)$ and its contributions to $G(\vec{x}_1)$ in directions parallel to the bond axis leads to a considerable decrease in $\overline{T}_{\parallel}$. $\overline{T}_{\perp}$ on the other hand is greatly increased over the original atomic contributions as a result of the contraction of the charge density in directions perpendicular to the bond axis.* The same conclusions regarding the relative behaviour of $\overline{T}_{\parallel}$ and $\overline{T}_{\perp}$ are to be found in the results obtained by Coulson[107] in his study of the momentum

* The average values of the parallel and perpendicular contributions to $\overline{T}$ have previously been calculated from a less accurate wavefunction for H_2 by Hoare and Linett[114]. A discussion of the binding in the H_2 molecule was given with reference to the properties of "a particle in a box".

TABLE 3.1

Values of $\overline{T}_{\parallel}$ and $\overline{T}_{\perp}$ for H_2 as a Function of R[a]

R	$\overline{T}$	$\overline{T}_{\parallel}$	$\overline{T}_{\perp}$	$(\overline{T}_{\perp} - \overline{T}_{\parallel})/\overline{T}$
1.0	1.4332	0.4032	1.0299	0.4373
1.2	1.2775	0.3465	0.9310	0.4574
1.3	1.2135	0.3238	0.8897	0.4663
1.4	1.1569	0.3043	0.8527	0.4740
1.6	1.0617	0.2728	0.7888	0.4860
2.0	0.9293	0.2343	0.6949	0.4956
4.0	0.9289	0.2885	0.6404	0.3789
8.0	0.9868	0.3288	0.6580	0.3336
∞	1.0000	0.3333^{+}	0.6666^{+}	0.3333^{+}

[a] All values are given in atomic units (a.u.).

distribution in the hydrogen molecule. He observed that the mean component of the velocity in the direction of the bond is decreased while the mean component of velocity perpendicular to the bond is increased.

In summary the charge density accumulated in the internuclear region, an accumulation which is necessary for the attainment of electrostatic equilibrium and the formation of a stable chemical bond, is distributed in such a way as to keep the increase in the kinetic energy to a minimum. The kinetic energy increase necessary for the decrease in the potential energy is restricted mainly to the perpendicular contributions of $G(\vec{x}_1)$. The relaxation of the curvature and gradient of $\rho(\vec{x}_1)$ in the parallel directions results in greatly reduced contributions to $G(\vec{x}_1)$ and hence to $\overline{T}$ while at the same time leading to an increase in the stability of the system (a more negative potential energy density) by decreasing the negative contributions to $L(\vec{x}_1)$ and $K(\vec{x}_1)$. Thus, both the relaxation of $\rho(\vec{x}_1)$ parallel to the bond axis and the contraction of $\rho(\vec{x}_1)$ perpendicular to this axis lead to a decrease in potential energy of the system but only the contractive effect results in large contributions to the kinetic energy. These properties of a one-electron charge distribution characteristic of a stable molecule will now be contrasted with those for the unstable He molecule, for which $\overline{T} > \frac{1}{2}|\overline{V}|$ for all values of R.

Contour maps of the total one-electron charge density $\rho(\vec{x}_1)$, the distribution $K(\vec{x}_1)$ and its components $L(\vec{x}_1)$ and $G(\vec{x}_1)$ for He_2 at R= 2.0 a.u. are given in Figure 3.2.* The charge density in He_2 is very peaked at the nuclei, but the value at the bond mid-point (0.164 a.u.) is considerably less than for H_2 (0.268 a.u.). A comparison of the difference density, $\Delta\rho(\vec{x}_1)$, contour maps for H_2 and He_2 (see Figures 3.3 and 3.4 respectively)

* The distributions for He_2 were calculated from the Hartree-Fock wavefunctions by Kestner[115].

Figure 3.2. Contour maps and profiles of $\rho(\vec{x}_1)$, $K(\vec{x}_1)$, $G(\vec{x}_1)$ and $L(\vec{x}_1)$ for He_2 at an internuclear separation of 2.0 a.u.

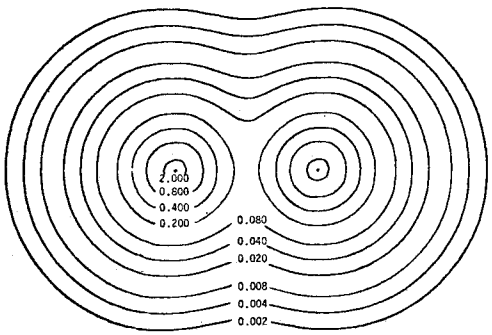

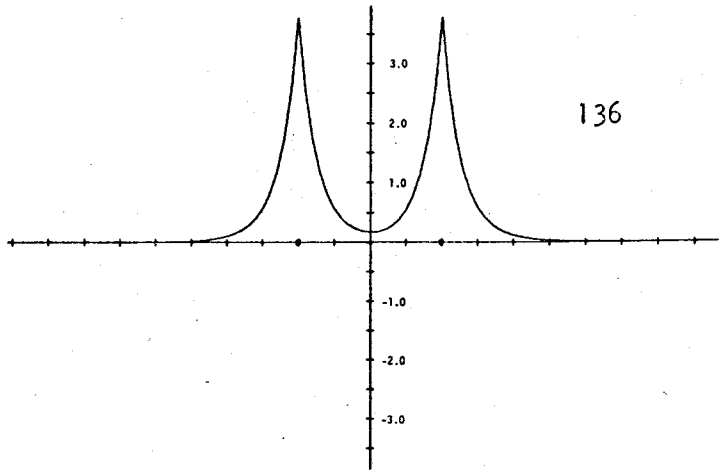

$\rho(\bar{x})$

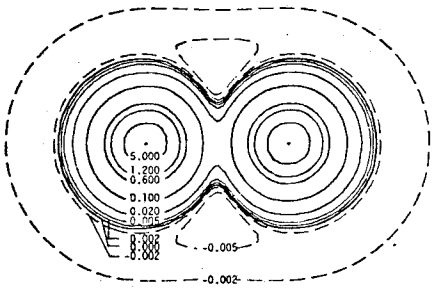

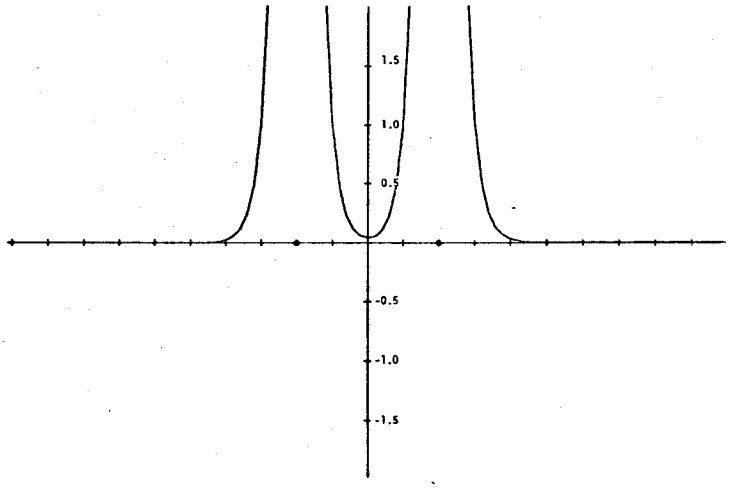

$K(\bar{x})$

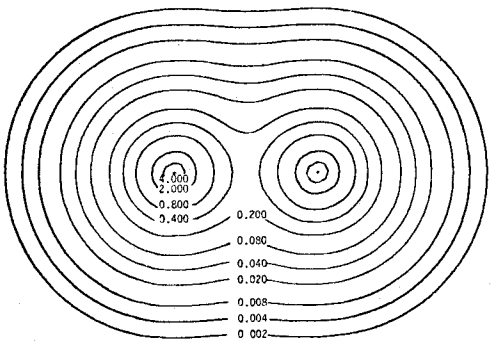

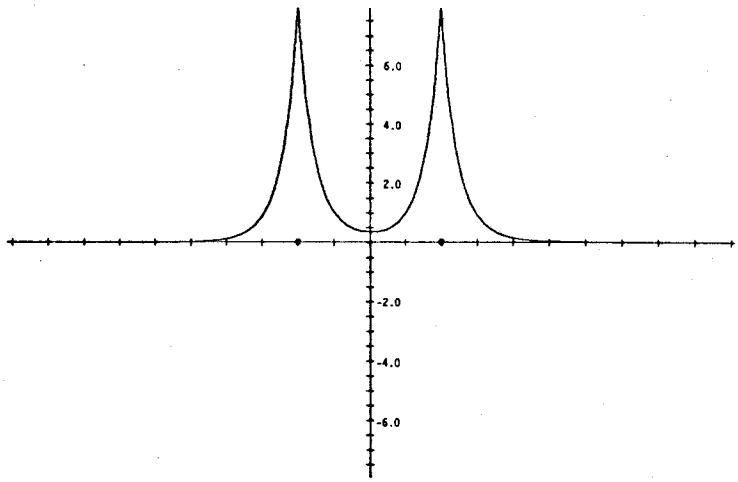

$G(\bar{x})$

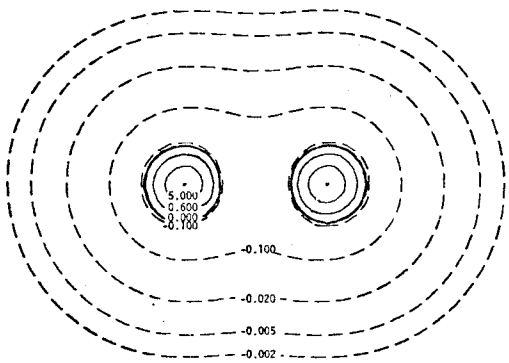

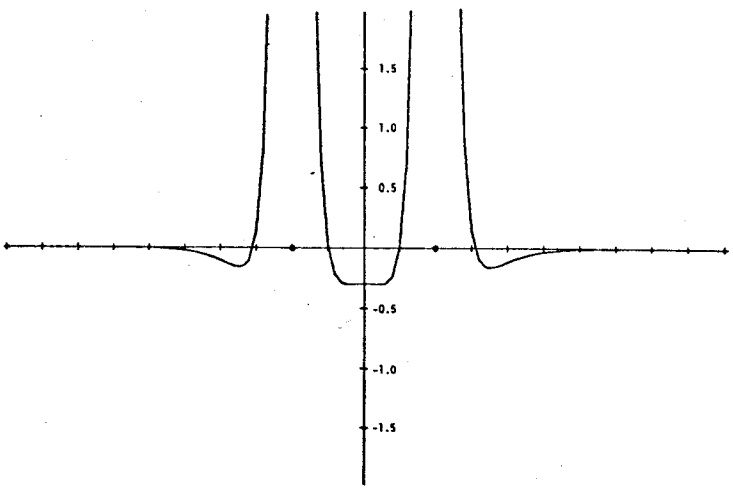

$L(\bar{x})$

indicates that aside from an increase in $\rho(\vec{x}_1)$ in the regions of the nuclei in both cases, the one-electron charge distributions exhibit opposite behaviour with respect to where the charge is removed and where it is accumulated. The large deficit in the binding region of the $\Delta\rho(\vec{x}_1)$ map for He_2 is a direct result of the anti-symmetry requirement of the Pauli exclusion principle which is discussed in Chapter II. The electrostatic analysis shows that a charge redistribution such as that pictured in the $\Delta\rho(\vec{x}_1)$ map for He_2 is inherently incapable of balancing the forces of nuclear repulsion[8,116]. The resulting instability of the system is now to be examined in terms of the energy distribution $K(\vec{x}_1)$ and its components.

The kinetic energy distribution $K(\vec{x}_1)$ is large and positive in the regions of the nuclei, as anticipated on the basis of the large charge accumulation in these regions. Its value in the region of the bond mid-point is however, very small, differing from that for hydrogen by roughly a factor of ten. Thus, the potential energy density cannot attain large negative values in this critical region of the potential energy surface.

The unfavourable distribution of the potential energy density may be traced directly to the topography of the charge distribution via the distribution function $L(\vec{x}_1)$. In He_2 the function $L(\vec{x}_1)$ is positive only in the immediate vicinity of the nuclei and thus only in these regions does the potential energy attain the extreme stabilities allowed in a quantum mechanical system. Because of the removal of charge density from the internuclear region, the curvature of $\rho(\vec{x}_1)$ in directions parallel to the bond axis is larger than the magnitude of the negative curvature per-

pendicular to the axis. As a result, $L(\vec{x}_1)$ attains its maximum negative values in the binding region and the stability of the potential energy density in the same region is reduced to a minimum. Thus, the Laplacian distributions for H_2 and He_2 exhibit opposite behaviour in their respective binding regions. The opposing effects which the accumulation or depletion of charge density in the binding region have on the potential energy of a system may therefore, be directly related to the sign of the dominant curvature of the one-electron charge distribution in this same region of space.

The differing topography of the charge distributions of H_2 and He_2 is further reflected in their kinetic energy contributions as determined by $G(\vec{x}_1)$, particularly in the binding region. The contours of $G(\vec{x}_1)$ for He_2 are similar in shape to those for $\rho(\vec{x}_1)$, indicating that the contours of equidensity represent lines of almost constant value for the classical-like contribution to the kinetic energy. In spite of a greatly reduced value for $\rho(\vec{x}_1)$ in the internuclear region of He_2 compared to H_2, the value of $G(\vec{x}_1)$ in this region of space is much greater than that for H_2, the values at the bond mid-point being 0.3344 and 0.0165 a.u. respectively. Because of the presence of the σ_u density component in He_2, $G(\vec{x}_1)$ does not exhibit a minimum at the bond mid-point as it does in the case of H_2. Instead, both the parallel and perpendicular contributions to $G(\vec{x}_1)$ and hence to $\overline{T}$ are large in He_2 as a consequence of the depletion of charge density in the binding region. The large value of the parallel gradient in the binding region of He_2 is reflected in the fact that at the discontinuity in $G(\vec{x}_1)$, which is too small to be shown in the profile of $G(\vec{x}_1)$ in Figure 3.2, the magnitude of the parallel gradient on the bonded side

of the nucleus exceeds that on the nonbonded side. Just the opposite behaviour is found in the profile of $G(\vec{x}_1)$ for H_2.

From this contrast in the behaviour of the $L(\vec{x}_1)$ and $G(\vec{x}_1)$ distributions for H_2 and He_2 it is concluded that a necessary (but not necessarily sufficient) criterion for molecular stability is the existence of a net negative curvature for $\rho(\vec{x}_1)$ in the binding region. A negative curvature for $\rho(\vec{x}_1)$ implies that $L(\vec{x}_1)$ is maximized in both parallel and perpendicular directions thus resulting in the maximum stability in the potential energy density. A negative curvature for $\rho(\vec{x}_1)$ insures at the same time that the increased stability is gained with the minimum increase in the kinetic energy, for while the perpendicular contributions to $G(\vec{x}_1)$ and $\overline{T}$ are increased, the parallel contributions are decreased with respect to the separated atoms. On the other hand, an overall positive curvature for $\rho(\vec{x}_1)$ in the binding region implies not only the absence of an excess stability in the potential energy density in the same region, but also a large total kinetic energy increase, since $G(\vec{x}_1)$ is increased both parallel and perpendicular to the bond axis. Table 3.2 indicates that this property of the $G(\vec{x}_1)$ distribution is again reflected in the average quantities $\overline{T}_{\parallel}$ and $\overline{T}_{\perp}$. In He_2 the values of $\overline{T}_{\parallel}$ and $\overline{T}_{\perp}$ are <u>both</u> increased above their atomic values, with $\overline{T}_{\parallel}$ increasing more than $\overline{T}_{\perp}$. Thus, the ratio $(\overline{T}_{\perp}-\overline{T}_{\parallel})/\overline{T}$ rather than increasing from its limiting value of 1/3 as in H_2, decreases to 0.290. The decrease in this ratio for He_2 indicates a greater overall tightening of the one-electron charge density parallel to the bond axis rather than perpendicular to it as in the case of H_2.

3.4 A Comparison of the Molecular and Atomic Kinetic Energy Distributions for H_2 and He_2

TABLE 3.2

Values of $\bar{T}_{\parallel}$ and $\bar{T}_{\perp}$ for He_2 as a Function of R[a]

R	$\bar{T}$	$\bar{T}_{\parallel}$	$\bar{T}_{\perp}$	$(\bar{T}_{\perp} - \bar{T}_{\parallel})/\bar{T}$
1.0	6.6190	2.4137	4.2053	0.2707
2.0	6.0803	2.1594	3.9209	0.2897
3.0	5.7985	1.9572	3.8413	0.3249
4.0	5.7381	1.9160	3.8221	0.3322
4.7	5.7265	1.9095	3.8169	0.3331
5.2	5.7237	1.9081	3.8156	0.3333
5.5	5.7239	1.9080	3.8158	0.3333
6.0	5.7249	1.9084	3.8165	0.3333
∞	5.7233	1.9078	3.8156	0.3333^{+}

[a] All values are given in atomic units (a.u.).

The discussion in Section 3.3 related the stability of a molecular system to the topographical features of $\rho(\vec{x}_1)$ itself through a comparison of the spatial distribution of the one-electron charge densities in the hydrogen and helium molecules. This section considers the question of molecular stability from the point of view of the changes which the formation of a molecule brings about in the kinetic and potential energies of the atoms. The difference distributions for $\rho(\vec{x}_1)$, $K(\vec{x}_1)$, $G(\vec{x}_1)$ and $L(\vec{x}_1)$ are shown in Figure 3.3 and 3.4 for H_2 and He_2 respectively. They are determined from the density difference distribution (defined here for a diatomic molecule AB)

$$\Delta\rho(\vec{x}_1) = \rho(\vec{x}_1) - [\rho_A(\vec{x}_1) + \rho_B(\vec{x}_1)] \ , \qquad (3.20)$$

where $\rho(\vec{x}_1)$ is the molecular one-electron charge distribution and $\rho_A(\vec{x}_1)$ and $\rho_B(\vec{x}_1)$ are the undistorted atomic densities separated by a distance R_e. The compression of the charge density accompanying the formation of the H_2 molecule, which is evident in the $\Delta\rho(\vec{x}_1)$ map, has an obvious parallel in the increase in $K(\vec{x}_1)$ evident in the $\Delta K(\vec{x}_1)$ map. The integral of $\Delta K(\vec{x}_1)$ over all space is a positive quantity, equal to the difference between the average kinetic energies of the molecule and the separated atoms, a difference which in turn is equal to the absolute value of the binding energy of the system. The $\Delta\rho(\vec{x}_1)$ and $K(\vec{x}_1)$ distributions are very similar in appearance; the increase or decrease in the charge density resulting in a corresponding increase or decrease in $K(\vec{x}_1)$ for the system. Transferring $G(\vec{x}_1)$ to the L.H.S. of Equation (3.14) gives an expression for $K(\vec{x}_1)$ in terms of the difference between the sum of the orbital energy densities and the potential energy density. Since $\sum_i \varepsilon_i \rho_i(\vec{x}_1)$ is everywhere negative, positive regions

Figure 3.3. Contour maps and profiles of the difference distributions $\Delta\rho(\vec{x}_1)$, $\Delta K(\vec{x}_1)$, $\Delta G(\vec{x}_1)$ and $\Delta L(\vec{x}_1)$ for H_2 at R = 1.4 a.u.

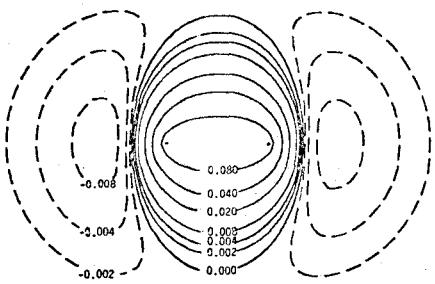

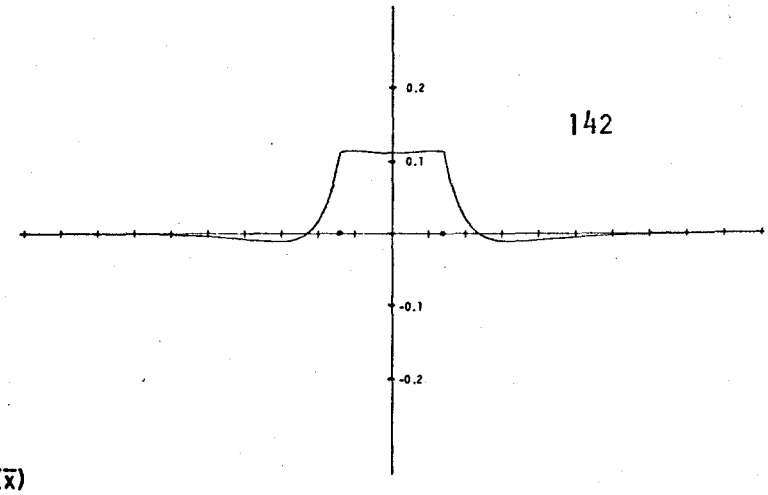

$\Delta\rho(\bar{x})$

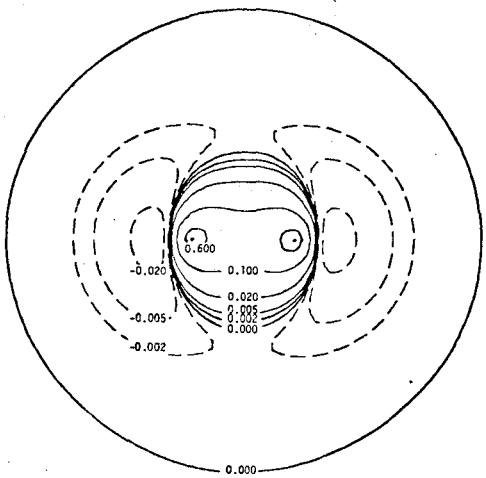

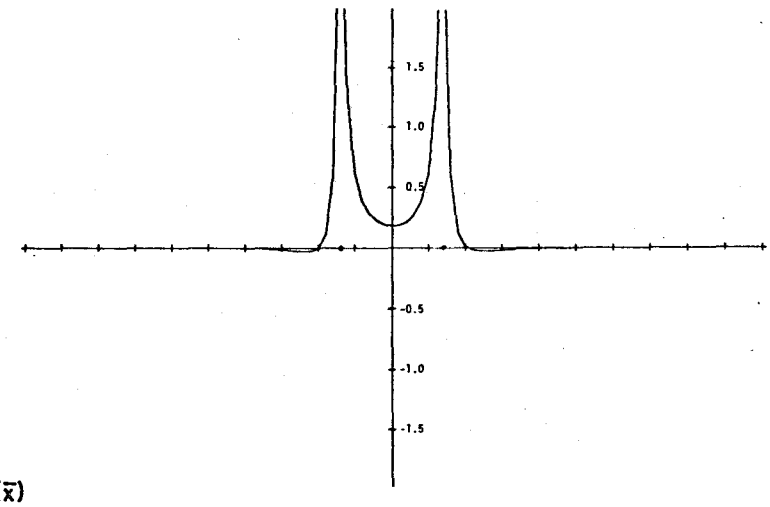

$\Delta K(\bar{x})$

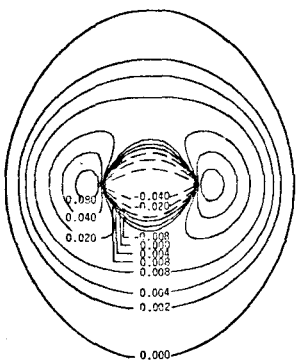

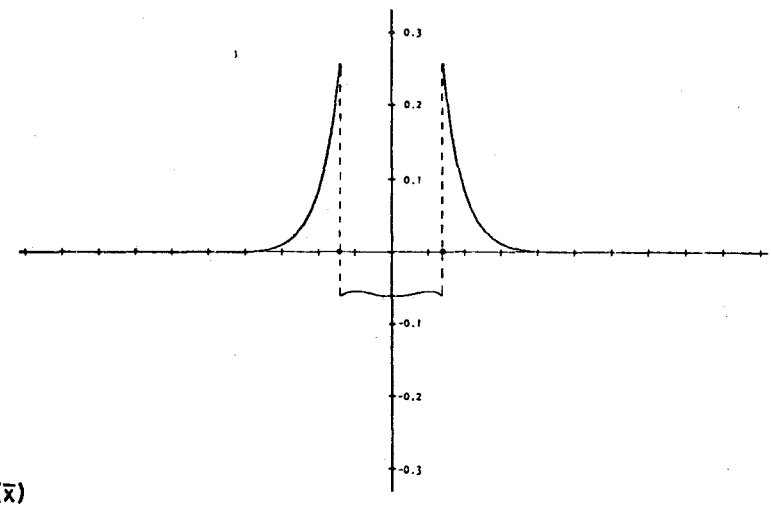

$\Delta G(\bar{x})$

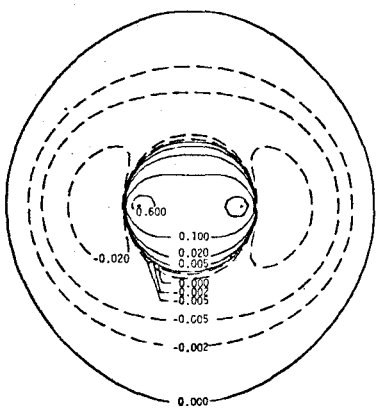

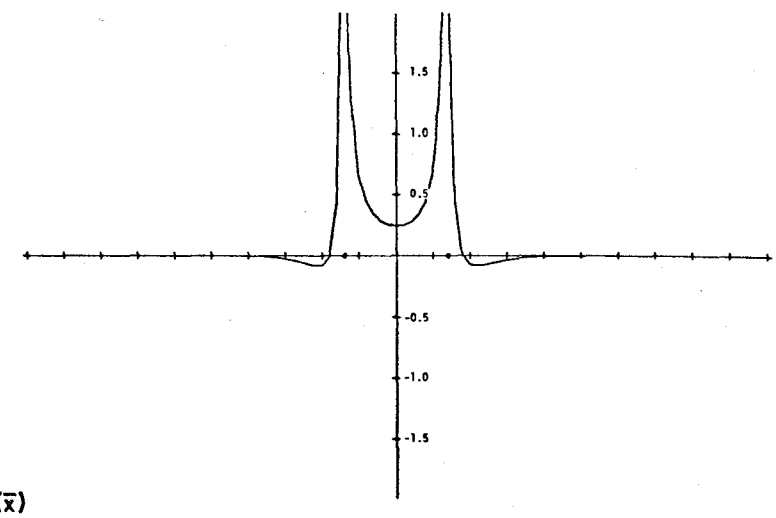

$\Delta L(\bar{x})$

Figure 3.4. Contour maps and profiles of the difference distributions for He_2 at R = 2.0 a.u.

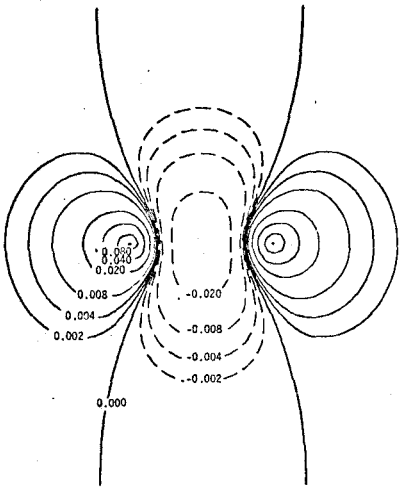

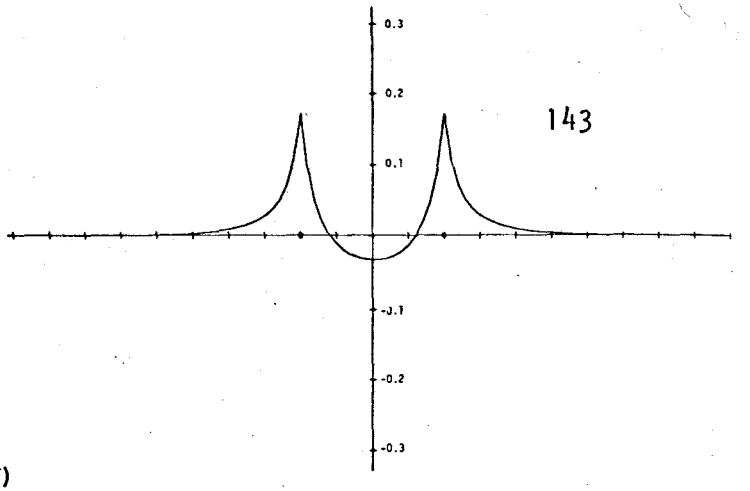

$\Delta\rho(\bar{x})$

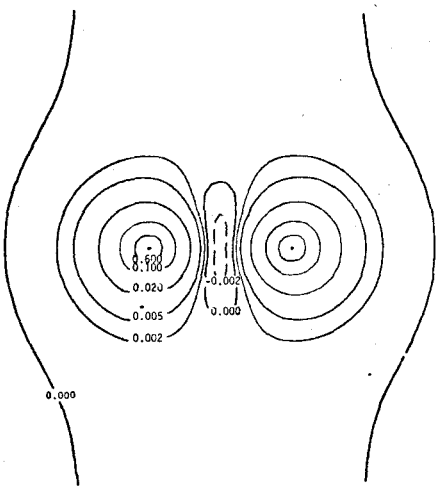

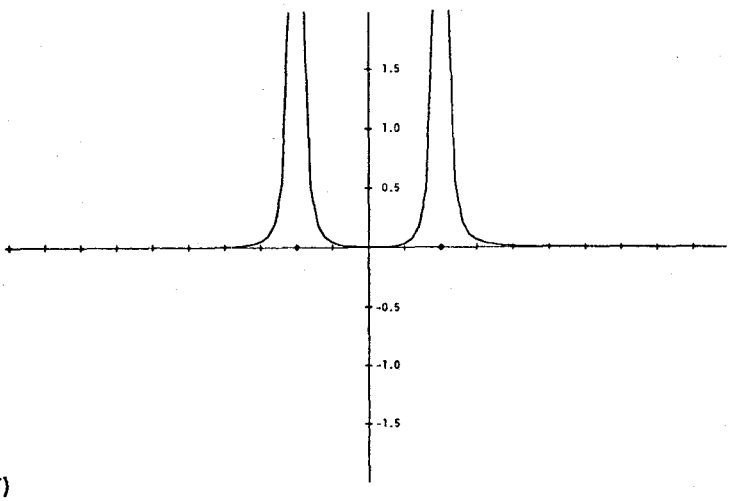

$\Delta K(\bar{x})$

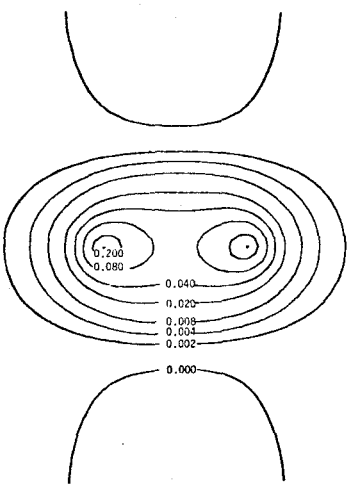

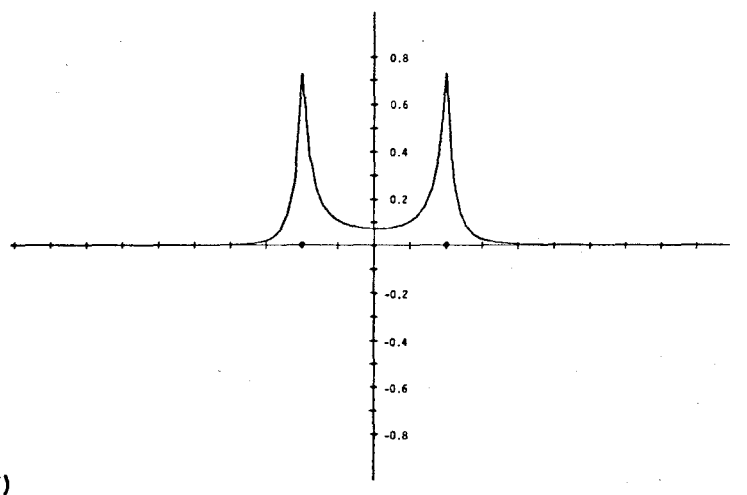

$\Delta G(\bar{x})$

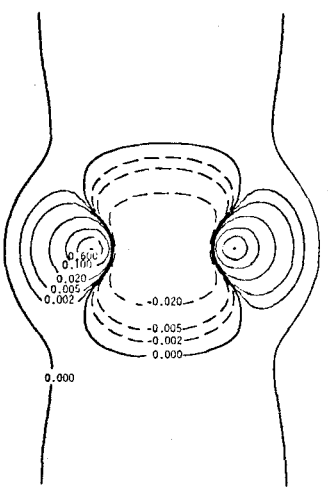

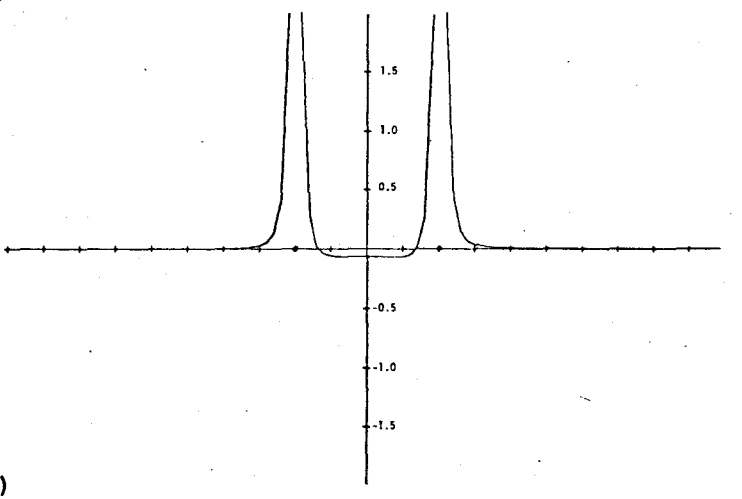

$\Delta L(\bar{x})$

of $K(\vec{x}_1)$ denote regions in which the potential energy density exceeds the energy density in absolute value. Similarly, an equation for $\Delta K(\vec{x}_1)$ in the Hartree-Fock approximation shows that for those regions of space in which both $\Delta\rho(\vec{x}_1)$ and $\Delta K(\vec{x}_1)$ are positive, the potential energy density of the molecule is more negative than that for the separated atoms. Not unexpectedly, the $\Delta K(\vec{x}_1)$ map demonstrates that the decrease in the potential energy occurs in the vicinity of the nuclei and in the internuclear regions. Since the region in which $\Delta K(\vec{x}_1) > 0$ is remarkably similar to that for which $\Delta\rho(\vec{x}_1) > 0$, almost the whole of the charge redistribution for the formation of H_2 results in a decrease in the potential energy density of the system.

A more direct view of the changes in the kinetic and potential energies of the atoms resulting from the charge redistribution depicted in the $\Delta\rho(\vec{x}_1)$ map is given in the difference maps for $G(\vec{x}_1)$ and $L(\vec{x}_1)$. The diagram of $\Delta G(\vec{x}_1)$ for H_2 (see Figure 3.3) indicates that, relative to the charge distribution obtained by the overlap of two undistorted atomic densities, the contributions to $G(\vec{x}_1)$ and hence to $\overline{T}$ for the molecular one-electron charge distribution have increased in the antibinding regions and have decreased in the binding region, a behaviour just opposite to that of charge density itself. Thus relative to the separated atom charge densities, the softening of the gradients of $\rho(\vec{x}_1)$ parallel to the bond axis (as is very evident in the profile of the $\Delta\rho(\vec{x}_1)$ map) dominate the change in $G(\vec{x}_1)$ in the internuclear region; the concentration of charge density in this region resulting in a decrease in $G(\vec{x}_1)$ and hence in decreased contributions to $\overline{T}$. The removal of charge density from the antibinding regions on the other hand, results in increased gradients for

the molecular distribution compared to the atomic ones and hence $G(\vec{x}_1)$ and $\overline{T}$ are increased. The integration of $G(\vec{x}_1)$ over all space yields $\Delta\overline{T}$, the difference in the kinetic energies of the molecule and the separated atoms. This is a positive quantity and the $\Delta G(\vec{x}_1)$ distribution indicates that relative to the separated atoms the increase in the kinetic energy is confined to the antibinding regions. It is important in the interpretation of the $\Delta G(\vec{x}_1)$ map to recall that the atomic contributions are determined for each atomic distribution separately and then added, as demanded by the expression for $\Delta\rho(\vec{x}_1)$ or if the integral of $\Delta G(\vec{x}_1)$ over all space is to equal $\Delta\overline{T}$. The $G(\vec{x}_1)$ distribution for the sum of the atomic distributions is <u>not</u> zero in the internuclear regions as profiles of $\rho(\vec{x}_1)$ for such a combined distribution would at first suggest. Thus, the negative values of $\Delta G(\vec{x}_1)$ in the binding region may be interpreted as arising from the ability of an electron in the molecule to move in the region of either nucleus rather than being confined to the region of a single nucleus as in the separated atoms. Or, alternatively, the decrease in the contributions to the kinetic energy from the binding region results from the charge density in the molecule being continuous over the whole of the binding region with a high probability density, rather than over half of it separately with a rapidly decreasing probability density as is the case for the atomic charge distributions. In the same way, the loss of charge density from the antibinding region decreases the effective volume available to the electrons and increases their kinetic energy contributions.

Ruedenberg[111] has previously stressed that the kinetic energy of the molecule is decreased as a result of the increased freedom of the electrons in the molecule over that present in the "promotion states" of

the atoms, in analogy with the behaviour of an electron in a box. However, we wish to point out that such an effect is evident in the binding region of the H_2 molecule with respect to the separated atoms themselves, and that it is not necessary to introduce a contractive promotion of the atomic charge densities to demonstrate the decrease in kinetic energy which arises from the increased "freedom" of the electrons, or better stated, from the change in the density distribution from a discontinuous one to one which is continuous over the whole of the binding region.

The $\Delta L(\vec{x}_1)$ distribution illustrates that the decrease in the potential energy which accompanies the formation of the hydrogen molecule occurs in the binding region and in the region of the nuclei. Thus, the decreases and increases in the charge density shown in the $\Delta\rho(\vec{x}_1)$ map correspond closely to regions of decrease and increase respectively in the absolute magnitude of the potential energy of the molecular one-electron charge distribution relative to that of the overlapping atomic distribution.

The $\Delta G(\vec{x}_1)$ map for He_2 is striking in that it illustrates that relative to the separated atom distributions the contribution to the kinetic energy from the molecular one-electron charge distribution are everywhere greater. Furthermore, the contributions from the internuclear region are greater than those from the antibinding regions in spite of greatly decreased values for $\rho(\vec{x}_1)$ in the binding region. The opposing behaviour of the parallel contributions to $\overline{T}$ in H_2 and He_2 (see Table 3.1 and 3.2 respectively) are made very evident by contrasting the properties of their $\Delta G(\vec{x}_1)$ distributions. The softening of the gradient and Laplacian of $\rho(\vec{x}_1)$ in directions parallel to the axis in the binding region of H_2 results in a $\Delta G(\vec{x}_1)$ distribution which is negative in this same region and attains its

minimum value along the internuclear axis. In He_2 the $\Delta G(\vec{x}_1)$ distribution exhibits a maximum along the bond axis. The $\Delta\rho(\vec{x}_1)$ map indicates that the charge density joining the two helium nuclei is smaller in value than that obtained from the overlapping atomic distributions. Unlike H_2, the formation of He_2 does not result in a greater freedom for the electrons since the originally isolated atoms are bridged by a probability density which is lower in value than that of the original atomic distributions. In effect, the parallel motions of the electrons in He_2, as gauged by the kinetic energy contributions from the binding region, are more restricted in the molecule than in the separated atoms.

As in the case of H_2, the features of the $\Delta L(\vec{x}_1)$ map for He_2 parallel closely those of the $\Delta\rho(\vec{x}_1)$ map. The $\Delta L(\vec{x}_1)$ map for He_2 illustrates that relative to the separated atoms, the potential energy density attains its maximum values in the antibinding regions and undergoes a decrease in stability in the critical binding region. The profile of $\Delta L(\vec{x}_1)$ and its implications about the changes in the potential energy density are of course a direct consequence of the curvatures exhibited by the $\Delta\rho(\vec{x}_1)$ profile.

The changes in the kinetic energy distributions necessary for the attainment of a stable molecular species can be examined by considering the H_2 molecule at a number of different bond lengths. Contour plots, without the corresponding profiles, of the total distributions $\rho(\vec{x}_1)$, $K(\vec{x}_1)$, $G(\vec{x}_1)$, $L(\vec{x}_1)$ and their difference distributions are shown in Figures 3.5, 3.6 and 3.7 for the H_2 molecule at internuclear separations of 1.2, 2.0 and 4.0 a.u. respectively. These distributions were obtained using the Das and Wahl[113] extended wavefunctions for H_2. The contour plots in Figure 3.5, which are for H_2 at a bond length of 1.2 a.u., are very similar to the

Figure 3.5. Contour maps of the total distributions $\rho(\vec{x}_1)$, $K(\vec{x}_1)$, $G(\vec{x}_1)$, $L(\vec{x}_1)$ and the difference distributions for H_2 at R = 1.2 a.u.

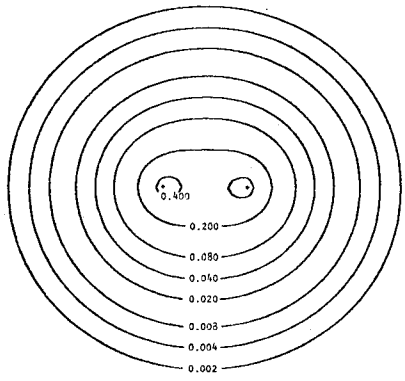

$\rho(\bar{x})$

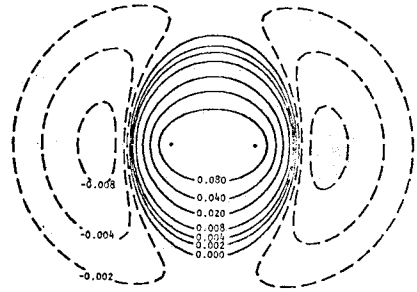

$\Delta\rho(\bar{x})$

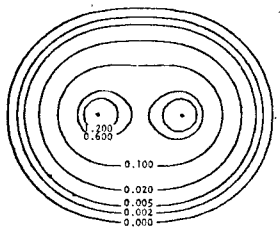

$K(\bar{x})$

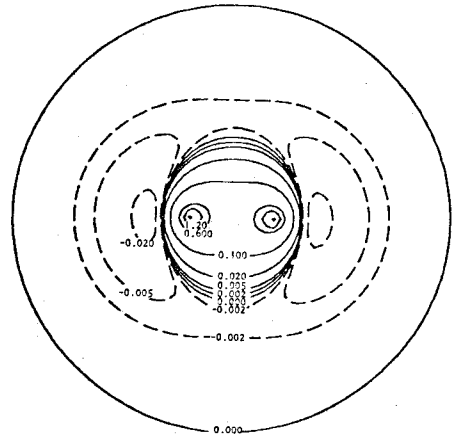

$\Delta K(\bar{x})$

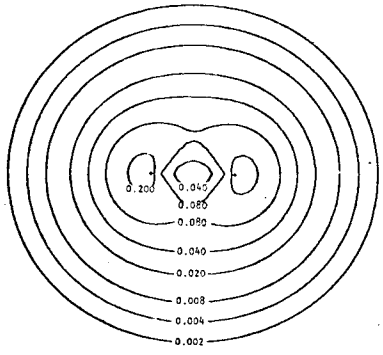

$G(\bar{x})$

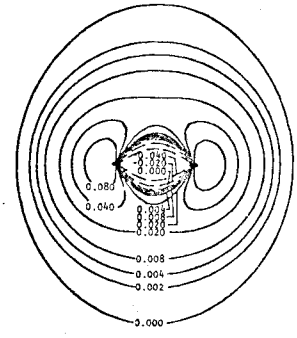

$\Delta G(\bar{x})$

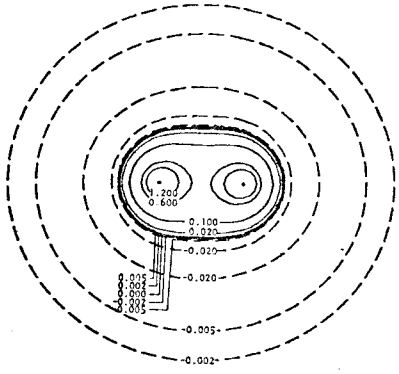

$L(\bar{x})$

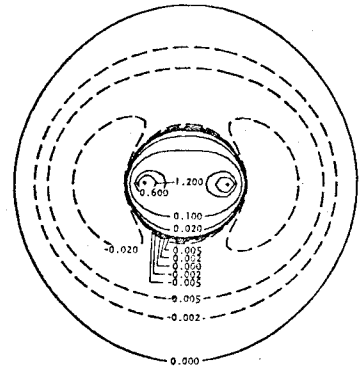

$\Delta L(\bar{x})$

Figure 3.6. Contour maps of the total distributions $\rho(\vec{x}_1)$, $K(\vec{x}_1)$, $G(\vec{x}_1)$, $L(\vec{x}_1)$ and the difference distributions for H_2 at R = 2.0 a.u.

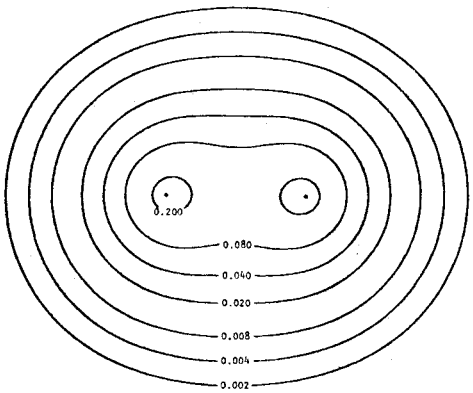

$\rho(\bar{x})$

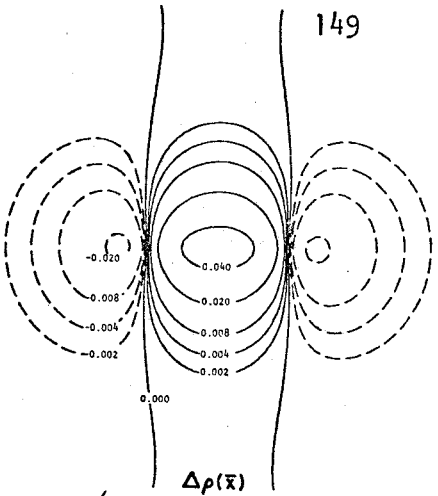

$\Delta\rho(\bar{x})$

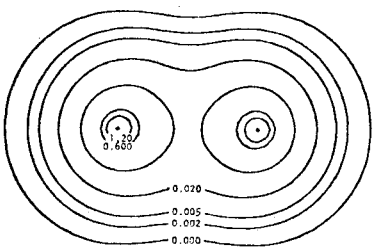

$K(\bar{x})$

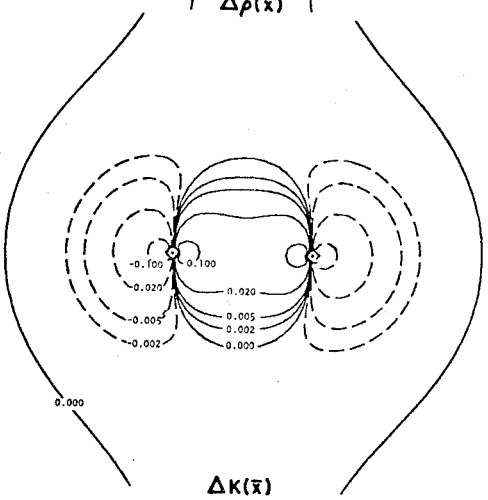

$\Delta K(\bar{x})$

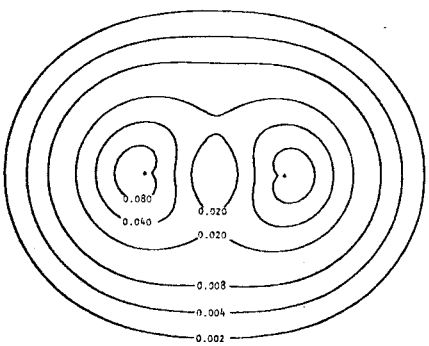

$G(\bar{x})$

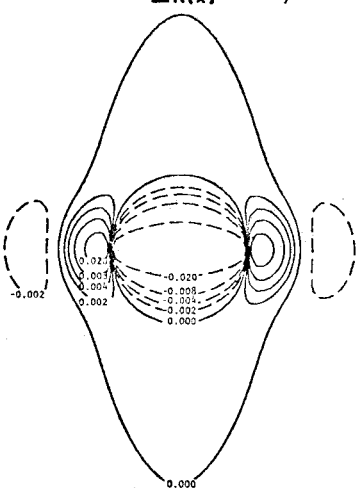

$\Delta G(\bar{x})$

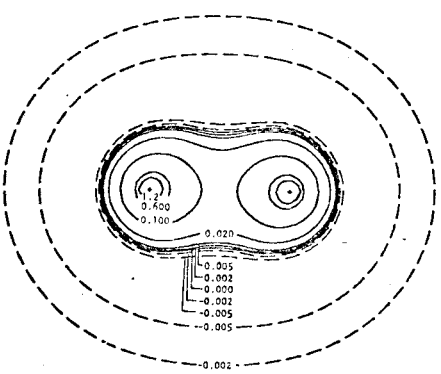

$I(\bar{x})$

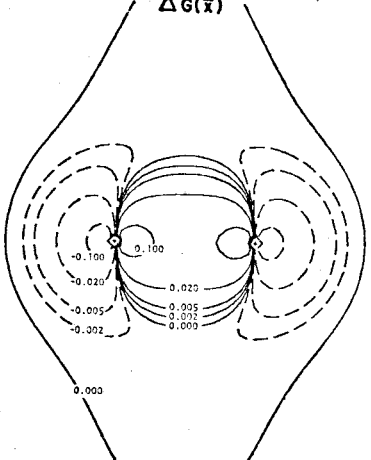

Figure 3.7. Contour maps of the total distributions $\rho(\vec{x}_1)$, $K(\vec{x}_1)$, $G(\vec{x}_1)$, $L(\vec{x}_1)$ and the difference distributions for H_2 at R = 6.0 a.u.

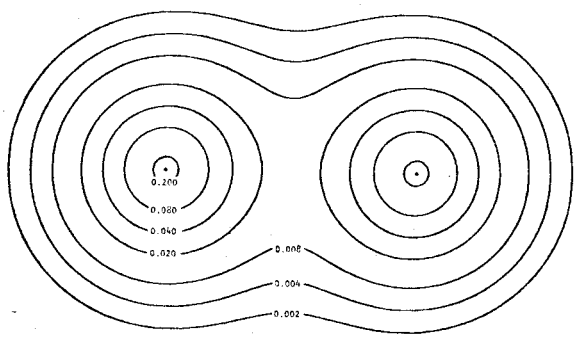

$\rho(\bar{x})$

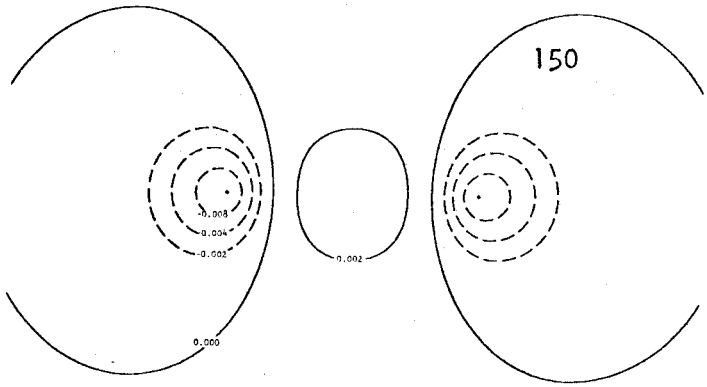

$\Delta\rho(\bar{x})$

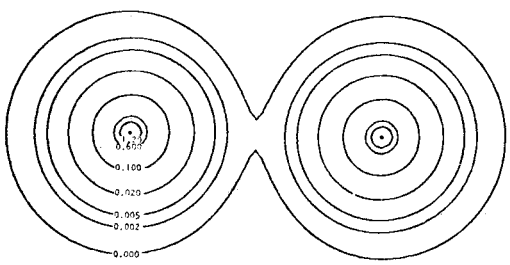

$K(\bar{x})$

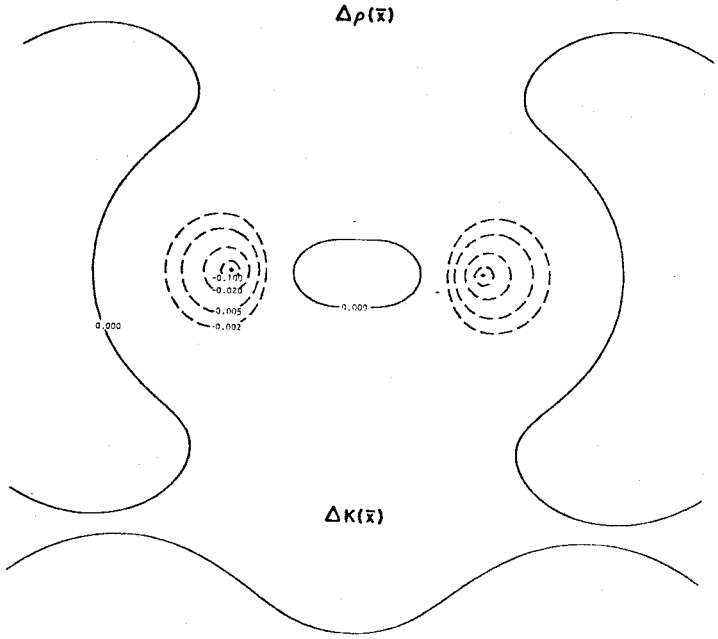

$\Delta K(\bar{x})$

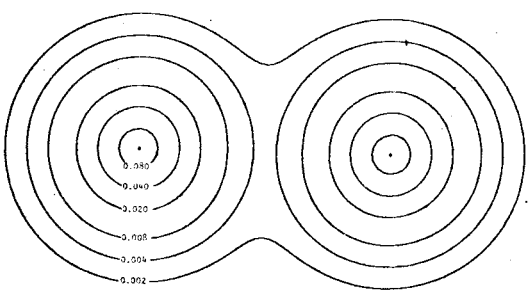

$G(\bar{x})$

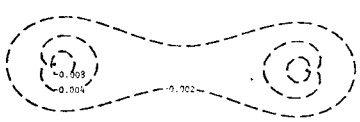

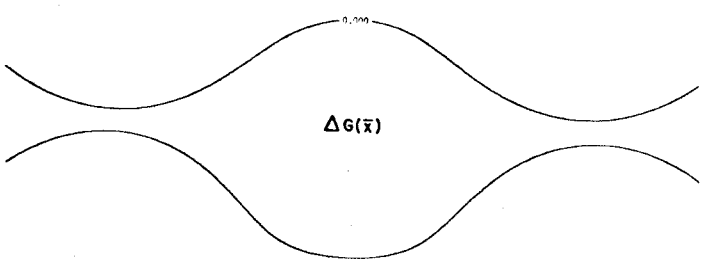

$\Delta G(\bar{x})$

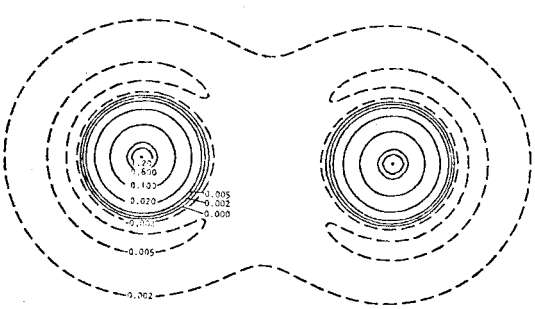

$L(\bar{x})$

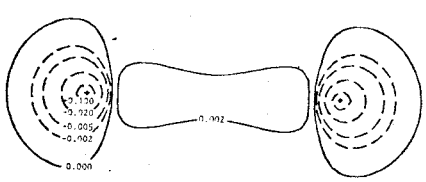

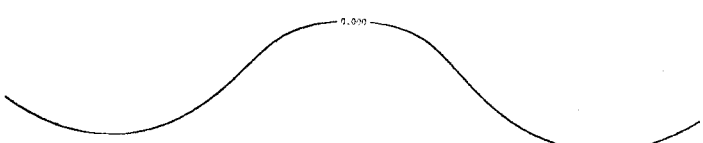

$\Delta L(\bar{x})$

corresponding plots for H_2 at the equilibrium bond length of 1.4 a.u. (see Figures 3.1 and 3.3). As the bond length is decreased the increase in kinetic energy, which tends to destabilize the system, can be seen to be the result of a large increase in $K(\vec{x}_1)$ or $G(\vec{x}_1)$, and thus an increase in $\overline{T}$, in the regions around the nuclei; the energy distributions in the internuclear or binding region are almost identical for the two different bond lengths. As the internuclear separation in H_2 is increased beyond the equilibrium value (see Figures 3.6 and 3.7) the <u>total</u> distributions $\rho(\vec{x}_1)$, $K(\vec{x}_1)$, $G(\vec{x}_1)$ and $L(\vec{x}_1)$ begin the resemble the corresponding distributions for He_2 (see Figures 3.2 and 3.4). At the largest internuclear separation considered for H_2, Figure 3.7, $L(\vec{x}_1)$ is negative in the internuclear region as in He_2 and the energy distributions clearly show the appearance of almost completely separated atoms.

The difference distributions at the different internuclear separations indicate the regions in which the contributions to the kinetic energy in the molecule have increased or decreased with respect to the separated atom values. For example, at a large separation of the hydrogen nuclei (see Figure 3.7) the difference distributions show that the rearrangement of the atomic charge densities does not produce large changes in the contributions to the kinetic energy from the binding region. Instead, the predominant changes in the contributions to the kinetic energy occur at the positions of nuclei and not in the binding region as found for He_2 and H_2 at shorter bond lengths.

The variation in the parallel, $\overline{T}_{\parallel}$, and perpendicular, $\overline{T}_{\perp}$, contributions to the total average kinetic energy for various bond lengths are shown in Tables 3.1 and 3.2 for H_2 and He_2 respectively. Reference to

Table 3.1 indicates that the total kinetic energy in the H_2 molecule is less than that of the separated atoms for values of $R \geq 2.0$ a.u. The $\Delta\rho(\vec{x}_1)$ maps for H_2 indicate that for $R > 2.0$ a.u. the charge decrease occurs in near spherical regions centered on each of the nuclei (see Figure 3.7). (Additional $\Delta\rho(\vec{x}_1)$ maps for H_2 at various other values of R are given in Reference 116.) The $\Delta G(\vec{x}_1)$ contour maps indicate that the decrease in $\overline{T}$ observed for large values of R arises from this decrease in the peaking of the charge density at the positions of the nuclei, an effect which decreases both the parallel and perpendicular contributions to $G(\vec{x}_1)$ and $\overline{T}$. For values of $R < 2.0$ a.u. charge density is accumulated in the vicinity of each nucleus and $\overline{T}$ increases above the atomic values.

3.5 The Kinetic Energy Distributions of the N_2 and Be_2 Molecules

The analysis of the kinetic energy distributions for H_2 and He_2 clearly indicates how molecular stability is related to the topographical features of the one-electron charge density $\rho(\vec{x}_1)$ in simple molecules formed from atoms which employ principally s-type orbitals. Because molecules formed from atoms which employ p-type orbitals differ from these simple molecules in that their $\Delta\rho(\vec{x}_1)$ plots show quadrupolar rather than dipolar polarizations of the atomic densities, it is of interest to further consider the kinetic energy distributions for more complex molecules such as N_2 and Be_2. In this section the stable molecule N_2 will be contrasted with the unstable molecule Be_2.

Contour maps for the total one-electron charge density $\rho(\vec{x}_1)$, the distribution $K(\vec{x}_1)$ and its contributions $G(\vec{x}_1)$ and $L(\vec{x}_1)$ for N_2 at the equilibrium internuclear separation of 2.068 a.u.* and for Be_2 at a bond

* The distributions for N_2 were calculated from the Hartree-Fock wavefunction determined by Cade, Sales and Wahl[117] for the $X^1\Sigma_g^+$ state.

length of 3.0 a.u.* are shown in Figures 3.8 and 3.9 respectively. A comparison of the $\rho(\vec{x}_1)$ and $K(\vec{x}_1)$ distributions for N_2 indicates that except for a deep negative ring around each nucleus $K(\vec{x}_1)$ is largest in those regions where the charge density is most concentrated, at the nuclei and in the internuclear or binding region. This feature is identical to that found for the stable H_2 molecule. The negative ring which appears around each nuclei in the $K(\vec{x}_1)$ and also the $L(\vec{x}_1)$ distribution for larger molecules such as N_2 arises from the large curvatures in the orbitals and the density near the nuclei as a result of the 1s core. This negative ring also appears in the component atomic distributions. As in the H_2 molecule, the accumulation of charge density between the nuclei in N_2 decreases the positive curvature in $\rho(\vec{x}_1)$ along the bond axis and increases the negative curvature perpendicular to the bond axis resulting in $L(\vec{x}_1) > 0$ in the internuclear or binding region. The values of $K(\vec{x}_1)$ and $L(\vec{x}_1)$ right at the bond mid point are 1.392 and 0.766 a.u. respectively. The large contribution of $L(\vec{x}_1)$ to $K(\vec{x}_1)$ in the binding region clearly indicates the excess stability achieved by the potential energy density in this critical region of space in the stable N_2 molecule. The shape of the contours of the gradient contribution $G(\vec{x}_1)$ are very similar to those for the $\rho(\vec{x}_1)$ distribution indicating that contours of equidensity represent lines of almost constant value for the classical-like contribution to the kinetic energy. The $G(\vec{x}_1)$ distribution for N_2 does not show a deep minimum at the bond mid point as found in the case of H_2. Orbitals of σ_u symmetry contribute

---

* The distributions for Be_2 were calculated from the Hartree-Fock wavefunction determined by Cade and Sales[118] for $^1\Sigma_g^+$ state. The Be_2 molecule being unstable has no equilibrium bond length. The stable neighbouring molecule B_2 has an equilibrium bond length of 3.005 a.u. and hence, a bond length of 3.0 a.u. is used to examine the properties of the charge density in Be_2.

Figure 3.8. Contour maps and profiles of $\rho(\vec{x}_1)$, $K(\vec{x}_1)$, $G(\vec{x}_1)$ and $L(\vec{x}_1)$ for N_2 at an internuclear separation of 2.068 a.u.

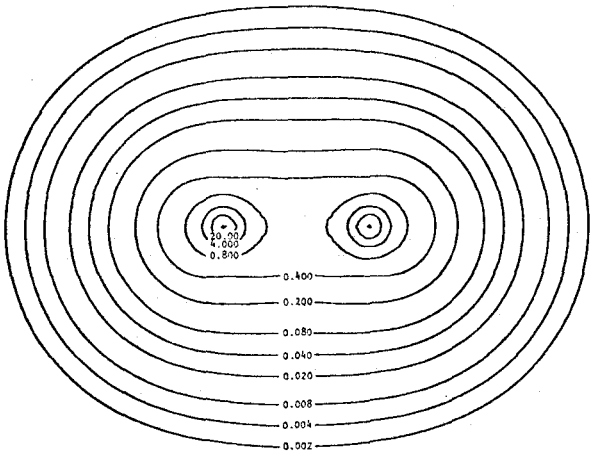

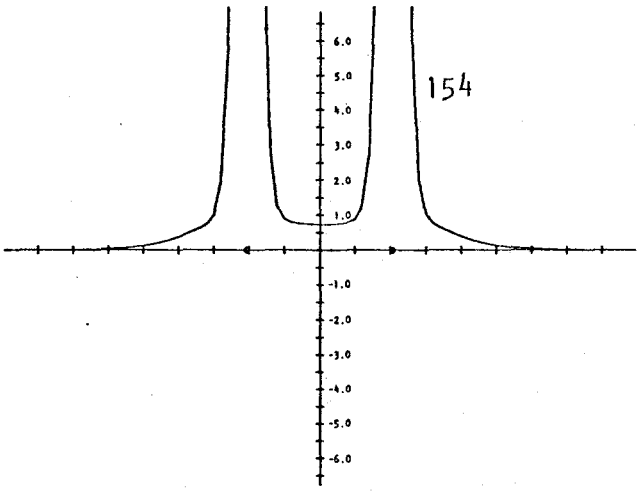

$\rho(\bar{x})$

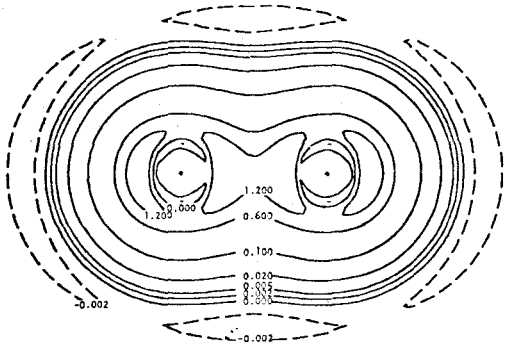

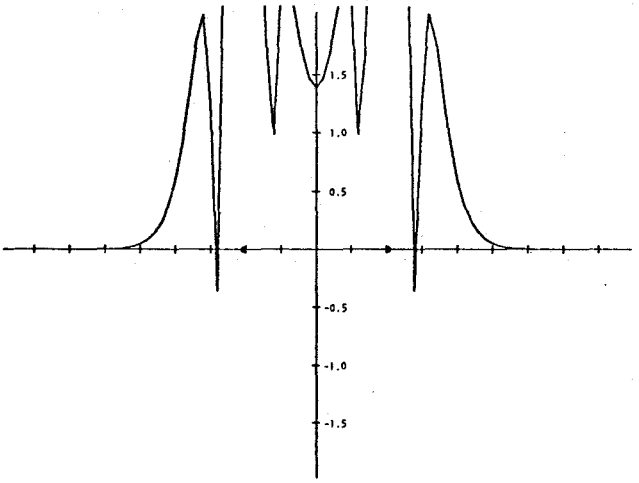

$K(\bar{x})$

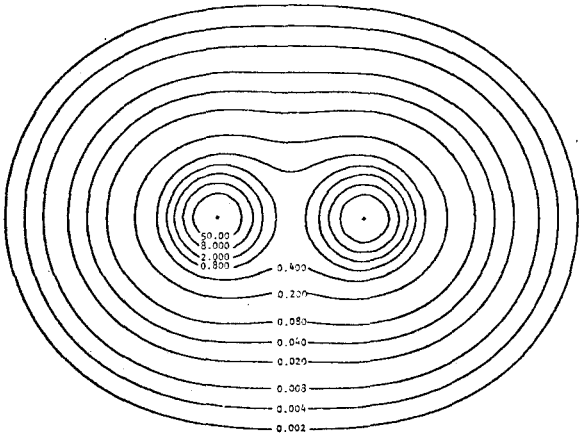

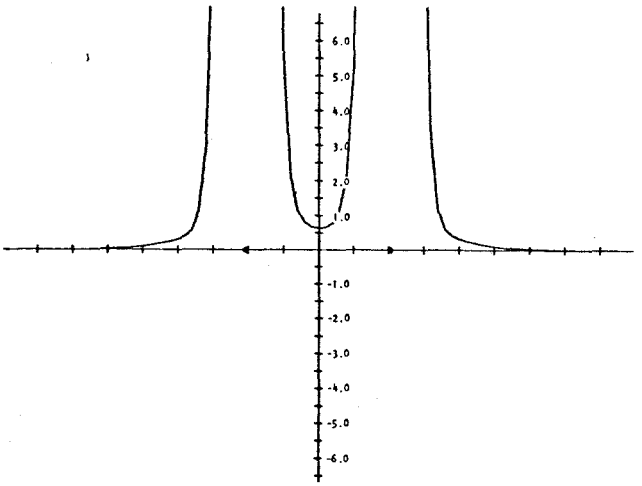

$G(\bar{x})$

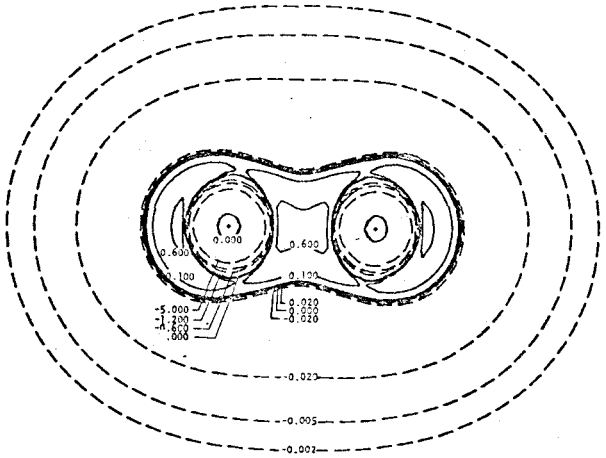

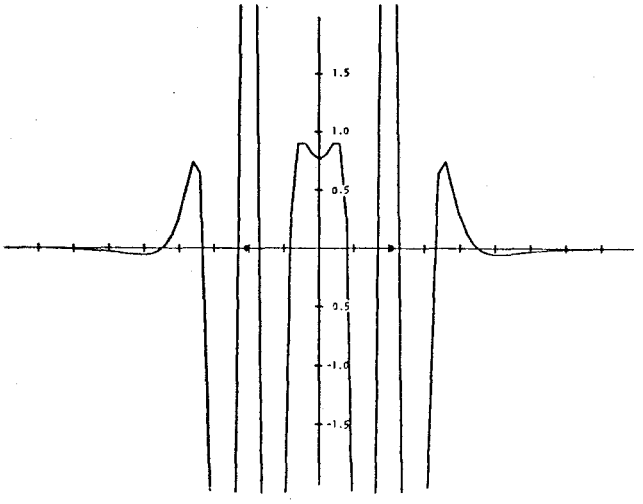

$L(\bar{x})$

Figure 3.9. Contour maps and profiles of $\rho(\vec{x}_1)$, $K(\vec{x}_1)$, $G(\vec{x}_1)$ and $L(\vec{x}_1)$ for Be_2 at R = 3.0 a.u.

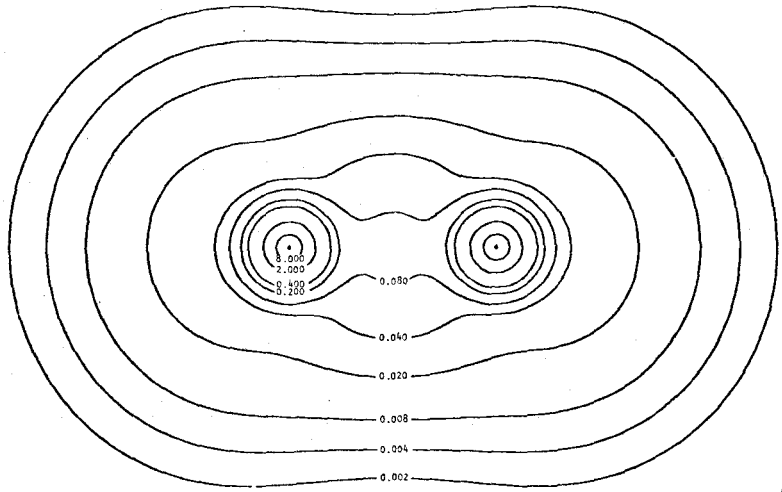

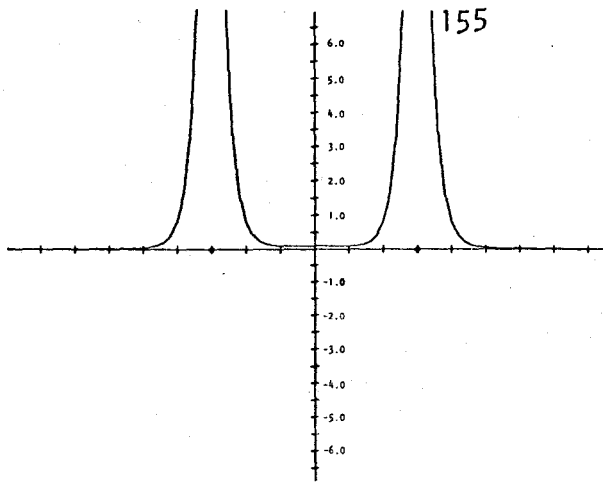

$\rho(\bar{x})$

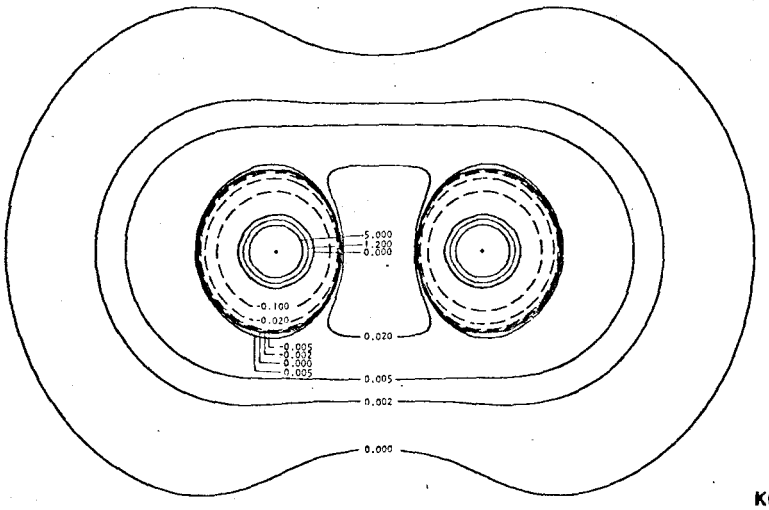

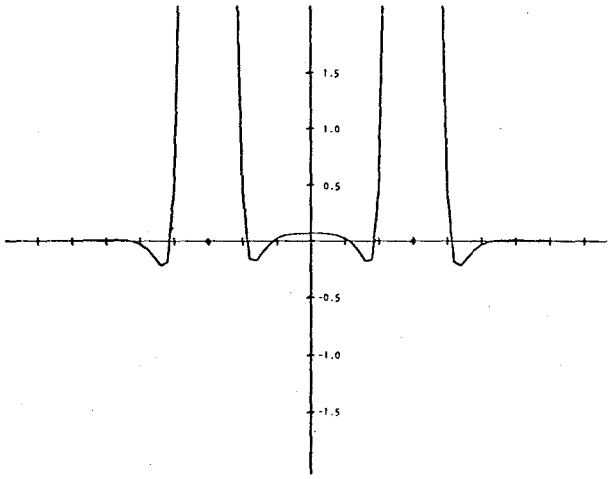

$K(\bar{x})$

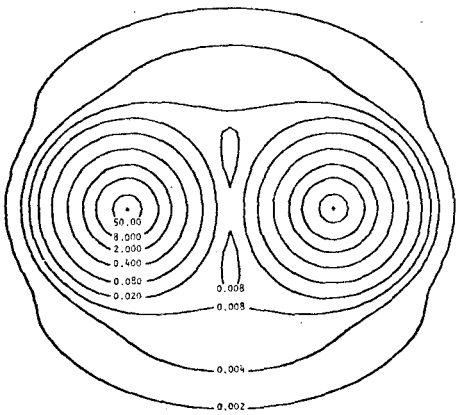

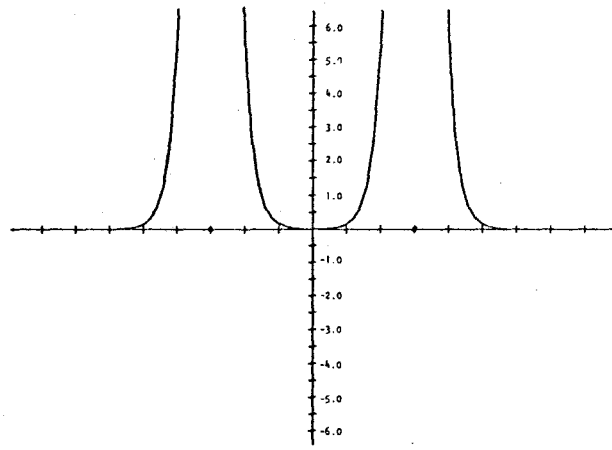

$G(\bar{x})$

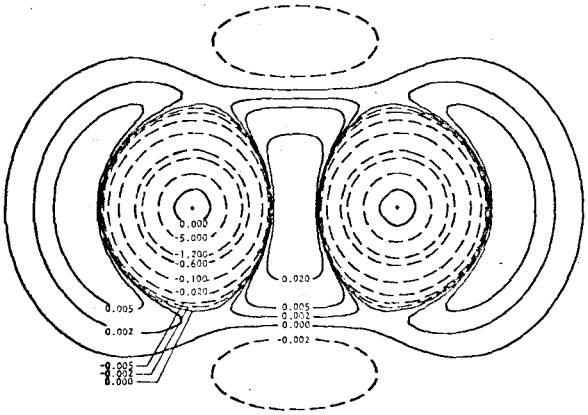

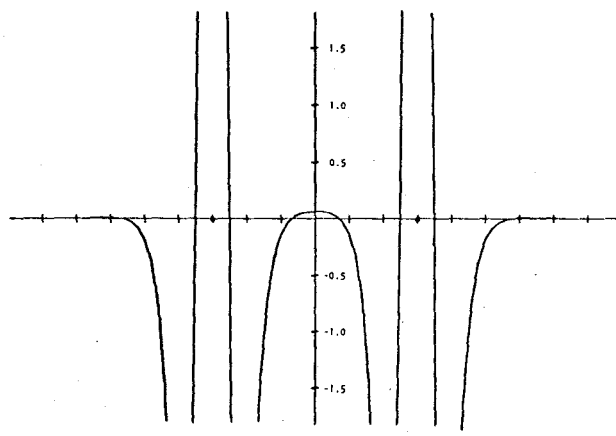

$L(\bar{x})$

heavily to the total one-electron density in N_2. It is the gradients of these orbitals which give large positive contributions to $G(\vec{x}_1)$ in the internuclear region, resulting in a value of 0.626 a.u. at the bond mid point. This value is much larger than the near zero value observed at the bond mid point in H_2. There are large peaks in the $G(\vec{x}_1)$ distribution at the nuclei clearly indicating the large contributions to the kinetic energy $\overline{T}$ from the 1s cores.

In contrast to the stable N_2 molecule, the kinetic energy distributions for the unstable Be_2 molecule exhibits many of the same characteristics as those found for He_2. The $\rho(\vec{x}_1)$ distribution for Be_2 (see Figure 3.9) indicates that the density in the internuclear region is very small (the value at the bond mid point is 0.091 a.u. compared to 0.724 a.u. at the bond mid point in N_2). This low value of the density in the binding region is a direct result of the antisymmetry requirements of the Pauli principle and a large internuclear separation. If a charge distribution with a smaller bond length were available for Be_2 the determined kinetic energy distributions would more strongly resemble the results found for He_2 rather than give the almost zero contributions to $K(\vec{x}_1)$, $G(\vec{x}_1)$ and $L(\vec{x}_1)$ at the bond mid point as found in the present example. The $K(\vec{x}_1)$ distribution shows large positive contributions near the nuclei, the regions of maximum charge accumulation and negative rings around the nuclei resulting from the 1s cores. The low value of $K(\vec{x}_1)$ at the bond mid point of Be_2 (0.073 a.u.), which is very small compared to the value for N_2 (1.392 a.u.), clearly indicates the low concentration of electron density in the internuclear region and thus the small contributions to the kineitc

energy from this critical binding region. Also, the very small values of $L(\vec{x}_1)$ in the binding region of Be_2 (0.064 a.u. at the bond mid point), although not negative as in the case of He_2, strongly reflects the very low stability of the potential energy density in this region of space. This feature contributes to the instability of the Be_2 molecule. The very small gradients of the orbitals in the internuclear region results in very small contributions to $G(\vec{x}_1)$ (0.009 a.u. at the bond mid point) in the binding region. The large peaks in $G(\vec{x}_1)$ at the nuclei show the large contributions to the kinetic energy from the 1s cores. Because of the large internuclear separation the energy distributions for Be are very characteristic of the component separated atoms.

The general features of the <u>total</u> kinetic energy distributions for N_2 and Be_2 are very similar to those for H_2 and He_2 respectively. It is not until we consider the difference distributions $\Delta\rho(\vec{x}_1)$, $\Delta K(\vec{x}_1)$, $\Delta G(\vec{x}_1)$ and $\Delta L(\vec{x}_1)$ for the N_2 and Be_2 molecules that the quadrupolar nature of the polarization of the atomic density distributions found in these more complex molecules results in marked differences in the interpretation given the simple molecules H_2 and He_2.

The difference distributions $\Delta\rho(\vec{x}_1)$, $\Delta K(\vec{x}_1)$, $\Delta G(\vec{x}_1)$ and $\Delta L(\vec{x}_1)$ for the N_2 and Be_2 molecules are shown in Figures 3.10 and 3.11 respectively. These distributions clearly show the typical quadrupolar polarizations found in molecules formed from atoms which employ p-type orbitals. The $\Delta\rho(\vec{x}_1)$ plots for both N_2 and Be_2 show a large build-up of charge in the antibinding regions behind the nuclei as well as in the internuclear or binding region. The density decreases occur in the antibinding regions perpendicular to the bond axis. The unstable molecule Be_2 does not

Figure 3.10. Contour maps and profiles of the difference distributions $\Delta\rho(\vec{x}_1)$, $\Delta K(\vec{x}_1)$, $\Delta G(\vec{x}_1)$, and $\Delta L(\vec{x}_1)$ for N_2 at R = 2.068 a.u.

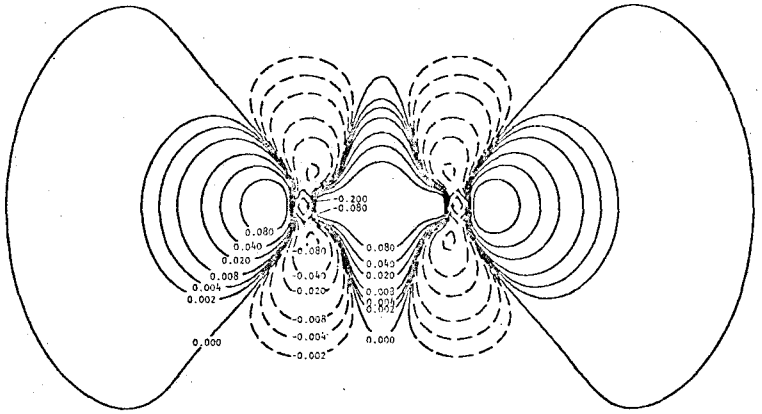

$\Delta\rho(\bar{x})$

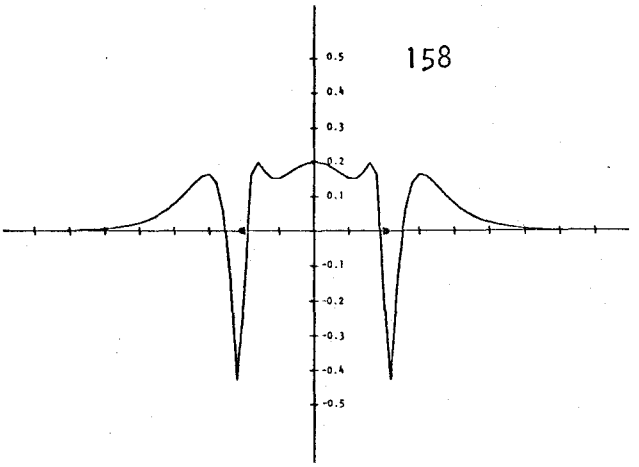

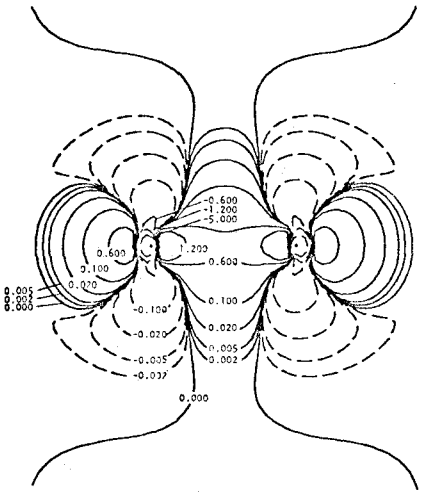

$\Delta K(\bar{x})$

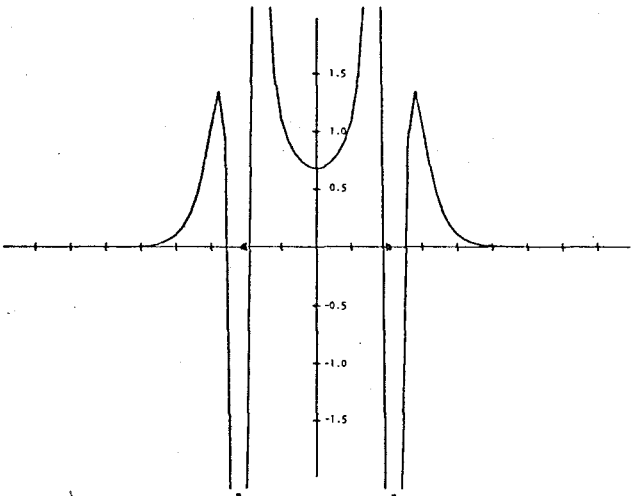

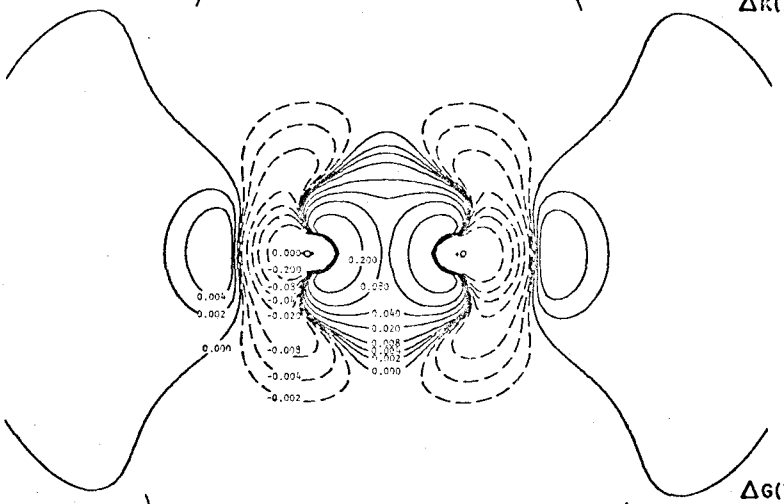

$\Delta G(\bar{x})$

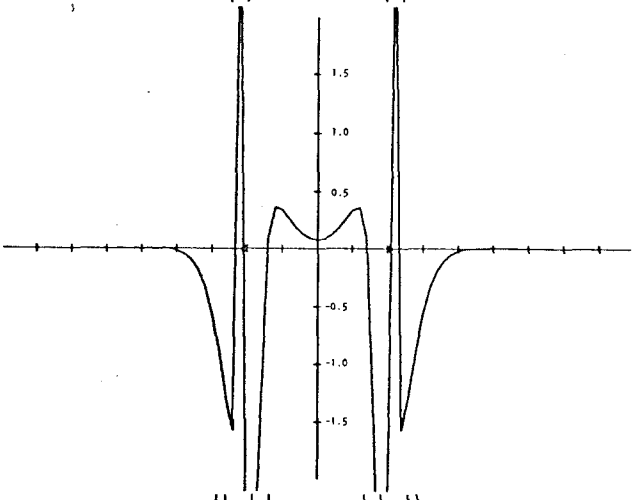

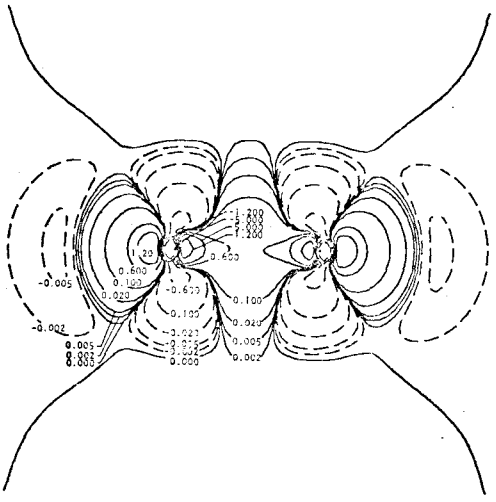

$\Delta L(\bar{x})$

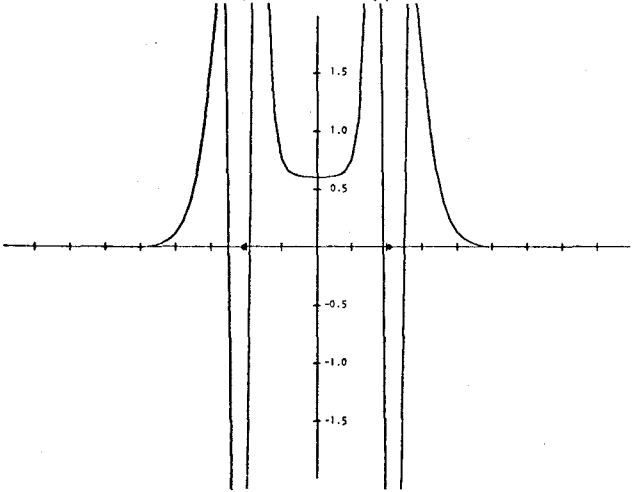

Figure 3.11. Contour maps and profiles of the difference distributions for Be_2 at R = 3.0 a.u.

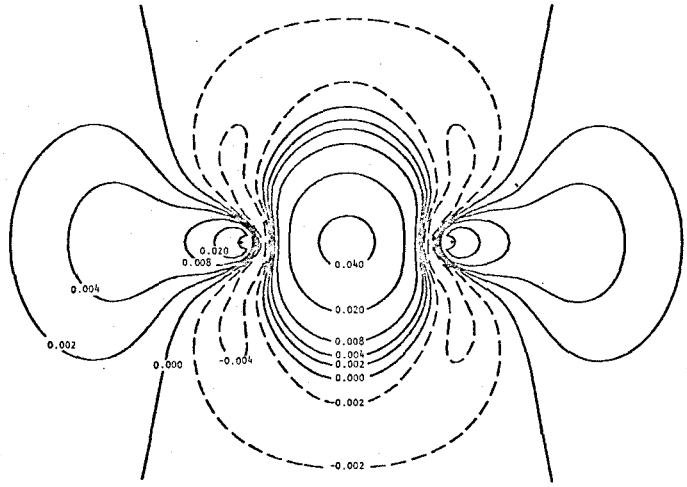

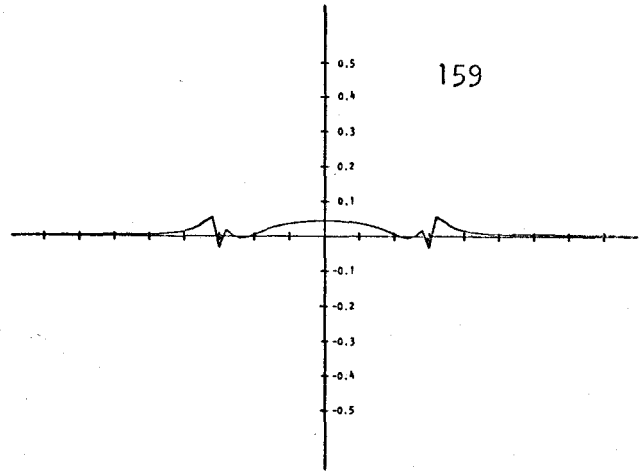

$\Delta\rho(\bar{x})$

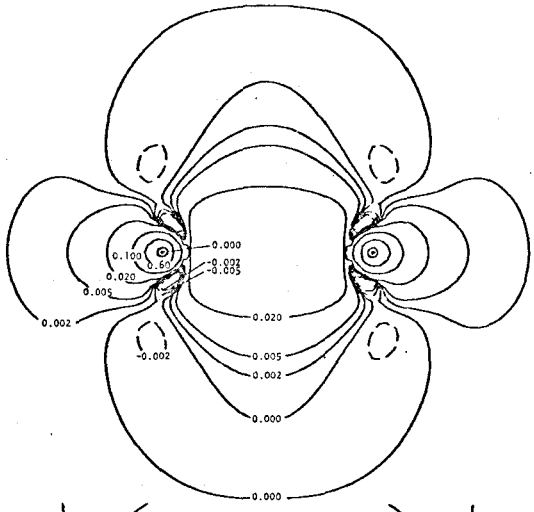

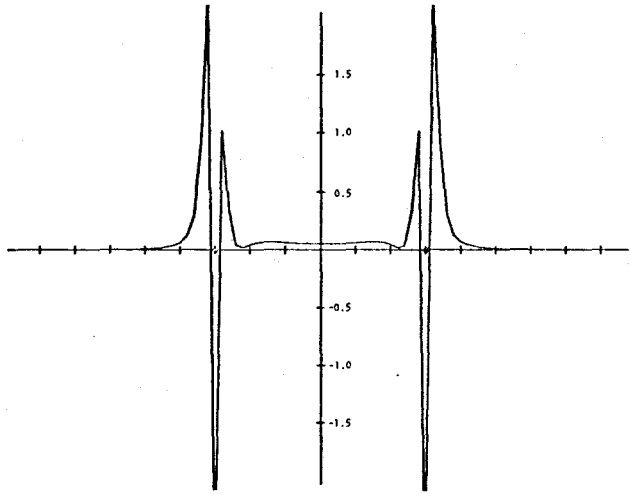

$\Delta K(\bar{x})$

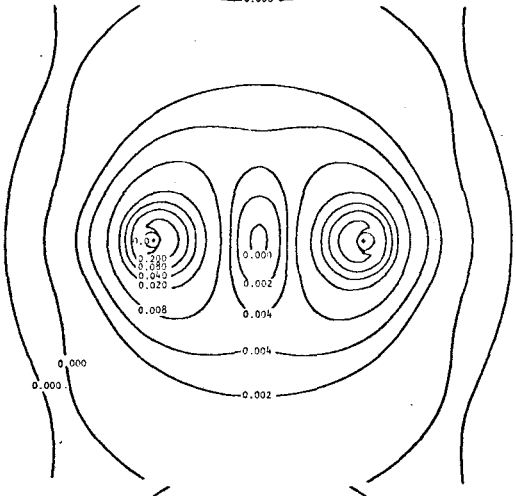

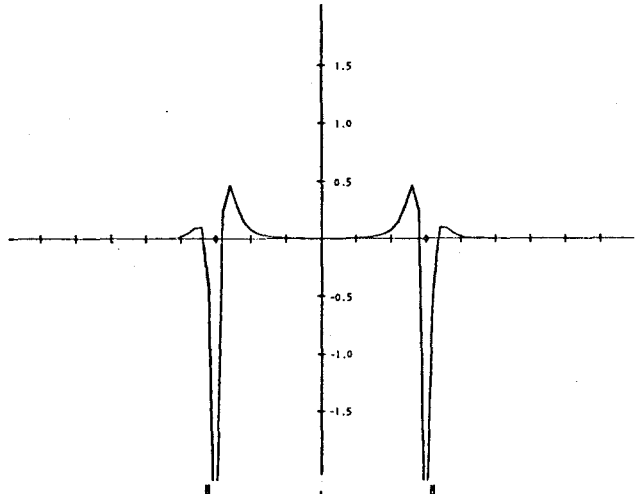

$\Delta G(\bar{x})$

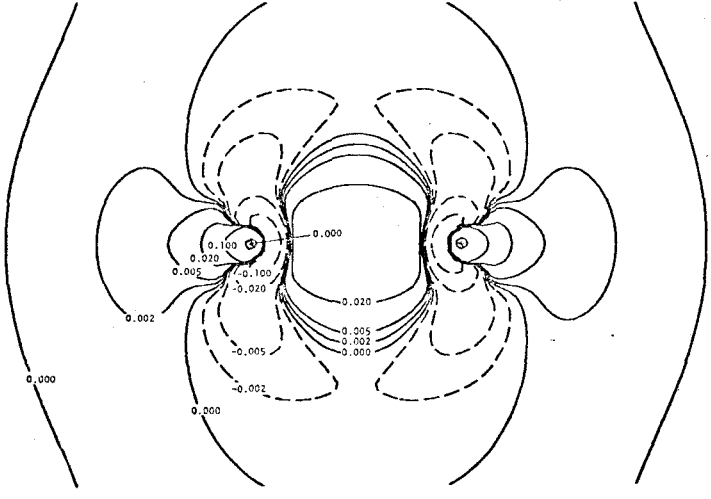

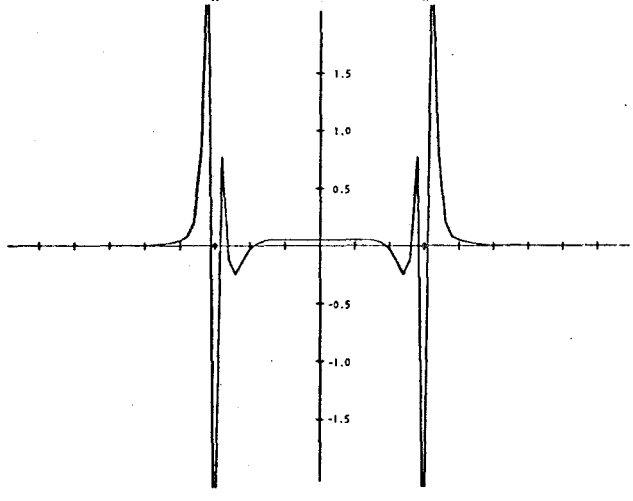

$\Delta L(\bar{x})$

concentrate sufficient density in the binding region to bind the nuclei[3]. The $\Delta K(\vec{x}_1)$ distribution for both molecules are very similar to their $\rho(\vec{x}_1)$ distributions; the increase or decrease in the charge density resulting in a corresponding increase or decrease in $K(\vec{x}_1)$ for the system. The regions of positive $\Delta K(\vec{x}_1)$ and thus, the regions in which the potential energy density of the molecule is more negative than that for the separated atoms, occur in the internuclear or binding regions and in the antibinding regions behind the nuclei. The $\Delta L(\vec{x}_1)$ distributions for both molecules also show the same regions of positive and negative contributions as found in the $\Delta\rho(\vec{x}_1)$ distributions. Thus, the potential energy density in molecules with quadrupolar polarizations of the atomic densities achieves its maximum stability in the binding region and in the antibinding regions behind the nuclei. This feature is in sharp contrast to that found for the simpler dipolar type molecules such as H_2 in which the potential energy density achieves its maximum stability only in the binding region between the nuclei.

The $\Delta G(\vec{x}_1)$ distribution for each molecule is of particular interest since this distribution clearly shows the instability of the density distribution for Be_2 as compared to that for N_2. Also, the $\Delta G(\vec{x}_1)$ distribution explains why the accumulation of charge density in the antibinding regions of a stable molecule is favourable on energetic grounds. The $\Delta G(\vec{x}_1)$ contour plot for N_2 shows that the contributions to $G(\vec{x}_1)$, and thus to $\overline{T}$, from the internuclear or binding region are larger in the molecule than in the separated atoms. It is the necessary inclusion of orbitals of σ_u symmetry in the molecular one-electron density distribution for N_2 which results in large orbital gradients and thus, in large contributions

to $G(\vec{x}_1)$ and $\overline{T}$ from the internuclear region. Thus unlike the situation in H_2, the accumulation of charge in the binding region of N_2 increases the kinetic energy of the molecular system with respect to the separated atoms. The accumulation of charge density in the antibinding regions behind the nuclei, however, does not lead to an increase in the contributions to $G(\vec{x}_1)$ and $\overline{T}$ upon the formation of a stable molecule from its component separated atoms. The $\Delta G(\vec{x}_1)$ contour map for N_2 clearly shows that the build-up of charge density behind the nuclei, as depicted in the $\Delta\rho(\vec{x}_1)$ map, results in a softening of the orbital gradients immediately behind the nuclei thus leading to a decrease in the contributions to $G(\vec{x}_1)$ and $\overline{T}$ for the molecule when compared to the separated atoms. The accumulation of charge density in the antibinding regions, since it results in a decrease in the contributions to the kinetic energy in the molecule, leads to a stabilization of a molecular system which is formed from atoms employing orbitals of non-zero angular momentum. Thus, the N_2 molecule achieves its stability from a reduction in the contributions to the kinetic energy from the antibinding regions behind the nuclei. By allowing the charge density in the molecule to have a high probability distribution in the antibinding regions, the resultant accumulation of charge in these regions softens the gradient of the density, decreases the contributions to $G(\vec{x}_1)$ and $\overline{T}$, and increases the effective volume available to the electrons. This was not the case in the simple H_2 molecule where it is the accumulation of charge in the binding region between the nuclei that decreases the contributions to $\overline{T}$ and gives the electrons greater freedom.

The $\Delta G(\vec{x}_1)$ contour map for Be_2 (Figure 3.11) is very different

from the $\Delta G(\vec{x}_1)$ map for N_2. The build-up of charge in both the binding and antibinding regions of the Be_2 molecule leads to an increase in the contributions to $G(\vec{x}_1)$ and $\overline{T}$. Since $\Delta G(\vec{x}_1)$ for Be_2 is positive nearly everywhere, clearly there is a large increase in the total kinetic energy of the molecule over that of the separated atoms. This increase in the kinetic energy is partially responsible for the instability found in the Be_2 molecule.

Stable diatomic molecules formed from atoms which employ p-type orbitals all show a quadrupolar polarization of the component separated atom densities in their $\Delta\rho(\vec{x}_1)$ contour diagrams[3,4,5,6]. These molecules accumulate large amounts of charge density in the antibinding regions behind the nuclei as well as in the binding region between the nuclei. In the example exemplified by N_2 the build-up of charge in the binding region leads to an unavoidable increase in the contributions to the kinetic energy. The increase in charge in the binding region is necessary for the attainment of electrostatic equilibrium but since this density increase is partially achieved by placing electrons in the $2\sigma_u$ orbital, which has a large parallel gradient in the internuclear regions, it leads to an increase in the kinetic energy. However, the accumulation of charge in the antibinding regions clearly results in a decrease in the contributions to the kinetic energy. Thus in molecules which show quadrupolar type polarizations, it is anticipated that it is energetically favourable, from a kinetic energy point of view, to accumulate charge density in the antibinding regions. This charge build-up in the non-binding regions leads to a decrease in the contributions to the kinetic energy and to the formation of a more stable molecular species with

respect to the separated atoms.

Since there is an increase in the contributions to the kinetic energy from the binding region and a decrease from the antibinding regions, there will be an obvious balance between the contributions from these two regions. The actual partitioning of the charge density between these separate regions will determine whether the parallel, $\overline{T}_{\parallel}$, and perpendicular, $\overline{T}_{\perp}$, contributions to the total average kinetic energy will separately increase or decrease with respect to the separated atom values. If the charge increase were confined to the binding region alone it is possible that both the parallel and perpendicular gradients of the density will increase as they do near the nuclei, thus resulting in an overall increase in both $\overline{T}_{\parallel}$ and $\overline{T}_{\perp}$. By allowing the charge density to accumulate in the antibinding regions behind the nuclei there is a reduction in the otherwise large orbital gradients in the internuclear region as well as a resultant decrease in the parallel gradients immediately behind the nuclei. Thus, the variation of $\overline{T}_{\parallel}$ and $\overline{T}_{\perp}$ in a stable molecule, when compared to the values for the separated atoms will be determined by the resulting balance between the increase in the binding region and the decrease in the antibinding regions of the contributions to $G(\vec{x}_1)$ and $\overline{T}$.

The contributions $\overline{T}_{\parallel}$ and $\overline{T}_{\perp}$ to the total average kinetic energy are given in Table 3.3 for a number of homonuclear diatomic molecules. It should be noted that these contributions are determined for each molecule using previously determined Hartree-Fock wavefunctions.* These

* The wavefunction for Li_2 ($X^1\Sigma_g^+$) is from Cade, Sales and Wahl[119]; for B_2 ($X^3\Sigma_g^-$) and C_2($X^1\Sigma_g^+$) from Greenshields[120]; for O_2 ($X^2\Sigma_g^-$) from Cade and Malli[121]; and for F_2 ($X^1\Sigma_g^+$) from Wahl[122]. The references to the wavefunctions for N_2 and Be_2 were given earlier.

TABLE 3.3

Values of $\overline{T}_{\shortparallel}$ and $\overline{T}_{\perp}$ for the First Row Homonuclear Diatomic Molecules[a]

		Molecular Values				Atomic Values at R = ∞[b]			
Molecule	R	$\overline{T}$	$\overline{T}_{\shortparallel}$	$\overline{T}_{\perp}$	$(\overline{T}_{\perp}-\overline{T}_{\shortparallel})/\overline{T}$	$\overline{T}$	$\overline{T}_{\shortparallel}$	$\overline{T}_{\perp}$	$(\overline{T}_{\perp}-\overline{T}_{\shortparallel})/\overline{T}$
Li_2	5.0510	14.8907	4.9575	9.9332	0.3334	14.8655	4.9552	9.9103	0.3333
Be_2	3.5000[c]	29.4116	9.9137	19.4979	0.3259	29.1460	9.7153	19.4306	0.3333
B_2	3.0050	49.1447	15.9979	33.1469	0.3489	49.0587	16.1539	32.9049	0.3414
C_2	2.3481	75.3938	24.4374	50.9564	0.3517	75.3771	24.4568	50.9203	0.3511
N_2	2.0680	108.7911	36.2774	72.5137	0.3331	108.8031	36.2674	72.5358	0.3333
O_2	2.2820	149.4219	49.0238	100.3981	0.3438	149.6196	49.1954	100.4242	0.3424
F_2	2.6800	198.5856	61.3945	137.1905	0.3817	198.8171	64.4909	134.3262	0.3513

[a] All values are given in atomic units (a.u.)

[b] The atomic values are for the proper valence states of the atoms.

[c] The bond length for Be_2 used here differs from the value 3.0 a.u. used in the contour diagrams.

wavefunctions do not satisfy the virial theorem accurately and give only a fraction of the total binding energy for each molecule (the F_2 molecule is predicted to have a negative binding energy). In general, the total kinetic energy as determined from the Hartree-Fock wavefunctions is low and, as can be seen from Table 3.3, in a number of cases there is a predicted decrease in the kinetic energy in going from the separated atoms to the stable molecule in strict violation of the virial theorem. The results considered here are not assumed to be as accurate as the results obtained for H_2 and He_2 where much more accurate wavefunctions are used. However, these calculated parallel and perpendicular contributions to the kinetic energy show trends that fit in well with the examples which have been considered.

From the values given in Table 3.3 we see that $\overline{T}_{\parallel}$ for the stable molecules is nearly equal to or less than the same value for the separated atoms. Thus, the accumulation of charge in the antibinding regions of these molecules reduces the orbital gradients parallel to the bond axis resulting in a decrease in $\overline{T}_{\parallel}$. However, the value of $\overline{T}_{\perp}$ for these molecules, except for some cases where there is a decrease in the total kinetic energy in going from the atoms to the stable molecule, increases considerably with respect to the atomic value indicating the crucial role played by the accumulation of charge in the antibinding regions. The build-up of charge in these regions increases the perpendicular gradients by contracting the density around the internuclear axis. Unlike the stable molecules, in Be_2 the parallel contribution to the kinetic energy, as well as the perpendicular contribution, has greatly increased above the atomic value. This fact reflects the instability found in Be_2. In a stable molecule

it is the perpendicular contribution, $\overline{T}_{\perp}$, which accounts for the overall increase in the average kinetic energy necessary to satisfy the virial theorem.

3.6 Summary

The study of the kinetic energy distributions for the molecules H_2, He_2, N_2 and Be_2 clearly indicate the importance of the charge distribution in determining the overall stability of a molecular system. Instead of just being able to discuss the forces operative in a molecular system as done earlier[3,4,5,6], we can now relate the energy of the system to the topographical features of the molecular one-electron charge distribution.

The analysis carried out in this chapter has shown that in simple molecules formed from atoms which employ s-type orbitals such as H_2 and He_2 the stability or instability of the system is determined by the charge density situated in the internuclear or binding region. The accumulation of charge in the binding region of H_2, as depicted in the $\Delta\rho(\vec{x}_1)$ distribution, leads to a lowering of the orbital gradients parallel to the bond axis resulting in a reduction in the contributions to $G(\vec{x}_1)$ and $\overline{T}$ when compared to the separated atoms. Thus, the build-up of charge in the binding region of a simple stable molecule is distributed in such a way as to keep the accompanying increase in kinetic energy to a minimum. In the unstable system typified by He_2 the depletion of charge density from the binding region leads to increased orbital gradients along the bond axis with a corresponding increase in the contributions to $G(\vec{x}_1)$ and $\overline{T}$. It is this large increase in the kinetic energy from the binding region,

compared to that for the separated atoms, which is responsible for the instability found in He_2.

The kinetic energy distributions for more complex molecules such as N_2 and Be_2, which are formed from atoms which employ p-type orbitals, show markedly different behaviours than those for the simple molecules H_2 and He_2. The accumulation of charge in the binding regions of these more complex molecules, as depicted in their $\Delta\rho(\vec{x}_1)$ distributions, leads to an increase and not a decrease in the contributions to $G(\vec{x}_1)$ and $\overline{T}$ when compared to the separated atom values. In stable molecules which show quadrupolar polarizations of their atomic densities it is the charge build-up behind the nuclei in the antibinding regions which is responsible for a decrease in the orbital gradients and a resultant reduction in the contributions to $G(\vec{x}_1)$ and $\overline{T}$ for the molecule. Thus, the stability in these more complex molecules is gained by a reduction in the kinetic energy owing to a charge increase in the antibinding regions. This is not the case in the unstable Be_2 molecule since the charge increase behind the nuclei, shown in the $\Delta\rho(\vec{x}_1)$ map, leads to an increase in the contributions to $G(\vec{x}_1)$ and $\overline{T}$ which results in Be_2 being non-bound.

In stable molecules the accumulation of charge in the binding and/or the antibinding regions decreases the orbital gradients parallel to the bond axis leading to a decrease in the contributions to $\overline{T}_{\parallel}$ and a greater axial freedom for the electrons when compared to the separated atoms. The same build-up of charge, since it contracts the density around the internuclear axis, creates larger orbital gradients perpendicular to the axis leading to an increase in the contributions to $\overline{T}_{\perp}$, an increase which is necessary to satisfy the virial theorem.

The discussion in this chapter has been based on a very few molecules, particularly in the case of the quadrupolar type molecules only N_2 and Be_2 have been considered. A large number of molecular systems should be investigated by this approach. Of particular interest will be a contrast of the results obtained from the homonuclear diatomic molecules with those obtained for heteronuclear molecules, which may exhibit either covalent or ionic binding. In this way a more complete understanding of the relationship between the topographical features of a molecular one-electron charge distribution and the kinetic energy of the system may be obtained.

IV. DISCUSSION OF THE DENSITY APPROACH

This thesis has been concerned with the analysis and interpretation of chemical binding based on the knowledge obtained from various density distributions. The distributions that have been considered are the total one-electron charge density $\rho(\vec{x}_1)$, the difference density $\Delta\rho(\vec{x}_1)$, the density shift which arises from a molecular vibration $\Delta\rho_D(\vec{x}_1)$, the density shift which arises from the orthogonality requirements of the Pauli exclusion principle $\Delta\rho_p(\vec{x}_1)$, the kinetic energy distributions $K(\vec{x}_1)$, $G(\vec{x}_1)$ and $L(\vec{x}_1)$, and the kinetic energy difference distributions $\Delta K(\vec{x}_1)$, $\Delta G(\vec{x}_1)$ and $\Delta L(\vec{x}_1)$. The particular features present in each of these individual distributions contribute to a more complete understanding of the electronic structure and chemical binding in molecular systems. The analyses carried out in this thesis clearly show the relationship between the stability of a molecular system and the topographical features of its one-electron charge distribution.

The one-electron charge distribution $\rho(\vec{x}_1)$ gives a three-dimensional picture of the arrangement of the static electron density in a molecule. It is this distribution which is responsible for all the electrical properties of the system (e.g., the electronic forces and multipole moments). In fact, the properties of the $\rho(\vec{x}_1)$ distribution are used to determine the "best" one-electron density distribution for the methane molecule. The near spherical shape of the $\rho(\vec{x}_1)$ distribution for CH_4 is partially responsible for its low reactivity. The properties of the $p(\vec{x}_1)$ distribution and the quantum mechanical conditions

imposed on it are important in determining the equilibrium geometry of a molecule.

The difference density distribution $\Delta\rho(\vec{x}_1)$ dramatically shows the rearrangement which the undistorted atomic densities undergo upon molecular formation. The stability of a molecular system with respect to the separated atoms is clearly understood in terms of the $\Delta\rho(\vec{x}_1)$ distribution and the forces operative in the system[3,4,5,6]. In order that a molecule be stable, stable with respect to the component separated atoms, there must be a build-up of charge (i.e., $\Delta\rho(\vec{x}_1)$ is positive) in the critical binding region. Molecules formed from atoms which employ p-type orbitals, such as N_2, also show an increase in charge in the antibinding regions behind the nuclei in their $\Delta\rho(\vec{x}_1)$ distribution. The analysis of the kinetic energy distributions has shown that this is an energetically favourable way of charge rearrangement. In Chapter I the $\Delta\rho(\vec{x}_1)$ distribution for methane shows that the binding in this molecule is the result of a large accumulation of charge density along the C-H bond axies. This build-up of charge strongly binds the carbon on hydrogen nuclei.

The $\Delta\rho_D(\vec{x}_1)$ distributions (see Chapter I) show that the change in the charge density accompanying a vibration in CH_4 aids in the motion of the nuclei as they vibrate from their equilibrium positions. The density shifts in such a way that charge is accumulated ahead of the moving nuclei thus resulting in a corresponding reduction in the force constant for the A_1 vibration. Since the major density shifts in the $\Delta\rho_D(\vec{x}_1)$ distributions occur along the C-H bond axies it is the charge situated in these regions which bind the nuclei together in the methane

molecule. The $\Delta\rho_D(\vec{x}_1)$ distributions for CH_4, together with the force constant analysis, indicate the crucial role played by the change in the one-electron charge distribution in lowering the otherwise large increase in energy of the system when the nuclei are displaced from their equilibrium positions.

The $\Delta\rho_p(\vec{x}_1)$ distributions (see Chapter II) are diagramtic models which demonstrate how the one-electron density $\rho(\vec{x}_1)$ in three-dimensional space must shift in order to satisfy the orthogonality requirements of the Pauli exclusion principle in the many-dimensional orbital space. The restraints imposed on the one-electron charge distribution by the Pauli principle will not permit the H_2O or the NH_3 molecule to have a tetrahedral geometry with a hybridization approaching sp^3. The $\Delta\rho_p(\vec{x}_1)$ distributions clearly show that such an arrangement of the one-electron charge distribution does not place sufficient charge in the molecular binding region to bind the nuclei and produce a state of electrostatic equilibrium. Using the $\Delta\rho(\vec{x}_1)$ distributions it is shown that one-electron charge distributions for H_2O and NH_3 which employ bonding orbitals of almost pure p character and one lone pair orbital of pure s character do place sufficient charge in the binding region to bind the nuclei. Such stable one-electrons charge distributions require "bent orbitals".

The kinetic energy distribution $K(\vec{x}_1)$ and its components $G(\vec{x}_1)$ and $L(\vec{x}_1)$ together with the corresponding difference distributions (see Chapter III) provide a new dynamic approach to the understanding of chemical binding in molecules. This approach is a complement to the electrostatic approach[3,4,5,6] which utilizes the $\Delta\rho(\vec{x}_1)$ distributions and force analyses to interpret the chemical binding in molecular systems.

The kinetic energy distributions are used in this thesis to examine the relationship between the topographical features of the molecular charge distribution and the kinetic energy of the system. The gradient distribution $G(\vec{x}_1)$, since it is a classical-like distribution which when integrated over all space yields $\overline{T}$, enables one to relate the final values of the kinetic energy to the spacial properties of the one-electron charge distribution. The Laplacian distribution $L(\vec{x}_1)$ in turn, whether it is greater than or less than zero, indicates the regions of space in which the charge density attains its maximum stability. Considering the $G(\vec{x}_1)$ and $L(\vec{x}_1)$ distributions together (i.e., $K(\vec{x}_1)$) provides a detailed explanation of the stability or instability of a molecular system in terms of the spatial distributions of the one-electron charge density.

The analysis of the kinetic energy distributions show that, with reference to the separated atom distributions, the accumulation of charge density in the binding region of a stable molecule formed from atoms which employ s-type orbitals, such as H_2, leads to a decrease in kinetic energy and to an increase in the magnitude of the potential energy. Just the opposite behaviour is obtained for the kinetic and potential energy in the binding region of a simple unstable molecule as typified by He_2. In contrast, in the more complex molecules such as N_2 and Be_2, which are formed from atoms employing p-type orbitals, the accumulation of charge in the binding region leads to an increase in kinetic energy. It is the charge build-up in the antibinding regions of these larger stable molecules which results in a decrease in kinetic energy and an overall stabilization of the molecular system. The

connections between the topographical features of the molecular charge distribution and the kinetic energy of the system, together with the other topic considered in this thesis, provide an increased understanding of the electronic structure and chemical binding in molecules.

APPENDIX

APPENDIX I

Atomic Orbitals Used for Methane

The accurate self-consistent field atomic orbital functions for the ^3P configuration of the carbon atom as determined by Clementi et al[53] were used to represent the $1s_c$, $2s_c$ and 2p atomic orbitals on carbon. These have the form

$$1s_c = C_1 1s_1 + C_2 1s_2 + C_3 2s_3 + C_4 2s_4 + C_5 2s_5 + C_6 2s_6$$

$$2s_c = C_1' 1s_1 + C_2' 1s_2 + C_3' 2s_3 + C_4' 2s_4 + C_5' 2s_5 + C_6' 2s_6$$

$$2p = C_7 2p_7 + C_8 2p_8 + C_9 2p_9 + C_{10} 2p_{10}$$

where the $1s_i$, $2s_i$ and $2p_i$ are Slater atomic orbitals given by

$$1s_i = \frac{\alpha_i^{3/2}}{\sqrt{\pi}} e^{-\alpha_i r} \qquad i = 1,2$$

$$2s_i = \frac{\alpha_i^{5/2}}{\sqrt{3\pi}} r\, e^{-\alpha_i r} \qquad i = 3,4,5,6$$

$$2p_i \begin{Bmatrix} z \\ x \\ y \end{Bmatrix} = \frac{\alpha_i^{5/2}}{\sqrt{\pi}} r \begin{Bmatrix} \cos\theta \\ \sin\theta\cos\phi \\ \sin\theta\sin\phi \end{Bmatrix} e^{-\alpha_i r} \qquad i = 7,8,9,10$$

and

i	1	2	3	4	5	6
α_i	5.41250	9.28630	1.03110	1.50200	2.58975	4.25950
C_i	0.92695	0.07665	0.00073	-0.00167	0.00539	0.00210
C_i'	-0.20786	-0.01175	0.06494	0.74109	0.34626	-0.13208

i	7	8	9	10
α_i	0.95540	1.42090	2.58730	6.34380
C_i	0.24756	0.57774	0.23563	0.01090

NOTE: The coefficients and exponents that appear in the above tables are the corrected values which appear in "Tables of Atomic Functions", published as a supplement to the paper by Enrico Clementi, "Ab Initio Computations in Atoms and Molecules", which appears in IBM Journal of Research and Development 9, 2 (1965).

The 1s atomic orbitals used on the hydrogens, designated as h_i (i = 1,2,3,4), are just simple Slater 1s atomic functions where the screening coefficient, α_H, is larger than the separated atom value of unity. The actual value used for α_H is given in the thesis.

APPENDIX 2

Equations for Wavefunction Determination

(a) Force Equations

For the convenience of notation the following identities will be used in this and the following appendicies.

$$\text{Sin}(\varepsilon b) \equiv SE$$

$$\text{Cos}(\varepsilon b) \equiv CE$$

$$Co \equiv \langle h_1 | 1s_c \rangle \cdot (1 - 3\delta) + \lambda \cdot CE \cdot \langle 1s_c | 2s_c \rangle / \mu$$

$$Fa \equiv \text{Cos}(\theta_{H1}) / r_{H1}^2$$

$$\langle \chi_b | Fa | \chi_c \rangle \equiv \int \chi_b Fa \chi_c d\tau$$

Here Fa is the force operator for the force on H_1 parallel to the C—H_1 bond axis. Since the force on each hydrogen is the same only the force on H_1 is considered. Also if b = c = a in the integral $\langle \chi_b | Fa | \chi_c \rangle$ then the integral is referred to as an atomic integral; if b = c ≠ a, the integral is a screening integral; and if b = a ≠ c, then the integral is an overlap integral. Finally, if b ≠ c ≠ a, the integral is a three center integral and this is denoted by a double prime on Fa. Using the above notation the orbital forces on H_1 parallel to the C—H_1 bond axis are

$$F_{11}(\phi_o^2) = 2\langle 1s_c | Fa | 1s_c \rangle$$

$$F_{11}(\phi_{b1}^2) = 2[\lambda^2(CE^2 \cdot \langle 2s_c | Fa | 2s_c \rangle + 2 \cdot CE \cdot SE \cdot \langle 2s_c | Fa | P_1 \rangle + SE^2 \cdot \langle P_1 | Fa | P_1 \rangle)$$
$$+ 2\lambda\mu(CE(\langle h_1 | Fa | 2s_c \rangle - 3\delta \cdot \langle h_2 | Fa'' | 2s_c \rangle - Co \cdot \langle 1s_c | Fa | 2s_c \rangle)$$

$$+ SE(\langle h_1|Fa|P_1\rangle - 3\delta\cdot\langle h_2|Fa''|P_1\rangle - Co\cdot\langle 1s_c|Fa|P_1\rangle)$$
$$+ \mu^2(3\delta^2(\sqrt{2/3}\cdot\langle h_2|Fa'|h_2\rangle^{*} + 2\langle h_2|Fa''|h_3\rangle)$$
$$+ 6\delta(Co\cdot\langle h_2|Fa''|1s_c\rangle - \sqrt{2/3}\cdot\langle h_1|Fa'|h_2\rangle)$$
$$- 2Co\cdot\langle h_1|Fa|1s_c\rangle + Co^2\cdot\langle 1s_c|Fa|1s_c\rangle)].$$

By symmetry $F_{11}(\phi_{b2}^2) = F_{11}(\phi_{b3}^2) = F_{11}(\phi_{b4}^2)$. $F_{11}(\phi_{b4}^2)$ is given by

$$F_{11}(\phi_{b4}^2) = 2[\lambda^2(CE^2\cdot\langle 2s_c|Fa|2s_c\rangle - 2\cdot CE\cdot SE\cdot\langle 2s_c|Fa|P_1\rangle/3$$
$$+ SE^2(\langle P_1|Fa|P_1\rangle + 8\langle P_{\pi 1}|Fa|P_{\pi 1}\rangle^{\dagger})/9)$$
$$+ 2\lambda\mu(CE(\{1-2\delta\}\cdot\langle h_2|Fa''|2s_c\rangle - \delta\cdot\langle h_1|Fa|2s_c\rangle - Co\cdot\langle 1s_c|Fa|2s_c\rangle)$$
$$+ SE(\{2\delta-1\}\cdot\langle h_2|Fa''|P_1\rangle + 2\sqrt{2}\cdot(1+\delta)\cdot\langle h_2|Fa''|P_{\pi 1}\rangle$$
$$+ \delta\cdot\langle h_1|Fa|P_1\rangle + Co\cdot\langle 1s_c|Fa|P_1\rangle)/3)$$
$$+ \mu^2(\sqrt{2/3}\cdot(1+2\delta^2)\cdot\langle h_2|Fa'|h_2\rangle - 2\delta\cdot(1-2\delta)\cdot\sqrt{2/3}\cdot\langle h_1|Fa'|h_2\rangle$$
$$- 2\delta\cdot(2-\delta)\cdot\langle h_2|Fa''|h_3\rangle - 2Co\cdot\langle h_2|Fa''|1s_c\rangle$$
$$+ 2\delta\cdot Co(\langle h_1|Fa|1s_c\rangle + 2\langle h_2|Fa''|1s_c\rangle) + Co^2\cdot\langle 1s_c|Fa|1s_c\rangle)].$$

The total electronic force on H_1 parallel to C—H_1 bond axis is

$$F_{11}^{e} = 2[4\lambda^2(CE^2\cdot\langle 2s_c|Fa|2s_c\rangle + SE^2\cdot(\langle P_1|Fa|P_1\rangle + 2\langle P_{\pi 1}|Fa|P_{\pi 1}\rangle)/3)$$
$$+ 2\lambda\mu(CE(\{1-3\delta\}\cdot(\langle h_1|Fa|2s_c\rangle + 3\langle h_2|Fa''|2s_c\rangle)$$
$$- 4Co\cdot\langle 1s_c|Fa|2s_c\rangle)$$
$$+ SE(\{1+\delta\}\cdot(\langle h_1|Fa|P_1\rangle - \langle h_2|Fa''|P_1\rangle + 2\sqrt{2}\cdot\langle h_2|F''|P_{\pi 1}\rangle)))$$
$$+ \mu^2(3(1+3\delta^2)\cdot\sqrt{2/3}\cdot\langle h_2|Fa'|h_2\rangle - 12\delta\cdot(1-\delta)\cdot\sqrt{2/3}\cdot\langle h_1|Fa'|h_2\rangle$$
$$- 12\delta\cdot(1-\delta)\langle h_2|Fa''|h_3\rangle$$
$$- 2(1-3\delta)\cdot Co\cdot(\langle h_1|Fa|1s_c\rangle + 3\langle h_2|Fa''|1s_c\rangle)$$
$$+ 4Co^2\cdot\langle 1s_c|Fa|1s_c\rangle) + \langle 1s_c|Fa|1s_c\rangle].$$

---

* The prime on Fa indicates that the integral gives the force along the bond axis between the two centers involved in the integral and that the component along C—H_1 axis has to be taken. This is done by multiplying by $\sqrt{2/3}$ in most cases.

† $P_{\pi 1} = \sqrt{2/3}\cdot(px - (py + pz)/2)$. This is a p type orbital perpendicular to the C—H_1 bond axis and in the H_1CH_2 plane.

(b) Magnetic Shielding Equations

The diamagnetic term of the proton magnetic shielding is obtained by averaging the wavefunction over the operator $1/r_{H1}$. This gives the shielding at the hydrogen H_1. The following identities are added to those given above.

$$\sigma a \equiv 1/r_{H1}$$

$$\langle \chi_b | \sigma a | \chi_c \rangle \equiv \int \chi_b \sigma a \chi_c d\tau$$

The orbital contributions to the magnetic shielding at H_1 are

$$\sigma(\phi_o^2) = 2\langle 1s_c | \sigma a | 1s_c \rangle$$

$$\begin{aligned}\sigma(\phi_{b1}^2) = 2[&\lambda^2(CE^2\cdot\langle 2s_c|\sigma a|2s_c\rangle + 2CE\cdot SE\cdot\langle 2s_c|\sigma a|P_1\rangle + SE^2\cdot\langle P_1|\sigma a|P_1\rangle)\\ &+ 2\lambda\mu(CE(\langle h_1|\sigma a|2s_c\rangle - 3\delta\cdot\langle h_2|\sigma a''|2s_c\rangle - Co\cdot\langle 1s_c|\sigma a|2s_c\rangle)\\ &+ SE(\langle h_1|\sigma a|P_1\rangle - 3\delta\cdot\langle h_2|\sigma a''|P_1\rangle - Co\cdot\langle 1s_c|\sigma a|P_1\rangle))\\ &+ \mu^2(\langle h_1|\sigma a|h_1\rangle + 3\delta^2\cdot(\langle h_2|\sigma a|h_2\rangle + 2\langle h_2|\sigma a''|h_3\rangle)\\ &+ 6\delta(Co\cdot\langle h_2|\sigma a''|1s_c\rangle - \langle h_1|\sigma a|h_2\rangle)\\ &- 2Co\cdot\langle h_1|\sigma a|1s_c\rangle + Co^2\langle 1s_c|\sigma a|1s_c\rangle)].\end{aligned}$$

By symmetry $\sigma(\phi_{b2}^2) = \sigma(\phi_{b3}^2) = \sigma(\phi_{b4}^2)$. $\sigma(\phi_{b4}^2)$ is given by

$$\begin{aligned}\sigma(\phi_{b4}^2) = 2[&\lambda^2(CE^2\cdot\langle 2s_c|\sigma a|2s_c\rangle - 2CE\cdot SE\cdot\langle 2s_c|\sigma a|P_1\rangle/3\\ &+ SE^2(\langle P_1|\sigma a|P_1\rangle + 8\langle P_{\pi 1}|\sigma a|P_{\pi 1}\rangle)/9)\\ &+ 2\lambda\mu(CE(\{1-2\delta\}\cdot\langle h_2|\sigma a''|2s_c\rangle - \delta\cdot\langle h_1|\sigma a|2s_c\rangle - Co\cdot\langle 1s_c|\sigma a|2s_c\rangle)\\ &+ SE(\{2\delta-1\}\cdot\langle h_2|\sigma a''|P_1\rangle + 2\sqrt{2}\cdot(1+\delta)\cdot\langle h_2|\sigma a''|P_{\pi 1}\rangle\\ &+ \delta\cdot\langle h_1|\sigma a|P_1\rangle + Co\cdot\langle 1s_c|\sigma a|P_1\rangle)/3)\\ &+ \mu^2(\{1+2\delta^2\}\cdot\langle h_2|\sigma a|h_2\rangle - 2\delta\cdot(1-2\delta)\cdot\langle h_1|\sigma a|h_2\rangle\\ &+ \delta^2\cdot\langle h_1|\sigma a|h_1\rangle - 2\delta\cdot(2-\delta)\cdot\langle h_2|\sigma a''|h_3\rangle - 2Co\cdot\langle h_2|\sigma a''|1s_c\rangle\\ &+ 2\delta\cdot Co(\langle h_1|\sigma a|1s_c\rangle + 2\langle h_2|\sigma a''|1s_c\rangle)\\ &+ Co^2\langle 1s_c|\sigma a|1s_c\rangle)].\end{aligned}$$

The total diamagnetic magnetic shielding at H_1 is

$$\begin{aligned}
\sigma^{(d)} = 2[&4\lambda^2(CE^2\cdot\langle 2s_c|\sigma a|2s_c\rangle + SE^2(\langle P_1|\sigma a|P_1\rangle + 2\langle P_{\pi 1}|\sigma a|P_{\pi 1}\rangle)/3) \\
&+ 2\lambda\mu(CE(\{1-3\delta\}\cdot(\langle h_1|\sigma a|2s_c\rangle + 3\langle h_2|\sigma a''|2s_c\rangle \\
&\quad - 4Co\cdot\langle 1s_c|\sigma a|2s_c\rangle) \\
&+ SE(\{1+\delta\}\cdot(\langle h_1|\sigma a|P_1\rangle - \langle h_2|\sigma a'|P_1\rangle + 2\sqrt{2}\cdot\langle h_2|\sigma a''|P_{\pi 1}\rangle))) \\
&+ \mu^2(\{1+3\delta^2\}\cdot(\langle h_1|\sigma a|h_1\rangle + 3\langle h_2|\sigma a|h_2\rangle) \\
&- 12\delta\cdot(1-\delta)\cdot(\langle h_1|\sigma a|h_2\rangle + \langle h_2|\sigma a''|h_3\rangle) \\
&- 2(1-3\delta)\cdot Co\cdot(\langle h_1|\sigma a|1s_c\rangle + 3\langle h_2|\sigma a''|1s_c\rangle) \\
&+ 4Co^2\cdot\langle 1s_c|\sigma a|1s_c\rangle) + \langle 1s_c|\sigma a|1s_c\rangle].
\end{aligned}$$

APPENDIX 3

Methods Used to Evaluate Integrals

A large number of integrals are required for the evaluation of all the theoretical properties recorded in this thesis. A list of the actual integrals is given in the following appendicies. This section is concerned with how these integrals were evaluated.

Consider a system of N electrons where the total wavefunction, ψ, is given by a single Slater determinant of the form

$$\psi(1,2,\ldots N) = \sqrt{1/N!}\ ||\phi_1(1)\alpha(1)\phi_1(2)\beta(2)\ldots\ldots\phi_{N/2}(N)\beta(N)|| \qquad (A3.1)$$

where the ϕ_i's are a set of orthonormal molecular space orbitals given by

$$\phi_i = \sum_j C_{ij}\chi_j \qquad (A3.2)$$

and χ_j are simple Slater-type functions centered on each of the different nuclei in the system. In order to evaluate the expectation value $\langle\psi|O_{op}|\psi\rangle$, where O_{op} is the quantum mechanical operator for the property of interest, for a polyatomic system (i.e., CH_4) one must calculate a large number of different types of integrals. For a two-electron operator (i.e., $O_{op} \equiv 1/r_{12}$) one can have one-, two-, three-, and four-center two-electron integrals of the general form $\langle\chi_a\chi_b|1/r_{12}|\chi_c\chi_d\rangle$*. If O_{op} is a one-electron operator (i.e., $O_{op} \equiv O_a$) then one can have only one-, two-, and three-center one-electron integrals. The actual method used to evaluate

---

* χ_a, χ_b, χ_c and χ_d refer to Slater atomic orbitals centered on nuclei a,b,c and d respectively.

each integral depends on the particular type of integral one is calculating.

(a) Two-Electron Integrals

All two-electron integrals used in this thesis were evaluated using a number of programs obtained from "Quantum Chemistry Program Exchange" (referred to as QCPE)[81]. These programs were all rewritten to operate on the IBM-7040 system at McMaster University. The one- and two-center $1/r_{12}$ integrals were evaluated using QCPE program #29-"DIAT". QCPE programs #22, #23, #24 and #25 were used to calculate the three- and four-center $1/r_{12}$ integrals. The input and output for these programs are the same as specified by QCPE.

(b) One-Electron Integrals

The atomic or one-center integrals, defined as $\langle \chi_a | O_a | \chi'_a \rangle$ are easily calculated using integral calculus. The two-center integrals are more difficult to evaluate. They are of two types, (a) overlap type, $\langle \chi_a | O_a | \chi_b \rangle$ and (b) screening type, $\langle \chi_b | O_a | \chi_b \rangle$. A number of methods were used to evaluate these two-center integrals depending on the form of the operator O_a. These methods are listed below. The three-center integrals, $\langle \chi_b | O_a | \chi_c \rangle$, were evaluated in nearly every case using modified versions of QCPE program #22. Here again the procedure is the same as specified by QCPE.

(c) Two-Center Integrals

Consider a two-center system as shown in Figure A3.1 with nuclei at A and B separated by a bond distance R. P is a variable point (usually the position of the electron), over all positions of which the integration

is performed.

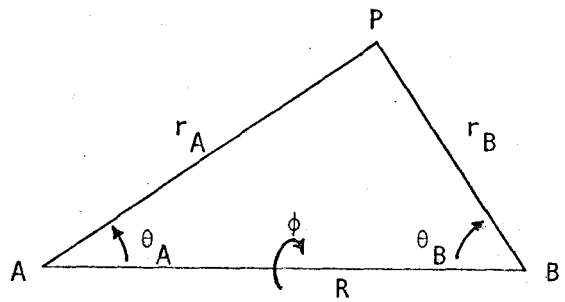

Figure A3.1

The spherical coordinates of P are (r_A, θ_A, ϕ) relative to origin A, and (r_B, θ_B, ϕ) relative to origin B.

i) Kotani "F" method

In this method the integrals are evaluated by a transformation to spheroidal coordinates λ, μ, ϕ. These coordinates are defined by $\lambda = (r_A + r_B)/R$, $\mu = (r_A + r_B)/R$ and ϕ is the azimath around AB. The ranges of these coordinates are

$$1 \leq \lambda \leq \infty, \qquad -1 \leq \mu \leq 1, \qquad 0 \leq \phi \leq 2\pi .$$

It is easily shown that

$$r_A = (\lambda + \mu)R/2 \tag{A3.3}$$

$$r_B = (\lambda - \mu)R/2 \tag{A3.4}$$

$$r_A \cos\theta_A = (1 + \lambda\mu)R/2 \tag{A3.5}$$

$$r_B \cos\theta_B = (1 - \lambda\mu)R/2 \tag{A3.6}$$

$$r_A \sin\theta_A = r_B \sin\theta_B = (\lambda^2 - 1)^{1/2}(1 - \mu^2)^{1/2}R/2 \tag{A3.7}$$

$$d\tau = (\lambda^2 - \mu^2)R^3/8 \; d\lambda d\mu d\phi \; . \tag{A3.8}$$

In this new coordinate system a large number of integrals can be expressed as products and/or sums of the following types of integrals.

$$A_N(\alpha) = \int_1^\infty \lambda^N e^{-\alpha\lambda} d\lambda \tag{A3.9}$$

$$B_N(\beta) = \int_{-1}^{1} \mu^N e^{-\beta\mu} d\mu \tag{A3.10}$$

$$F_{KMN}(\alpha,\beta) = \int_1^{\infty}\int_{-1}^{1} \frac{(\lambda^2-1)^K}{(\lambda+\mu)^{K+1}} \lambda^M \mu^N e^{-\alpha\lambda} e^{-\beta\mu} d\lambda d\mu \tag{A3.11}$$

where

$$\alpha = (Z_1 + Z_2)R/2 \tag{A3.12}$$

$$\beta = (Z_1 - Z_2)R/2 \text{ (for overlap-type integrals)} \tag{A3.13}$$

$$\beta = -(Z_1 + Z_2)R/2 \text{ (for screening-type integrals).} \tag{A3.14}$$

The symbols Z_1 and Z_2 refer to the two screening coefficients of the Slater-type functions χ_1 and χ_2 respectively which are used in the integral $\langle\chi_1|O_A|\chi_2\rangle$. χ_2 is always on center B, but χ_1 is on center A if calculating an overlap-type integral and on center B is calculating a screening-type integral.

Kotani et al[123] give general expressions and recursion relations to evaluate the integrals (A3.9), (A3.10) and (A3.11). Dr. J. Goodisman at the University of Illinois used these relations as the basis of a program to calculate two-center integrals. This program was modified and rewritten as a subroutine, called FØRINT, in double precision for the IBM-7040. The subroutine has α and β as input parameters and it evaluates and provides as output the values for $A_N(\alpha)$, $B_N(\beta)$, $F_{0MN}(\alpha,\beta)$, $F_{1MN}(\alpha,\beta)$ and $F_{MN}(\alpha,\beta)$ where

$$F_{MN}(\alpha,\beta) = F_{0,M+1,N}(\alpha,\beta) - F_{1,M,N}(\alpha,\beta) . \tag{A3.15}$$

Whenever an integral is calculated, a call to FØRINT is made using the correct input parameters α and β, then the integral is evaluated using an appropriate expression in terms of the output values A_N, B_N, F_{0MN}, F_{1MN} and F_{MN}. In the subroutine FØRINT these output parameters are designated as subscripted variables where the following notation is used.

$A(N + 1) \equiv A_N(\alpha)$

$B(N + 1) \equiv B_N(\beta)$

$FO(N + 1, M + 1) \equiv F_{0MN}(\alpha, \beta)$

$F1(N + 1, M + 1) \equiv F_{1MN}(\alpha, \beta)$

$FMN(N + 1, M + 1) \equiv F_{MN}(\alpha, \beta)$

The Kotani "F" method was used to evaluate most screening integrals of the type $\langle \chi_b | 0_a | \chi_b \rangle$ and most overlap integrals of the form $\langle \chi_a | 0_a | \chi_b \rangle$. This computational method can not be used to calculate overlap integrals where Z_1 equals Z_2. In this case β equals zero and the Kotani "F" method blows up. To calculate integrals where Z_1 equals Z_2 and also field gradient integrals of the overlap-type the following method was used.

ii) The Barnett-Coulson zeta-function method

The overlap-type integrals with which we are concerned can often be reduced, by the use of the relations $r_A \sin\theta_A = r_B \sin\theta_B$ and $r_A \cos\theta_A = R - r_B \cos\theta_B$ (see Figure A3.1), to sums of integrals of the general form

$$J(k,\ell,m) = \int e^{-Z_1 r_A} e^{-Z_2 r_B} \cos^k\theta_A r_A^{\ell-1} r_B^{m-1} d\tau . \qquad (A3.16)$$

In the Barnett-Coulson[124] zeta-function technique, the remaining terms on center B in Equation (A3.16) are expanded in terms of a coordinate system centered on A. The expansion is

$$r_B^{m-1} e^{-Z_2 r_B} = \sum_{n=0}^{\infty} \frac{(2n+1)}{\sqrt{r_A R}} P_n(\cos\theta_A) \xi_{mn}(Z_2, r_A; R) \qquad (A3.17)$$

$$= Z^{-m+1} \sum_{n=0}^{\infty} \frac{(2n+1)}{\sqrt{t\tau}} P_n(\cos\theta_A) \xi_{mn}(1, t; \tau) \qquad (A3.18)$$

where t and τ are the dimensionless variables

$$t = Z_2 r_A$$

$$\tau = Z_2 R$$

and P_n is the Legendre polynomial of order n. The $\xi_{mn}(Z_2, r_A; R)$ functions are products of Bessel functions of purely imaginary argument. The $J(k,\ell,m)$ integrals can then be expressed as

$$J(k,\ell,m) = \frac{4\pi}{Z_2^{(\ell+m+1)}\sqrt{\tau}} \int_0^\infty e^{-\kappa t} t^{\ell+\frac{1}{2}} f(m,k;t)\,dt \qquad \text{(A3.19)}$$

where

$$f(m,k;t) = \sum_{j=0}^{k} \frac{(2j+1)}{2} \int_{-1}^{1} P_j(x) x^k dx \xi_{mj}(1,t;\tau) \qquad \text{(A3.20)}$$

and

$$\kappa = Z_1/Z_2 \ .$$

Making use of the definition that

$$Z_{m,n,\ell+\frac{1}{2}}(\kappa,\tau) = \int_0^\infty e^{-\kappa t} \xi_{m,n}(1,t;\tau) t^{\ell+\frac{1}{2}}\,dt \qquad \text{(A3.21)}$$

it is easily seen that the $J(k,\ell,m)$ integrals can be expressed as sums of $Z_{m,n,\ell+\frac{1}{2}}(\kappa,\tau)$ integrals. The recursion relations and the methods for evaluating these expressions are given by Barnett and Coulson[124]. General use will be made of the following definitions.

$$G_{n,\ell+\frac{1}{2}}(\kappa,\tau) = Z_{0,n,\ell+\frac{1}{2}}(\kappa,\tau) \qquad \text{(A3.22)}$$

$$P_{n,\ell+\frac{1}{2}}(\kappa,\tau) = Z_{1,n,\ell+\frac{1}{2}}(\kappa,\tau) \qquad \text{(A3.23)}$$

All integrals evaluated by this method can be expressed as sums of these $G_{n,\ell+\frac{1}{2}}$ and $P_{n,\ell+\frac{1}{2}}$ functions. A general subroutine called ØVLINT, which has κ and τ as input parameters, was designed to calculate these $G_{n,\ell+\frac{1}{2}}$ and $P_{n,\ell+\frac{1}{2}}$ functions. The program calculates and gives as

output the subscripted variables G(I,J), CP(I,J) where

$$G(N + 2, L + 2) \equiv G_{N,L+\frac{1}{2}} \quad (\kappa,\tau)$$

$$CP(N + 2, L + 2) \equiv P_{N,L+\frac{1}{2}} \quad (\kappa,\tau) .$$

A third method was used to calculate the screening-type field gradient integrals.

iii) Method of Pitzer, Kern and Lipscomb

The integrals of concern here are the screening-type field gradient integrals which have the form

$$\int (Z_1,n_1\ell_1,m)_B \begin{Bmatrix} \cos m\phi \\ \sin m\phi \end{Bmatrix} \frac{P_2^o(\cos\theta_A)}{r_A^3} (Z_2,n_2,\ell_2,m)_B \begin{Bmatrix} \cos m\phi \\ \sin m\phi \end{Bmatrix} d\tau . \quad (A3.24)$$

This type of integral has been discussed by Pitzer, Kern and Lipscomb[125]. The method used in solving integrals of this type makes general use of the Spherical Harmonic expansion given by Hobson[126].

$$\frac{P_n^m(\cos\theta_A)}{r_A^{n+1}} = \frac{1}{R^n} \sum_{\ell=m}^{\infty} \binom{\ell+n}{n-m} \frac{r_B^\ell}{R^{\ell+1}} P_\ell^m(\cos\theta_B) \qquad \text{if } r_B < R \quad (A3.25)$$

$$= \frac{(-1)^{n-m}}{R^n} \sum_{\ell=n}^{\infty} \binom{\ell-m}{n-m} \frac{R^\ell}{r_A} P_\ell^m(\cos\theta_B) \qquad \text{if } r_B > R \quad (A3.26)$$

It is easily shown that the integrals given by Equation (A3.24) can be reduced to sums of functions of the form

$$G(2,0,n,\ell,\rho) = \binom{\ell+2}{2} \int_0^1 t^{n+\ell} e^{-\rho t} dt + \binom{\ell}{2} \int_1^\infty t^{n-\ell-1} e^{-\rho t} dt \quad (A3.27)$$

where $\rho = (Z_1 + Z_2)R$, $n = n_1 + n_2$ and $|\ell_1 + \ell_2| \geq \ell \geq |\ell_1 - \ell_2|$.

It must be noted that a singularity exists at $r_B = R$ for $n - m \geq 2$,

which is the case for the field gradient operator $[P_2(\cos\theta_a)/r_a^3]$, and an additional term $-\frac{4}{3}\pi\delta(r_B-R)$ must be added to either Equation (A3.25) or (A3.26) to give the correct result in this type of expansion.

A function subprogram called PNINT was designed to compute the functions $G(2,0,n,\ell,\rho)$. The input parameters for the program are ρ, n and ℓ. The functional output has the defining relation

$$PNINT(\rho,N,L) \equiv G(2,0,N,L,\rho).$$

General equations for all the two-center one-electron integrals used in this thesis are given in the following appendicies. These integrals are expressed as products and/or sums of the parameters $A_N(\alpha)$, $B_N(\beta)$, $F_{0MN}(\alpha,\beta)$, $F_{1MN}(\alpha,\beta)$, $F_{MN}(\alpha,\beta)$, $G_{n,\ell+\frac{1}{2}}(\kappa,\tau)$, $P_{n,\ell+\frac{1}{2}}(\kappa,\tau)$ and $G(2,0,n,\ell,\rho)$ which have already been discussed in this section.

APPENDIX 4

Integrals Required for Wavefunction Determination

All the expressions for the integrals in this and the following appendicies are for the single Slater 1s, 2s and 2p orbitals and not for the SCF atomic orbitals $1s_c$, $2s_c$ and $2p_c$ which are linear combinations of the Slater orbitals as given in Appendix 1.

(a) Overlap Integrals

Defining an overlap integral as $\langle \chi_i | \chi_j \rangle$ where χ_i has a screening coefficient Z_1 and χ_j has a screening coefficient Z_2 then we can write

$$\langle h_1 | 1s \rangle = \frac{Z_1^{3/2} Z_2^{3/2} R^3}{4} [A_2B_0 - A_0B_2]$$

$$\langle h_1 | 2s \rangle = \frac{Z_1^{3/2} Z_2^{5/2} R^4}{8\sqrt{3}} [A_3B_0 + A_0B_3 - A_1B_2 - A_2B_1]$$

$$\langle h_1 | 2p\sigma \rangle = \frac{Z_1^{3/2} Z_2^{5/2} R^4}{8} [A_2B_0 + A_1B_3 - A_3B_1 - A_0B_2]$$

where R is the C—H_1 bond distance. When Z_1 equals Z_2 the overlap has a different form

$$\langle h_1 | h_2 \rangle = \frac{Z_1^3 R_1^3}{6} [3A_2 - A_0]$$

where now R_1 is the H_1—H_2 bond distance.

(b) Force Integrals

These integrals involve the average over the force operator $Fa \equiv \cos(\theta_{H_1})/r_{H_1}^2$, where the force is on H_1 and directed along the C—H_1

bond axis. The non-zero elements are given by the following expressions.

The screening-type integrals are

$$\langle 1s|Fa|1s\rangle = Z_1^{3/2} Z_2^{3/2} R[F_{10} - F_{01}]$$

$$\langle 2s|Fa|1s\rangle = \frac{Z_1^{5/2} Z_2^{3/2} R^2}{2\sqrt{3}} [F_{20} + F_{02} - 2F_{11}]$$

$$\langle 2s|Fa|2s\rangle = \frac{Z_1^{5/2} Z_2^{5/2} R^3}{12} [3(F_{12} - F_{21}) + F_{30} - F_{03}]$$

$$\langle 2p\sigma|Fa|1s\rangle = \frac{Z_1^{5/2} Z_2^{3/2} R^2}{2} [F_{10} - F_{01} + F_{12} - F_{21}]$$

$$\langle 2p\sigma|Fa|2s\rangle = \frac{Z_1^{5/2} Z_2^{5/2} R^3}{4\sqrt{3}} [2(F_{22} - F_{11}) + F_{20} + F_{02} - F_{13} - F_{31}]$$

$$\langle 2p\sigma|Fa|2p\sigma\rangle = \frac{Z_1^{5/2} Z_2^{5/2} R^3}{4} [2(F_{12} - F_{21}) + F_{10} + F_{32} - F_{01} - F_{23}]$$

$$\langle 2p\pi|Fa|2p\pi\rangle = \frac{Z_1^{5/2} Z_2^{5/2} R^3}{8} [F_{110} + F_{121} + F_{103} + F_{114} - F_{101} - F_{123} - 2F_{112}]$$

$$\langle h_2|F\dot{a}|h_2\rangle^{*} = Z_1^{3/2} Z_2^{3/2} R_1 [F_{10} - F_{01}] .$$

The overlap-type integrals are

$$\langle h_1|Fa|1s\rangle = Z_1^{3/2} Z_2^{3/2} R [F_{10} - F_{01}]$$

$$\langle h_1|Fa|2s\rangle = \frac{Z_1^{3/2} Z_2^{5/2} R^2}{2\sqrt{3}} [F_{02} + F_{20} - 2F_{11}]$$

$$\langle h_1|Fa|2p\sigma\rangle = \frac{Z_1^{3/2} Z_2^{5/2} R^2}{2} [F_{10} + F_{12} - F_{01} - F_{21}]$$

and when Z_1 equals Z_2 we have

---

* See the first footnote on page 178.

$$\langle h_1|Fa|h_2\rangle = \frac{Z_1^{3/2} Z_2^{1/2}}{\sqrt{Z_2 R_1}} 4P_{1,1+\frac{1}{2}} \quad .$$

The three-center integrals were evaluated using QCPE program #22 where the operator is $Fa \equiv Z_a/r_a^3$.

(c) Proton Magnetic Shielding Integrals

To determine the magnetic shielding at the proton H_1 the operator is $\sigma a \equiv 1/r_{H_1}$. The non-zero integrals have the following expressions. The only atomic-type integral is

$$\langle h_1|\sigma a|h_1\rangle = Z_1$$

where Z_1 equals Z_2. The screening-type integrals are

$$\langle 1s|\sigma a|1s\rangle = \frac{Z_1^{3/2} Z_2^{3/2} R^2}{2} [F_{020} - F_{002}]$$

$$\langle 2s|\sigma a|1s\rangle = \frac{Z_1^{5/2} Z_2^{3/2} R^3}{4\sqrt{3}} [F_{030} + F_{003} - F_{012} - F_{021}]$$

$$\langle 2s|\sigma a|2s\rangle = \frac{Z_1^{5/2} Z_2^{5/2} R^4}{24} [F_{040} + 2(F_{013} - F_{031}) - F_{004}]$$

$$\langle 2p\sigma|\sigma a|1s\rangle = \frac{Z_1^{5/2} Z_2^{3/2} R^3}{4} [F_{020} + F_{013} - F_{002} - F_{031}]$$

$$\langle 2p\sigma|\sigma a|2s\rangle = \frac{Z_1^{5/2} Z_2^{5/2} R^4}{8\sqrt{3}} [F_{030} + F_{003} + F_{032} + F_{023} - F_{041}$$

$$\langle 2p\sigma|\sigma a|2p\sigma\rangle = \frac{Z_1^{5/2} Z_2^{5/2} R^4}{8} [F_{020} + F_{042} + 2(F_{013} - F_{031}) - F_{002} - F_{024}]$$

$$\langle 2p\pi|\sigma a|2p\pi\rangle = \frac{Z_1^{5/2} Z_2^{5/2} R^4}{16} [F_{040} + F_{002} + F_{024} - F_{020} - F_{042} - F_{004}]$$

$$\langle h_2|\sigma a|h_2\rangle = \frac{Z_1^{3/2} Z_2^{3/2} R_1^2}{2} [F_{020} - F_{002}] \quad .$$

The overlap-type integrals are

$$\langle h_1|\sigma a|1s\rangle = \frac{Z_1^{3/2} Z_2^{3/2} R^2}{2} [F_{020} - F_{002}]$$

$$\langle h_1|\sigma a|2s\rangle = \frac{Z_1^{3/2} Z_2^{5/2} R^3}{4\sqrt{3}} [F_{030} + F_{003} - F_{021} - F_{012}]$$

$$\langle h_1|\sigma a|2p\sigma\rangle = \frac{Z_1^{3/2} Z_2^{5/2} R^3}{4} [F_{020} + F_{013} - F_{002} - F_{031}]$$

and when Z_1 equals Z_2 we have

$$\langle h_1|\sigma a|h_2\rangle = Z_1(1 + Z_1R_1)e^{-Z_1R_1} .$$

All the three-center integrals were evaluated using QCPE[81] program #22 where the operator is $\sigma a \equiv 1/r_a$.

APPENDIX 5

Diamagnetic Susceptibility

The diamagnetic susceptibility is obtained by averaging the wavefunction over the operator $\chi a \equiv r_c^2$ where r_c is the distance from the center of mass. Using the additional definition that

$$\langle \chi_b' | \chi a | \chi_c' \rangle \equiv \int \chi_b' \chi a \chi_c' d\tau$$

then the orbital contributions to the diamagnetic susceptibility are

$$\chi(\phi_o^2) = 2\langle 1s_c | \chi a | 1s_c \rangle$$

$$\begin{aligned}\chi(\phi_{b1}^2) = 2[&\lambda^2(CE^2 \cdot \langle 2s_c | \chi a | 2s_c \rangle + SE^2 \cdot \langle P_1 | \chi a | P_1 \rangle) \\ &+ 2\lambda\mu(CE(\{1 - 3\delta\} \cdot \langle h_1 | \chi a | 2s_c \rangle - Co \cdot \langle 1s_c | \chi a | 2s_c \rangle) \\ &+ SE \cdot (1 + \delta) \cdot \langle h_1 | \chi a | P_1 \rangle) \\ &+ \mu^2(\{1 + 3\delta^2\} \cdot \langle h_1 | \chi a | h_1 \rangle - 6\delta \cdot (1 - \delta) \cdot \langle h_1 | \chi \ddot{a} | h_2 \rangle \\ &- 2Co \cdot (1 - 3\delta) \cdot \langle h_1 | \chi a | 1s_c \rangle + Co^2 \cdot \langle 1s_c | \chi a | 1s_c \rangle)] \ .\end{aligned}$$

By symmetry $\chi(\phi_{b2}^2) = \chi(\phi_{b3}^2) = \chi(\phi_{b4}^2) = \chi(\phi_{b1}^2)$. The total diamagnetic susceptibility is

$$\begin{aligned}\chi^{(d)} = 8[&\lambda^2(CE^2 \cdot \langle 2s_c | \chi a | 2s_c \rangle + SE^2 \cdot \langle P_1 | \chi a | P_1 \rangle) \\ &+ 2\lambda\mu(CE \cdot (\{1 - 3\delta\} \cdot \langle h_1 | \chi a | 2s_c \rangle - Co \cdot \langle 1s_c | \chi a | 2s_c \rangle) \\ &+ SE \cdot (1 + \delta) \cdot \langle h_1 | \chi a | P_1 \rangle) \\ &+ \mu^2(\{1 + 3\delta^2\} \cdot \langle h_1 | \chi a | h_1 \rangle - 6\delta \cdot (1 - \delta) \cdot \langle h_1 | \chi \ddot{a} | h_2 \rangle \\ &- 2\ Co \cdot (1 - 3\delta) \cdot \langle h_1 | \chi a | 1s_c \rangle + Co^2 \cdot \langle 1s_c | \chi a | 1s_c \rangle)] \\ &+ 2\langle 1s_c | \chi a | 1s_c \rangle \ .\end{aligned}$$

The non-zero integrals required for the evaluation of the susceptibility have the following expressions. The atomic-type integrals are

$$\langle 1s|\chi a|1s\rangle = 96\,\frac{Z_1^{3/2}Z_2^{3/2}}{(Z_1+Z_2)^5}$$

$$\langle 2s|\chi a|1s\rangle = 480\,\frac{Z_1^{5/2}Z_2^{3/2}}{\sqrt{3}(Z_1+Z_2)^6}$$

$$\langle 2s|\chi a|2s\rangle = 960\,\frac{Z_1^{5/2}Z_2^{5/2}}{(Z_1+Z_2)^7}$$

$$\langle 2p\sigma|\chi a|2p\sigma\rangle = \langle 2p\pi|\chi a|2p\pi\rangle = 960\,\frac{Z_1^{5/2}Z_2^{5/2}}{(Z_1+Z_2)^7}\ .$$

The only screening-type integral is

$$\langle h_1|\chi a|h_1\rangle = \frac{Z_1^{3/2}Z_2^{3/2}R^5}{16}\,[A_4B_0 + 2(A_3B_1 - A_1B_3) - A_0B_4]\ .$$

The overlap-type integrals are

$$\langle 1s|\chi a|h_1\rangle = \frac{Z_1^{3/2}Z_2^{3/2}R^5}{16}\,[A_4B_0 + 2(A_3B_1 - A_1B_3) - A_0B_4]$$

$$\langle 2s|\chi a|h_1\rangle = \frac{Z_1^{5/2}Z_2^{3/2}R^6}{32\sqrt{3}}\,[A_5B_0 - A_0B_5 + 2(A_3B_2 - A_2B_3) + 3(A_4B_1 - A_1B_4)]$$

$$\langle 2p\sigma|\chi a|h_1\rangle = \frac{Z_1^{5/2}Z_2^{3/2}R^6}{32}\,[A_4B_0 + A_5B_1 - A_0B_4 - A_1B_5 + 2(A_3B_1 + A_4B_2 - A_1B_3 - A_2B_4)]\ .$$

The only three-center integral has the form

$$\langle h_1|\chi''a|h_2\rangle = \frac{R^2Z_1^3R_1^3}{6}\,[3A_2 - A_0] + \frac{Z_1^3R_1^5}{8}\,[A_4 - A_0/5] - 2R\sqrt{2/3}\,\frac{Z_1^3R_1^4}{12}\,[3A_2 - A_0]$$

where Z_1 equals Z_2 and the integral has been transformed into a two-center overlap-type integrals between the centers H_1 and H_2.

APPENDIX 6

Bond Dipole

The dipole operator is $Da \equiv r_c \cos\theta_c$ where θ_c is the angle measured from the C—H_1 bond axis and r_c is the distance from the carbon nucleus. The expectation value of this operator gives the electronic dipole at carbon in the direction along the C—H_1 bond axis. Since the dipole due to ϕ_o is zero we are interested only in the bond dipole resulting from the bonding orbital ϕ_{b1}. This orbital contribution is

$$\begin{aligned} D(\phi_{b1}^2) = 2[&2\lambda^2 \cdot CE \cdot SE \cdot \langle 2s_c|Da|P_1\rangle + 2\lambda\mu(CE \cdot (1+\delta) \cdot \langle 2s_c|Da|h_1\rangle \\ &+ SE(\langle P_1|Da|h_1\rangle - 3\delta\langle P_1|Da|h_2\rangle^{*} - Co \cdot \langle 1s_c|Da|P_1\rangle)) \\ &+ \mu^2(\{1-\delta^2\} \cdot \langle h_1|Da|h_1\rangle - 6\delta \cdot (1+\delta) \cdot \langle h_1|D\ddot{a}|h_2\rangle \\ &- 2Co \cdot (1+\delta) \cdot \langle 1s_c|Da|h_1\rangle)] \end{aligned}$$

where

$$\langle \chi_b|Da|\chi_c\rangle \equiv \int \chi_b Da \chi_c d\tau \ .$$

The non-zero integrals required for the calculation of the bond dipole have the following expressions. The atomic-type integrals are

$$\langle 1s|Da|2p\sigma\rangle = \frac{32 Z_1^{3/2} Z_2^{5/2}}{(Z_1+Z_2)^5}$$

$$\langle 2s|Da|2p\sigma\rangle = \frac{160 Z_1^{5/2} Z_2^{5/2}}{\sqrt{3}(Z_1+Z_2)^6} \ .$$

---

* Note that $\langle P_1|Da|h_2\rangle = (\langle P_1|Da|h_1\rangle + 8\langle P_{\pi 1}|D\pi a|h_1\rangle)/9$ where $P_{\pi 1}$ is given in the second footnote on page 178 and $D\pi a \equiv r_c \sin\theta_c \cos\phi$.

The only screening-type integral is

$$\langle h_1|Da|h_1\rangle = \frac{Z_1^3 R^4}{8}[A_2B_0 + A_3B_1 - A_0B_2 - A_1B_3] = R$$

where Z_1 equals Z_2. The overlap-type integrals are

$$\langle 1s|Da|h_1\rangle = \frac{Z_1^{3/2} Z_2^{3/2} R^4}{8}[A_2B_0 + A_3B_1 - A_0B_2 - A_1B_3]$$

$$\langle 2s|Da|h_1\rangle = \frac{Z_1^{5/2} Z_2^{3/2} R^5}{16\sqrt{3}}[A_3(B_0 + B_2) + (A_2 + A_4)B_1 - A_1(B_2 + B_4) - (A_0 + A_2)B_3]$$

$$\langle 2p\sigma|Da|h_1\rangle = \frac{Z_1^{5/2} Z_2^{3/2} R^5}{16}[A_2(B_0 + B_4) - (A_0 + A_4)B_2 + 2(A_3B_1 - A_1B_3)]$$

$$\langle 2p\pi|D\pi a|h_1\rangle = \frac{Z_1^{5/2} Z_2^{3/2} R^5}{32}[A_4(B_0 - B_2) + (A_2 - A_0)B_4 + A_0B_2 - A_2B_0]$$

where $D\pi a \equiv r_c \sin\theta_c \cos\phi$. The resulting three center integral has the form

$$\langle h_1|D''a|h_2\rangle = \frac{Z_1^3 R_1^3}{2}(R - \sqrt{2/3}\cdot R_1/2)\cdot(A_2 - A_0/3)$$

where Z_1 equals Z_2 and the integral has been transformed into a two-center overlap-type integral between centers H_1 and H_2.

APPENDIX 7

Octupole Moment

The expectation value for the octupole moment is obtained by averaging the wavefunction over the operator $\Phi a \equiv \sqrt{15}\, x_c y_c z_c$. The origin of the operator is at the center of mass and the coordinate axies have the directions indicated in Figure 1.1. Using the previous notation together with the identity

$$\langle \chi_b | \Phi a | \chi_c \rangle \equiv \int \chi_b \Phi a \chi_c \, d\tau$$

the orbital contributions to the octupole moment are

$$\Phi(\phi_o^2) = 0$$

$$\begin{aligned}\Phi(\phi_{b1}^2) = 2[&2\lambda\mu(CE\cdot(1 - 3\delta)\cdot\langle 2s_c|\Phi a|h_1\rangle + SE\cdot(1 + \delta)\cdot\langle 2P_1|\Phi a|h_1\rangle) \\ &+ \mu^2(\{1 + 3\delta^2\}\cdot\langle h_1|\Phi a|h_1\rangle - 6\delta\cdot(1 - \delta)\cdot\langle h_1|\Phi a''|h_2\rangle \\ &- 2Co\cdot(1 - 3\delta)\cdot\langle 1s_c|\Phi a|h_1\rangle)] \ .\end{aligned}$$

By symmetry $\Phi(\phi_{b2}^2) = \Phi(\phi_{b3}^2) = \Phi(\phi_{b4}^2) = \Phi(\phi_{b1}^2)$. Thus the total electronic octupole moment, I_3^e, is

$$I_3^e = 4\Phi(\phi_{b1}^2)$$

All the atomic octupole moment integrals are zero. In order to carry out the evaluation of the two-center integrals the operator, Φa, was written in terms of a new coordinate system x', y', z', where z' points at H_1, x' is perpendicular to the C—H_1 bond and in the H_1CH_2 plane and y' is perpendicular to both the C—H_1 bond and the H_1CH_2 plane forming a right-

handed system. The operator thus can be expressed as

$$\Phi a = \sqrt{15}[z'^3/3 - y'^2 z'/2 - x'^2 z'/2 - y'^2 x'/\sqrt{2} + x'^3/\sqrt{2}]/\sqrt{3}$$

$$= \sqrt{15}\, r_c^3 \left[\frac{\cos^3\theta_c}{3\sqrt{3}} - \frac{\sin^2\theta_c \cos\theta_c}{2\sqrt{3}} - \frac{\sin^3\theta_c \sin^2\phi \cos\phi}{\sqrt{6}} + \frac{\sin^3\theta_c \cos^3\phi}{3\sqrt{6}}\right]$$

where θ_c is the angle measured from the C—H_1 bond axis. Using this new form of the operator the non-zero integrals required to evaluate the octupole moment have the following expressions. The single screening-type integral is

$$\langle h_1|\Phi a|h_1\rangle = \frac{\sqrt{15}Z_1^3 R^6}{192\sqrt{3}}[3(A_0B_4 + A_1B_5 - A_4B_0 - A_5B_1) + 5(A_2B_0 + A_5B_3 - A_0B_2 - A_3B_5) + 9(A_3B_1 + A_4B_2 - A_1B_3 - A_2B_4)]$$

where the orbital exponents are equal (i.e., Z_1 equals Z_2). The overlap-type integrals are

$$\langle 1s|\Phi a|h_1\rangle = \frac{\sqrt{15}Z_1^{3/2} Z_2^{3/2} R^6}{192\sqrt{3}}[3(A_0B_4 + A_1B_5 - A_4B_0 - A_5B_1) + 5(A_2B_0 + A_5B_3 - A_0B_2 - A_3B_5) + 9(A_3B_1 + A_4B_2 - A_1B_3 - A_2B_4)]$$

$$\langle 2s|\Phi a|h_1\rangle = \frac{\sqrt{15}Z_1^{5/2} Z_2^{3/2} R^7}{1152}[3(A_0B_5 - A_1B_6 - A_5B_0 - A_6B_1) + 5(A_3B_0 + A_6B_3 + A_2B_1 + A_5B_4 - A_0B_3 - A_3B_6 - A_1B_2 - A_4B_5) + 6(A_4B_1 + A_5B_2 - A_1B_4 - A_2B_5) + 9(A_3B_2 + A_4B_3 - A_2B_3 - A_3B_4)]$$

$$\langle 2p\sigma|\Phi a|h_1\rangle = \frac{\sqrt{15}Z_1^{5/2} Z_2^{3/2} R^7}{384\sqrt{3}}[3(A_0B_4 + A_2B_6 - A_4B_0 - A_6B_2) + 5(A_2B_0 + A_6B_4 - A_0B_2 - A_4B_6) + 6(A_1B_5 - A_5B_1) + 14(A_3B_1 + A_5B_3 - A_1B_3 - A_3B_5) + 18(A_4B_2 - A_2B_4)].$$

One three-center integral is required for the octupole moment calculation. This integral was obtained by transforming the operator to center H_1. The integral was then evaluated as a two-center integral of the overlap-type between the two centers H_1 and H_2. The integral has the expression

$$\langle h_1 | \Phi_a'' | h_2 \rangle = \sqrt{15}\, Z_1^3 R R_1^3 \left[\frac{R_1^2}{40\sqrt{3}} (3A_2 - A_0) + R(R/\sqrt{3} - R_1/\sqrt{2})(A_2 - A_0/3)/6\right]$$

where Z_1 equals Z_2.

APPENDIX 8

Field Gradients and Force Constants

In this appendix we are interested in finding the expectation value of the field gradient operator $Ga \equiv (3\cos^2\theta_{H_1} - 1)/r^3_{H1}$, where r_{H_1} is the distance measured from H_1 and θ_{H_1} is the angle measured from the C—H_1 bond axis. This operator gives the field gradient at the proton H_1. Using the identity

$$\langle\chi_b|Ga|\chi_c\rangle \equiv \int \chi_b Ga \chi_c d\tau$$

the orbital contributions to the field gradient are

$$G(\phi_{b0}^2) = 2\langle 1s_c|Ga|1s_c\rangle$$

$$\begin{aligned} G(\phi_{b1}^2) = 2[&\lambda^2(CE^2\cdot\langle 2s_c|Ga|2s_c\rangle + 2\cdot CE\cdot SE\cdot\langle 2s_c|Ga|P_1\rangle \\ &+ SE^2\cdot\langle P_1|Ga|P_1\rangle) \\ &+ 2\lambda\mu(CE(\langle h_1|Ga|2s_c\rangle - 3\delta\cdot\langle h_2|G\ddot{a}|2s_c\rangle - Co\cdot\langle 1s_c|Ga|2s_c\rangle) \\ &+ SE(\langle h_1|Ga|P_1\rangle - 3\delta\cdot\langle h_2|G\ddot{a}|P_1\rangle - Co\cdot\langle 1s_c|Ga|P_1\rangle)) \\ &+ \mu^2(3\delta^2(0.5\cdot\langle h_2|G\acute{a}|h_2\rangle^* + 2\langle h_2|G\ddot{a}|h_3\rangle) \\ &+ 6\delta(Co\cdot\langle h_2|G\ddot{a}|1s_c\rangle - 0.5\cdot\langle h_1|G\acute{a}|h_2\rangle) \\ &- 2Co\cdot\langle h_1|Ga|1s_c\rangle + Co^2\cdot\langle 1s_c|Ga|1s_c\rangle)] \ . \end{aligned}$$

---

* The prime on Ga indicates that the integral gives the tensor component along the H_1-H_2 bond axis. In order to get the correct tensor component along the C-H_1 bond axis the integral is multiplied by the factor $(\cos^2\alpha - 1/2\ \sin^2\alpha) = 0.5$, where α is the angle between the H_1-H_2 bond and the C-H_1 bond.

By symmetry $G(\phi_{b2}^2) = G(\phi_{b3}^2) = G(\phi_{b4}^2)$. $G(\phi_{b4}^2)$ is given by

$$G(\phi_{b4}^2) = 2[\lambda^2(CE^2\cdot\langle 2s_c|Ga|2s_c\rangle - 2\cdot CE\cdot SE\cdot\langle 2s_c|Ga|P_1\rangle/3$$

$$+ SE^2(\langle P_1|Ga|P_1\rangle + 8\langle P_{\pi 1}|Ga|P_{\pi 1}\rangle^*)/9)$$

$$+ 2\lambda\mu(CE(\{1 - 2\delta\}\cdot\langle h_2|\overset{''}{Ga}|2s_c\rangle - \delta\cdot\langle h_1|Ga|2s_c\rangle$$

$$- Co\cdot\langle 1s_c|Ga|2s_c\rangle)$$

$$+ SE(\{2\delta - 1\}\cdot\langle h_2|\overset{''}{Ga}|P_1\rangle + 2\sqrt{2}\cdot(1 + \delta)\cdot\langle h_2|\overset{''}{Ga}|P_{\pi 1}\rangle$$

$$+ \delta\cdot\langle h_1|Ga|P_1\rangle + Co\cdot\langle 1s_c|Ga|P_1\rangle)/3)$$

$$+ \mu^2(0.5\cdot(1 + 2\delta^2)\cdot\langle h_2|\overset{'}{Ga}|h_2\rangle - 2\delta\cdot(1 - 2\delta)\cdot 0.5\cdot\langle h_1|\overset{'}{Ga}|h_2\rangle$$

$$- 2\delta\cdot(2 - \delta)\cdot\langle h_2|\overset{''}{Ga}|h_3\rangle - 2Co\cdot\langle h_2|\overset{''}{Fa}|1s_c\rangle$$

$$+ 2\delta\cdot Co(\langle h_1|Ga|1s_c\rangle + 2\langle h_2|\overset{''}{Ga}|1s_c\rangle) + Co^2\cdot\langle 1s_c|Ga|1s_c\rangle)] \ .$$

The total electronic field gradient at the proton H_1 is given by

$$G^e = G(\phi_{b0}^2) + G(\phi_{b1}^2) + 3(\phi_{b4}^2) \ .$$

The non-zero integrals required to evaluate the field gradient at the proton are given by the following expressions. The screening-type integrals are

$$\langle 1s|Ga|1s\rangle = 8\ Z_1^{3/2} Z_2^{3/2}[-\tfrac{1}{3}\exp(-\rho) + G(2,0,2,0,\rho)]$$

$$\langle 2s|Ga|1s\rangle = \frac{8\ Z_1^{5/2} Z_2^{3/2} R}{\sqrt{3}}[-\tfrac{1}{3}\exp(-\rho) + G(2,0,3,0,\rho)]$$

$$\langle 2s|Ga|2s\rangle = \frac{8\ Z_1^{5/2} Z_2^{5/2} R^2}{3}[-\tfrac{1}{3}\exp(-\rho) + G(2,0,4,0,\rho)]$$

---

* See second footnote on page 178.

$$\langle 2p\sigma|Ga|1s\rangle = \frac{8\, Z_1^{5/2} Z_2^{3/2} R}{3} [-\exp(-\rho) + G(2,0,3,1,\rho)]$$

$$\langle 2p\sigma|Ga|2s\rangle = \frac{8\, Z_1^{5/2} Z_2^{5/2} R^2}{3\sqrt{3}} [-\exp(-\rho) + G(2,0,4,1,\rho)]$$

$$\langle 2p\sigma|Ga|2p\sigma\rangle = \frac{8\, Z_1^{5/2} Z_2^{5/2} R^2}{3} [-\exp(-\rho) + G(2,0,4,0,\rho) + \frac{2}{5} G(2,0,4,2,\rho)]$$

$$\langle 2p\pi|Ga|2p\pi\rangle = \frac{8\, Z_1^{5/2} Z_2^{5/2} R^2}{3} [G(2,0,4,0,\rho) - \frac{1}{5} G(2,0,4,2,\rho)]$$

where $\rho = (Z_1 + Z_2)R$. Also, when Z_1 equals Z_2 we have

$$\langle h_2|Ga'|h_2\rangle = 8\, Z_1^3 [-\frac{1}{3} \exp(-2Z_1R_1) + G(2,0,2,0,2Z_1R_1)] \ .$$

The overlap-type integrals are

$$\langle h_1|Ga|1s\rangle = \frac{8\, Z_1^{3/2} Z_2}{5R^{\frac{1}{2}}} [Z_2R(G_{1,-1+\frac{1}{2}} - G_{3,-1+\frac{1}{2}})]$$

$$\langle h_1|Ga|2s\rangle = \frac{8\, Z_1^{3/2} Z_2}{\sqrt{3}\, R^{\frac{1}{2}}} [G_{2,0+\frac{1}{2}} + Z_2^2R^2G_{2,-2+\frac{1}{2}} - \frac{Z_2R}{5} (4G_{1,-1+\frac{1}{2}} + 6G_{3,-1+\frac{1}{2}})]$$

$$\langle h_1|Ga|2p\sigma\rangle = \frac{8\, Z_1^{3/2} Z_2}{5R^{\frac{1}{2}}} [Z_2^2R^2(G_{1,-1+\frac{1}{2}} - G_{3,-1+\frac{1}{2}}) - 2P_{1,-1+\frac{1}{2}} - 3P_{3,-1+\frac{1}{2}}]$$

and when Z_1 equals Z_2 we have

$$\langle h_1|Ga'|h_2\rangle = \frac{8\, Z_1^{5/2}}{5R^{\frac{1}{2}}} [Z_1R_1(G_{1,-1+\frac{1}{2}} - G_{3,-1+\frac{1}{2}})] \ .$$

The three-centre field gradient integrals were evaluated using a modified version of QCPE program #22. The required revisions were to set TJ(7,1) = 96.0 and TJ(8,1) = -16.0 in the subroutine LITLJ1. Making these changes the QCPE program was used to calculate the correct tensor components

for the field gradient operator, which were then used to evaluate the appropriate three-center integrals.

In this appendix consideration is given to how one might determine the theoretical contribution to the force constant for one of the infra-red active T_2 modes of the methane molecule. The actual numerical calculations were not carried out but the mathematical expressions that are required have been worked out and are given here.

Considering one of the infra-red active normal coordinates, Q_{4a}, referred to hereafter as Q_4, the force constant associated with this normal mode can be determined theroetically from Equation (1.60). Thus

$$k_4 = \left(\frac{\partial^2 E}{\partial Q_4^2}\right)_0 = \left.\frac{\partial^2 V_N}{\partial Q_4^2}\right|_0 + \left.\int \frac{\partial^2 V_1}{\partial Q_4^2}\,\rho(\vec{x}_1)\,d\tau_1\right|_0 + \left.\int \frac{\partial V_1}{\partial Q_4}\,\frac{\partial \rho(\vec{x}_1)}{\partial Q_4}\,d\tau_1\right|_0 . \tag{A8.1}$$

The normal coordinate Q_4 is a linear function of the symmetry coordinates S_{3a} and S_{4a}[92], hereafter referred to as S_3 and S_4 (see Equations (1.63) and (1.64)) and thus it is easily shown that

$$\frac{\partial^2 V_N}{\partial Q_4^2} = \sum_{i=3}^{4}\sum_{j=3}^{4} \frac{\partial S_i}{\partial Q_4}\,\frac{\partial S_j}{\partial Q_4}\,\frac{\partial^2 V_N}{\partial S_i\,\partial S_j}\,, \tag{A8.2}$$

and

$$\frac{\partial^2 V_1}{\partial Q_4^2} = \sum_{i=3}^{4}\sum_{j=3}^{4} \frac{\partial S_i}{\partial Q_4}\,\frac{\partial S_j}{\partial Q_4}\,\frac{\partial^2 V_1}{\partial S_i\,\partial S_j}\,. \tag{A8.3}$$

Using Equations (A8.2) and (A8.3) in Equation (A8.1) one obtains

$$k_4 = \left(\frac{\partial S_3}{\partial Q_4}\right)^2 \left[\left.\frac{\partial^2 V_N}{\partial S_3^2}\right|_0 + \left.\int \frac{\partial^2 V_1}{\partial S_3^2}\,\rho(\vec{x}_1)\,d\tau_1\right|_0\right]$$

$$+ 2\left(\frac{\partial S_3}{\partial Q_4}\right)\left(\frac{\partial S_4}{\partial Q_4}\right)\left[\frac{\partial^2 V_N}{\partial S_3 \partial S_4}\Bigg|_0 + \int \frac{\partial^2 V_1}{\partial S_3 \partial S_4}\rho(\vec{x}_1)d\tau_1\Bigg|_0\right]$$

$$+ \left(\frac{\partial S_4}{\partial Q_4}\right)^2\left[\frac{\partial^2 V_N}{\partial S_4{}^2}\Bigg|_0 + \int \frac{\partial^2 V_1}{\partial S_4{}^2}\rho(\vec{x}_1)d\tau_1\Bigg|_0\right]$$

$$+ \int \frac{\partial V_1}{\partial Q_4}\frac{\partial \rho(\vec{x}_1)}{\partial Q_4}d\tau_1\Bigg|_0 . \qquad \text{(A8.4)}$$

Mills[92] has shown that the matrix transformation relating the normal coordinates Q_3 and Q_4 to the symmetry coordinates S_3 and S_4 is given by

$$\begin{pmatrix} Q_3 \\ Q_4 \end{pmatrix} = \begin{pmatrix} 0.9559 & -0.0211 \\ -0.0994 & 0.6474 \end{pmatrix}\begin{pmatrix} S_3 \\ S_4 \end{pmatrix} . \qquad \text{(A8.5)}$$

The inverse transformation is

$$\begin{pmatrix} S_3 \\ S_4 \end{pmatrix} = \begin{pmatrix} 1.04970 & 0.03421 \\ 0.16117 & 1.54990 \end{pmatrix}\begin{pmatrix} Q_3 \\ Q_4 \end{pmatrix} \qquad \text{(A8.6)}$$

From matrix Equation (A8.6) it can be easily shown that the constants $(\partial S_3/\partial Q_4)$ and $(\partial S_4/\partial Q_4)$, required in Equation (A8.4), are given by

$$\frac{\partial S_3}{\partial Q_4} = 0.16117 \ , \ \frac{\partial S_4}{\partial Q_4} = 1.54990 . \qquad \text{(A8.7)}$$

The remaining derivatives in Equation (A8.4), $(\partial^2 V_N/\partial S_3{}^2)$, $(\partial^2 V_1/\partial S_3{}^2)$, $(\partial^2 V_N/\partial S_3 \partial S_4)$, $(\partial^2 V_1/\partial S_3 \partial S_4)$, $(\partial^2 V_N/\partial S_4{}^2)$ and $(\partial^2 V_1/\partial S_4{}^2)$, can be simplified.

Since S_3 is a linear function of the internal coordinates r_i (see Equation (1.63)), it follows that

$$\frac{\partial^2 V_N}{\partial S_3{}^2} = \sum_{i=1}^{4}\sum_{j=1}^{4}\frac{\partial r_i}{\partial S_3}\frac{\partial r_j}{\partial S_3}\frac{\partial^2 V_N}{\partial r_i \partial r_j} . \qquad \text{(A8.8)}$$

Similar expressions can be obtained for all the other derivative in terms of the internal coordinates r_i and α_{ij}. If all displacements are assumed to be equivalent it is easily shown that

$$\frac{\partial r_1}{\partial S_3} = \frac{\partial r_4}{\partial S_3} = -\frac{\partial r_2}{\partial S_3} = -\frac{\partial r_3}{\partial S_3} = \frac{1}{2} \tag{A8.9}$$

and thus Equation (A8.8) becomes

$$\frac{\partial^2 V_N}{\partial S_3^2} = \frac{\partial^2 V_N}{\partial r_1^2} - \frac{\partial^2 V_N}{\partial r_1 \partial r_2} \tag{A8.10}$$

Similar expressions can be obtained for the other derivatives. These expressions are

$$\frac{\partial^2 V_1}{\partial S_3^2} = \sum_{i=1}^{4} \sum_{j=1}^{4} \frac{\partial r_i}{\partial S_3} \frac{\partial r_j}{\partial S_3} \frac{\partial^2 V_1}{\partial r_i \partial r_j} = \frac{\partial^2 V_1}{\partial r_1^2} - \frac{\partial^2 V_1}{\partial r_1 \partial r_2} . \tag{A8.11}$$

$$\frac{\partial^2 V_N}{\partial S_3 \partial S_4} = \sum_{i=1}^{4} \sum_{j=1}^{2} \frac{\partial r_i}{\partial S_3} \frac{\partial \alpha_j}{\partial S_4} \frac{\partial^2 V_N}{\partial r_i \partial \alpha_j}$$

$$= \frac{\sqrt{2}}{R} \frac{\partial^2 V_N}{\partial r_1 \partial \alpha_{23}} - \frac{\sqrt{2}}{R} \frac{\partial^2 V_1}{\partial r_2 \partial \alpha_{23}} . \tag{A8.12}$$

$$\frac{\partial^2 V_1}{\partial S_3 \partial S_4} = \sum_{i=1}^{4} \sum_{j=1}^{2} \frac{\partial r_i}{\partial S_3} \frac{\partial \alpha_j}{\partial S_4} \frac{\partial^2 V_1}{\partial r_i \partial \alpha_j}$$

$$= \frac{\sqrt{2}}{R} \frac{\partial^2 V_1}{\partial r_1 \partial \alpha_{23}} - \frac{\sqrt{2}}{R} \frac{\partial^2 V_1}{\partial r_2 \partial \alpha_{23}} . \tag{A8.13}$$

$$\frac{\partial^2 V_N}{\partial S_4^2} = \sum_{i=1}^{2} \sum_{j=1}^{2} \frac{\partial \alpha_i}{\partial S_4} \frac{\partial \alpha_j}{\partial S_4} \frac{\partial^2 V_N}{\partial \alpha_i \partial \alpha_j}$$

$$= \frac{1}{R^2} \frac{\partial^2 V_N}{\partial \alpha_{23}^2} - \frac{1}{R^2} \frac{\partial^2 V_N}{\partial \alpha_{23} \partial \alpha_{14}} . \tag{A8.14}$$

$$\frac{\partial^2 V_1}{\partial S_4^2} = \sum_{i=1}^{2} \sum_{j=1}^{2} \frac{\partial \alpha_i}{\partial S_4} \frac{\partial \alpha_j}{\partial S_4} \frac{\partial^2 V_1}{\partial \alpha_i \partial \alpha_j}$$

$$= \frac{1}{R^2} \frac{\partial^2 V_1}{\partial \alpha_{23}^2} - \frac{1}{R^2} \frac{\partial^2 V_1}{\partial \alpha_{23} \partial \alpha_{14}} . \tag{A8.15}$$

Using the potential energy functions V_N and V_1, defined by Equations

(I.70) and (I.71) respectively for the methane molecule, all the derivatives required in the above expressions have been worked out in detail[127]. The final expressions evaluated at the equilibrium configuration, for the different terms appearing in Equation (A8.4) are then given by

$$\left.\frac{\partial^2 V_N}{\partial S_3^2}\right|_0 = (48\sqrt{2} + \sqrt{3})/4\sqrt{2}\ R^3. \tag{A8.16}$$

$$\left.\int \frac{\partial^2 V_1}{\partial S_3^2}\rho(\vec{x}_1)d\tau_1\right|_0 = -\int \frac{(3\cos^2\theta_{H_1}-1)}{r_{H_1}^3}\rho(\vec{x}_1)d\tau_1 + \frac{4\pi}{3}\rho_o(H_1). \tag{A8.17}$$

$$\left.\frac{\partial^2 V_N}{\partial S_3 \partial S_4}\right|_0 = -\sqrt{3}/8\sqrt{2}\ R^3. \tag{A8.18}$$

$$\left.\int \frac{\partial^2 V_1}{\partial S_3 \partial S_4}\rho(\vec{x}_1)d\tau_1\right|_0 = \frac{1}{\sqrt{2}}\int \frac{(3\cos\theta_{H_1}\sin\theta_{H_1}\cos\phi)}{r_{H_1}^3}\rho(\vec{x}_1)d\tau_1 - \frac{1}{\sqrt{2}R}\int \frac{\sin\theta_{H_1}\cos\phi}{r_{H_1}^2}\rho(\vec{x}_1)d\tau_1 . \tag{A8.19}$$

$$\left.\frac{\partial^2 V_N}{\partial S_4^2}\right|_0 = 5\sqrt{3}/16\sqrt{2}\ R^3. \tag{A8.20}$$

$$\left.\int \frac{\partial^2 V_1}{\partial S_4^2}\rho(\vec{x}_1)d\tau_1\right|_0 = -\frac{1}{2}\int \frac{(3\sin^2\theta_{H_1}\cos^2\phi-1)}{r_{H_1}^3}\rho(\vec{x}_1)d\tau_1 - \frac{1}{2R}\int \frac{\cos\theta_{H_1}}{r_{H_1}^2}\rho(\vec{x}_1)d\tau_1 + \frac{2\pi}{3}\rho_o(H_1) . \tag{A8.21}$$

Substituting the expressions given in Equations (A8.16) to (A8.21) into Equation (A8.4) the theoretical contributions to the force constant k_4 can be determined. However, the field gradient integrals appearing in Equations (A8.19) and (A8.21) have not been evaluated and thus no numerical values have been tabulated in this thesis. The theoretical expressions,

having been worked out, are given in this appendix for future reference. If all these expressions from (A8.16) to (A8.21) were evaluated for the derived one-electron density distribution for methane and if the experimental force constant for this T_2 mode was obtained then the theoretical contributions to the force constant for this infra-red active mode could be determined in the same manner as was done in this thesis (see page 77) for the breathing mode force constant.

APPENDIX 9

Equations and Integrals Used in Kinetic Energy Determinations

The orbitals of interest in this section are Slater-type orbitals defined as

$$\chi(n,\ell,m) = (2\alpha)^{n+1/2}[(2n)!]^{-1/2} r^{n-1} e^{-\alpha r} S_{\ell,m}(\theta,\phi) \tag{A9.1}$$

where $S_{\ell,m}(\theta,\phi)$ are the normalized real spherical harmonics given by

$$S_{\ell,o}(\theta,\phi) = \left[\frac{(2\ell+1)}{4\pi}\right]^{1/2} P_\ell^o(\cos\theta) \tag{A9.2}$$

$$S_{\ell,|m|}(\theta,\phi) = \left[\frac{2\ell+1}{2\pi} \cdot \frac{(\ell-|m|)!}{(\ell+|m|)!}\right]^{1/2} P_\ell^{|m|}(\cos\theta) \cos|m|\phi \tag{A9.3}$$

$$S_{\ell,-|m|}(\theta,\phi) = \left[\frac{2\ell+1}{2\pi} \cdot \frac{(\ell-|m|)!}{(\ell+|m|)!}\right]^{1/2} P_\ell^{|m|}(\cos\theta) \sin|m|\phi \tag{A9.4}$$

and the $P_\ell^{|m|}(\cos\theta)$ are the associated Legendre polynomials. In this appendix expressions are given for the operation of the operators ∇^2 and ∇_z^2 on the Slater orbitals χ_i where

$$\nabla^2 = -\frac{1}{2}\left(\frac{\partial^2}{\partial x_a^2} + \frac{\partial^2}{\partial y_a^2} + \frac{\partial^2}{\partial z_a^2}\right) \tag{A9.5}$$

and

$$\nabla_z^2 = -\frac{1}{2}\frac{\partial^2}{\partial z_a^2} . \tag{A9.6}$$

Also expressions for the expectation values $\langle\chi_i|\nabla_z^2|\chi_j\rangle$, which were used to

calculate the parallel component to the kinetic energy in a diatomic system, are listed. Using this component and the total $\overline{T}$, the perpendicular component is obtained.

It is easily shown[128] that

$$\nabla^2\chi(n,\ell,m)_a = -\frac{\alpha^2}{2}\frac{(2\alpha)^{n+1/2}}{(2n!)^{1/2}}\left[r_a^{n-1} - \frac{2nr_a^{n-2}}{\alpha} + \frac{(n+\ell)(n-\ell+1)}{\alpha^2}r_a^{n-3}\right] e^{-\alpha r_a} S_{\ell,m}(\theta_a,\phi) \quad . \tag{A9.7}$$

Using this equation the operation of ∇^2 on the Slater orbitals gives

$$\nabla^2|1s\rangle = -\frac{\alpha^{7/2}}{2\sqrt{\pi}}\left[1 - 2/(\alpha r_a)\right] e^{-\alpha r_a} \tag{A9.8}$$

$$\nabla^2|2s\rangle = -\frac{\alpha^{9/2}}{2\sqrt{3\pi}}\left[r_a - 4/\alpha + 2/(\alpha^2 r_a)\right] e^{-\alpha r_a} \tag{A9.9}$$

$$\nabla^2|2p\sigma\rangle = -\frac{\alpha^{9/2}}{2\sqrt{\pi}}\left[r_a - 4/\alpha\right] \cos\theta_a e^{-\alpha r_a} \tag{A9.10}$$

$$\nabla^2|2p\pi\rangle = -\frac{\alpha^{9/2}}{2\sqrt{\pi}}\left[r_a - 4/\alpha\right] \sin\theta_a\cos\phi\ e^{-\alpha r_a} \tag{A9.11}$$

$$\nabla^2|3s\rangle = -\frac{\alpha^{11/2}\sqrt{2}}{6\sqrt{5\pi}}\left[r_a^2 - 6r_a/\alpha + 6/\alpha^2\right] e^{-\alpha r_a} \tag{A9.12}$$

$$\nabla^2|3p\sigma\rangle = -\frac{\alpha^{11/2}\sqrt{2}}{2\sqrt{15\pi}}\left[r_a^2 - 6r_a/\alpha + 4/\alpha^2\right] \cos\theta_a\ e^{-\alpha r_a} \tag{A9.13}$$

$$\nabla^2|3p\pi\rangle = -\frac{\alpha^{11/2}\sqrt{2}}{2\sqrt{15\pi}}\left[r_a^2 - 6r_a/\alpha + 4/\alpha^2\right] \sin\theta_a\cos\phi\ e^{-\alpha r_a} \tag{A9.14}$$

$$\nabla^2|3d\sigma\rangle = -\frac{\alpha^{11/2}}{2\sqrt{18\pi}}\left[r_a^2 - 6r_a/\alpha\right](3\cos^2\theta_a - 1)\ e^{-\alpha r_a} \tag{A9.15}$$

$$\nabla^2|3d\pi\rangle = -\frac{\alpha^{11/2}\sqrt{2}}{2\sqrt{3\pi}}\left[r_a^2 - 6r_a/\alpha\right] \sin\theta_a\cos\theta_a\cos\phi\ e^{-\alpha r_a} \tag{A9.16}$$

$$\nabla^2|4f\sigma\rangle = -\frac{\alpha^{13/2}}{2\sqrt{180\pi}}[r_a^3 - 8r_a^2/\alpha](5\cos^3\theta_a - 3\cos\theta_a)\, e^{-\alpha r_a} \qquad (A9.17)$$

$$\nabla^2|4f\pi\rangle = -\frac{\alpha^{13/2}}{2\sqrt{120\pi}}[r_a^3 - 8r_a^2/\alpha]\sin\theta_a(5\cos^2\theta_a - 1)\cos\phi\, e^{-\alpha r_a}. \qquad (A9.18)$$

The Expressions (A9.8) - (A9.18) were used to evaluate the contributions $\chi_i(\vec{x})\nabla^2\chi_j(\vec{x})$ to the function $L(\vec{x}_i)$ given in the thesis. These expressions could also be used to calculate the kinetic energy integrals $\langle\chi_i|\nabla^2|\chi_j\rangle$ but in the present work QCPE[81] program #29 was used to evaluate these one- and two-center integrals.

Considering the operator ∇_z^2 it can be shown that

$$\begin{aligned}\nabla_z^2\chi(n,\ell,m)_a &= -\frac{1}{2}\frac{\partial^2}{\partial z_a^2}(n,\ell,m)_a \\ &= -\frac{1}{2}\frac{(2\alpha)^{n+1/2}}{(2n!)^{1/2}}[(\{n-1\}(1 + \{n-3\}\cos^2\theta_a)r_a^{n-3} \\ &\quad - \alpha(1 + \{2n-3\}\cos^2\theta_a)\, r_a^{n-2} + \alpha^2\cos^2\theta_a r_a^{n-1})e^{-\alpha r_a}S_{\ell,m}(\theta_a,\phi) \\ &\quad + 2\cos\theta_a(\{n-1\}\, r_a^{n-2} - \alpha r_a^{n-1})\, e^{-\alpha r_a}\frac{\partial}{\partial z_a}S_{\ell,m}(\theta_a,\phi) \\ &\quad + r_a^{n-1}\, e^{-\alpha r_a}\frac{\partial^2}{\partial z_a^2}S_{\ell,m}(\theta_a,\phi)]\,. \end{aligned} \qquad (A9.19)$$

Using this equation the following expressions are obtained for the operation of ∇_z^2 on the Slater orbitals.

$$\nabla_z^2|1s\rangle = -\frac{\alpha^{3/2}}{2\sqrt{\pi}}[\alpha^2\cos^2\theta_a - \alpha(1 - \cos^2\theta_a)/r_a]e^{-\alpha r_a} \qquad (A9.20)$$

$$\nabla_z^2|2s\rangle = -\frac{\alpha^{5/2}}{2\sqrt{3\pi}}[\alpha^2\cos^2\theta_a r_a - \alpha(1 + \cos^2\theta_a) + (1 - \cos^2\theta_a)/r_a]e^{-\alpha r_a} \qquad (A9.21)$$

$$\nabla_z^2|2p\sigma\rangle = -\frac{\alpha^{5/2}}{2\sqrt{\pi}}[\alpha^2\cos^2\theta_a r_a - \alpha(3-\cos^2\theta_a)]\cos\theta_a e^{-\alpha r_a} \quad \text{(A9.22)}$$

$$\nabla_z^2|2p\pi\rangle = -\frac{\alpha^{5/2}}{2\sqrt{\pi}}[\alpha^2\cos^2\theta_a r_a - \alpha(1-\cos^2\theta_a)] \sin\theta_a\cos\phi e^{-\alpha r_a} \quad \text{(A9.23)}$$

$$\nabla_z^2|3s\rangle = -\frac{\alpha^{7/2}\sqrt{2}}{2\sqrt{45\pi}}[\alpha^2\cos^2\theta_a r_a^2 - \alpha(1+3\cos^2\theta_a)r_a + 2]e^{-\alpha r_a} \quad \text{(A9.24)}$$

$$\nabla_z^2|3p\sigma\rangle = -\frac{\alpha^{7/2}\sqrt{2}}{2\sqrt{15\pi}}[\alpha^2\cos^2\theta_a r_a^2 - \alpha(3+\cos^2\theta_a)r_a + (3-\cos^2\theta_a)]\cos\theta_a e^{-\alpha r_a} \quad \text{(A9.25)}$$

$$\nabla_z^2|3p\pi\rangle = -\frac{\alpha^{7/2}\sqrt{2}}{2\sqrt{15\pi}}[\alpha^2\cos^2\theta_a r_a^2 - \alpha(1+\cos^2\theta_a)r_a + (1-\cos^2\theta_a)]\sin\theta_a\cos\phi e^{-\alpha r_a} \quad \text{(A9.26)}$$

$$\nabla_z^2|3d\sigma\rangle = -\frac{\alpha^{7/2}}{6\sqrt{2\pi}}\left[\alpha^2\cos^2\theta_a r_a^2 - \frac{\alpha(-3\cos^4\theta_a + 12\cos^2\theta_a - 1)r_a + 4}{(3\cos^2\theta_a - 1)}\right] (3\cos^2\theta_a - 1)e^{-\alpha r_a} \quad \text{(A9.27)}$$

$$\nabla_z^2|3d\pi\rangle = -\frac{\alpha^{7/2}\sqrt{2}}{2\sqrt{3\pi}}[\alpha^2\cos^2\theta_a r_a^2 - \alpha(3-\cos^2\theta_a)r_a] \sin\theta_a\cos\theta_a\cos\phi e^{-\alpha r_a} \quad \text{(A9.28)}$$

$$\nabla_z^2|4f\sigma\rangle = -\frac{\alpha^{9/2}}{2\sqrt{180\pi}}\left[\alpha^2\cos^2\theta_a r_a^3 + \frac{\alpha\cos\theta_a(5\cos^4\theta_a - 26\cos^2\theta_a + 9)r_a^2 + 12\cos\theta_a r_a}{(5\cos^3\theta_a - 3\cos\theta_a)}\right] (5\cos^3\theta_a - 3\cos\theta_a)e^{-\alpha r_a} \quad \text{(A9.29)}$$

$$\nabla_z^2|4f\pi\rangle = -\frac{\alpha^{9/2}}{2\sqrt{120\pi}}\left[\alpha^2\cos^2\theta_a r_a^3 + \frac{\alpha(5\cos^4\theta_a - 22\cos^2\theta_a + 1)r_a^2 + 8r_a}{(5\cos^2\theta_a - 1)}\right]$$

$$\sin\theta_a(5\cos^2\theta_a - 1)\cos\phi e^{-\alpha r_a} \qquad \text{(A9.30)}$$

The Expressions (A9.20) - (A9.30) were used to evaluate the integrals $\langle\chi_i|\nabla_z^2|\chi_j\rangle$. If χ_i has a screening coefficient Z_1 and χ_j has a screening coefficient Z_2 then the non-zero elements can be given by the following expressions. The one-center or atomic integrals, represented as $\langle\chi_a|\nabla_z^2|\chi_a'\rangle_1$, are

$$\langle 1s|\nabla_z^2|1s\rangle_1 = \frac{4Z_1^{5/2}Z_2^{5/2}}{3(Z_1+Z_2)^3}$$

$$\langle 2s|\nabla_z^2|1s\rangle_1 = \frac{4Z_1^{5/2}Z_2^{5/2}}{3\sqrt{3}(Z_1+Z_2)^4}(2Z_1 - Z_2)$$

$$\langle 2s|\nabla_z^2|2s\rangle_1 = \frac{8Z_1^{5/2}Z_2^{5/2}}{9(Z_1+Z_2)^5}(-Z_1^2 + 4Z_1Z_2 - Z_2^2)$$

$$\langle 2p\sigma|\nabla_z^2|2p\sigma\rangle_1 = \frac{48Z_1^{7/2}Z_2^{7/2}}{5(Z_1+Z_2)^5}$$

$$\langle 2p\pi|\nabla_z^2|2p\pi\rangle_1 = \frac{16Z_1^{7/2}Z_2^{7/2}}{5(Z_1+Z_2)^5}$$

$$\langle 3s|\nabla_z^2|1s\rangle_1 = \frac{8\sqrt{2}\,Z_1^{7/2}Z_2^{5/2}}{3\sqrt{5}\,(Z_1+Z_2)^5}(Z_1 - Z_2)$$

$$\langle 3s|\nabla_z^2|2s\rangle_1 = \frac{8\sqrt{2}\,Z_1^{7/2}Z_2^{5/2}}{3\sqrt{15}\,(Z_1+Z_2)^6}(-Z_1^2 + 6Z_1Z_2 - 3Z_2^2)$$

$$\langle 3s|\nabla_z^2|3s\rangle_1 = \frac{64Z_1^{7/2}Z_2^{7/2}}{15(Z_1+Z_2)^7}(-Z_1^2 + 3Z_1Z_2 - Z_2^2)$$

$$\langle 3d\sigma|\nabla_z^2|1s\rangle_1 = -\frac{16Z_1^{7/2}Z_2^{5/2}}{15\sqrt{2}\,(Z_1+Z_2)^5}(Z_1 + 5Z_2)$$

$$\langle 3d\sigma|\nabla_z^2|2s\rangle_1 = \frac{16Z_1^{7/2}Z_2^{5/2}}{15\sqrt{6}\,(Z_1+Z_2)^6}(Z_1 + 6Z_1Z_2 - 15Z_2^2)$$

$$\langle 3d\sigma|\nabla_z^2|3s\rangle_1 = \frac{64Z_1^{7/2}Z_2^{9/2}}{\sqrt{45}\,(Z_1+Z_2)^7}(Z_1 - Z_2)$$

$$\langle 3d\sigma|\nabla_z^2|3d\sigma\rangle_1 = \frac{704Z_1^{9/2}Z_2^{9/2}}{21(Z_1+Z_2)^7}$$

$$\langle 3d\pi|\nabla_z^2|3d\pi\rangle_1 = \frac{192Z_1^{9/2}Z_2^{9/2}}{7(Z_1+Z_2)^7}$$

$$\langle 4f\sigma|\nabla_z^2|2p\sigma\rangle_1 = -\frac{32Z_1^{9/2}Z_2^{7/2}}{7\sqrt{5}\,(Z_1+Z_2)^7}(Z_1 + 7Z_2)$$

$$\langle 4f\sigma|\nabla_z^2|4f\sigma\rangle_1 = \frac{5888\,Z_1^{11/2}Z_2^{11/2}}{45(Z_1+Z_2)^9}$$

$$\langle 4f\pi|\nabla_z^2|2p\pi\rangle_1 = -\frac{64Z_1^{9/2}Z_2^{7/2}}{7\sqrt{30}\,(Z_1+Z_2)^7}(Z_1 + 7Z_2)$$

$$\langle 4f\pi|\nabla_z^2|4f\pi\rangle_1 = \frac{1792Z_1^{11/2}Z_2^{11/2}}{15(Z_1+Z_2)^9}\,.$$

In the above list the integrals involving the $3p\sigma$ and $3p\pi$ orbitals have been omitted since they were not required for the calculations carried out in this thesis. Because of the hermitian properties of the operator ∇_z^2 it must be noted, for example, that the integral $\langle 3d\sigma|\nabla_z^2|1s\rangle_1$ is equal to the integral $\langle 1s|\nabla_z^2|3d\sigma\rangle_1$. This property was used to verify the expressions listed above and can be used to obtain the integrals of this form that are not listed.

Since the operator ∇_z^2 defined on center A in a diatomic system as shown in Figure A3.1 can be equally well-represented by the operator ∇_z^2 defined on center B the screening-type two-center integrals are easily reduced to the atomic integrals already listed above. The overlap-type integrals, defined as $\langle\chi_b|\nabla_z^2|\chi_a\rangle_2$ where χ_b has a screening coefficient Z_1

and χ_a has a screening coefficient Z_2, have the following expressions where again integrals involving $3p\sigma$ and $3p\pi$ orbitals have been omitted.

$$\langle 1s|\nabla_z^2|1s\rangle_2 = -\frac{Z_1^{3/2}Z_2^{5/2}R^2}{4}[F_{112}+F_{101}-F_{110}-F_{103}+\frac{Z_2R}{2}(F_{010}+F_{032}+2(F_{021}-F_{012})-F_{001}-F_{023})]$$

$$\langle 2s|\nabla_z^2|1s\rangle_2 = -\frac{Z_1^{5/2}Z_2^{5/2}R^3}{8\sqrt{3}}[F_{122}+F_{104}-F_{120}-F_{102}+2(F_{111}-F_{113})+\frac{Z_2R}{2}(F_{020}+F_{002}+F_{042}+F_{024}+2(F_{031}+F_{013}-F_{011}-F_{033})-4F_{022})]$$

$$\langle 2s|\nabla_z^2|2s\rangle_2 = -\frac{Z_1^{5/2}Z_2^{5/2}R^3}{24}[F_{120}+F_{102}-F_{122}-F_{104}+2(F_{113}-F_{111})-\frac{Z_2R}{2}(F_{040}+F_{020}+F_{042}+F_{004}+F_{002}+F_{024}+2(F_{031}+F_{013}-F_{011}-F_{033})-6F_{022})+\frac{Z_2^2R^2}{4}(A_2B_0+A_4B_2+A_0B_2+A_2B_4+2(A_3B_1+A_1B_3-A_1B_1-A_3B_3)-4A_2B_2)]$$

$$\langle 2p\sigma|\nabla_z^2|1s\rangle_2 = -\frac{Z_1^{5/2}Z_2^{5/2}R^3}{8}[F_{121}+F_{114}+F_{101}-F_{110}-F_{103}-F_{123}+\frac{Z_2R}{2}(F_{010}+F_{021}+F_{023}+F_{034}-F_{001}-F_{012}-F_{032}-F_{043})]$$

$$\langle 2p\sigma|\nabla_z^2|2s\rangle_2 = -\frac{Z_1^{5/2}Z_2^{5/2}R^3}{8\sqrt{3}}[F_{110}+F_{103}+F_{123}-F_{101}-F_{121}-F_{114}-\frac{Z_2R}{2}(F_{030}+F_{010}+F_{014}+F_{034}-F_{003}-F_{001}-F_{041}-F_{043}+2(F_{021}+F_{023}-F_{012}-F_{032}))+\frac{Z_2^2R^2}{4}(A_1B_0+A_2B_1+A_2B_3+A_3B_4-A_0B_1-A_1B_2-A_3B_2-A_4B_3)]$$

$$\langle 2p\sigma|\nabla_z^2|2p\sigma\rangle_2 = -\frac{Z_1^{5/2}Z_2^{7/2}R^4}{16}[F_{112}+F_{101}+F_{132}+F_{125}$$

$$- F_{110} - F_{103} - F_{123} - F_{134}$$

$$- 2(A_1B_0 + A_2B_3 - A_0B_1 - A_3B_2)$$

$$+ \frac{Z_2R}{2}(F_{010} + F_{045} - F_{001} - F_{054} + 2(F_{021} + F_{034} - F_{012} - F_{043}))]$$

$$\langle 2p\pi|\nabla_z^2|2p\pi\rangle_2 = -\frac{Z_1^{5/2}Z_2^{7/2}R^4}{32}[F_{121} + F_{125} + F_{110} + F_{114} - F_{130}$$

$$- F_{134} - F_{101} - F_{105}$$

$$+ 2(F_{132} + F_{103} - F_{123} - F_{112})$$

$$+ \frac{Z_2R}{2}(F_{030} + F_{052} + F_{045} + F_{001} - F_{003} - F_{025} - F_{054} - F_{010}$$

$$+ 2(F_{041} - F_{014}) + 3(F_{034} + F_{012} - F_{043} - F_{021})$$

$$+ 4(F_{023} - F_{032}))]$$

$$\langle 3s|\nabla_z^2|1s\rangle_2 = -\frac{\sqrt{2}\,Z_1^{7/2}Z_2^{5/2}R^4}{48\sqrt{5}}[F_{132} + F_{103} - F_{130} - F_{105}$$

$$+ 3(F_{121} + F_{114} - F_{123} - F_{112})$$

$$+ \frac{Z_2R}{2}(F_{030} + F_{052} - F_{003} - F_{025} + 2(F_{041} - F_{014})$$

$$+ 3(F_{012} + F_{034} - F_{021} - F_{043}) + 6(F_{023} - F_{032}))]$$

$$\langle 3s|\nabla_z^2|2s\rangle_2 = -\frac{\sqrt{2}\,Z_1^{7/2}Z_2^{5/2}R^4}{48\sqrt{15}}[F_{130} + F_{105} - F_{132} - F_{103}$$

$$+ 3(F_{123} + F_{112} - F_{121} - F_{114})$$

$$- \frac{Z_2R}{2}(F_{050} + F_{041} + F_{030} + F_{052} - F_{005} - F_{014} - F_{003} - F_{025}$$

$$+ 3(F_{012} + F_{034} - F_{021} - F_{043}) + 8(F_{023} - F_{032}))$$

$$+ \frac{Z^2R^2}{4}(A_3B_0 + A_5B_2 - A_0B_3 - A_2B_5 + 2(A_4B_1 - A_1B_4)$$

$$+ 3(A_1B_2 + A_3B_4 - A_2B_1 - A_4B_3) + 6(A_2B_3 - A_3B_2))]$$

$$\langle 3s|\nabla_z^2|2p\sigma\rangle_2 = -\frac{\sqrt{2}\,Z_1^{7/2}Z_2^{7/2}R^5}{96\sqrt{5}}[F_{143} + F_{103} - F_{130} - F_{141} - F_{105} - F_{116}$$

$$+ 3(F_{121} + F_{125} - F_{112} - F_{134})$$

$$+ 4(F_{114} + F_{132}) - 6F_{123}$$

$$- 2(A_3B_0 + A_4B_1 - A_0B_3 - A_1B_4 + 3(A_1B_2 + A_2B_3 - A_2B_1 - A_3B_2))$$

$$+\frac{Z_1R}{2}(F_{030}+F_{063}-F_{003}-F_{036}+3(F_{041}+F_{052}+F_{012}+F_{045}-F_{014}-F_{025}-F_{021}-F_{054})+9(F_{023}+F_{034}-F_{032}-F_{043}))]$$

$$\langle 3s|\nabla_z^2|3s\rangle_2 = -\frac{Z_1^{7/2}Z_2^{7/2}R^5}{720}[2(A_4B_0+2A_1B_3-A_0B_4-2A_3B_1)-\frac{Z_2R}{2}(F_{060}-F_{006}+3(F_{040}+F_{062}-F_{004}-F_{026})+6(F_{051}+F_{013}+F_{035}-F_{015}-F_{031}-F_{053})+15(F_{024}-F_{042}))+\frac{Z_2^2R^2}{4}(A_4B_0+A_6B_2-A_0B_4-A_2B_6+2(A_5B_1+A_1B_3+A_3B_5-A_1B_5-A_3B_1-A_5B_3)+4(A_2B_4-A_4B_2))]$$

$$\langle 3d\sigma|\nabla_z^2|1s\rangle_2 = -\frac{Z_1^{7/2}Z_2^{5/2}R^4}{48\sqrt{2}}[F_{130}+F_{105}+3(F_{101}+F_{121}+F_{114}+F_{034}-F_{110}-F_{125})-4(F_{103}+F_{132})+\frac{Z_2R}{2}(F_{003}+F_{025}-F_{030}-F_{052}+2(F_{014}-F_{041})+3(F_{010}+F_{021}+F_{043}+F_{054}-F_{001}-F_{012}-F_{034}-F_{045}))]$$

$$\langle 3d\sigma|\nabla_z^2|2s\rangle_2 = -\frac{Z_1^{7/2}Z_2^{5/2}R^4}{48\sqrt{6}}[-F_{130}-F_{105}+3(F_{110}+F_{125}-F_{101}-F_{121}-F_{114}-F_{134})+4(F_{103}+F_{132})-\frac{Z_2R}{2}(F_{005}-F_{050}+2(F_{030}+F_{052}-F_{003}-F_{025})+3(F_{010}+F_{054}-F_{001}-F_{045})+4(F_{023}-F_{032})+6(F_{021}+F_{043}-F_{012}-F_{034})+7(F_{014}-F_{041}))+\frac{Z^2R^2}{4}(A_0B_3+A_2B_5-A_3B_0-A_5B_2+2(A_1B_4-A_4B_1)+3(A_1B_0+A_2B_1+A_4B_3+A_5B_4-A_0B_1-A_1B_2-A_3B_4-A_4B_5))]$$

$$\langle 3d\sigma|\nabla_z^2|2p\sigma\rangle_2 = -\frac{Z_1^{7/2}Z_2^{7/2}R^5}{96\sqrt{2}}[F_{130}+F_{141}+F_{105}+F_{116}-F_{132}-F_{114}$$

$$+ 3(F_{112} + F_{101} + F_{145} + F_{134} - F_{110} - F_{136})$$

$$- 4(F_{103} + F_{143}) - 2(A_0B_3 + A_1B_4 - A_3B_0 - A_4B_1$$

$$+ 3(A_1B_0 + A_4B_3 - A_0B_1 - A_3B_4))$$

$$+ \frac{Z_1R}{2}(F_{003} + F_{036} - F_{030} - F_{063} + 3(F_{010} + F_{065} + F_{032}$$

$$+ F_{043} + F_{014} + F_{025} - F_{001} - F_{056}$$

$$- F_{023} - F_{034} - F_{041} - F_{052})$$

$$+ 6(F_{021} + F_{054} - F_{012} - F_{045}))]$$

$$\langle 3d\sigma|\nabla_z^2|3s\rangle_2 = -\frac{Z_1^{7/2}Z_2^{7/2}R^5}{288\sqrt{5}}[2(A_0B_4 - A_4B_0 + 3(A_2B_0 + A_4B_2 - A_0B_2 - A_2B_4)$$

$$+ 4(A_1B_3 - A_3B_1))$$

$$-\frac{Z_2R}{2}(F_{006} - F_{060} + 9(F_{020} + F_{064} - F_{002} - F_{046})$$

$$+ 12(F_{031} + F_{053} + F_{015} - F_{013} - F_{035} - F_{051})$$

$$+ 15(F_{024} - F_{042}))$$

$$+ \frac{Z_2^2R^2}{4}(A_0B_4 + A_2B_6 - A_4B_0 - A_6B_2 + 2(A_3B_1 + A_2B_4 + A_5B_3$$

$$+ A_1B_5 - A_1B_3 - A_4B_2 - A_3B_5 - A_5B_1)$$

$$+ 3(A_2B_0 + A_6B_4 - A_0B_2 - A_4B_6))]$$

$$\langle 3d\sigma|\nabla_z^2|3d\sigma\rangle_2 = -\frac{Z_1^{7/2}Z_2^{7/2}R^5}{576}[\frac{Z_2R}{2}(F_{116} + F_{141} - F_{107} - F_{150}$$

$$+ 6(F_{130} + F_{127} - F_{121} - F_{136}) + 7(F_{152} + F_{105} - F_{114} - F_{143})$$

$$+ 9(F_{101} + F_{156} - F_{110} - F_{147}) + 10(F_{123} + F_{134} - F_{132} - F_{125})$$

$$+ 15(F_{112} + F_{145} - F_{103} - F_{154}))$$

$$+ \frac{Z^2R^2}{4}(F_{072} + F_{050} - F_{027} - F_{005} + 2(F_{061} - F_{016})$$

$$+ 6(F_{003} + F_{047} - F_{030} - F_{074}) + 9(F_{010} + F_{076} - F_{001} - F_{067})$$

$$+ 13(F_{014} + F_{036} - F_{041} - F_{063}) + 14(F_{025} - F_{052})$$

$$+ 20(F_{043} - F_{034}) + 24(F_{021} + F_{065} - F_{012} - F_{056})$$

$$+ 25(F_{032} + F_{054} - F_{023} - F_{045}))$$

$$- 4Z_2R(A_0B_3 + A_2B_5 - A_3B_0 - A_5B_2 + 2(A_1B_4 - A_4B_1)$$

$$+ 3(A_1B_0 + A_2B_1 + A_4B_3 + A_5B_4 - A_0B_1 - A_1B_2 - A_3B_4 - A_4B_5))$$

$$+ 4(A_0B_4 - A_4B_0 + 3(A_2B_0 + A_4B_2 - A_0B_2 - A_2B_4)$$

$$+ 4(A_1B_3 - A_3B_1))]$$

$$\langle 3d\pi|\nabla_z^2|2p\pi\rangle_2 = -\frac{Z_1^{7/2}Z_2^{7/2}R^5}{32\sqrt{6}}[F_{132} + F_{110} + F_{141} + F_{134} + F_{145} + F_{116}$$

$$- F_{130} - F_{112} - F_{101} - F_{105} - F_{136} - F_{114}$$

$$+ 2(F_{103} - F_{143})$$

$$+ \frac{Z_2R}{2}(F_{030} + F_{041} + F_{001} + F_{023} + F_{043} + F_{065} + F_{025} + F_{036}$$

$$- F_{003} - F_{014} - F_{010} - F_{032} - F_{034} - F_{056} - F_{052} - F_{063}$$

$$+ 2(F_{012} + F_{054} - F_{021} - F_{045}))]$$

$$\langle 3d\pi|\nabla_z^2|3d\pi\rangle_2 = -\frac{Z_1^{7/2}Z_2^{9/2}R^6}{192}[F_{110} + F_{114} + F_{132} + F_{121} + F_{134} + F_{156}$$

$$+ F_{127} + F_{152} - F_{105} - F_{130} - F_{123} - F_{101}$$

$$- F_{125} - F_{136} - F_{147} - F_{143}$$

$$+ 2(F_{103} + F_{145} - F_{112} - F_{154})$$

$$- 2(A_3B_0 + A_1B_2 + A_0B_1 + A_4B_3 + A_5B_4 + A_2B_5 - A_0B_3 - A_2B_1$$

$$- A_1B_0 - A_3B_4 - A_4B_5 - A_5B_2)$$

$$+ \frac{Z_2R}{2}(F_{030} + F_{001} + F_{076} + F_{047} - F_{003} - F_{010} - F_{067} - F_{074}$$

$$+ 2(F_{041} + F_{036} - F_{014} - F_{063})$$

$$+ 3(F_{012} + F_{023} + F_{054} + F_{065} - F_{021} - F_{032} - F_{045} - F_{056}))]$$

$$\langle 4f\sigma|\nabla_z^2|1s\rangle_2 = -\frac{Z_2^{9/2}Z_2^{5/2}R^5}{192\sqrt{5}}[F_{134} - F_{112} + 3(F_{130} + F_{105} - F_{141} - F_{126})$$

$$+ 5(F_{136} + F_{101} - F_{110} - F_{145})$$

$$+ 6(F_{121} - F_{125}) + 8(F_{143} - F_{103}) + 9(F_{114} - F_{132})$$

$$+\frac{Z_2R}{2}(F_{043}+F_{023}-F_{034}-F_{032}+3(F_{052}+F_{063}+F_{003}+F_{014}-F_{025}-F_{036}-F_{030}-F_{041})+4(F_{045}+F_{021}-F_{054}-F_{012})+5(F_{010}+F_{056}-F_{001}-F_{065}))]$$

$$\langle 4f\sigma|\nabla_z^2|2s\rangle_2 = -\frac{Z_1^{9/2}Z_2^{5/2}R^5}{192\ 15}[F_{112}-F_{134}+3(F_{141}+F_{116}-F_{130}-F_{105})+5(F_{110}+F_{145}-F_{101}-F_{136})+6(F_{125}-F_{121})+8(F_{103}-F_{143})+9(F_{132}-F_{114})$$
$$+\frac{Z_2R}{2}(2(F_{030}+F_{036}-F_{003}-F_{063})+3(F_{061}+F_{005}-F_{016}-F_{050})+5(F_{010}+F_{056}-F_{001}-F_{065})+9(F_{021}+F_{045}-F_{012}-F_{054})+10(F_{043}+F_{023}-F_{034}-F_{032})+15(F_{052}+F_{014}-F_{041}-F_{025}))$$
$$+\frac{Z_2^2R^2}{4}(A_2B_3+A_4B_3-A_3B_2-A_3B_4+3(A_5B_2+A_6B_3+A_0B_3+A_1B_4-A_2B_5-A_3B_6-A_3B_0-A_4B_1)+4(A_4B_5+A_2B_1-A_5B_4-A_1B_2)+5(A_1B_0+A_5B_6-A_0B_1-A_6B_5))]$$

$$\langle 4f\sigma|\nabla_z^2|2p\sigma\rangle_2 = -\frac{Z_1^{9/2}Z_2^{7/2}R^6}{384\sqrt{5}}[F_{134}+F_{121}+F_{114}-F_{123}-F_{143}-F_{136}+3(F_{125}+F_{130}+F_{105}-F_{132}-F_{152}-F_{127})+4(F_{112}-F_{145})+5(F_{101}+F_{147}-F_{110}-F_{156})+8(F_{154}-F_{103})-2(A_4B_3+A_1B_2-A_3B_4-A_2B_1+3(A_5B_2+A_0B_3-A_2B_5-A_3B_0)+5(A_1B_0+A_4B_5-A_0B_1-A_5B_4)$$
$$+\frac{Z_2R}{2}(3(F_{032}+F_{003}+F_{074}+F_{045}-F_{023}-F_{030}-F_{047}-F_{054})+5(F_{010}+F_{067}-F_{001}-F_{076})+6(F_{014}+F_{063}-F_{041}-F_{036})+9(F_{021}+F_{056}-F_{012}-F_{065}))]$$

$$\langle 4f\sigma|\nabla_z^2|3s\rangle_2 = -\frac{\sqrt{2}\ Z_1^{9/2}Z_2^{7/2}R^6}{5760}[2(3(A_5B_1+A_0B_4-A_1B_5-A_4B_0)$$

$$+ 5(A_2B_0 + A_3B_5 - A_0B_2 - A_5B_3) + 9(A_4B_2 + A_1B_3 - A_2B_4 - A_3B_1))$$
$$- \frac{Z_2R}{2}(3(F_{071} + F_{006} - F_{017} - F_{060})$$
$$+ 4(F_{004} + F_{073} - F_{040} - F_{037})$$
$$+ 13(F_{031} + F_{046} - F_{013} - F_{064}) + 15(F_{020} + F_{057} - F_{002} - F_{075})$$
$$+ 24(F_{062} + F_{015} - F_{026} - F_{051}) + 33(F_{053} + F_{024} - F_{035} - F_{042}))$$
$$+ \frac{Z_2^2R^2}{4}(A_3B_1 + A_4B_6 - A_1B_3 - A_6B_4 + 3(A_6B_2 + A_7B_3 + A_0B_4 + A_1B_5$$
$$- A_2B_6 - A_3B_7 - A_4B_0 - A_5B_1) + 4(A_5B_3 + A_2B_4 - A_3B_5 - A_4B_2)$$
$$+ 5(A_2B_0 + A_5B_7 - A_0B_2 - A_7B_5))]$$

$$\langle 4f\sigma|\nabla_z^2|3d\sigma\rangle_2 = -\frac{Z_1^{9/2}Z_2^{7/2}R^6}{1152\sqrt{10}}\left[\frac{Z_2R}{2}(3(F_{127} + F_{118} + F_{161} - F_{150} - F_{141} - F_{107})\right.$$
$$+ 4(F_{154} - F_{114}) + 6(F_{152} - F_{116})$$
$$+ 7(F_{147} - F_{121}) + 9(F_{143} - F_{125}) + 13(F_{123} - F_{145})$$
$$+ 14(F_{130} - F_{138}) + 15(F_{101} + F_{158} - F_{110} - F_{167})$$
$$+ 17(F_{105} - F_{163}) + 20(F_{136} - F_{132}) + 22(F_{112} - F_{156})$$
$$+ 29(F_{165} - F_{103}))$$
$$+ \frac{Z_2^2R^2}{4}(3(F_{050} + F_{061} + F_{027} + F_{038} - F_{005} - F_{016} - F_{072} - F_{083})$$
$$+ 11(F_{025} + F_{063} - F_{052} - F_{036}) + 13(F_{043} + F_{045} - F_{034} - F_{054})$$
$$+ 14(F_{003} + F_{085} - F_{030} - F_{058}) + 15(F_{010} + F_{078} - F_{001} - F_{087})$$
$$+ 25(F_{014} + F_{074} - F_{041} - F_{047}) + 35(F_{032} + F_{056} - F_{023} - F_{065})$$
$$+ 37(F_{021} + F_{067} - F_{012} - F_{076}))$$
$$- 4Z_2R(A_4B_3 + A_2B_3 - A_3B_4 - A_3B_2 + 3(A_5B_2 + A_6B_3 + A_0B_3$$
$$+ A_1B_4 - A_2B_5 - A_3B_6 - A_3B_0 - A_4B_1)$$
$$+ 4(A_2B_1 + A_4B_5 - A_1B_2 - A_5B_4) + 5(A_1B_0 + A_5B_6 - A_0B_1 - A_6B_5))$$
$$+ 4(3(A_5B_1 + A_0B_4 - A_1B_5 - A_4B_0)$$
$$+ 5(A_2B_0 + A_3B_5 - A_0B_2 - A_5B_3) + 9(A_4B_2 + A_1B_3 - A_2B_4 - A_3B_1))]$$

$$\langle 4f\sigma|\nabla_z^2|4f\sigma\rangle_2 = -\frac{Z_1^{9/2}Z_2^{9/2}R^7}{23040}[12(3(A_0B_4 + A_6B_2 - A_4B_0 - A_2B_6)$$

$$+ 4(A_1B_3 + A_5B_3 - A_3B_1 - A_3B_5) + 5(A_2B_0 + A_4B_6 - A_0B_2 - A_6B_4))$$

$$- Z_2R(9(A_5B_0 + A_2B_7 - A_0B_5 - A_7B_2)$$

$$+ 33(A_1B_4 + A_6B_3 - A_4B_1 - A_3B_6) + 39(A_3B_2 + A_4B_5 - A_2B_3 - A_5B_4)$$

$$+ 42(A_0B_3 + A_7B_4 - A_3B_0 - A_4B_7) + 45(A_1B_0 + A_6B_7 - A_0B_1 - A_7B_6)$$

$$+ 66(A_2B_1 + A_5B_6 - A_1B_2 - A_6B_5))$$

$$+ \frac{Z_2R}{2}(9(F_{136} + F_{116} + F_{141} + F_{152} + F_{172} + F_{129} - F_{143} - F_{150}$$

$$- F_{107} - F_{163} - F_{127} - F_{138}) + 25(F_{101} + F_{169} - F_{110} - F_{178})$$

$$+ 27(F_{134} + F_{154} - F_{125} - F_{145}) + 30(F_{130} + F_{158} - F_{121} - F_{149})$$

$$+ 39(F_{105} + F_{165} - F_{114} - F_{174}) + 55(F_{112} + F_{176} - F_{103} - F_{167})$$

$$+ 57(F_{123} + F_{147} - F_{132} - F_{156}))$$

$$+ \frac{Z_2^2R^2}{4}(9(F_{050} + F_{049} - F_{005} - F_{094})$$

$$+ 18(F_{061} + F_{038} - F_{016} - F_{083}) + 25(F_{010} + F_{089} - F_{001} - F_{098})$$

$$+ 30(F_{003} + F_{096} - F_{030} - F_{069}) + 48(F_{025} + F_{074} - F_{052} - F_{047})$$

$$+ 69(F_{014} + F_{085} - F_{041} - F_{058}) + 80(F_{021} + F_{078} - F_{012} - F_{087})$$

$$+ 84(F_{043} + F_{056} - F_{034} - F_{065})$$

$$+ 112(F_{032} + F_{067} - F_{023} - F_{076}))]$$

$$\langle 4f\pi|\nabla_z^2|2p\pi\rangle_2 = -\frac{Z_1^{9/2}Z_2^{7/2}R^6}{256\sqrt{30}}[F_{107} + F_{150} - 2(F_{123} + F_{134} + F_{136} + F_{121})$$

$$- 3(F_{112} + F_{145}) + 5(F_{110} + F_{147} - F_{101} - F_{156})$$

$$- 6(F_{130} + F_{127}) + 7(F_{141} + F_{116} - F_{105} - F_{152})$$

$$- 9(F_{143} + F_{114}) + 10(F_{132} + F_{125}) + 11(F_{103} + F_{154})$$

$$+ \frac{Z_2R}{2}(F_{005} + F_{027} - F_{050} - F_{072} + 2(F_{025} + F_{016} - F_{052} - F_{061})$$

$$+ 4(F_{034} - F_{043}) + 5(F_{041} + F_{045} + F_{001} + F_{023} + F_{063} + F_{067}$$

$$- F_{014} - F_{054} - F_{010} - F_{032} - F_{036} - F_{076})$$

$$+ 6(F_{030} + F_{074} - F_{003} - F_{047}) + 8(F_{012} + F_{056} - F_{021} - F_{065}))]$$

$$\langle 4f\pi|\nabla_z^2|3d\pi\rangle_2 = -\frac{Z_1^{9/2} Z_2^{9/2} R^7}{1536\sqrt{5}} [F_{125} + F_{143} + F_{127} + F_{141} + F_{150} + F_{161} + F_{107}$$
$$+ F_{118} + 2(F_{114} + F_{154}) + 3(F_{121} + F_{147})$$
$$- 4F_{134} + 5(F_{110} + F_{158} - F_{145} - F_{123} - F_{101} - F_{167})$$
$$- 6(F_{130} + F_{138}) - 7(F_{105} + F_{163}) + 8(F_{136} + F_{132} - F_{112} - F_{156})$$
$$+ 11(F_{103} + F_{165})$$
$$- 2(A_1B_4 + A_2B_5 + A_0B_5 + A_1B_6 - A_4B_1 - A_5B_2 - A_5B_0 - A_6B_1$$
$$+ 2(A_2B_3 + A_3B_4 - A_3B_2 - A_4B_3) + 3(A_1B_2 + A_4B_5 - A_2B_1 - A_5B_4)$$
$$+ 5(A_0B_1 + A_5B_6 - A_1B_0 - A_6B_5) + 6(A_3B_0 + A_6B_3 - A_0B_3 - A_3B_6))$$
$$+ \frac{Z_2R}{2} (F_{005} + F_{038} - F_{050} - F_{083} + 3(F_{052} + F_{063} + F_{016} + F_{027}$$
$$- F_{025} - F_{036} - F_{061} - F_{072})$$
$$+ 5(F_{001} + F_{078} - F_{010} - F_{087}) + 6(F_{030} + F_{085} - F_{003} - F_{058})$$
$$+ 9(F_{034} + F_{045} - F_{043} - F_{054}) + 11(F_{041} + F_{074} - F_{014} - F_{047})$$
$$+ 13(F_{023} + F_{012} + F_{056} + F_{067} - F_{032} - F_{021} - F_{065} - F_{076}))]$$

$$\langle 4f\pi|\nabla_z^2|4f\pi\rangle_2 = -\frac{Z_1^{9/2} Z_2^{9/2} R^7}{30720} [\frac{Z_2R}{2} (F_{161} + F_{118} - F_{170} - F_{109}$$
$$+ 11(F_{150} + F_{129} - F_{141} - F_{138}) + 12(F_{107} + F_{172} - F_{116} - F_{163})$$
$$+ 20(F_{143} + F_{136} - F_{152} - F_{127}) + 25(F_{110} + F_{169} - F_{101} - F_{178})$$
$$+ 35(F_{121} + F_{158} - F_{130} - F_{149}) + 42(F_{154} + F_{125} - F_{145} - F_{134})$$
$$+ 46(F_{114} + F_{165} - F_{174} - F_{105}) + 60(F_{103} + F_{176} - F_{112} - F_{167})$$
$$+ 68(F_{132} + F_{147} - F_{123} - F_{156}))$$
$$+ \frac{Z_2^2R^2}{4} (F_{070} + F_{092} - F_{007} - F_{029} + 2(F_{081} - F_{018})$$
$$+ 11(F_{005} + F_{049} - F_{050} - F_{094}) + 23(F_{016} + F_{038} - F_{061} - F_{083})$$
$$+ 24(F_{027} - F_{072}) + 25(F_{001} + F_{089} - F_{010} - F_{098})$$
$$+ 35(F_{030} + F_{096} - F_{003} - F_{069}) + 40(F_{063} - F_{036})$$

$$+ 66(F_{052} + F_{074} - F_{025} - F_{047}) + 81(F_{041} + F_{085} - F_{014} - F_{058})$$
$$+ 84(F_{045} - F_{054}) + 85(F_{012} + F_{078} - F_{021} - F_{087})$$
$$+ 110(F_{034} + F_{056} - F_{043} - F_{065})$$
$$+ 128(F_{023} + F_{067} - F_{032} - F_{076}))$$
$$+ 8(A_0B_6 - A_6B_0 + 5(A_0B_2 + A_4B_6 - A_2B_0 - A_6B_4)$$
$$+ 6(A_4B_0 + A_6B_2 - A_0B_4 - A_2B_6) + 8(A_5B_3 + A_3B_1 + A_1B_5 - A_3B_5$$
$$- A_1B_3 - A_5B_1) + 11(A_2B_4 - A_4B_2))$$
$$- 8Z_2R(A_0B_5 + A_2B_7 - A_5B_0 - A_7B_2 + 2(A_2B_5 + A_1B_6 - A_5B_2 - A_6B_1)$$
$$+ 4(A_3B_4 - A_4B_3) + 5(A_2B_3 + A_0B_1 + A_4B_1 + A_4B_5 + A_6B_3 + A_6B_7$$
$$- A_3B_2 - A_1B_0 - A_1B_4 - A_5B_4 - A_3B_6 - A_7B_6)$$
$$+ 6(A_3B_0 + A_7B_4 - A_0B_3 - A_4B_7) + 8(A_1B_2 + A_5B_6 - A_2B_1 - A_6B_5))]$$

The expressions given above for these two-center integrals can be checked by considering the hermitian property of the operator ∇_z^2. For example consider the integral $\langle 3s|\nabla_z^2|2p\sigma\rangle_2$. If the 3s orbital has a screening coefficient 5.37670, the 2pσ orbital has a screening coefficient 3.11196, and the bond length is 2.132 a.u. then the appropriate expression given above yields a value of -0.18763329 for this integral. But because of the hermitian property of the operator this integral could equally well be evaluated by considering the integral $\langle 2p\sigma|\nabla_z^2|3s\rangle_2$. The expression for the integral in this form is different from that listed above for the integral in the reverse form and is given by

$$\langle 2p\sigma|\nabla_z^2|3s\rangle_2 = -\frac{\sqrt{2}\, Z_1^{5/2} Z_2^{7/2} R^4}{48\sqrt{5}} [2(A_2B_0 + A_1B_3 - A_0B_2 - A_3B_1)$$
$$- \frac{Z_2R}{2}(F_{040} + F_{015} - F_{004} - F_{051} + 3(F_{020} + F_{035} - F_{002} - F_{053})$$
$$+ 5(F_{031} + F_{024} - F_{013} - F_{042}))$$
$$+ \frac{Z_2^2R^2}{4}(A_2B_0 + A_3B_1 + A_2B_4 + A_3B_5 - A_0B_2 - A_1B_3 - A_4B_2 - A_5B_3)]$$

If the orbitals have the same screening coefficients as before then this new expression yields a value of -0.18763329 for the specified integral. Thus these two expressions, which give identical results for the integral, are consistent and correct. All the expressions listed previously were checked in this manner. The remaining expressions for the integrals in the reverse order are not listed here but are given in a research notebook for future reference.[127]

All the expressions that have been listed for the two-center overlap-type integrals are valid only if Z_1 is not equal to Z_2. If Z_1 equals Z_2, which is the case for homonuclear diatomic molecules, new expressions must be obtained for certain integrals. These new expressions use the Barnett-Coulson zeta method instead of the Kotani "F" method. The required expressions are

$$\langle 1s|\nabla_z^2|1s\rangle_2 = -\frac{2Z_2^{5/2}}{3Z_1R^{1/2}}\left[2\left(P_{2,0+\frac{1}{2}} - P_{0,0+\frac{1}{2}}\right) + \frac{Z_2}{Z_1}\left(P_{0,1+\frac{1}{2}} + 2P_{2,1+\frac{1}{2}}\right)\right]$$

$$\langle 2s|\nabla_z^2|2s\rangle_2 = -\frac{2Z_2^{5/2}}{9Z_1R^{1/2}}\left[2\left(G_{0,2+\frac{1}{2}} - G_{2,2+\frac{1}{2}} + Z_1^2R^2\left(G_{0,0+\frac{1}{2}} - G_{2,0+\frac{1}{2}}\right)\right.\right.$$

$$\left. - 6Z_1R\left(G_{1,1+\frac{1}{2}} - G_{3,1+\frac{1}{2}}\right)/5\right)$$

$$- \frac{Z_2}{Z_1}\left(4\left(G_{0,3+\frac{1}{2}} + Z_1^2R^2G_{0,1+\frac{1}{2}} - 2Z_1RG_{1,2+\frac{1}{2}}\right)\right.$$

$$\left. + 2\left(G_{2,3+\frac{1}{2}} + Z_1^2R^2G_{2,1+\frac{1}{2}} - 2Z_1R\left(2G_{1,2+\frac{1}{2}} + 3G_{3,2+\frac{1}{2}}\right)/5\right)\right)$$

$$+ \frac{Z_2^2}{Z_1^2}\left(G_{0,4+\frac{1}{2}} + Z_1^2R^2G_{0,2+\frac{1}{2}} - 2Z_1RG_{1,3+\frac{1}{2}}\right.$$

$$\left.\left. + 2\left(G_{2,4+\frac{1}{2}} + Z_1^2R^2G_{2,2+\frac{1}{2}} - 2Z_1R\left(2G_{1,3+\frac{1}{2}} + 3G_{3,3+\frac{1}{2}}\right)/5\right)\right)\right]$$

$$\langle 2p\sigma|\nabla_z^2|2p\sigma\rangle_2 = -\frac{2Z_2^{7/2}}{Z_1 R^{1/2}}\left[R\left(2P_{3,1+1/2} - 12P_{1,1+1/2} + \frac{Z_2}{Z_1}\left(3P_{1,2+1/2} + 2P_{3,2+1/2}\right)\right)/5\right.$$

$$- \left(-28P_{0,2+1/2} - 50P_{2,2+1/2} + 8P_{4,2+1/2}\right.$$

$$\left.\left. + \frac{Z_2}{Z_1}\left(7P_{0,3+1/2} + 20P_{2,3+1/2} + 8P_{4,3+1/2}\right)\right)/(35Z_1)\right]$$

$$\langle 2p\pi|\nabla_z^2|2p\pi\rangle_2 = -\frac{Z_2^{7/2}}{Z_1^2 R^{1/2}}\left[-\frac{8}{15}P_{0,2+1/2} + \frac{16}{21}P_{2,2+1/2} - \frac{8}{35}P_{4,2+1/2}\right.$$

$$\left. + \frac{Z_2}{Z_1}\left(\frac{2}{15}P_{0,3+1/2} + \frac{2}{21}P_{2,3+1/2} - \frac{8}{35}P_{4,3+1/2}\right)\right]$$

$$\langle 3s|\nabla_z^2|3s\rangle_2 = -\frac{4Z_2^{7/2}}{45Z_1^2 R^{1/2}}\left[2\left(P_{0,3+1/2} + Z_1^2R^2P_{0,1+1/2} - 2Z_1RP_{1,2+1/2}\right)\right.$$

$$- \frac{Z_2}{Z_1}\left(2\left(P_{0,4+1/2} + P_{2,4+1/2} + Z_1^2R^2\left(P_{0,2+1/2} + P_{2,2+1/2}\right)\right.\right.$$

$$\left.\left. - 2Z_1R\left(7P_{1,3+1/2} + 3P_{3,3+1/2}\right)/5\right)\right)$$

$$\left. + \frac{Z_2^2}{Z_1^2}\left(P_{0,5+1/2} + Z_1^2R^2P_{0,3+1/2} - 2Z_1RP_{1,4+1/2}\right.\right.$$

$$\left.\left. + 2\left(P_{2,5+1/2} + Z_1^2R^2P_{2,3+1/2} - 2Z_1R\left(2P_{1,4+1/2} + 3P_{3,4+1/2}\right)/5\right)\right)/3\right]$$

$$\langle 3d\sigma|\nabla_z^2|3d\sigma\rangle_2 = -\frac{Z_2^{7/2}}{9R^{1/2}}\left[\frac{Z_2}{Z_1}\left(\left(-\frac{88}{35}P_{0,4+1/2} - \frac{56}{7}P_{2,4+1/2} - \frac{336}{55}P_{4,4+1/2}\right.\right.\right.$$

$$\left.\left.\left. + \frac{48}{77}P_{6,4+1/2}\right)/Z_1^2\right.\right.$$

$$\left.\left. + 2R^2\left(-\frac{12}{5}P_{0,2+1/2} - \frac{44}{7}P_{2,2+1/2} + \frac{24}{35}P_{4,2+1/2}\right)\right.\right.$$

$$- \frac{4R}{Z_1}\left(- \frac{172}{35} P_{1,3+\frac{1}{2}} - \frac{52}{15} P_{3,3+\frac{1}{2}} + \frac{24}{63} P_{5,3+\frac{1}{2}}\right)\Big)$$

$$+ \frac{Z_2^2}{Z_1^2}\left(\left(\frac{44}{105} P_{0,5+\frac{1}{2}} + \frac{32}{21} P_{2,5+\frac{1}{2}} + \frac{552}{385} P_{4,5+\frac{1}{2}} + \frac{144}{231} P_{6,5+\frac{1}{2}}\right)/Z_1^2\right.$$

$$+ 2R^2\left(\frac{4}{15} P_{0,3+\frac{1}{2}} + \frac{22}{21} P_{2,3+\frac{1}{2}} + \frac{24}{35} P_{4,3+\frac{1}{2}}\right)$$

$$- \frac{4R}{Z_1}\left(\frac{24}{35} P_{1,4+\frac{1}{2}} + \frac{42}{45} P_{3,4+\frac{1}{2}} + \frac{24}{63} P_{5,4+\frac{1}{2}}\right)\Big)$$

$$+ 8\left(\frac{1}{Z_1^2} P_{2,3+\frac{1}{2}} + R^2 P_{0,1+\frac{1}{2}} - \frac{2R}{Z_1} P_{1,2+\frac{1}{2}}\right)\Big]$$

$$\langle 3d\pi \left| \nabla_z^2 \right| 3d\pi \rangle_2 = - \frac{2Z_2^{9/2}}{3Z_1^2 R^{\frac{1}{2}}}\Big[R\left(- \frac{36}{35} P_{1,3+\frac{1}{2}} + \frac{52}{45} P_{3,3+\frac{1}{2}} - \frac{8}{63} P_{5,3+\frac{1}{2}}\right.$$

$$+ \frac{Z_2}{Z_1}\left(\frac{6}{35} P_{1,4+\frac{1}{2}} - \frac{2}{45} P_{3,4+\frac{1}{2}} - \frac{8}{63} P_{5,4+\frac{1}{2}}\right)\Big)$$

$$+ \frac{1}{Z_1}\left(\frac{12}{35} P_{0,4+\frac{1}{2}} + \frac{28}{147} P_{2,4+\frac{1}{2}} - \frac{232}{385} P_{4,4+\frac{1}{2}} + \frac{16}{231} P_{6,4+\frac{1}{2}}\right.$$

$$- \frac{Z_2}{Z_1}\left(\frac{2}{35} P_{0,5+\frac{1}{2}} + \frac{2}{21} P_{2,5+\frac{1}{2}} - \frac{32}{385} P_{4,5+\frac{1}{2}} - \frac{16}{231} P_{6,5+\frac{1}{2}}\right)\Big)\Big]$$

$$\langle 4f\sigma \left| \nabla_z^2 \right| 4f\sigma \rangle_2 = - \frac{Z_2^{9/2}}{90R^{\frac{1}{2}}}\Big[R\left(\frac{24}{Z_1^2} P_{3,4+\frac{1}{2}} - \frac{16R}{Z_1}\left(P_{0,3+\frac{1}{2}} + 2P_{2,3+\frac{1}{2}}\right) + 24R^2 P_{1,2+\frac{1}{2}}\right.$$

$$+ \frac{Z_2}{Z_1}\left(\frac{1}{Z_1^2}\left(- \frac{736}{105} P_{1,5+\frac{1}{2}} - \frac{2296}{495} P_{3,5+\frac{1}{2}} - \frac{10880}{819} P_{5,5+\frac{1}{2}}\right.\right.$$

$$\left.\left.\left. + \frac{400}{429} P_{7,5+\frac{1}{2}}\right)\right.$$

$$- \frac{4R}{Z_1}\left(- \frac{52}{35} P_{0,4+\frac{1}{2}} - \frac{136}{21} P_{2,4+\frac{1}{2}} - \frac{1688}{385} P_{4,4+\frac{1}{2}} + \frac{80}{231} P_{6,4+\frac{1}{2}}\right)$$

$$+ 2R^2 \left(- \frac{156}{35} P_{1,3+\frac{1}{2}} - \frac{368}{45} P_{3,3+\frac{1}{2}} + \frac{40}{63} P_{5,3+\frac{1}{2}}\right)\Big)$$

$$+ \frac{Z_2^2}{Z_1^2} \left(\frac{1}{Z_1^2} \left(\frac{92}{105} P_{1,6+\frac{1}{2}} + \frac{144}{165} P_{3,6+\frac{1}{2}} + \frac{360}{273} P_{5,6+\frac{1}{2}} + \frac{400}{429} P_{7,6+\frac{1}{2}}\right)\right.$$

$$- \frac{4R}{Z_2} \left(\frac{4}{35} P_{0,5+\frac{1}{2}} + \frac{2}{3} P_{2,5+\frac{1}{2}} + \frac{48}{55} P_{4,5+\frac{1}{2}} + \frac{80}{231} P_{6,5+\frac{1}{2}}\right)$$

$$+ 2R^2 \left(\frac{12}{35} P_{1,4+\frac{1}{2}} + \frac{46}{45} P_{3,4+\frac{1}{2}} + \frac{40}{63} P_{5,4+\frac{1}{2}}\right)\Big)\Big)$$

$$- \left(\frac{1}{Z_1^3} \left(\frac{72}{7} P_{2,5+\frac{1}{2}} + \frac{96}{7} P_{4,5+\frac{1}{2}}\right) - \frac{48R}{Z_1^2} \left(\frac{3}{5} P_{1,4+\frac{1}{2}} + \frac{2}{5} P_{3,4+\frac{1}{2}}\right)\right.$$

$$+ \frac{8R^2}{Z_1} \left(P_{0,3+\frac{1}{2}} + 2P_{2,3+\frac{1}{2}}\right)$$

$$+ \frac{Z_2}{Z_1} \left(\frac{1}{Z_1^3} \left(- \frac{736}{315} P_{0,6+\frac{1}{2}} - \frac{4616}{693} P_{2,6+\frac{1}{2}} - \frac{478368}{55055} P_{4,6+\frac{1}{2}}\right.\right.$$

$$\left.\left. - \frac{4720}{693} P_{6,6+\frac{1}{2}} + \frac{640}{1287} P_{8,6+\frac{1}{2}}\right)\right.$$

$$- \frac{4R}{Z_1^2} \left(- \frac{428}{105} P_{1,5+\frac{1}{2}} - \frac{2888}{495} P_{3,5+\frac{1}{2}} - \frac{1864}{819} P_{5,5+\frac{1}{2}} + \frac{80}{429} P_{7,5+\frac{1}{2}}\right)$$

$$+ \frac{2R^2}{Z_1} \left(- \frac{52}{35} P_{0,4+\frac{1}{2}} - \frac{136}{21} P_{2,4+\frac{1}{2}} - \frac{1688}{385} P_{4,4+\frac{1}{2}} + \frac{80}{231} P_{6,4+\frac{1}{2}}\right)\Big)$$

$$+ \frac{Z_2^2}{Z_1^2} \left(\frac{1}{Z_1^3} \left(\frac{92}{315} P_{0,7+\frac{1}{2}} + \frac{664}{693} P_{2,7+\frac{1}{2}} + \frac{60456}{55055} P_{4,7+\frac{1}{2}} + \frac{800}{693} P_{6,7+\frac{1}{2}}\right.\right.$$

$$\left.\left. + \frac{640}{1287} P_{8,7+\frac{1}{2}}\right)\right.$$

$$- \frac{4R}{Z_1^2} \left(\frac{8}{21} P_{1,6+\frac{1}{2}} + \frac{26}{33} P_{3,6+\frac{1}{2}} + \frac{176}{273} P_{5,6+\frac{1}{2}} + \frac{80}{429} P_{7,6+\frac{1}{2}}\right)$$

$$+ \frac{2R^2}{Z_1}\left(\frac{4}{35} P_{0,5+\frac{1}{2}} + \frac{2}{3} P_{2,5+\frac{1}{2}} + \frac{48}{55} P_{4,5+\frac{1}{2}} + \frac{80}{231} P_{6,5+\frac{1}{2}}\right)\Big)\Big)\Big]$$

$$\langle 4f\pi | \nabla_z^2 | 4f\pi \rangle_2 = - \frac{Z_2^{9/2}}{120 Z_1 R^{\frac{1}{2}}}\Big[\frac{Z_2}{Z_1}\Big(\frac{5}{Z_1^2}\Big(- \frac{128}{225} P_{0,6+\frac{1}{2}} - \frac{4096}{3465} P_{2,6+\frac{1}{2}} + \frac{13952}{25025} P_{4,6+\frac{1}{2}}$$

$$+ \frac{128}{99} P_{6,6+\frac{1}{2}} - \frac{128}{1287} P_{8,6+\frac{1}{2}}\Big)$$

$$+ 4R^2\Big(- \frac{208}{105} P_{0,4+\frac{1}{2}} - \frac{16}{7} P_{2,4+\frac{1}{2}} + \frac{1776}{385} P_{4,4+\frac{1}{2}} - \frac{80}{231} P_{6,4+\frac{1}{2}}\Big)$$

$$- \frac{8R}{Z_1}\Big(- \frac{304}{105} P_{1,5+\frac{1}{2}} + \frac{112}{165} P_{3,5+\frac{1}{2}} + \frac{656}{273} P_{5,5+\frac{1}{2}} - \frac{80}{429} P_{7,5+\frac{1}{2}}\Big)\Big)$$

$$+ \frac{Z_2^2}{Z_1^2}\Big(\frac{5}{Z_1^2}\Big(\frac{16}{225} P_{0,7+\frac{1}{2}} + \frac{656}{3465} P_{2,7+\frac{1}{2}} + \frac{16}{25025} P_{4,7+\frac{1}{2}} - \frac{16}{99} P_{6,7+\frac{1}{2}}$$

$$- \frac{128}{1287} P_{8,7+\frac{1}{2}}\Big)$$

$$+ 4R^2\Big(\frac{16}{105} P_{0,5+\frac{1}{2}} + \frac{8}{21} P_{2,5+\frac{1}{2}} - \frac{77}{385} P_{4,5+\frac{1}{2}} - \frac{80}{231} P_{6,5+\frac{1}{2}}\Big)$$

$$- \frac{8R}{Z_1}\Big(\frac{32}{105} P_{1,6+\frac{1}{2}} + \frac{8}{55} P_{3,6+\frac{1}{2}} - \frac{24}{91} P_{5,6+\frac{1}{2}} - \frac{80}{429} P_{7,6+\frac{1}{2}}\Big)\Big)$$

$$+ 8\Big(\frac{8}{7Z_1^2}\Big(P_{2,5+\frac{1}{2}} - P_{4,5+\frac{1}{2}}\Big) + \frac{8}{3} R^2\Big(P_{0,3+\frac{1}{2}} - P_{2,3+\frac{1}{2}}\Big)$$

$$- \frac{16R}{5Z_1}\Big(P_{1,4+\frac{1}{2}} - P_{3,4+\frac{1}{2}}\Big)\Big)\Big] \ .$$

These final expressions, which are valid if Z_1 equals Z_2 or not, were checked by computing the integrals where $Z_1 \neq Z_2$ and comparing them with the results for the same integrals from the previous method. The

results agreed to seven or eight significant figures thus verifying the above expressions.

All the integral expressions that have been listed were used to calculate the Z-component for the total average kinetic energy, $\overline{T}_{zz}$, (i.e., $\langle\psi|\nabla_z^2|\psi\rangle$) for a number of homonuclear molecules. The results are given in the thesis.

Finally, in the kinetic energy determinations the function $G(\vec{x}_1) = \frac{1}{2}\sum_i \lambda_i \vec{\nabla}\phi_i(\vec{x})\cdot\vec{\nabla}\phi_i(\vec{x})$ was evaluated at different points of space. In order to carry out these calculations the following expressions were used. Letting $\nabla_x = \frac{\partial}{\partial x_a}$, $\nabla_y = \frac{\partial}{\partial y_a}$ and $\nabla_z = \frac{\partial}{\partial z_a}$ then

$$\nabla_x\chi(n,\ell,m)_a = (2\alpha)^{n+1/2}(2n!)^{-1/2}[((n-1)r_a^{n-2} - \alpha r_a^{n-1})$$

$$\sin\theta_a\cos\phi S_{\ell,m}(\theta_a,\phi) + r_a^{n-1}\frac{\partial}{\partial x_a}S_{\ell,m}(\theta_a,\phi)]e^{-\alpha r_a} \qquad \text{(A9.31)}$$

$$\nabla_y\chi(n,\ell,m)_a = (2\alpha)^{n+1/2}(2n!)^{-1/2}[((n-1)r_a^{n-2} - \alpha r_a^{n-1})$$

$$\sin\theta_a\sin\phi S_{\ell,m}(\theta_a,\phi) + r_a^{n-1}\frac{\partial}{\partial y_a}S_{\ell,m}(\theta_a,\phi)]e^{-\alpha r_a} \qquad \text{(A9.32)}$$

$$\nabla_z\chi(n,\ell,m)_a = (2\alpha)^{n+1/2}(2n!)^{-1/2}[((n-1)r_a^{n-2} - \alpha r_a^{n-1})$$

$$\cos\theta_a S_{\ell,m}(\theta_a,\phi) + r_a^{n-1}\frac{\partial}{\partial z_a}S_{\ell,m}(\theta_a,\phi)]e^{-\alpha r_a}\ . \qquad \text{(A9.33)}$$

Using Equation (A9.33) one obtains

$$\nabla_z|1s\rangle = \frac{\alpha^{3/2}}{\sqrt{\pi}}[-\alpha]\cos\theta_a\ e^{-\alpha r_a}$$

$$\nabla_z|2s\rangle = \frac{\alpha^{5/2}}{\sqrt{3\pi}}[1 - \alpha r_a]\cos\theta_a\, e^{-\alpha r_a}$$

$$\nabla_z|2p\sigma\rangle = \frac{\alpha^{5/2}}{\sqrt{\pi}}[1 - \alpha r_a\cos^2\theta_a]e^{-\alpha r_a}$$

$$\nabla_z|2p\pi x\rangle = \frac{\alpha^{5/2}}{\sqrt{\pi}}[-\alpha r_a]\cos\theta_a\sin\theta_a\cos\phi\, e^{-\alpha r_a}$$

$$\nabla_z|2p\pi y\rangle = \frac{\alpha^{5/2}}{\sqrt{\pi}}[-\alpha r_a]\cos\theta_a\sin\theta_a\sin\phi\, e^{-\alpha r_a}$$

$$\nabla_z|3s\rangle = \frac{\sqrt{2}\,\alpha^{7/2}}{3\sqrt{5\pi}}[2r_a - \alpha r_a^2]\cos\theta_a\, e^{-\alpha r_a}$$

$$\nabla_z|3p\sigma\rangle = \frac{\sqrt{2}\,\alpha^{7/2}}{\sqrt{15\pi}}[(r_a - \alpha r_a^2)\cos^2\theta_a + r_a]e^{-\alpha r_a}$$

$$\nabla_z|3p\pi x\rangle = \frac{\sqrt{2}\,\alpha^{7/2}}{\sqrt{15\pi}}[r_a - \alpha r_a^2]\cos\theta_a\sin\theta_a\cos\phi\, e^{-\alpha r_a}$$

$$\nabla_z|3p\pi y\rangle = \frac{\sqrt{2}\,\alpha^{7/2}}{\sqrt{15\pi}}[r_a - \alpha r_a^2]\cos\theta_a\sin\theta_a\sin\phi\, e^{-\alpha r_a}$$

$$\nabla_z|3d\sigma\rangle = \frac{\alpha^{7/2}}{\sqrt{18\pi}}[(-\alpha r_a^2)\cos\theta_a(3\cos^2\theta_a - 1) + 4r_a\cos\theta_a]e^{-\alpha r_a}$$

$$\nabla_z|3d\pi x\rangle = \frac{\sqrt{2}\,\alpha^{7/2}}{\sqrt{3\pi}}[(-\alpha r_a^2)\cos^2\theta_a\sin\theta_a\cos\phi + r_a\sin\theta_a\cos\phi]e^{-\alpha r_a}$$

$$\nabla_z|3d\pi y\rangle = \frac{\sqrt{2}\,\alpha^{7/2}}{\sqrt{3\pi}}[(-\alpha r_a^2)\cos^2\theta_a\sin\theta_a\sin\phi + r_a\sin\theta_a\sin\phi]e^{-\alpha r_a}$$

$$\nabla_z|4f\sigma\rangle = \frac{\alpha^{9/2}}{\sqrt{180\pi}}[(-\alpha r_a^3)\cos\theta_a(5\cos^3\theta_a - 3\cos\theta_a) + 3r_a^2(3\cos^2\theta_a - 1)]e^{-\alpha r_a}$$

$$\nabla_z|4f\pi x\rangle = \frac{\alpha^{9/2}}{\sqrt{120\pi}}[(-\alpha r_a^3)\cos\theta_a\sin\theta_a(5\cos^2\theta_a - 1)\cos\phi + 8r_a^2\cos\theta_a\sin\theta_a\cos\phi]e^{-\alpha r_a}$$

$$\nabla_z|4f\pi y\rangle = \frac{\alpha^{9/2}}{\sqrt{120\pi}}\left[(-\alpha r_a^3)\cos\theta_a\sin\theta_a(5\cos^2\theta_a-1)\sin\phi + 8r_a^2\cos\theta_a\sin\theta_a\sin\phi\right]e^{-\alpha r_a} .$$

Similar expressions can be obtained for the operators ∇_x and ∇_y using Equations (A9.31) and (A9.32) respectively. These expressions were then used to evaluate the function $G(\vec{x}_1)$.

BIBLIOGRAPHY

1. P. Hohenberg and W. Kohn, Phys. Rev. 136B, 864 (1964).

2. R. J. Gillespie and R. S. Nyholm, Quart. Rev. (London) 11, 339 (1957); R. J. Gillespie, J. Am. Chem. Soc. 82, 5978 (1960).

3. R. F. W. Bader, W. H. Henneker and P. E. Cade, J. Chem. Phys. 46, 3341 (1967).

4. R. F. W. Bader, I. Keaveny and P. E. Cade, J. Chem. Phys. 47, 3381 (1967).

5. R. F. W. Bader and A. D. Bandrauk, J. Chem. Phys. 49, 1653 (1968).

6. P. E. Cade, R. F. W. Bader, W. H. Henneker and I. Keaveny, J. Chem. Phys. 50, 0000 (1969).

7. The material in Chapter III has been accepted for publication in the International Journal of Quantum Chemistry.

8. R. F. W. Bader and H. J. T. Preston, Can. J. Chem. 44, 1131 (1966).

9. R. A. Buckingham, H. S. W. Massey and S. R. Tibbs, Proc. Roy. Soc. (London) A178, 119 (1941).

10. H. Hartmann, Z. Naturforch. 2A, 489 (1947).

11. M. J. M. Bernal, Proc. Phys. Soc. A66, 514 (1953).

12. C. Carter, Proc. Roy. Soc. (London) A235, 321 (1956).

13. K. Funabashi and J. L. Magee, J. Chem. Phys. 26, 407 (1957).

14. S. Kaide, H. Sekijama and T. Nagashima, J. Phys. Soc. Japan, 12, 1016 (1957).

15. H. Hartmann and G. Gliemann, Z. Physik. Chem. (Frankfurt) 15, 108 (1958).

16. R. K. Nesbet, J. Chem. Phys. 32, 1114 (1960).

17. I. M. Mills, Mol. Phys. 1, 99 (1958); 4, 57 (1961).

18. E. L. Albasiny and J. R. A. Cooper, Mol. Phys. 4, 353 (1961).

19. F. Grein, Theoret. Chim. Acta 1, 52 (1962).

20. J. R. Hoyland and F. W. Lampe, J. Chem. Phys. 37, 1066 (1962).

21. M. Krauss, J. Chem. Phys. 38, 564 (1963).

22. R. Moccia, J. Chem. Phys. 37, 910 (1962); 40, 2164 (1964).

23. J. J. Sinai, J. Chem. Phys. 39, 1575 (1963).

24. B. J. Woznick, J. Chem. Phys. 40, 2860 (1964).

25. M. Klessinger and R. McWeeny, J. Chem. Phys. 42, 3343 (1965).

26. W. E. Palke and W. N. Lipscomb, J. Am. Chem. Soc. 88, 2384 (1966).

27. R. M. Pitzer, J. Chem. Phys. 46, 4871 (1967).

28. C. D. Ritchie and H. F. King, J. Chem. Phys. 47, 564 (1967).

29. G. P. Arrighini, C. Guidolti, M. Maestro, R. Moccia and O. Salvetti, J. Chem. Phys. 49, 2224 (1968).

30. A. F. Saturno and R. G. Parr, J. Chem. Phys. 33, 22 (1960); D. M. Bishop, Mol. Phys. 6, 305 (1963); A. G. Turner, A. F. Saturno, P. Hauk and R. G. Parr, J. Chem. Phys. 40, 1919 (1964).

31. A. D. McLean and M. Yoshimine, "Tables of Linear Molecule Wave Functions", published as a supplement to the I.B.M. Journal of Research and Development, 1967; Internat. J. Quantum Chem. Symposium 1, 313 (1967).

32. P. E. Cade and W. M. Huo, J. Chem. Phys. 47, 614 (1967).

33. L. C. Allen, J. Chem. Phys. 37, 200 (1962).

34. C. C. J. Roothaan, Rev. Mod. Phys. 23, 69 (1951).

35. R. F. W. Bader and G. A. Jones, Can. J. Chem. 39, 1253 (1961); 41, 586 (1963).

36. I. T. Keaveny, "The Nature of the Binding in Hydride Molecules", Ph.D. Thesis, McMaster University, 1967.

37. G. N. Lewis, J. Amer. Chem. Soc. 38, 762 (1916).

38. W. Heitler, Z. Physik, 46, 47 (1927).

39. F. London, Z. Physik, 46, 455 (1928).

40. H. M. Powell and N. V. Sidgwick, Proc. Roy. Soc. (London) A176, 153 (1940).

41. J. E. Lennard-Jones, J. Chem. Phys. 20, 1024 (1952).

42. J. A. Pople, Quart. Rev. (London) 11, 291 (1957).

43. O. Sinanoglu, Advan. Chem. Phys. 6, 315 (1964).

44. M. Born and R. Oppenheimer, Am. Physik, 87, 457 (1927).

45. V. Fock, Z. Physik, 61, 126 (1930).

46. P. R. Hartree, Proc. Com. Phil. Soc. 24, 89 (1928).

47. R. G. Parr, "Quantum Theory of Molecular Electronic Structure", New York, W. A. Benjamin, Inc., 1964.

48. P. O. Löwdin, Phys. Rev. 97, 1474 (1955).

49. A. Mukherji and M. Karplus, J. Chem. Phys. 38, 44 (1963).

50. H. Hellmann, "Einführing in die Quantemchemie", F. Deuticke, Leipzig, 1937, p. 285; R. P. Feynman, Phys. Rev. 56, 340 (1939).

51. J. E. Lennard-Jones, Proc. Roy. Soc. (London) A198, 1, 14 (1949); G. G. Hall and J. E. Lennard-Jones, ibid, A202, 155 (1950); A205, 357 (1951); J. E. Lennard-Jones and J. A. Pople, ibid, A202, 166 (1950).

52. P. O. Löwdin and B. Pullman, "Molecular Orbitals in Chemistry, Physics, and Biology", Academic Press, New York and London (1964), p. 165.

53. E. Clementi, C. C. J. Roothaan, M. Yoshimine, Phys. Rev. 127, 1618 (1962).

54. L. Suttan, Chem. Soc. (London), Spec. Pub. 11 (1958).

55. N. F. Ramsey, Phys. Rev. 78, 699 (1950).

56. R. F. Ramsey, Am. Scientist, 49, 509 (1961); C. H. Anderson and N. F. Ramsey, Phys. Rev. 149, 14 (1966).

57. R. Hegstrom and W. N. Lipscomb, J. Chem. Phys. 46, 4538 (1967).

58. R. F. Schwartz, "Magnetic Effects in Free Molecules", Ph.D. Thesis, Harvard University, 1952.

59. T. Myint, D. Kleppner, N. F. Ramsey and H. G. Robinson, Phys. Rev. Letters, 17, 405 (1966).

60. J. A. Pople, W. G. Schneider and H. J. Bernstein, High-Resolution Nuclear Magnetic Resonance (McGraw-Hill Book Co., New York, 1959), p. 90.

61. R. F. W. Bader, Can. J. Chem. 38, 2117 (1960).

62. J. H. Van Vleck, "The Theory of Electric and Magnetic Susceptibilities"(Oxford University Press, New York, 1932).

63. J. R. Eshback and M. W. P. Strandberg, Phys. Rev. 85, 24 (1952); W. Weltner, J. Chem. Phys. 28, 477 (1958).

64. C. Barter, R. G. Meisenheimer and D. P. Stevenson, J. Phys. Chem. 64, 1312 (1960). An earlier result by F. Bitter, Phys. Rev. 33, 389 (1929), gives χ = -12.2 e.m.u. but this is taken to be less accurate than the more recent value.

65. C. A. Coulson, Trans. Faraday Soc. 33, 388 (1937); Proc. Phys. Soc. (London) A54, 51 (1942).

66. K. E. Banyard, J. Chem. Phys. 33, 832 (1960).

67. W. C. Hamilton, J. Chem. Phys. 26, 345 (1957).

68. A. M. Thorndike, A. J. Wells, and E. B. Wilson, J. Chem. Phys. 15, 157 (1947).

69. D. F. Hornig and P. C. McKean, J. Phys. Chem. 59, 1133 (1955).

70. J. J. Sinai, J. Chem. Phys. 40, 3596 (1964).

71. D. E. Strogryn and A. P. Strogryn, Mol. Phys. 11, 371 (1966).

72. E. L. Albasiny and J. R. A. Cooper, Proc. Phys. Soc. (London) 82, 289 (1963).

73. A. G. Turner, A. F. Saturno, P. Hauk, and R. G. Parr, J. Chem. Phys. 40, 1919 (1964).

74. W. T. King, J. Chem. Phys. 39, 2141 (1963).

75. S. Kielich, Acta Phys. Polom. 24, 289 (1963).

76. S. Kielich, Mol. Phys. 9, 549 (1965); D. R. Johnston, G. J. Oudemans and R. H. Cale, J. Chem. Phys. 33, 1310 (1960).

77. H. M. James and T. A. Keenan, J. Chem. Phys. 31, 12 (1959).

78. H. Narumi and T. Watanabe, Bull. Am. Phys. Soc. 9, 11 (1964); J. P. Auffray, Phys. Rev. Letters, 6, 120 (1961) obtains 2.82×10^{-27} cm^2.

79. T. Caves and M. Karplus, J. Chem. Phys. 45, 1670 (1966).

80. C. H. Anderson and N. F. Ramsey, Phys. Rev. 149, 14 (1966).

81. R. M. Pitzer, J. P. Wright and M. P. Barnett, "Some Programs to Evaluate Multicenter Integrals by the Zeta Function Method", Programs 22-25, and the FORTRAN IV versions, Programs 86 and 87; A. C. Switendick and F. J. Corbato, "Diatomic Molecular Integral Program", Program 29, Quantum Chemistry Program Exchange, Indiana University (1966).

82. C. Hollister and O. Sinanoglu, J. Am. Chem. Soc. 88, 13 (1966).

83. D. D. Wagman, W. H. Evans, I. Halow, V. B. Parker, S. M. Bailey and R. H. Schumm, Nat. Bur. Std. Tech. Note, 270-4, October, 1965.

84. R. F. W. Bader and G. A. Jones, J. Chem. Phys. 38, 2791 (1963).

85. R. F. W. Bader and G. A. Jones, Can. J. Chem. 41, 2251 (1963).

86. R. L. Matcha, J. Chem. Phys. 47, 4595 (1967); 47, 5295 (1967).

87. T. Berlin, J. Chem. Phys. 19, 208 (1951).

88. R. F. W. Bader, J. Am. Chem. Soc. 86, 5070 (1964).

89. R. F. W. Bader and A. D. Bandrauk, J. Chem. Phys. 49, 1666 (1968).

90. L. Salem, J. Chem. Phys. 46, 4474 (1967).

91. J. Gerratt and I. M. Mills, J. Chem. Phys. 49, 1719, 1730 (1968).

92. I. M. Mills, Mol. Phys. 4, 57 (1961).

93. J. N. Murrell, J. Mol. Spect. 4, 446 (1960).

94. L. H. Jones and R. S. McDowell, J. Mol. Spect. 3, 632 (1959).

95. W. Byres Brown, Proc. Cambridge Phil. Soc. 54, 251 (1958).

96. R. H. Schwendeman, J. Chem. Phys. 44, 556 (1966).

97. L. Salem, Proc. Roy. Soc. (London), A264, 379 (1961).

98. Per-Olov Löwdin, Advan. Chem. Phys. 2, 207 (1959).

99. D. Peters, J. Chem. Soc. (London), 2003 (1963).

100. B. J. Ransil, Rev. Mod. Phys. 32, 245 (1960).

101. C. Edmiston and K. Ruedenberg, J. Chem. Phys. 43, S97 (1965).

102. R. J. Gillespie, J. Chem. Educ. 40, 295 (1963).

103. N. L. Balàzs, Phys. Rev. 156, 42 (1967).

104. C. F. v. Weizsacker, Z. Physik, 96, 431 (1935).

105. Per-Olov Löwdin, Phys. Rev. 97, 1474 (1955).

106. R. McWeeny, Rev. Mod. Phys. 32, 335 (1960).

107. C. A. Coulson, Proc. Cambridge Phil. Soc. 37, 55, 74 (1941); C. A. Coulson and W. E. Duncanson, ibid, 37, 67, 406 (1941).

108. W. H. Henneker and P. E. Cade, Chem. Phys. Letters (in press).

109. D. Bohm, Phys. Rev. 85, 166 (1952).

110. C. K. Jørgensen, Internat. J. Quantum Chem. 2, 49 (1968).

111. K. Ruedenberg, Rev. Mod. Phys. 34, 326 (1962).

112. J. C. Slater, J. Chem. Phys. 1, 687 (1933).

113. G. Das and A. C. Wahl, J. Chem. Phys. 44, 87 (1966).

114. M. F. Hoar and J. W. Linett, Trans. Faraday Soc. 46, 885 (1950).

115. N. R. Kestner, J. Chem. Phys. 48, 252 (1968).

116. R. F. W. Bader and A. K. Chandra, Can. J. Chem. 46, 953 (1968).

117. P. E. Cade, K. D. Sales and A. C. Wahl, J. Chem. Phys. 44, 1973 (1966).

118. P. E. Cade and K. D. Sales (unpublished calculations for $Be_2\ ^1\Sigma_g^+$).

119. P. E. Cade, K. D. Sales and A. C. Wahl (unpublished results).

120. J. B. Greenshields (unpublished results).

121. P. E. Cade and G. Malli (unpublished results).

122. A. C. Wahl, J. Chem. Phys. 41, 2600 (1964).

123. M. Kotani, A. Amemiya, E. Ishiguro and T. Kimura, "Table of Molecular Integrals", (Tokyo, Maruzen Co., Limited, 1955).

124. M. P. Barnett and C. A. Coulson, Phil. Trans. Roy. Soc. A243, 221 (1951).

125. R. M. Pitzer, C. W. Kern and W. N. Lipscomb, J. Chem. Phys. 32, 267 (1962).

126. E. W. Hobson, "The Theory of Spherical and Ellipsoidal Harmonics", (Chalsea Publishing Company, New York, 1955).

127. For a more detailed analysis, see the work recorded in the author's research notebook.

128. C. C. J. Roothaan, J. Chem. Phys. 19, 1445 (1951).